

5907

STUDIES IN X-RAY ASTRONOMY

A THESIS
SUBMITTED FOR THE DEGREE OF
DOCTOR OF PHILOSOPHY
OF THE
GUJARAT UNIVERSITY

by

DHARMA PAL SHARMA
PHYSICAL RESEARCH LABORATORY
AHMEDABAD - 380009
INDIA

September 1974.

043



B5907

TO THE MEMORY OF
MY BROTHER

LATE SHRI SATYA PAL

S T A T E M E N T

Realising the advantage of conducting experiments near the magnetic equator due to the presence of very low charged particle background, the X-ray astronomy group at the Physical Research Laboratory, Ahmedabad planned a comprehensive programme in this field. The author as member of the X-ray astronomy group under Prof.U.R. Rao has been deeply involved in the design and fabrication of both balloon and rocket borne payloads for conducting these experiments, and in the analysis of the data obtained. This thesis presents a comprehensive account of the results obtained by the author and their interpretation.

For the rocket borne payloads Xenon-methane proportional counters with slit collimators have been extensively used. Most of the rocket experiments conducted so far from the Thumba Equatorial Rocket Launching Station (TERLS), Trivandrum ($\phi = 8^{\circ} 32'N$, $\lambda = 76^{\circ} 51'E$) have mainly concentrated in the 2-20 keV range. Consequently gas filled counters with 50-100 micron thick window of Beryllium were used as detectors. In addition balloon experiments have also been conducted from a low latitude station - Hyderabad ($\phi \approx 17^{\circ}N$), using 3 million cubic feet balloons. For all these experiments sodium iodide crystals were used as the main detectors, with plastic scintillator anticoincidence shield along with lead, tin and copper-graded shield. The balloon borne detectors were mounted on oriented platforms so that the tracking of the pre-selected stars for periods longer than an hour could be achieved with a pointing accuracy better than 1.5° .

The main body of the thesis deals with the study of variable X-ray stars and their detection through rocket borne, balloon borne and ground based techniques. The first chapter briefly reviews the important observational results on some of the important variable sources. The second chapter contains a detailed description of the rocket experiment and the results obtained therefrom. In the third chapter we have described the three balloon experiments and the results obtained during these observations. Fourth chapter contains the method and discussion of monitoring the X-ray sources using ground based techniques, through the ionization produced by their radiation in the night time D-region of the ionosphere. Additional material such as the optimal suitability of low latitude stations for conducting X-ray astronomy experiments and the methods of analysis are briefly described in the appendices.

The rocket borne instrumentation was mainly used to study the spectacular flare star Cen X-4 and the irregular variable Nor X-2. Besides these, useful information on the cosmic X-ray background has also been obtained. The important results which have come out of the present study are summarized below.

1) RESULTS ON CEN X-4:

- a) The most significant feature of these sources is that they erupt into sudden brightness, reach a maximum in a few days and then decay more or less exponentially over a period of months.

- b) The general behaviour of such sources is quite comparable to that of optical novae. Short period fluctuations are found to be superimposed on the smooth decay profile as in the case of optical novae. Similarly, the X-ray novae also show a definitive relationship between their peak emission and their decay time, the higher the intensity at the peak the lower is the decay time.
- c) The energy released in the X-ray region during these explosions is very high, usually comparable or more than the emission from the strongest X-ray source Sco X-1 ($\approx 2 \times 10^{-7}$ ergs.cm⁻².sec⁻¹) in the 2-20 keV energy band.
- d) All the sources of this type seem to exhibit basically an exponential spectrum with a temperature of $\approx 10^7$ °K corresponding to the peak of their intensity.

2. RESULTS ON NOR X-2:

- a) The flux in the X-ray band of 2-18 keV follows an exponential spectrum having a plasma temperature of $kT = 5.25$ keV corresponding to $T = 6 \times 10^7$ °K. The flux received in the 2-10 keV energy range is $\approx 1.75 \times 10^{-8}$ ergs.cm⁻².sec⁻¹.

b) The source spectrum as well as the intensity show large variability whereas the X-ray flux changes by factors as large as 6, the temperature of the emitting region in the source derived under the assumption of an exponential spectrum also shows variations from $kT = 4 \text{ keV}$ to $kT = 11 \text{ keV}$.

The study on background cosmic X-rays was made during two rocket flights in the energy range 2-18 keV. The cosmic background has been evaluated for the first time using earth as the occulting body. The spectrum derived in the 2-18 keV range from the present measurement is found to obey a power law spectrum with an index of $\alpha \approx 1.73 \pm .15$ having an average integrated flux of $\approx 10^{-8} \text{ ergs.cm}^{-2}.\text{sec}^{-1}.\text{sr}^{-1}$ in the 2-10 keV range. The results have indicated the effectiveness of the method using earth as a shutter, for deriving the diffuse background flux particularly in the energy band 2-30 keV and at low latitudes. With larger area counters in conjunction with secondary background rejection techniques such as the veto counters and pulse shape discrimination, this method can be very powerful tool for obtaining an accurate estimation of the diffuse cosmic X-ray background spectrum.

The balloon borne observations have been conducted mainly to study binary stars Cyg X-1 and Her X-1 in the hard X-ray region. The experiments conducted by the author provided the first evidence for the emission of the Her X-1 source at energies $> 40 \text{ keV}$ during ON state. Subsequently the same source was also monitored during the OFF state. The main results obtained by the author are summarized below.

1) RESULTS ON HER X-1:

- a) The spectrum of the source above 20 keV obeys a power law with a spectral index of $\alpha \approx -2.05 \pm .33$. The observations clearly show that the spectrum in this range ($20 < E < 100$ keV) steepens considerably compared to the spectrum observed below 20 keV ($\alpha \approx -1.0$). The average integrated flux of X-rays in the energy range 20-100 keV observed during the ON state is $\approx 2.77 \times 10^{-10}$ ergs.cm⁻².sec⁻¹.
- b) The present results along with the other observations show that the emission in the hard X-ray region also fluctuates considerably depending on the phase of 1.7 day orbital period as well as the epoch in the ON state of 35 day period.
- c) No emission during the OFF state of the source was detected. The upper limits derived were $\leq 1.44 \times 10^{-10}$ ergs.cm⁻².sec⁻¹. Thus the intensity in the ON state is atleast a factor of ~ 2 greater than its intensity in the OFF state.
- d) The arguments presented in the main body of the thesis show that the X-ray emitting source in Her X-1 should be a neutron star with its magnetic field axis not coinciding with the rotational axis and neutron star being a member of a close binary system.

2. RESULTS ON CYG X-1:

- a) The observations indicate that the source has two distinct levels of emission one corresponding to the 'quiet' condition and the other to the 'flare' condition.
- b) During the quiet condition the spectrum of the source can be fitted with a power law of index $\alpha \approx -1.9$ with an average integrated intensity in 20-100 keV amounting to $\approx 1.8 \times 10^{-8} \text{ erg.cm}^{-2}.\text{sec}^{-1}$. Even though the spectral behaviour seems to be almost same over long periods of time, the level of intensity of emission shows considerable long term variation by factors as large as ≈ 4 .
- c) During the flaring condition, the flux from the source is enhanced by factors of ~ 2.0 for a short duration of time (~ 10 mts) after which the level returns back to the pre-flare condition. The spectrum of the source during the flare hardens considerably and can be fitted with a power law spectrum having an index of $\alpha = -1.0$ with average integrated intensity of $\approx 2.86 \times 10^{-8} \text{ ergs.cm}^{-2}.\text{sec}^{-1}$ in 20-100 keV range.
- d) The results of present flight which is substantiated by subsequent observations of other experimenters show that the flaring occurs for $\sim 10\%$ of the observation time usually coincident with the maximum

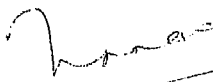
emission of light during its binary cycle. Similarly, the enhancement of flux during the flare in the higher energy channels seems to precede the enhancement of the lower energy channels by as much as 5 minutes.

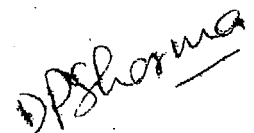
- e) The arguments presented in the thesis show that the X-ray emission of this source is due to accretion of matter on to a black hole from its binary companion in a close binary system.

Recently it has become evident from the work carried out at PRL and elsewhere that ground based ionospheric techniques can be very useful to monitor the presence of X-ray stars. The main observations are centered on Sco X-1 and Tau X-1 whose effect on enhancing the ionization in the night time D-region has been unambiguously identified. In the present thesis we evaluate the importance of the potentiality of the method both from theoretical and from experimental point of view. In addition, the thesis also provides evidence to establish the nova like character of one of the X-ray stars for which (Cet X-2) very meagre observational data is available. Finally the possible effects of the recently discovered gamma ray bursts on the night time D-region of the ionosphere and their possible detection has been critically discussed. The most important results obtained by the author on this topic are summarized below:

- a) Evidence is quite strong both from observational and theoretical standpoint for the detection of ionospheric effect due to strong celestial X-ray sources. Presently available evidence shows that the contribution to night time ionization of equatorial D-region ionosphere from cosmic X-rays, cosmic rays and $\text{Ly}\alpha$ are comparable with each other. There is also reasonable agreement between the theoretically expected nature of the effect and the experimental observations of VLF propagation.
- b) The effect of these sources persists for about 2-3 hours on either side of the time corresponding to the peak effect, the extent of the spread depending upon the declination of the source. The investigation shows that the ionosphere behaves as a X-ray telescope with a large opening angle so far as the transit of celestial sources is concerned.
- c) In general, since the contribution from $\text{Ly}\alpha$ can become significant during disturbed periods, the effect of celestial X-ray sources should be more frequently observed during solar quiet periods.
- d) On an average basis, it should be possible to study systematic long term variations of the intensity of strong X-ray sources, in the time scales of a few months to a few years, using the data on VLF propagation.

- e) There now exists a real possibility for the detection of such rare celestial events as flaring X-ray stars or super novae through their transient ionospheric effects using ground based VLF observations.
- f) Owing to the fact that NO (Nitric Oxide) is very important minor constituent at D-region altitudes for deciding the ambient electron density, accurate knowledge of its altitude ion-concentration profile is very vital. The present work shows that the detectability of X-ray sources implies a concentration of NO atleast a factor of 7-10 lower than that determined by direct experiments.


(U.R. RAO)
Professor-in-Charge


(D.P. SHARMA)

PUBLICATIONS

1. X-ray observations of Cen XR-4 and Nor XR-2

U.R. Rao, E.V. Chitnis, D.P. Sharma, A.S. Prakasarao and U.B. Jayanthi. Nature 229 (1971) 248.

2. Diffuse X-ray background measurements in the energy range 2-18 keV.

A.S. Prakasarao, D.P. Sharma, U.B. Jayanthi and U.R. Rao. Astrophys. and Space Sc. 10 (1971) 150.

3. Possibility of continuous monitoring of celestial X-ray sources through their effects in the nocturnal D-region ionosphere.

D.P. Sharma, A.K. Jain, S.C. Chakravarty, K. Kasturirangan K.R. Ramanathan and U.R. Rao. Astrophys. and Space Sc. 17 (1972) 409.

4. Balloon born observations of celestial X-rays: Part I

A.K. Jain, U.B. Jayanthi, D.P. Sharma, K. Kasturirangan and U.R. Rao. Proc. 13th Int. Conf. on Cosmic Rays, Denver, U.S.A. (August 17 - August 31, 1973).

5. Balloon born observations of celestial X-rays: Part II

D.P. Sharma, A.K. Jain, U.B. Jayanthi, K. Kasturirangan, and U.R. Rao. Proc. 13th Int. Conf. on Cosmic Rays, Denver, U.S.A. (August 17 - August 31, 1973).

6. Hard X-ray emissions from Her X-1

D.P. Sharma, A.K. Jain, K. Kasturirangan, U.B. Jayanthi and U.R. Rao. Nature Phys. Sc. 246 (1973) 107.

7. Detection of celestial gamma ray burst through ground based techniques (Nature, in press, 1974).

K. Kasturirangan, U.R. Rao, D.P. Sharma, S.C. Chakravarty and R.G. Rastogi.

8. On the detection of X-rays from celestial sources through their ionization of the terrestrial atmosphere.

U.R. Rao, D.P. Sharma, A.K. Jain, S.C. Chakravarty, K. Kasturirangan, and K.R. Ramanathan (Published in

A C K N O W L E D G E M E N T S

I am highly indebted to Prof.U.R. Rao who initiated me to Scientific research and introduced me to the subject of X-ray astronomy. I would like to express my sincere gratitude to him for his constant encouragement, guidance and supervision in all the phases of the work.

Author is very grateful to Dr.K. Kasturirangan for going through the thesis critically and for many useful suggestions and encouragement during the various stages of work. The author also thanks Prof.L.E. Peterson for discussions on various topics.

Some of the experimental work was done in association with my colleagues Drs.A.S. Prakasarao, U.B. Jayanthi and Mr.A.K. Jain. Their co-operation and encouragement at various stages of work are gratefully acknowledged.

The technical support for the work presented here was provided by Messers K.S.V. Seshadri, N.J.N. Sarma and B.L. Agrawal who all deserve my thanks. I am grateful to Messers J.S. Sidhu, S.K. Banerjee, D.P. Devgan, K.S.B. Manian, and K.A. Panchal for the help in the construction of various electronic circuits and systems at different stages of payload fabrication and its launching. The computational help provided by Mrs.H.S. Shah, is gratefully acknowledged.

Thanks are also due to Mr.A.C. Dave for the excellent drafting of the diagrams for the thesis and to Mr.M.V. Joseph for typing the final manuscript of the thesis.

The co-operation shown by the TERLS staff in launching the rocket, under the guidance of Mr.H.G.S. Murthy is gratefully acknowledged. The balloons were launched under the leadership of Mr.R.T. Redkar of TIFR Balloon Facility who along with his team deserve thanks.

The research work was done using the funds from the Department of Atomic Energy and Department of Space, Government of India.

Finally, I express my sincere gratitude to my wife and parents for constant encouragements throughout the period of this work.

DP Sharma
(D. P. SHARMA)

C O N T E N T S

CHAPTER I

1.1.	INTRODUCTION	1.1
1.2.	The present status of X-ray astronomy	1.3
1.2.1	General aspects	1.3
1.3	Galactic sources	1.6
1.3.1	General remarks	1.6
1.3.2	Periodic variable sources	1.10
1.3.3	Binary systems	1.11
1.3.4	Her X-1	1.16
1.3.5	Cyg X-1	1.25
1.4.	Irregular variables	1.34
1.4.1	Flaring X-ray sources	1.35
1.4.2	Fluctuating X-ray sources	1.37
1.5	X-ray background	1.39
1.5.1	Introduction	1.39
1.5.2	Observational results	1.42
1.6	Models for diffuse X-ray background	1.49
1.6.1	Models not involving cosmology	1.49
1.6.2	Models involving cosmology	1.51

CHAPTER II

	The rocket experiment	2.1
2.1	Brief description of the rocket payload	2.1
2.2.1	Results and discussion	2.6
2.2.2	Cen X-4	2.10
2.2.3	Cen X-1	2.17
2.2.4	Cen X-2	2.18

2.2.5	Discussion	2.20
2.3	Source in Norma/Lupus constellation	2.32
2.3.1	Discussion	2.35
2.4	Derivation of background spectrum	2.40
CHAPTER III		
	Balloon experiment	
3.1	Introduction	3.1
3.2	X-ray telescope	3.1
3.2.1	The detector	3.1
3.3	Orientation system and magnetic sensors	3.6
3.4	Tracking the X-ray source	3.9
3.5	Electronics and associated instrumentation	3.9
3.6	Inflight calibration and altitude measurements	3.12
3.7	The details of the balloon flights	3.14
3.8	Observations on binary X-tars	3.17
	A. Her X-1	
3.8.1	Programme of observation	3.17
3.8.2	Results	3.20
3.8.2a	Observation during ON state	3.20
3.8.2b	Observation in OFF state	3.22
3.8.2c	Comparison with the results of other experimenters	3.24
3.8.3	Discussion	3.26
3.8.3a	Brief introduction	3.26
3.8.3b	Discussion on source models	3.27
3.8.4	The 35 day period of Her X-1	3.31
	B. Cyg X-1	
3.9.1	Observational programme	3.33

3.9.2	Results	3.35
3.9.2a	Observations of Cyg X-1 during first flight	3.35
3.9.2b	The results of second flight	3.41
3.9.2c	Contribution due to Cyg X-3	3.43
3.9.3	Discussion	3.44
3.9.3a	Flare phenomena in Cyg X-1	3.44
3.9.3b	Time variation of flux from Cyg X-1	3.49
3.9.4	Models for Cyg X-1	3.53

CHAPTER IV

Monitoring of X-tars through ionosphere

4.1	Introduction	4.1
4.2	Ionization due to celestial X-ray sources	4.5
4.3	Ionization due to other sources in the night time D-region	4.9
4.4	Ionization due to the diffuse cosmic X-rays	4.11
4.5	Ionization due to galactic cosmic rays	4.11
4.6	Ionization from night time $Ly\alpha$	4.12
4.6.1	Night time $Ly\alpha$	4.12
4.6.2	Molecular oxygen density	4.13
4.6.3	Nitric oxide density	4.14
4.6.4	Ionization calculations	4.19
4.7	Ionization due to $Ly\alpha$	4.20
4.8	Ionization due to meteors	4.20
4.9	The electron density profiles	4.20
4.10	164 KHz VLF observations at Ahmedabad	4.27
4.11	Detection of flare stars	4.33
4.12	Detection of gamma ray bursts	4.38

Appendix A 1	A 1.1
Appendix A 2	A 2.1
A 2.1 Altitude determination of rocket	A 2.1
A 2.2 Magnetometer data reduction	A 2.7
A 2.3 Solar sensor data reduction	A 2.12
Appendix A 3	
A 3.1a Efficiency, resolution and escape X-rays of the detector	A 3.1
A 3.1b Escape X-rays correction	A 3.2
A 3.2 Exposure efficiency of the detector	A 3.5
A 3.3 Separation of source from background	A 3.7
A 3.4 Spectrum folding	A 3.8

References

CHAPTER - I

1.1 INTRODUCTION:

The electromagnetic and particle radiations reaching the Earth from outside the solar system carry with them the signature of various dynamical processes that characterize the universe. In the last two decades, with the advances in the space technology, it has become possible to deploy detectors outside the deleterious effects of the atmosphere thereby throwing open, the entire spectrum of the electromagnetic and particle radiation to direct observations. This in turn has opened up completely new vistas in the field of astronomy and astrophysics, revealing celestial phenomena hitherto unsuspected or explored only through theoretical means.

The discovery of strong and nearly exclusive emitter of X-rays in the constellation Scorpius in 1962 by Giacconi et al (1962) which haralded the beginning of astronomy is one such remarkable example, that revealed the existence of high energy processes in the universe. For the first time, the observation in the X-ray end of the electromagnetic spectrum revealed the presence of dense magnetic fields ($\approx 10^{12}$ gauss), high temperatures ($\approx 10^9$ °K) and high energy electrons (≈ 10 GeV) in localized and extended regions both inside and outside our galaxy. Detailed investigations using rocket, balloon and satellite borne detectors have since then revealed the existence of a large number of such objects, both discrete and extended, besides a diffuse

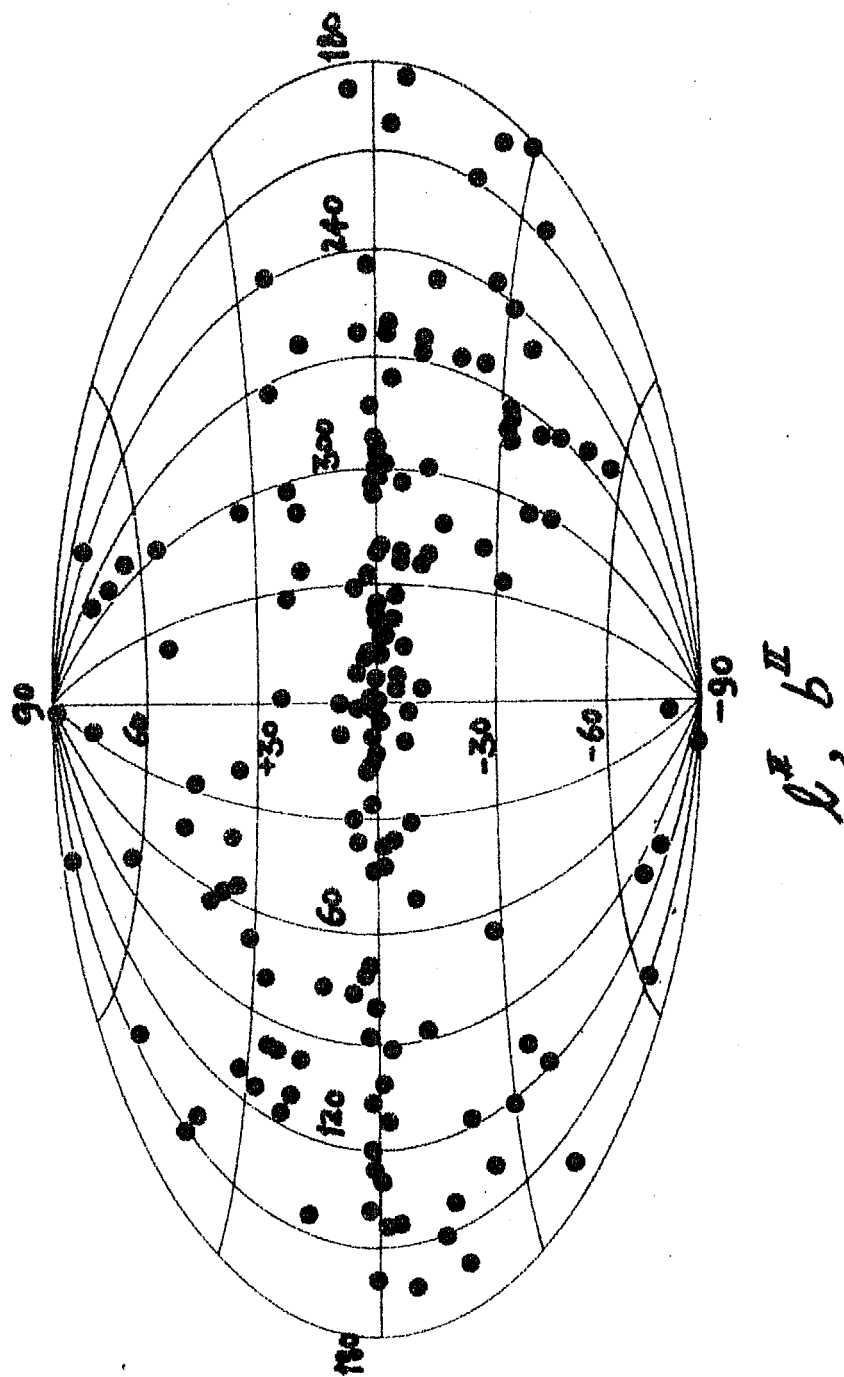


FIG: 1.2 THE X-RAY SOURCES DISCOVERED SO FAR (DECEMBER 1973) SHOWN IN GALACTIC COORDINATES.

X-ray background that is nearly isotropic over the sky.

One striking aspect of these X-ray sources is the enormous amount of power emitted at X-ray wave lengths, typically in the range $10^{36} - 10^{38}$ ergs. sec^{-1} for galactic sources. For example, Sco X-1 radiates 2×10^{36} ergs. sec^{-1} in the 1-10 keV range which is $\approx 10^3$ times the energy radiated in the optical band. Further, the X-ray luminosity of Sco X-1 is $\approx 2 \times 10^3$ times the optical luminosity and $\approx 10^{10}$ times the X-ray luminosity of the quiet sun. The fact that many of these sources are not identified with optical or radio objects means that the X-ray emission is the dominant form of energy conversion in these objects.

The X-ray background is primarily of extragalactic origin because of its high degree of isotropy with little enhancement in the direction of galactic plane and has an energy flux of $\approx 10^{-8}$ ergs. $\text{cm}^{-2}.\text{sec}^{-1}$ in 2-10 keV region (Prakasarao et al 1971, Schwartz and Gursky 1973).

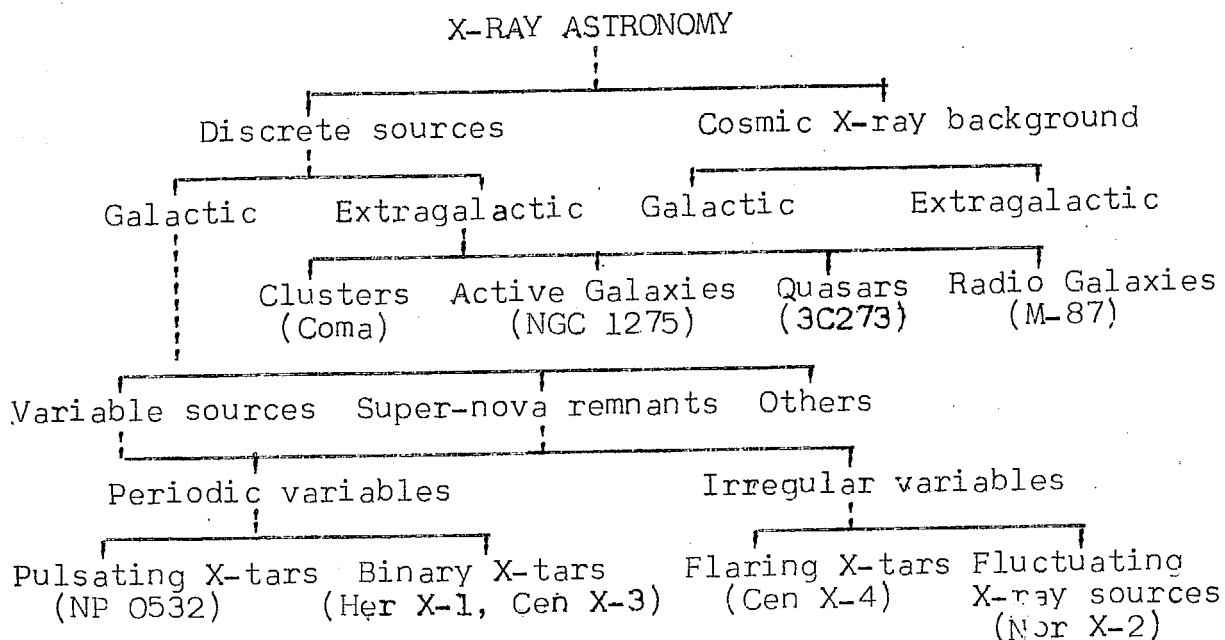
1.2. THE PRESENT STATUS OF X-RAY ASTRONOMY:

1.2.1 GENERAL ASPECTS:

About 170 sources have been discovered so far in the 2-20 keV energy interval, bulk of which is through observations by Uhuru, the first satellite for exclusive investigation in the X-ray astronomy (Giacconi et al 1971 1973a; Seward 1970). The X-ray sky as seen by Uhuru with other known sources is shown in figure 1.1 and is prepared from the

latest available data (Giacconi et al 1973a, Seward 1970).

The sources discovered so far can be broadly categorised as given in the following chart.



As shown in the chart, the discrete sources can be broadly classified under two categories galactic and extragalactic. Nearly half of the sources discovered so far are interpreted to be galactic, because of their closeness to the galactic plane ($b^{\text{II}} \leq 20^\circ$) by their concentration in Sgr-Sco region and from their apparent association with the spiral arms particularly those in Cygnus, Serpens and Centaurus (Giacconi et al 1973a).

Identification of extragalactic sources is observationally based on their direct association with known external galaxies as well as by their distribution in

galactic coordinates. Broadly, they fall in the category of extragalactic clusters, active galaxies, quasars and radio galaxies. Prominent active galaxies like NGC 5128 and NGC 1275 have been identified as X-ray sources (Fritz et al 1971, Giacconi et al 1973a) with emission originating most likely from a very restricted region in the galactic nucleus (Forman et al 1972b, Tucker et al 1972, Lampton et al 1971, 72).

X-rays have also been detected from galactic clusters such as Virgo Cluster, Perseus Cluster and Coma Cluster where the extent of X-ray emission is beyond the confines of a single galaxy (Kellogg et al 1973). Only one quasar that is, 3C 273 has been found to be an emitter of X-rays (Byram et al 1966, Giacconi et al 1973a). Some of the galaxies like NGC 1275, discovered so far are essentially X-ray galaxies as they are found (Giacconi et al 1973a) to emit X-rays with a power that is roughly an order of magnitude higher than that in the optical region. The intensity of emission varies from 10^{40} ergs.sec⁻¹ for a typical extragalactic like SMC X-1 to 10^{44} ergs.sec⁻¹ for sources such as 3C 273, the most distant X-ray source (Hoover et al 1972).

As the present thesis deals with only certain classes of galactic sources no further reference to extragalactic sources will be made in this chapter.

The diffuse background above 1 keV is of extragalactic origin because of its high degree of isotropy. Of the two principal hypotheses with regard to its origin viz.

superposition of a large number of extragalactic sources or inverse compton radiation by fast electrons colliding with 3°K microwave radiation (Silk 1970), the former is gaining more favour recently because of the discovery of a large number of discrete extragalactic sources that could contribute a significant portion of the background.

1.3. GALACTIC SOURCES:

1.3.1. GENERAL REMARKS:

With the discovery of a large number of galactic X-ray sources their distribution in the galaxy can be studied. A typical log N-logS plot for these objects (see figure 1.2, Matilsky et al 1973) similar to that in radio astronomy leads to a slope of ≈ 0.5 , a reasonable value should the sources belong to our galaxy and clustered along the spiral arms. However, for comparatively stronger sources, as the figure shows the slope obtained is ≈ 1.5 typical of intermediate populations II or disk population objects (Blaauw 1965) and would be simply a fortuitous result of the intrinsic range of luminosities for these sources ($10^{38} \geq L_X \leq 10^{39}$ in the range from 2-10 keV). Primarily it is possible to identify two kinds of populations for the galactic sources; a small number of intense sources in the central region of our galaxy out to typical distance of $|Z| = 650$ pc and a large number dispersed through the galaxy out to $|Z| = 200$ pc.

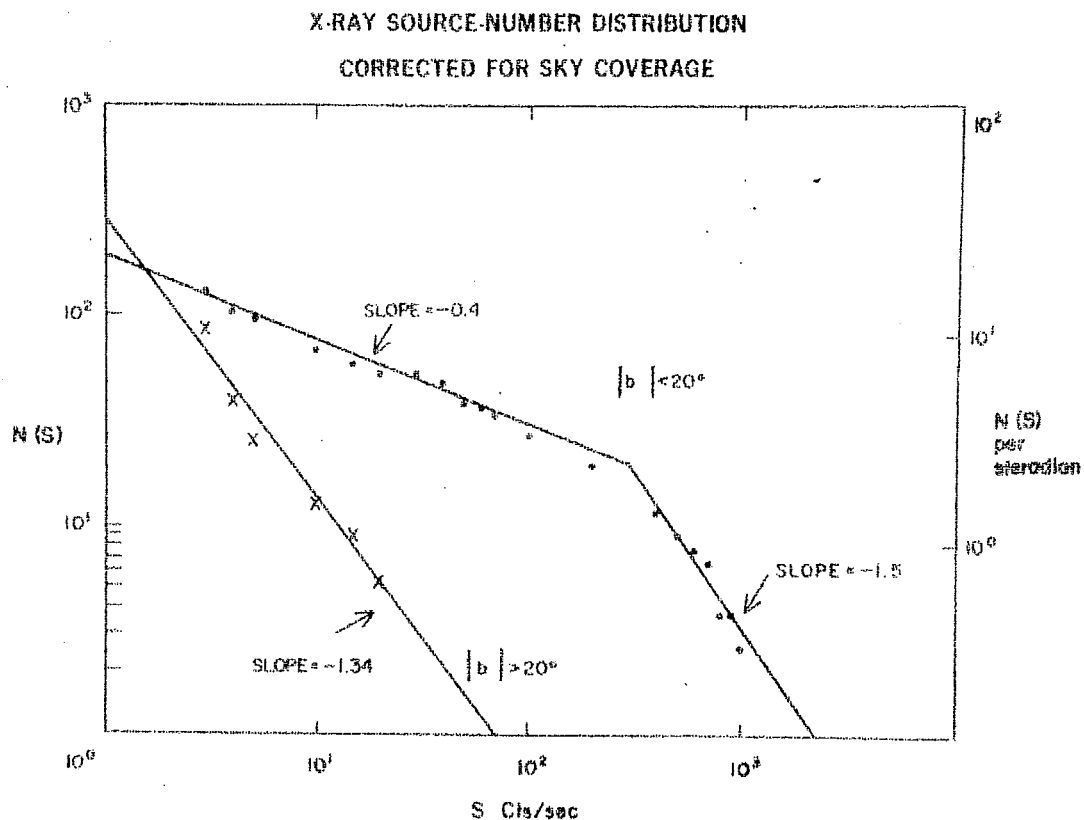


FIG.1.2. $N(S)$, THE NUMBER OF SOURCES GREATER THAN OR EQUAL TO INTENSITY S IN THE 2-6 KEV ENERGY RANGE IS PLOTTED AS A FUNCTION OF S . THE LOW LATITUDE SOURCES ($|b| \leq 20^\circ$) ARE SHOWN AS DOTS, THE HIGH LATITUDE SOURCES AS CROSSES. THE BEST FIT LINES ARE MARKED. THE RIGHT HAND SIDE SCALE APPLIES ONLY TO THE $|b| \geq 20^\circ$ SOURCES (MATILSKY ET AL 1973).

The galactic sources in general can be classified into supernova remnants, binary systems, and those not covered by either of these two, based on their physical properties.

Some of the well known supernova remnants have been found to be X-ray emitters. The known supernova remnants (SNRS) about 15 in number, range in their age from 250 years to 50,000 years. The Crab-nebula, Cassiopeia A and Tycho supernovae are those whose age is less than thousand years. Others such as Cygnus loop, Vela X and Puppis A are estimated to be more than 10^4 years and have been found to emit (Burginyon 72) predominantly in the soft X-ray region (Hoover et al 1972). Considering that supernova remnant sources in general emit in the radio region, study of X-rays from these objects therefore could lead to estimates of their intrinsic luminosity as the distance of these sources can also be independently established through radio observations. Further, since the presence of synchrotron process is well established in many of the supernova remnants, simultaneous radio and X-ray measurements are in principle capable of giving a very thorough insight into the acceleration processes that are taking place in such sources. The detection of pulsar effects in two of the well known sources viz. Crab-nebula and Vela both in the X-ray and radio regions have provided evidence for the presence of compact objects in them, the rotational energy from which could provide the necessary continual supply of energy to keep these sources radiating (Gold 1968).

VARIABLE SOURCES

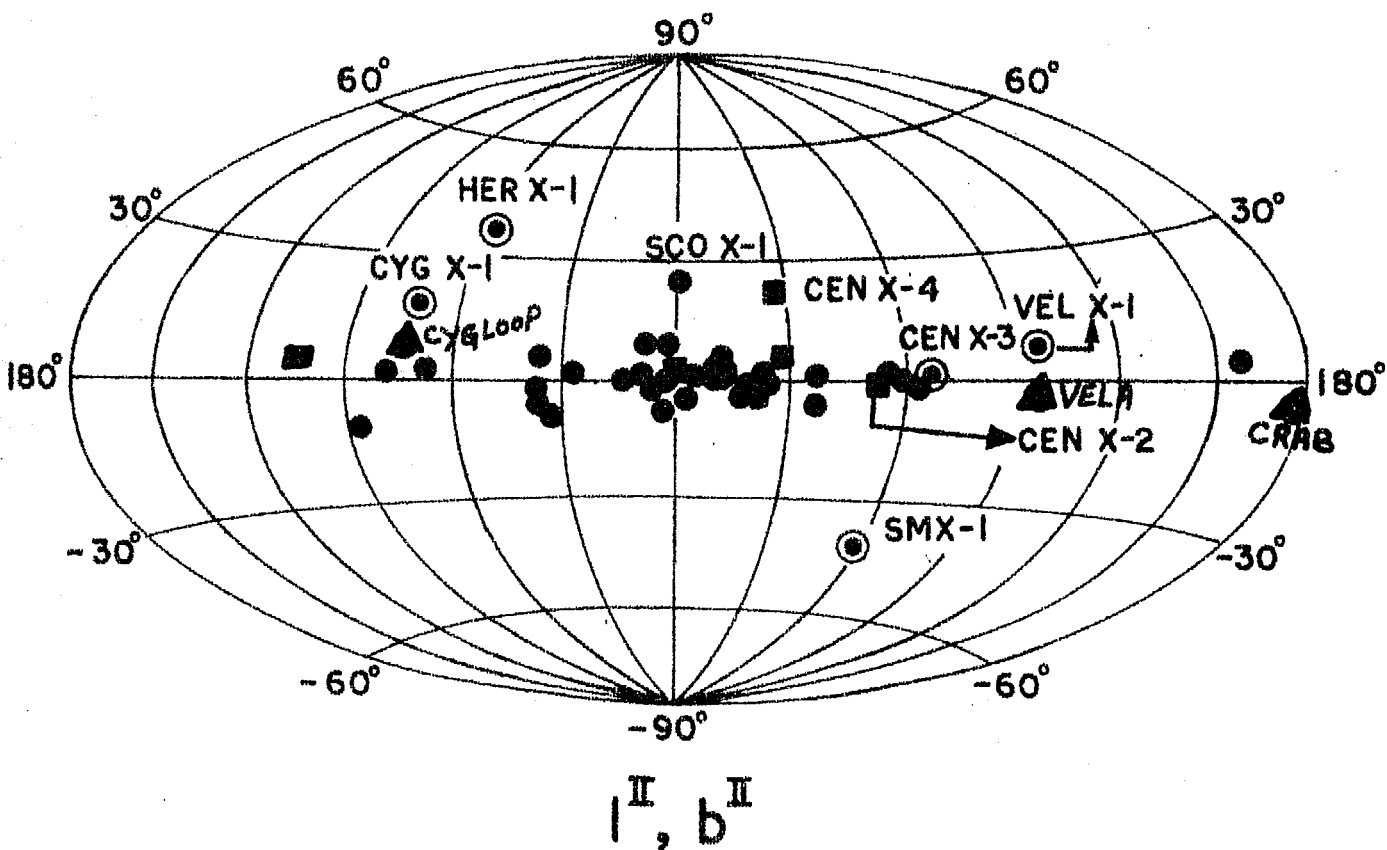


FIG: 1.3 THE VARIABLE SOURCE DISTRIBUTION IN GLACTIC COORDINATES. ■ FLARE STARS, ⊙ BINARY SOURCES
 ▲ PULSARS, ● irregular.

1.3.2. PERIODIC VARIABLE SOURCES:

Out of the total X-ray sources discovered so far, about 40 sources are found to be variable on time scales of a few seconds to days to months and years. Among these forty sources (see figure 1.3), about 20 show periodic variations. The study of variable sources whose time profiles carry the unmistakable signature of the physical processes is vital to the understanding of a variety of astrophysical phenomena. An interesting aspect of the investigations of the variable sources stems from the fact that the time scales of variations are in general representative of the size of the emitting region. As an example in the case of pulsars, the fact that the time structure in the pulsations is reproduced in successive pulses suggests that the radiation comes from a single source. Assuming the maximum possible rate of information transfer i.e. the speed of light, the upper limit of the diameter of the emitting region should be ≈ 30 kms if the line width is of the order of 100 microsecond. On the other hand if the source is of an extended nature, the time scales of observed variations are correspondingly large.

Many of the galactic X-ray sources are now known to be members of the binary systems, where the X-ray generation is explained in terms of mass transfer between the primary star on to the X-ray star. The time duration of X-ray eclipse in such systems can provide an upper limit of the size of the photosphere of the larger star.

The most important aspect of the study of the time variations relates to the simultaneous observations in different bands of the electromagnetic spectrum. The different modes of radiation mechanisms responsible for their production and transfer as well as the particle densities and magnetic field configurations at different distances from the stellar surface are important aspects of such a study. Thus the time variation studies provide vital information on the physical nature of the source and the matter surrounding them. Further, since the positional coincidence with optical or radio counterparts cannot provide an unambiguous identification of the X-ray source, especially when there is no a priori basis for such coincidences, simultaneous observations of distinctive signatures in the X-ray, radio and optical time profiles helps to a large extent in clarifying the situation.

1.3.3. BINARY SYSTEMS:

Of the periodic variable sources discovered so far, at least seven are known to be members of binary systems. In some of the X-ray binaries such as Her X-1, the X-ray emitting companion could also be a pulsating compact object such as a neutron star, the pulsation periodicity corresponding to the rotational motion of the neutron star. Under these conditions the binary nature of the system can be conclusively established through the measurement of Doppler shift of the pulsation period during the orbital motion of the X-ray star around

1-11a

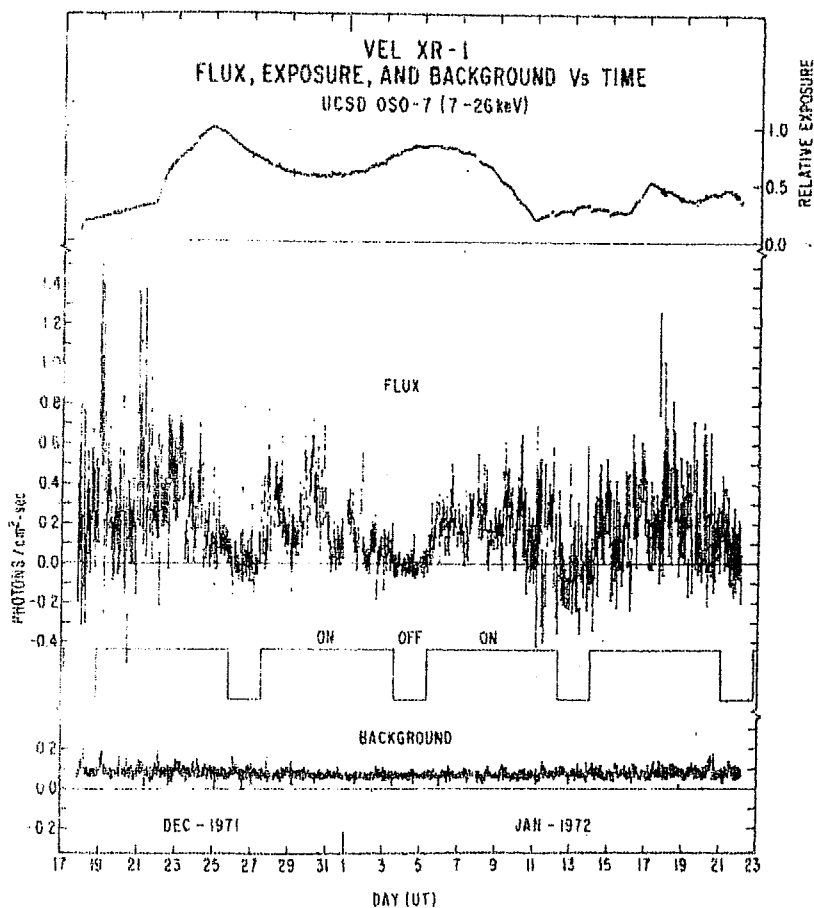


FIG. 1.4 - THE FIGURE SHOWS THE
OBSERVED COUNTING RATE OF A
X-RAY BINARY VELA XR-1
BY OSO-7 EXPERIMENT OF UCSD.
(ULMER ET AL 1972b)

the main companion (Tananbaum et al 1972a). The longer time periodicity in intensity corresponding to the orbital period can be separately measured and the phase of the eclipse correlated with the extent of Doppler shift to derive a limited picture of the X-ray binary system.

Whereas all the binary systems behave essentially as eclipsing binaries at the X-ray wavelengths, at the optical wavelengths they do show considerable differences. Sources such as Her X-1, Vala X-1, Cen X-3 etc. behave as eclipsing binaries even in the optical region due to the occultation of the bigger star by the compact X-ray companion. On the other hand sources such as Cyg X-1 and 3 U 1700-47 are only spectroscopic binaries where the optical intensity of the star does not show any variation, the evidence of the binary motion coming from the radial velocity measurements. The light curve of a typical X-ray binary observed is shown in figure 1.4.

Table 1.1 presents summary of the available data on the known binary X-ray sources. Based on this it is possible to draw a few general conclusions regarding emission of X-rays from these binary systems (Schreier et al 1972b, Jones et al 1973a, Ulmer et al 1972, 1973, Canizares 1973, Krzeminski, 1973 etc.),

(1): In addition to the intensity variations arising from the orbital motion, all the binary X-ray sources show short duration periodic or non-periodic pulsations that are suggestive of emission coming from highly localized regions.

Table 1.1 - Binary X-ray sources

Source	Binary period (days)	Short term variability	Long term variability	Power law energy index (2-20keV)	Low energy cut off (keV)	Optical candidate	Radio candidate	Distance \sim kpc	Peak X-ray luminosity (2-10 keV) ergs.sec ⁻¹
Cyg X-3	.19960 \pm .0007 (=4.8hrs)	Short duration non-periodic pulsations are observed. Freq. is constant 1 part in 1500 over 7 months	--	0.0-1.2	--	--	A flaring strong radio source of strength $> 20\text{fu}$	10.4	10^{37}
Her X-1	1.700167 \pm .000006	1.23782 second pulsations which decrease by 4.5 microsecond in 6 months	Extended pulsations with average cycle of ~ 35 days of which it remains ON for 11-12 days	-1.3-0.2	1.5-3.2	Hz Her $m_V = 13$	None	5.8	1×10^{37}
Cen X-3	2.08712 \pm .00004	4.84 second pulsations which decrease by ~ 200 microsecond in 6 months	Extended pulsations of non-periodic nature	-0.4-0.6	1.5-4.2	WRA795 $m_V = 11.4$	--	10	3.5×10^{37}

contd.....

:2:

Source	Binary period (days)	Short term variability	Long term variability	Power law energy index (2-20 keV)	Low energy cut-off (keV)	Optical candidate	Radio candidate	Distance kpc	Peak X-ray luminosity (2-10 keV) ergs.sec ⁻¹
3U1700-37	3.41 ± .002	Non-periodic pulsations as short as 0.1 sec	No extended lows	-0.4-1.0	2.1-5.1	HD153919 m _V =6.56	--	3.7	3 × 10 ³⁶
Cyg X-1	5.600 ± .003 (only optical)	Non-periodic pulsations as short as 50 m sec, also shows flares at high energy having durations of few minutes	Single low energy transition	0.0-1.2	1.5	HD226868 m _V =9	Weak radio source of average strength ~.015fu which also shows short term fluctuations of factors as large as ~3	2.5	1.7 × 10 ³⁷ before transition and 3 × 10 ³⁶ after
Vela X-1	8.96 ± .05	Non-periodic pulsations on time scale of seconds	No extended lows	-0.2-0.7	2.5-4.4	HD7781 m _V =6.87	--	1.3	4 × 10 ³⁶
SMC X-1 only extra-galactic binary	3.8927 ± .001	Non-periodic pulsations on time scales of minutes	Extended lows	0.0-0.3	1.5-3.0	SK 160 m _V =13	--	61	3 × 10 ³⁸

(2):-

All the binary X-ray sources listed in the table show high luminosity. Some of the most powerful galactic sources come under this category.

(3):-

All these sources have X-ray spectra that could be approximated by a power law and the spectral shape below 10 keV is almost flat (Power law energy index $\alpha \approx 0.0$). The spectral index seems to steepen considerably at energies above 20 keV.

(4):-

The X-ray spectra in all the cases show low energy turnover possibly due to the absorption of radiation by the mass present in the line of sight. Comparison of the column density derived from X-ray turnover with that derived from 21 cm radio data indicates the presence of matter around the X-ray emitter. This is further confirmed by the dependence of the extent of low energy cut-off on the phase of the eclipsing binary X-ray source.

(5):-

Most of the binary X-ray systems are also associated with the known optical binary systems.

In what follows, two prominent binary X-ray sources Her X-1 and Cyg X-1 are discussed in detail since they are of direct relevance to the investigations described in this thesis.

134.O. HER X-1:

This source, first detected by Uhuru observatory (Schreier et al 1972), has subsequently been studied by many workers (Tananbaum et al 1972a, Ulmer et al 1972, 1973a, Clark et al 1972, Giacconi et al 1973b, Doxsey et al 1973, McClintock et al 1974) mainly at energies below 20 keV. At energies above 20 keV there exist very few observations. In fact, the observations presented in the body of this thesis are the first high energy observations to be made on this star above 40 keV. The important properties of Her X-1 established through observations in the various regions of the electromagnetic spectrum are summarized below.

(1):-

The X-ray emission of Her X-1 shows a very prominent periodicity in the form of regular pulsations of duration 1.24 seconds. This periodicity is attributable to the rotation of the star. The 1.24 second pulses which seem to have a double peak structure have sharp fall and rise time ($\approx 20\%$ duty cycle) and show significant changes of shape on the time scale of hours. The two peaks have same maximum amplitude but markedly different widths (Doxsey et al 1973, Giacconi et al 1973b. The trailing edge of the second peak falls very quickly in 30-40 milliseconds with a minimum following immediately, about 60% of the source counts occur during the major double pulse corresponding to a phase $\sim 140^\circ$ of the pulse and at least 80% of the source power is

contained in the form of 1.24 second pulsations (Giacconi et al 1973b, Doxsey et al 1973, McClintock et al 1974).

(2):-

In addition to the 1.24 second period, the X-ray emission of Her X-1 also shows a distinct level of intensity variation having a period of 1.7 day. In other words the average intensity contained in the 1.24 second pulsations is further modulated over a variation in the average intensity having a period of ≈ 1.7 day (Tananbaum et al 1972a). The Doppler variations in the 1.24 second pulsation period indicate that this variation is due to the orbital motion of Her X-1, X-ray source going around its binary companion star resulting in the periodic eclipsing of the X-ray intensity. During this 1.7 day orbital period the X-rays are observed for about 1.46 days and the source remains in eclipse for ≈ 0.24 days (Giacconi et al 1973b, Tananbaum et al 1972a, Ulmer et al 1973a, McClintock et al 1974, Clark et al 1972).

(3):-

In addition to the 1.24 second pulsation and the 1.7 day orbital period the X-ray emission of Her X-1 also shows intensity variations over a period of ≈ 35 days whose origin is still obscure. During each 35 day period the X-ray emission is observed for 11-12 days which is referred to as the 'ON' state (Ulmer et al 1972, Giacconi et al 1973b) of the source. The source remains in the 'OFF' state for the rest of the 23 days when no significant X-ray emissions above 2 keV

have been detected so far. Although there have been some reports (Fabian et al 1973 a,b) of the detection of small amount of X-ray flux ($\approx 5-17 \times 10^{-10} \text{ erg cm}^{-2} \text{ sec}^{-1}$) in the 3-6 keV range during the 'OFF' state by instruments aboard the 'Copernicus' satellite, this emission appears to be very short lived (≈ 2 hours).

(4):-

The evidence seems to indicate that the onset of the 'ON' state bears some definite relationship to the phase of the 1.7 day cycle (Giacconi et al 1973b, McClintock et al 1974). Detailed observations from Uhuru and OSO-7 show that the turn on of the 'ON' state occurs when the phase of the 1.7 day orbital period lies between .22-.24 and .67-.70.

(5):-

An important result that has emerged out of the long term X-ray observations by Uhuru is that the time period of ^{sec.} the 1.24/pulsations decreases by ≈ 4.5 microseconds in about 6 months period (Giacconi et al 1973b). This result can be directly interpreted as due to the speeding up of the pulsar in the Her X-1 which is contrary to the normal slowing down behaviour of pulsars. The result clearly indicates that there must be significant amount of matter accreting on to the X-tar from its binary companion causing the observed perturbation in the rotational motion of the X-tar.

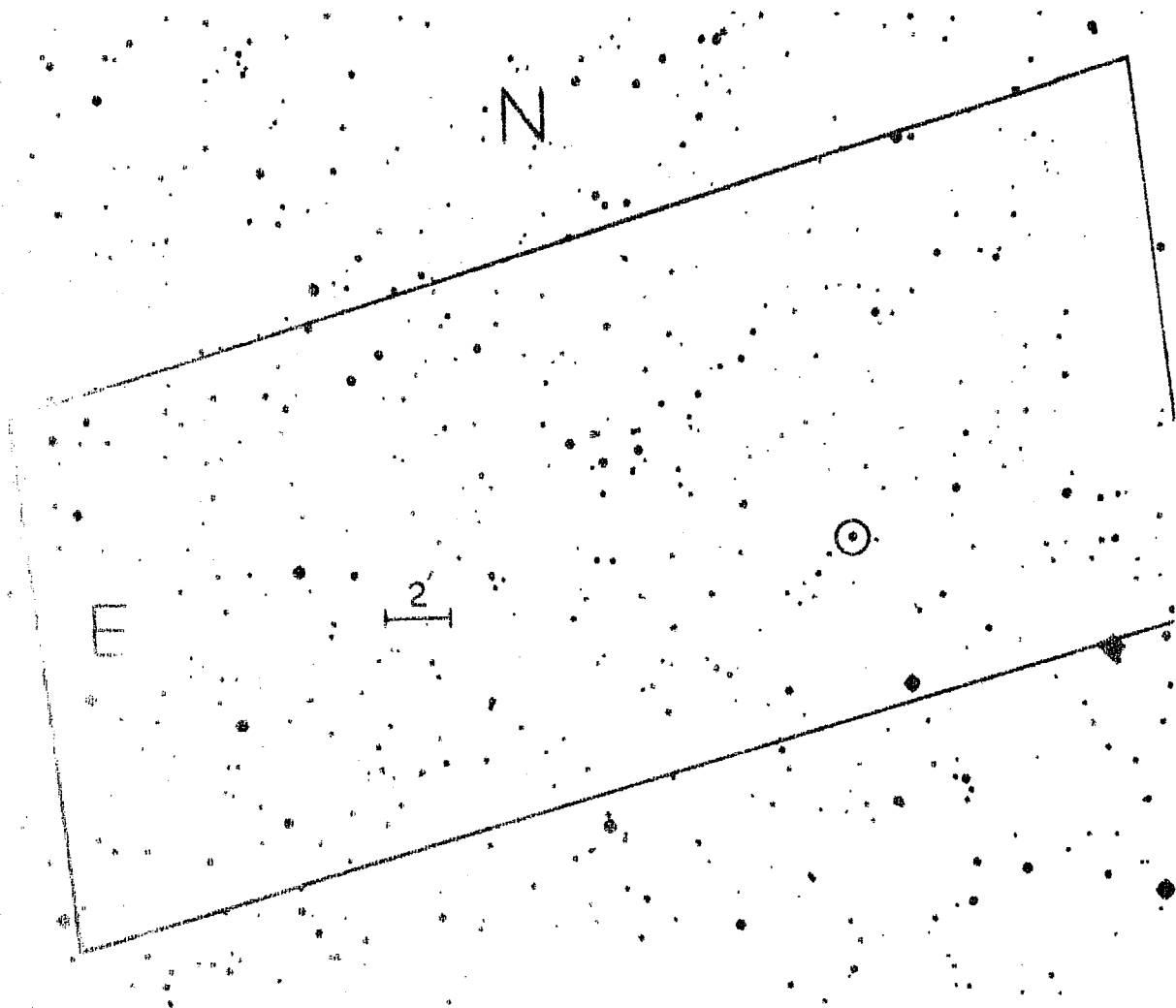


FIG. 1.5 - THE ENLARGEMENT OF A BLUE PALOMER SKY SURVEY PRINT CONTAINING HER X-1. THE CIRCLE SHOWS THE MIT POSITION AND PARALLELOGRAM SHOWS THE UHURU AND OSO-7 POSITIONS.

(6):-

At energies below 10 keV the observed spectrum is nearly flat, and can be represented with a power law having an index of $\alpha \approx 1.0$ (Giacconi et al 1973b, Clark et al 1972). The spectrum also shows low energy turn over around 2-4 keV depending on the phase of the orbital period. The luminosity in the 2-10 keV range is $\approx 10^{37}$ ergs.sec⁻¹ if the source distance is assumed to be ≈ 5.8 kpc (Jones et al 1973b), the same as for the optical counterpart Hz Hercules.

(7):-

The observations at high energies ($10 < E < 40$ keV) by the UCSD experiment aboard OSO-7 also show the 1.7 day periodicity (Ulmer et al 1972, 1973a) superposed over the 35 day cyclic variation. However, no significant pulsations at 1.24 second have been observed above 20 keV (Peterson, private communication). The spectrum in this energy range steepens considerably and can be represented by a power law with an index of $\alpha \approx -2.5$ as compared to $\alpha \approx -1.0$ observed at low energies (≤ 20 keV).

(8):-

Her X-1 has been identified with the binary system where the main star is a ≈ 13.5 magnitude star Hz Hercules (see figure 1.5, Liller 1972 and also Davidson et al 1972a, Doxsey et al 1973, Bahcall and Bahcall 1972, Forman et al 1972a, Jones et al 1973b etc.). Whereas the long term 35 day periodicity has not been reported in this region

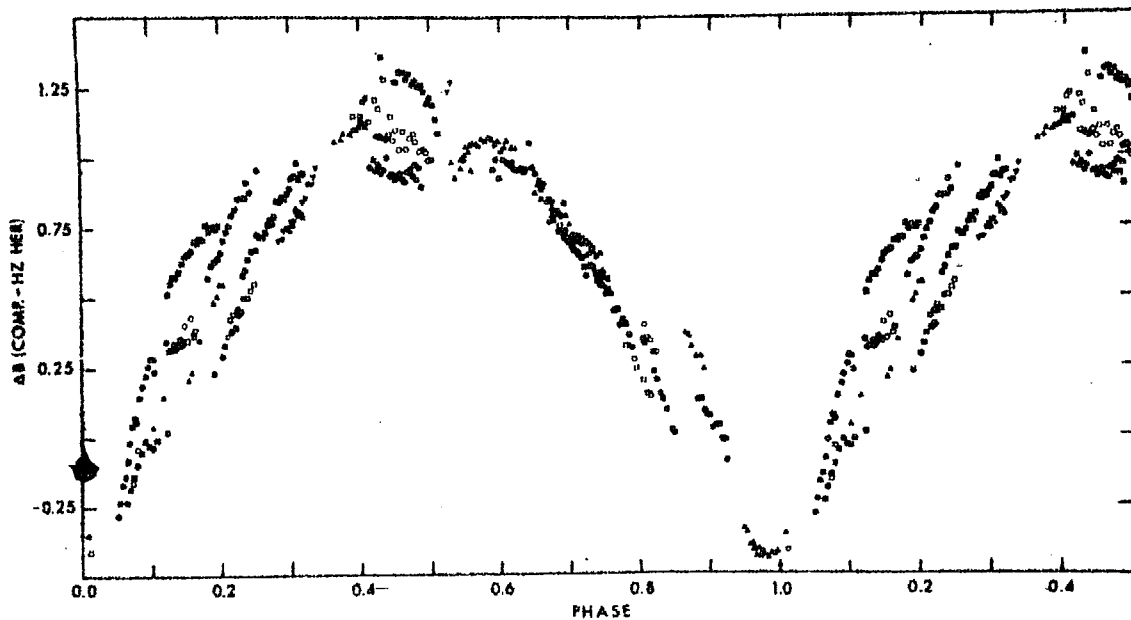


FIG.1.6 - THE FIGURE SHOWS THE LIGHT CURVE OF THE BINARY Hz HER WHICH HAS BEEN IDENTIFIED AS THE OPTICAL COUNTERPART OF HER X-1.
(PATRO & HILTNER 1973).

of the electromagnetic spectrum the 1.24 second and 1.7 day periods have been observed at optical wavelengths also.

(9):-

The 1.7 day light curve (see figure 1.6) has a broad minima which begins well before the X-ray eclipse (at least by $.2 \phi$, where ϕ represents the total phase; Davidson et al 1972a). At its peak intensity in the 1.7 day cycle, the star shows the greatest ultraviolet excess as indicated by $U-B = + 0.3$. In the optical region, where very long period observations exist, it has been verified that the optical period has remained constant at 1.70017 day within 2 parts in 10^5 since 1900 (Jones et al 1972b). Further, the star has also shown long period blackouts some times lasting over many years (see figure 1.7a,b; Jones et al 1972b).

(10):-

The 1.24 second pulsations at optical wavelengths are observed only when the X-ray source is in the 'ON' state (Cocke et al 1973) which indicates that the origin of 1.24 second pulsations observed even at optical wavelengths is related to the X-ray source. It is generally accepted that the X-ray emission from Her X-1 irradiates Hz Her through the thermal heating thus causing the 1.24 second pulsation.

(11):-

Chevalier and Ilovaisky (1973), while monitoring the optical behaviour of Hz Her when the X-ray source was 'OFF' have apparently detected short duration decrease in the

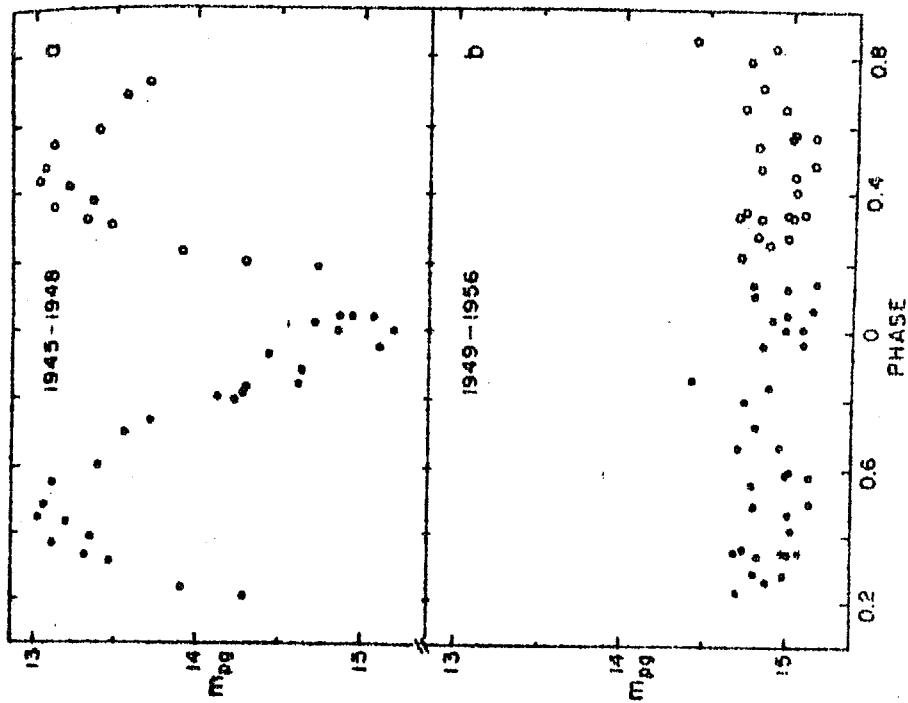


FIG. 17a - THE FIGURE SHOWS THE VARIATION OF MAGNITUDE OF HZ HER AT PHASE .5 FROM YEAR 1990-1972.

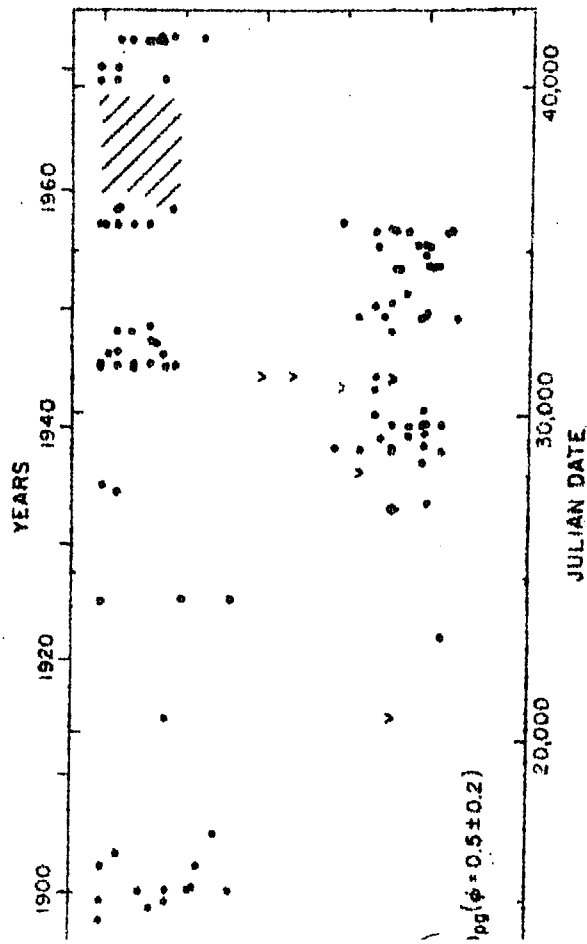


FIG. 17b - THE LONG TERM BEHAVIOUR OF HZ HER ASSOCIATED WITH HER-X-1. IT SHOULD BE NOTED THAT SOURCE WAS INACTIVE FOR PERIOD 1949-54.

optical emission. It is interesting to note that coincident with one such decrease in the optical emission, Fabian et al (1973a,b) have observed detectable X-ray emission during the 'OFF' state. However, this result needs further confirmation.

(12):-

So far no infrared or radio emission from Her X-1 have been detected (Doxsey et al 1972, Elliot et al 1973).

(13):-

Based on the X-ray observations in particular prominent pulsations at 1.24 seconds and its Doppler shift as a result of the orbital motion of the binary system, following physical parameters have been derived (Tananbaum et al 1972a) for the X-tar for a given inclination of the binary orbit of $i = 90^\circ$;

$$M_x = 0.22 \text{ to } 3.0 M_\odot$$

$$M_2 = 1.2 \text{ to } 3.2 M_\odot$$

$$\text{Mass function, } f(m) = 0.35 M_\odot$$

$$\text{Eccentricity of the orbit, } = 0.1.$$

Discussion of possible models to explain the observations is postponed to chapter 3 where our own detailed observations on this source are also presented.

1.3.5. Cyg X-1:

Cyg X-1 was amongst the first few sources discovered in the early days of X-ray astronomy (Byram et al 1966). Since then this source has been studied extensively by a number of rocket and balloon borne instruments. Among all the sources observable at balloon altitudes, Cyg X-1 is one of the strongest. Based on the available observations the main features of this source are summarized below.

(1):-

At low energies (≤ 20 keV) the intensity of Cyg X-1 is characterized by large fluctuations some time as much as by a factor of 200 in extreme cases (Giacconi et al 1973, Oda et al 1971, Schreier et al 1971). The fluctuations (see figure 1.8; Schreier et al 1971) are observed as trains of pulses that rise and decay in time scales of the order of seconds. Such pulsations seem to exhibit wide ranging periods from less than 0.3 second to over 10 seconds. As seen in figure 1.8, the power spectral analysis of the observations however, indicates that no particular periodicity is preferred. Besides the occurrence of short period fluctuations, variation in intensity on time scales of days are also observed in the data, again, no preference being shown for any particular periodicity to repeat.

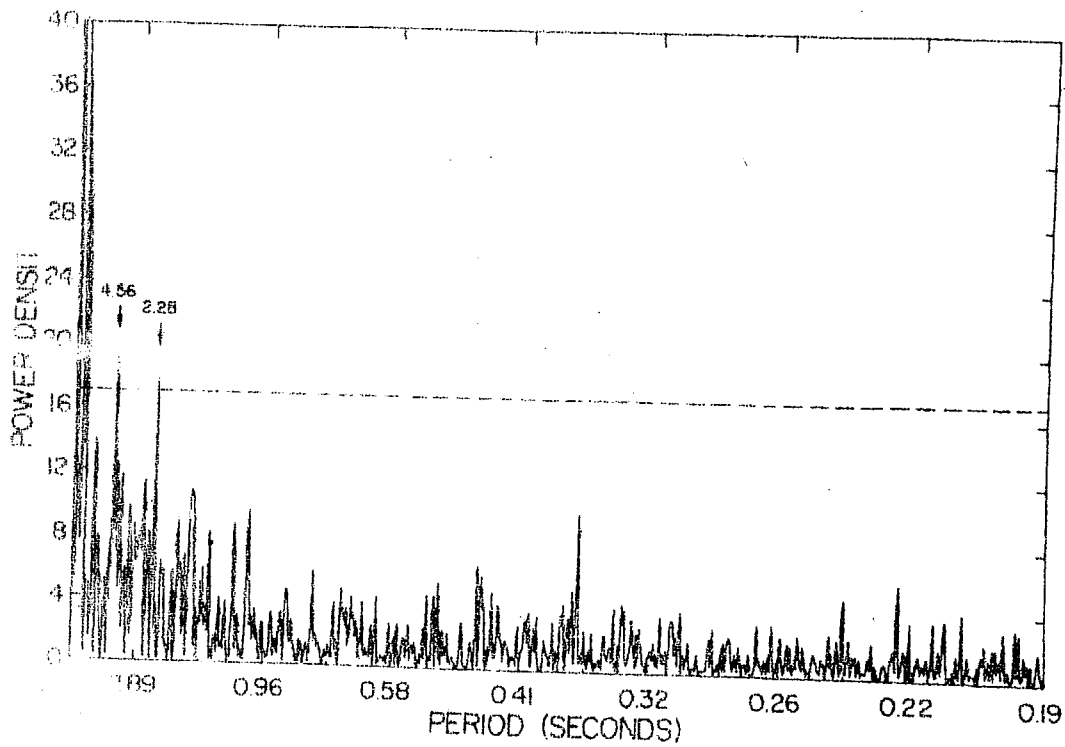


FIG. 1-8 - THE POWER SPECTRUM OF X-RAY EMISSION FROM CYG X-1 (2-6 keV).

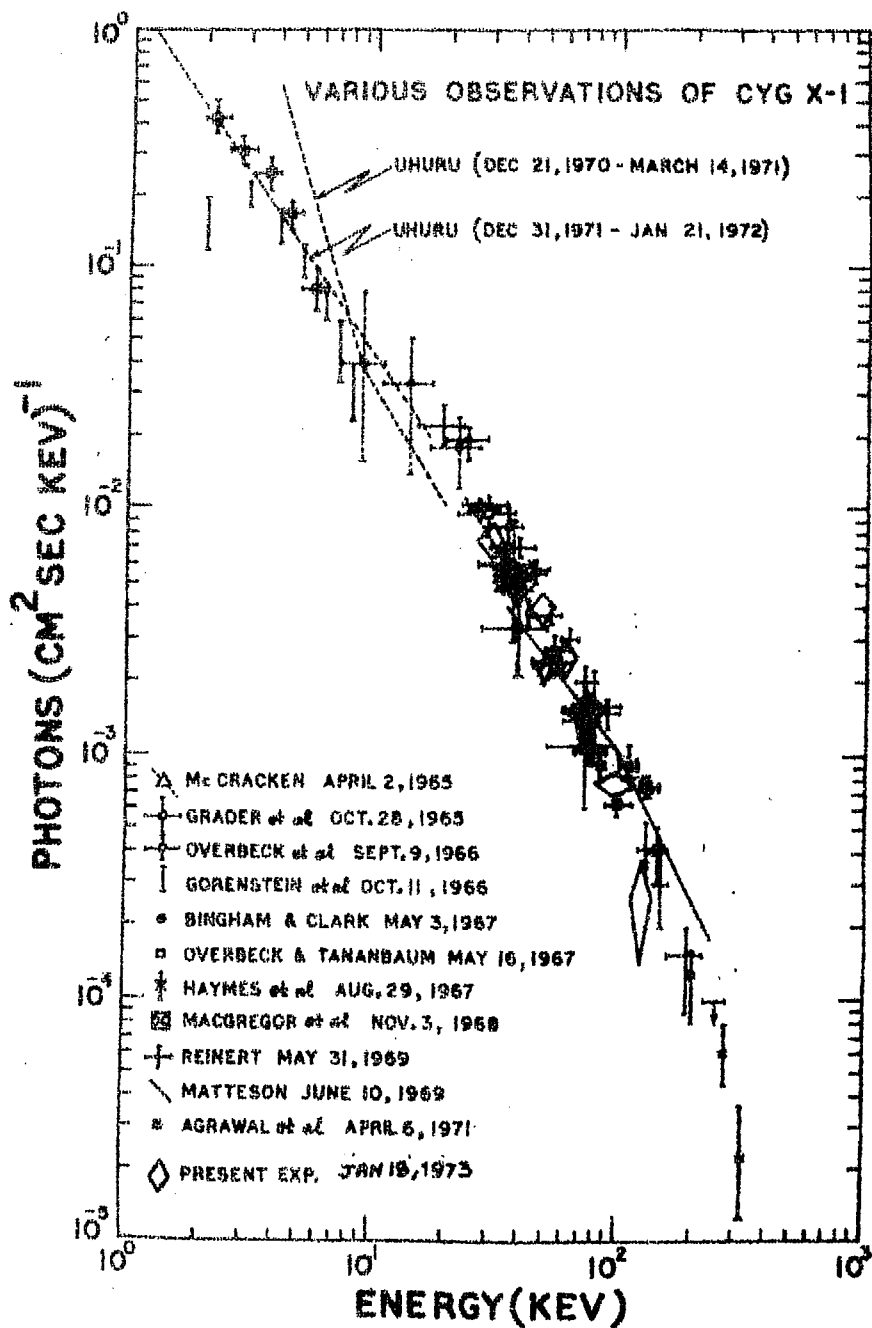


FIG.1.9 - A COMPILATION OF SOME OF THE OBSERVATIONS ON CYG X-1.

(2):-

At energies below 20 keV the detailed Uhuru observations (Schreier et al 1971) indicate that considerable changes in the spectral shape occur corresponding to the long term time variations in intensity observed over the time scales of days. Two such observations are shown in figure 1.9, where the spectras of Cyg X-1 observed during two distinct periods are plotted. By and large the spectral function can be represented well by the equation

$$\frac{dN}{dE} = A.E^{-\alpha} \text{ Photons cm}^{-2}.\text{sec}^{-1}.\text{keV}^{-1}$$

with A and α both showing variations (figure 1.9).

(3):-

At hard X-ray energies (≥ 20 keV) the behaviour of the source is found to be similar to that at lower energies (Manchanda et al 1971, Oda et al 1972 , Dolan 1970) i.e. both short term pulsations and long term variations with no preference being shown for the occurrence of regularly periodic variations.

(4):-

At hard X-ray energies the most spectacular property of the source is the occasional flare like enhancement in the intensity of the source which seems to last only for a few minutes at a time (Matteson 1971 , Agrawal 1972 , present results of our own experiment, Nakagawa et al 1973 and Fulgini et al 1973). During these flares the intensity

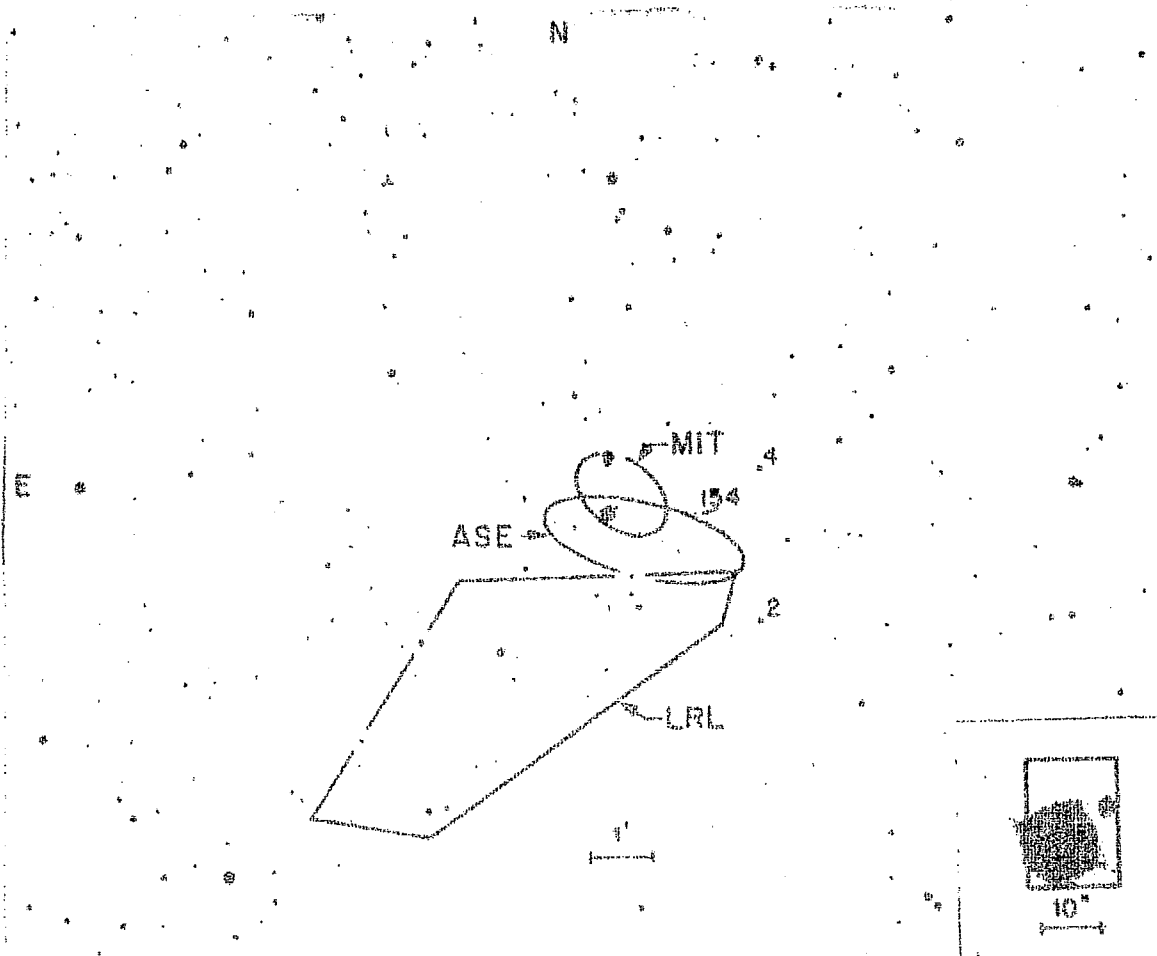


FIG.1.10 - A 16'x 16' FIELD OF VIEW OF SKY CONTAINING CYG X-1. THE STAR CONTAINED IN THE INTERSECTION BETWEEN MIT & ASE POSITIONS IS HDE 226868 IDENTIFIED WITH CYG X-1. THE INSET SHOWS AN ENLARGEMENT OF THIS AND THE CROSS IN THE INSET REPRESENTS THE POSITION OF THE STAR OBTAINED BY RADIO OBSERVATIONS.

shows enhancement by several factors and then drops back to its original value at the end of the flare event. The flare event seems to be very complex in that the presently available evidence is not able to clearly establish the nature of the spectral variations during the flare event i.e. softening (Nakagawa et al 1973 , Fulgini et al 1973), hardening (Present) as well as no spectral changes have been reported (Agrawal 1972)by different observers.

(5):-

Cyg X-1 has been identified with a spectroscopic binary HDE 226868 having an orbital period of 5.60 days and magnitude $M_V \approx 9.0$ (see figure 1.10; Kristian et al 1971 , Rappaport et al 1971 , Webster and Murdin 1972 , Bolton 1972a). The star is of the spectral type BOIb having a blue excess in its emission indicated by $B-V = 0.24$ (Margon et al 1973 , Smith et al 1973 , Bolton 1972a,b). The optical variation in blue (Brucato and Kristian 1972 , Bolton 1972a,b, Hutchings et al 1973) shows that the He II, $\lambda 4686$ emission features are essentially in antiphase (see figure 1.11; Bolton 1972b) with the stellar absorption lines. From this observation it has been concluded that the He emission line is intimately connected with the unseen companion of the star HDE 226868. Solving the binary system using these results the following estimates have been obtained for the physical parameters of the Cyg X-1 source (Bolton 1972a,b);

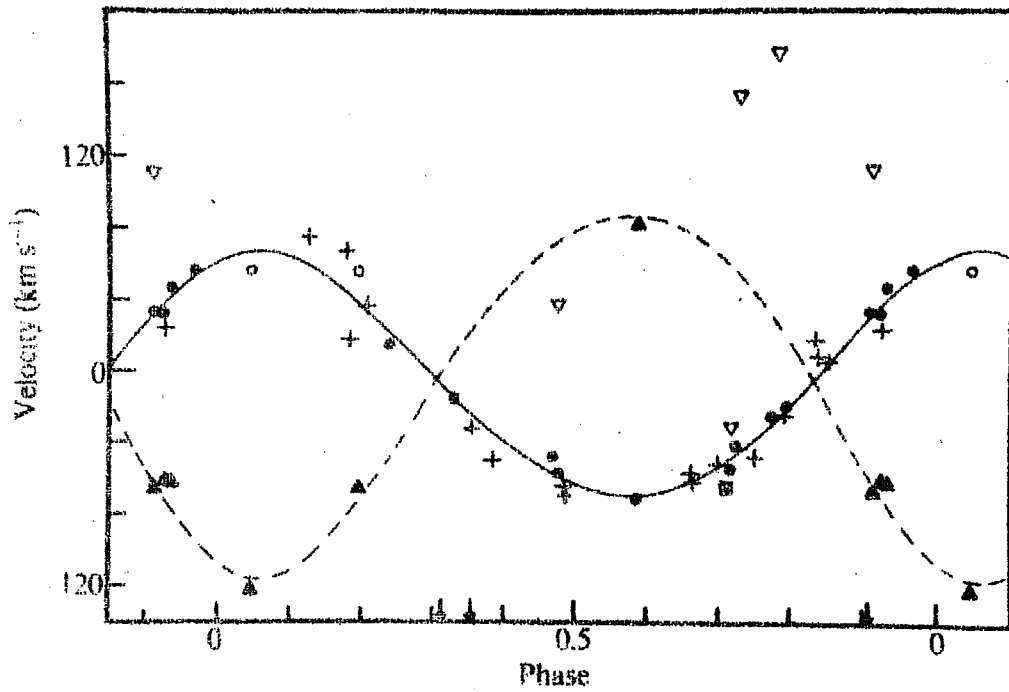


FIG.1.11 - THE RADIAL VELOCITY LIGHT CURVE OF HDE 226868, THE STAR ASSOCIATED WITH CYG X-1. THE DOTTED LINE IS He II λ 4686 AND IS CONSIDERED TO BE EMITTED FROM THE MASS ASSOCIATED WITH THE UNSEEN LIGHTER COMPANION (= X-TAR). (BOLTON 1972b)

Mass function $f(m) \approx 0.182$

$$M_1 \approx 30 M_{\odot}^*, \quad M_2 \approx 14.4 M_{\odot}$$

$$R_1 \approx 23 R_{\odot}, \quad R \text{ (Roche)} \approx 24.5 R_{\odot}$$

Distance of the source ≈ 2.5 kpc.

(6):- *Derived from spectral type (Sothers 1972)

Cyg X-1 has been identified with a weak radio source of average strength $\sim .015$ flux units (Tananbaum et al 1972b, Hjellming and Waade 1971, Braes and Miley 1972, Waade and Hjellming 1971 and Hjellming 1973). The radio flux has also shown short duration enhancements on several occasions (Hjellming 1973). Besides, at radio wavelengths also no regular periodicity has been observed (Mohanty et al 1972) although fluctuations by factors as large as 3 at 2695 MHz have been reported on the time scales of days (Hjellming 1973).

(7):-

Simultaneous observations in optical and X-ray regions have not been very successful. However, recent reports of Sanford et al (1974) and Li et al (1974) through their observations with the instruments aboard 'Copernicus' and OSO-7 satellites respectively are quite interesting. They have detected some enhancement and dip below 20 keV corresponding to the optical maximum and minimum of the optical counterpart. At hard X-ray energies, even though there is an indication of increase in the X-ray flux almost by 50% (Peterson, private communication) corresponding to the time of optical maximum, statistics are rather poor to make any meaningful conclusion.

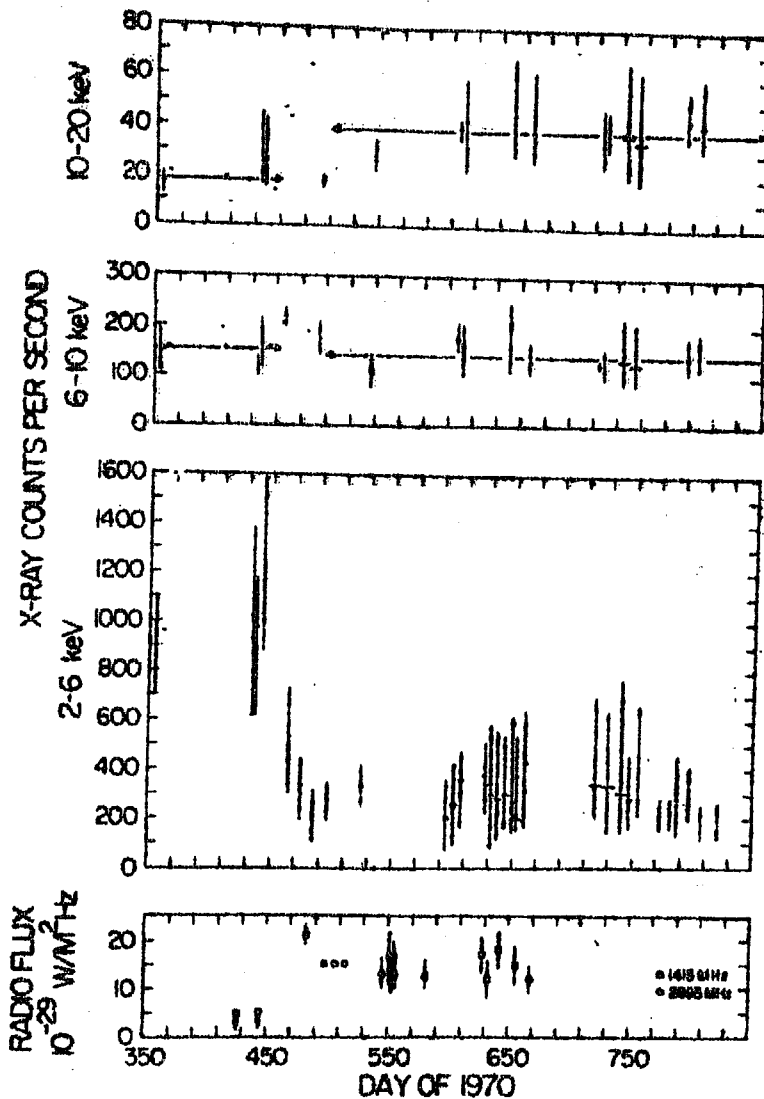


FIG. 1/12 - THIS FIGURE SHOWS THE SIMULTANEOUS X-RAY OF CYG X-1 AND RADIO OBSERVATION OF HDE 226868

(8):-

Simultaneous X-ray observations by Uhuru and radio observations by NARO radio telescope have shown correlated changes in the emission from this source (Schreier et al 1971). The radio flux variation corresponding to an increase in flux of $\sim .02$ flux units during March 1971 seems to have occurred coincident with the decrease in the 2-6 keV average intensity by a factor of four (see figure 1.12; Schreier et al 1971) and an increase in the 10-20 keV intensity by a factor of two. No such observations are reported at hard X-ray energies.

A discussion of possible models for this source to explain all the observations is postponed to chapter III along with our own observations.

1.4.0. IRREGULAR VARIABLES:

In addition to the sources which show periodic variation in their flux there is a large number of sources which do not reflect any periodicity in their emission. These sources which may be called as "Irregular Variables" are characterized by large and irregular variations in their intensity. Depending upon the time scales and the nature of variations in their emission, they can be loosely classified into two classes: 'Flaring' X-ray sources and 'Fluctuating' X-ray sources as depicted in the chart shown earlier.

We present here a short description of some of the sources under each of these categories as their study is relevant to the observations presented in this thesis.

1.4.1. 'FLARING' X-RAY SOURCES:

Characteristic property of this type of sources is that they appear rather suddenly with very large X-ray flux emission some times even more than twice the intensity of the strongest known X-ray source Sco X-1. The intensity of these 'X-tars' then decays with time scales of the order of many days or some time even months and at the end of the decay, reach an intensity level which is normally below the detectable threshold. In fact, the behaviour of these sources is very much like optical novae.

Cen X-2 was the first source of this type discovered during a rocket flight by Harries et al (1967) and later studied by a number of experimenters (see chapter second section 2.2). Since a continuous monitoring of the sky is necessary to detect sources of this type, to date only six 'flare' type X-tars have been reported. These include Cen X-2, Cen X-4, Cet X-2, 3U1543-47 (= Lup X-2) and Ceph X-4. Of these Cen X-4, Lup X-2, 3U1543-47 and Ceph X-4 were detected by satellite borne instruments. The X-tar Cet X-2 discovered in a rocket flight was seen only once (Shukla and Wilson 1970). Since this source is located at high galactic latitude ($b^{\text{II}} \approx -52^\circ$), it is conceivable that this could be an extragalactic source.

Amongst all the sources of this type discovered so far Cen X-4 was the strongest (Conner et al 1969) which, at its maximum, reached an intensity more than twice the strongest

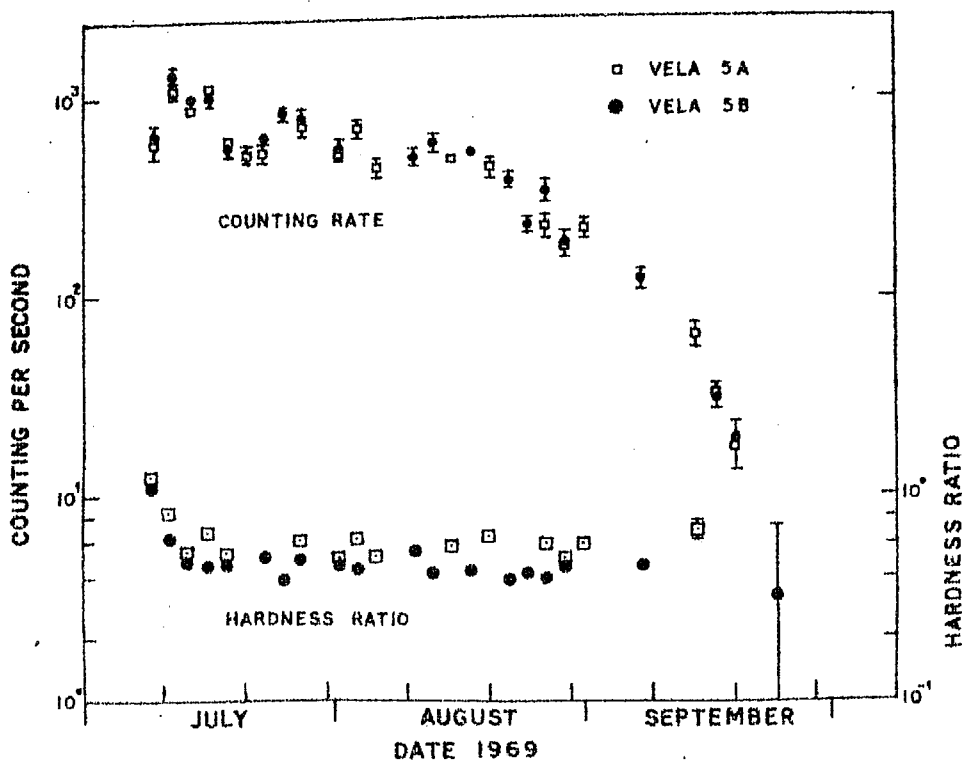
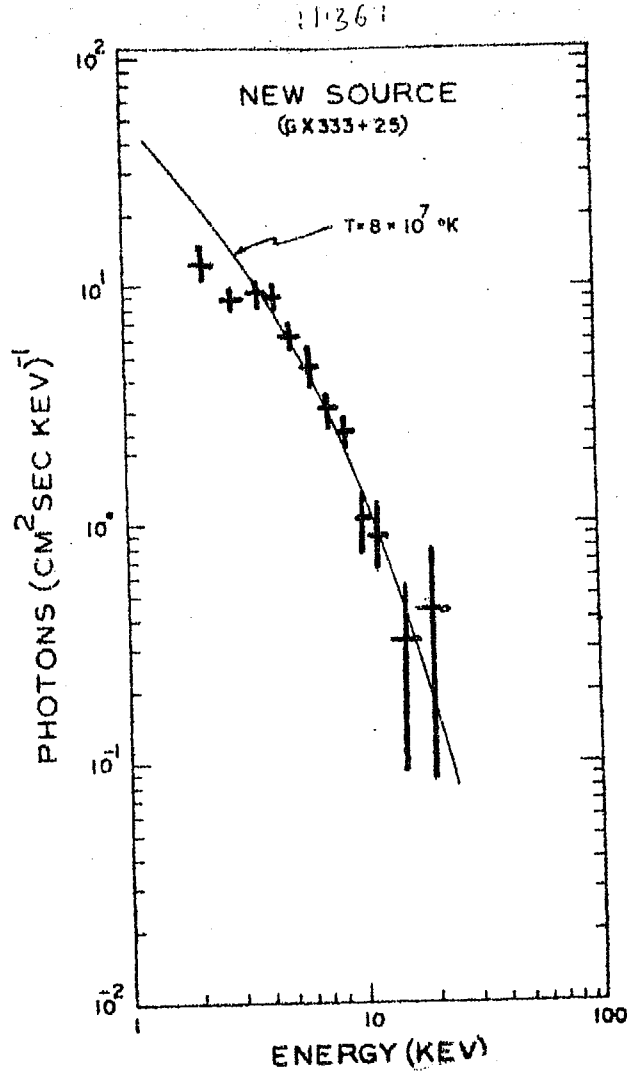


FIG. 112a. OBSERVATIONS OF CEN X .4 (UPPER) BY
TRANSIT GROUP ON AUG. 2 (LOWER) BY VELA

X-ray source Sco X-1, ($\approx 2 \times 10^{-7}$ ergs.cm⁻².sec⁻¹, in 2-10 keV range). Further, this source is probably the best tracked amongst all sources which belong to this class. Cen X-4 was monitored above back ground level for ~ 80 days after its eruption. The light curve of Cen X-4 as observed by Vela satellites (Evans. et al 1970) and its spectrum near the maximum (Kitamura et al 1969) are shown in figure 1.12a. Lup X-2 as compared to Cen X-4 was found to have an intensity above back-ground level even as late as ~ 270 days after its eruption (Matilsky et al 1972).

Ulmer et al (1973b) first reported the detection of Ceph X-4 from observation with their detector on board the satellite OSO-7. However the poor statistics preclude us from clearly establishing the true nature of the source as to whether it was a flare type star or a binary star.

From a detailed comparison of the profile of the X-ray emission from one of the sources of this type (i.e. Cen X-4) with optical emission profile of a typical nova, Rao et al (1971) showed the striking similarity in the time profile of flaring stars and optical novae.

1.4.2. FLUCTUATING X-RAY SOURCES:

Among about forty, variable X-ray sources (see figure 1.3) discovered till now majority of these show non-periodic fluctuations in their intensity and can be called as "fluctuating" X-tars. The most important source which belongs to this class Sco X-1 for example, shows fluctuations

in its intensity by factors as large as ≈ 600 in extreme cases in the 2-6 keV range (Giacconi et al 1973a, Nor X-2 is also a similar irregular variable which was within the field of view of our detector in our present rocket experiment. Hence, a brief description of this source will be given below:

Nor X-2 was discovered by NRL group in their early survey flight of 1962 (Friedman et al 1967). Later this source has been studied extensively by many experimenters (Rao et al 1971, MacGregor et al 1970, Cooke et al 1971, Cruddace et al 1971, Touhy et al 1973, Harries et al 1971, Giacconi et al 1973a) at energies below 20 keV as well as above 20 keV (Lewin et al 1968, Peterson 1973, and Baity et al 1974, Guo 73). This source has shown highly variable spectrum on the time scale of days and its intensity in the 2-6 keV energy range has been found to vary by factors as large as ≈ 36 (Giacconi et al 1973a). Although the source was recently suggested to be a binary (Spada et al 1974) detailed observations by OSO-7 (Peterson, private communication) do not show any such periodicity. Margon et al (1971) reported it to be a short period variable ($P \approx 680$ m sec) but others have not seen any such periodicity (Harries et al 1970, Schreier et al 1971 and Tuohy et al 1973). The detailed observation by Uhuru and OSO-7 (Giacconi et al 1973a, Baity et al 1974) indicate that this source has the same type of character as shown by Cyg X-1.

This source is situated very near to a supernova remnant (Poveda and Woltjer 1968, Rao et al 1971). If this association is confirmed it should give information on many aspects of this type of sources such as emission mechanisms, magnetic fields and distances etc.

1.5. X-RAY BACK GROUND:

1.5.1. INTRODUCTION:

Besides the existence of discrete X-ray emitting objects, the earlier observations (Giacconi et al 1962, Bowyer et al 1964) also revealed the presence of a diffuse cosmic back ground of X-rays which is more or less isotropic at energies above 2 keV. Detailed energy spectral observations above 2 keV show that a power law function is a good approximation above 2 keV. However, owing to the isotropy of the radiation, it is presumed that the bulk of this radiation, if not all, emanate from outside our galaxy. Detailed investigations of this radiation is of considerable interest from the stand point of cosmology.

Table 1.2 summarises briefly the various techniques used to derive the back ground. Since the correct estimation of cosmic back ground requires an exact knowledge of the internal back grounds. Hence various techniques used here differ mainly in the manner with which the internal back ground is estimated. Basically, these can be broadly classified as under (Schwartz and Gursky 1973).

(1):-

The earth, assumed to emit no X-rays has been used as a "Shutter" and the entire instrument output obtained when the earth occupied the field of view of the collimator was assumed to be internal. This technique was used for the first time by the present author and the results as well the technique used are described in detail in chapter II.

Table 1.2. Summary of various method used to determine the X-ray background spectrum (Schwartz & Gursky 1973).

Method of deduction	Used by	Possible contamination by	Comments
1. Earth occultation	PRL (Present Rocket expt.)	Albedo	For experiments at low latitudes and below 30 keV the effect is negligible
2. Opaque Shutter	LLL,Bologna, AS & E	Production in shutter	--
3. Variable solid angle	GSFC	Precipitating electrons	Effect would be negligible at equatorial stations like Thumba
4. Modulation with vehicle motion	PRL(Balloons) OSO III , TIFR,Saclay	Radio activity and atmospheric scattering	For equatorial orbits in case of satellites and at low latitude stations for balloon experiments the effect would be minimum

(2):

The physical shutter that is opaque to the X-rays of the energy range of interest have also been used. In this case either the shutter was moved into and out of place over the aperture or else used to cover one of several

(3):-

Different collimator solid angles have also been used, again either by motion of a shutter over one detector or fixed collimator over several identical detectors.

(4):-

Observation of modulation of the internal background as a function of varying geomagnetic conditions has also been used mainly in satellite experiments. By this, the internal background can be separated from the constant isotropic X-rays.

The background determination using the first technique (below 10 keV) can suffer by the sporadic emission of X-rays due to auroral type of events. But at stations like Thumba ($\phi_{\text{mag}} \approx 0^\circ$) there are no such contaminations possible (Seward 1974). However, above 30 keV the atmospheric albedo becomes comparable to the diffuse X-ray background. Below 30 keV, this is undoubtedly an extremely good technique which can be used to great advantages particularly at low latitude stations.

All the rest of the techniques suffer from a common problem in that X-rays generated by interactions in the mechanical shutter can contribute significantly to the internal background when shutter is closed but would not be present when the shutter is open. This will introduce the errors in the estimation of the true celestial background. In addition, the contamination due to the geomagnetically trapped electrons which produce X-rays could also be a significant contributor.

However, outside the trapped zone (Seward 1974) and away from the Polar-auroral electron zones this effect may not be significant.

In the last method, however, a truly constant internal background component, for example, radio activity within the detector or vehicle, will not be modulated as function of geomagnetic conditions and thus affecting the estimation of celestial X-ray background.

1.5.2. OBSERVATIONAL RESULTS:

The observational status of this important radiation can be summarized as follows:

(1):-

Above 2 keV the radiation is more or less isotropic in intensity (Reviewed by Schwartz and Gursky 1973, Silk 1970, 1973) within 5% in accordance with the detailed investigations by the OSO-III payload which gave upper limits of about 2% for 12 and 24 hour components. This information has further led to the deduction that the relative motion of the earth relative to rest frame of reference of the universe must be less than 800 km sec^{-1} (Schwartz 1969, Ph.D. thesis).

(2):-

The energy spectrum in the 2-100 keV range can be reasonably represented by a power law function, which according to OSO III observations has a break at 40 keV. However, detailed critical examination of the available

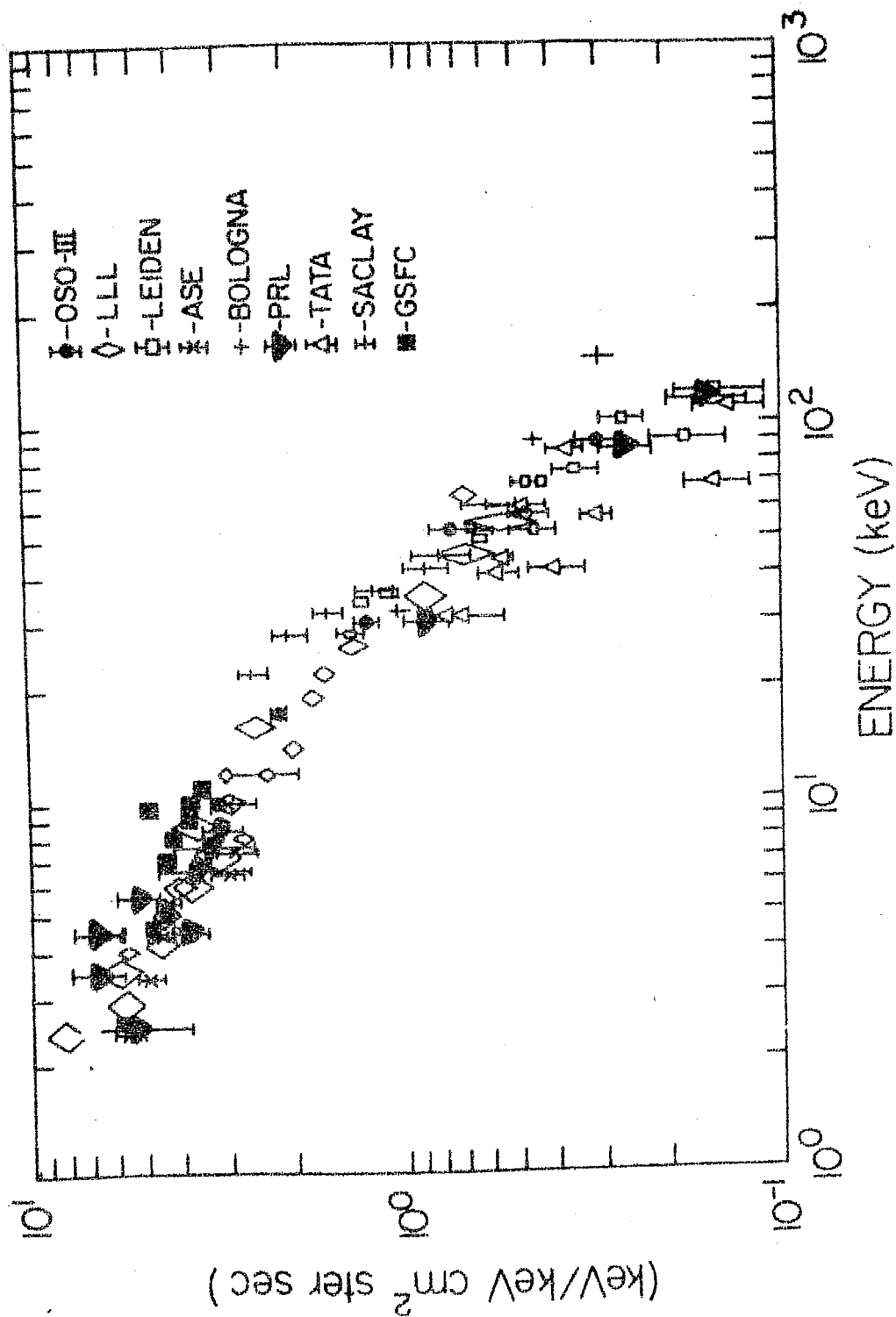


FIG.1.13: THE FIGURE SHOWS THE X-RAY BACKGROUND OBSERVATIONS. PRL RESULTS INCLUDE ROCKET AS WELL AS BALLOON OBSERVATIONS. THE RESULTS ARE NOT CORRECTED FOR COMPTON SCATTERING.

data (Kasturirangan and Rao, 1972) from balloons and rocket observations suggests that the spectrum over the range 2 keV-1 MeV can be fairly well represented by a single power law spectrum of the type

$$\frac{dN}{dE} = 30 E^{-2.0 \pm 0.2} \text{ photons.cm}^{-2}.\text{sec}^{-1}.\text{keV}^{-1}.\text{Sr}^{-1}$$

These authors have shown that the earlier difference in spectrum at different energy ranges were finally due to the fact that no corrections were applied for taking into account the multiple Compton scattering in balloon observations. The data obtained from rocket borne instruments which cover a larger energy range from 2 keV to beyond 20 keV (see figs.1.13, 1.14) confirm this view. The 40 keV break observed by satellite borne instrumentation has been quantitatively explained as due to the induced radio activity effects in the detector system arising from the particle bombardment during the time the spacecraft passes through the trapped radiation belts (Dyer and Morfil 1972). Recent results from OSO-5 (Dennis et al 1973) also do not show any such break in the spectrum. It should be remarked here that from a theoretical stand point of view it is not possible to explain (Cowsik and Kobetich, 1971) the presence of a break in the spectrum even if a corresponding break is assumed to be present in the electron spectrum.

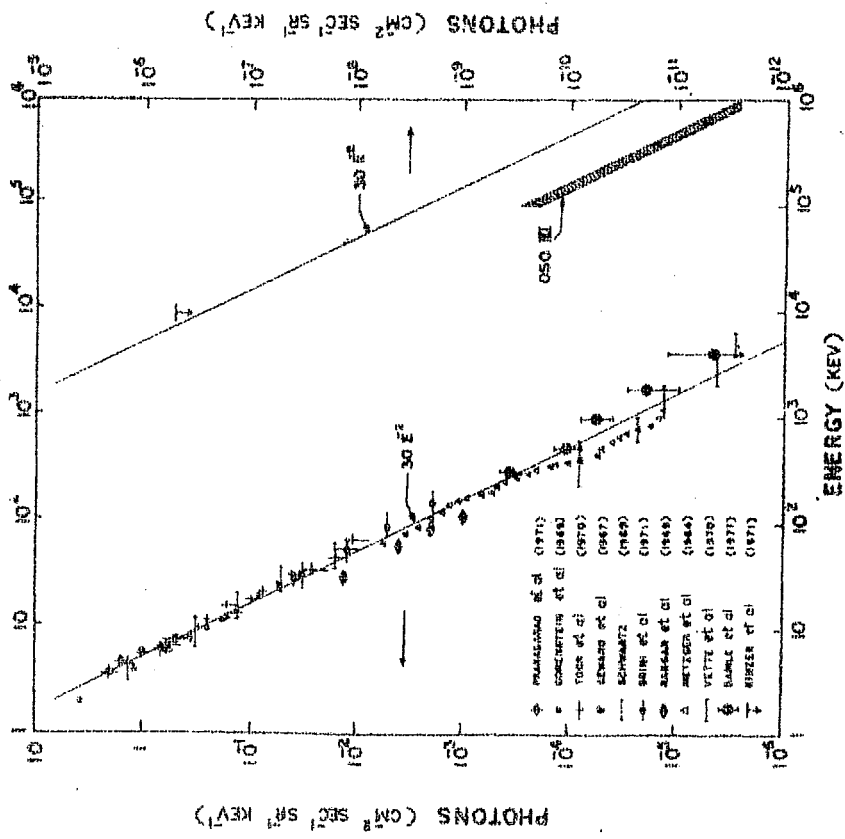


Fig. 14 - Spectrum of the diffuse X-ray and Gamma rays with the balloon observations corrected for multiple compton scattering of X-rays.

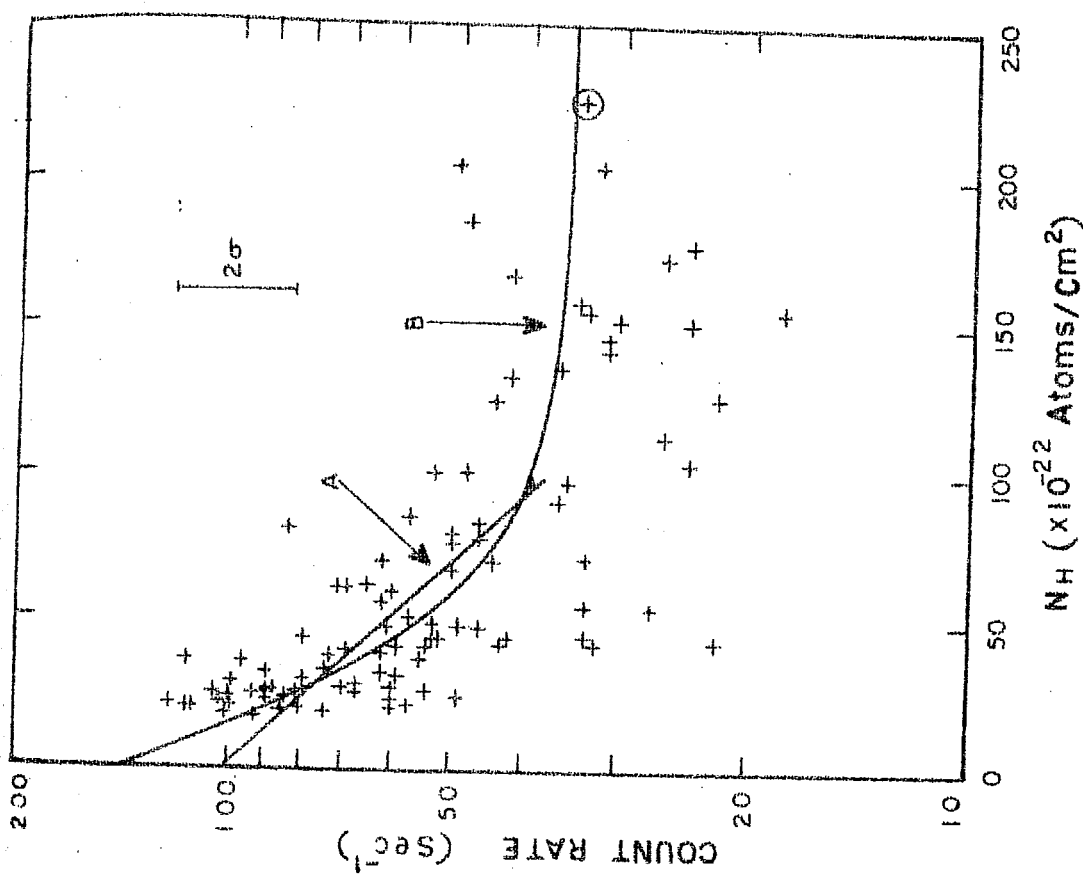


Fig. 15 - Correlation plot of the 250 eV X-ray background flux versus the hydrogen density.

(3):-

At energies below 2 keV, usually denoted as soft X-rays, the observations reveal that although the maximum intensity is from the direction of galactic poles, the decrease observed as the galactic plane is approached is what is expected from purely galactic absorption effects. This strongly indicates the existence of a galactic component at these energies, the contribution of which has been assessed in some of the experiments (Henry et al 1971, Bunner et al 1971, Kato 1972, Gorenstein and Tucker 1972, Davidson et al 1972b, Novick et al 1972, Hayakawa et al 71,73, Yentis et al 1973 a,b).

(4):-

The extragalactic soft X-ray component appears to have a hard spectrum which can be reasonably approximated to a power law (Gorenstein et al 1972, Hayakawa et al 1973) whereas the galactic component seems to have an exponential spectrum with $KT \leq 0.1$ keV. It is conjectured that the soft galactic component is the result of a number of diffuse sources e.g. Cygnus loop and Vela X (Grader et al 1970, Gorenstein et al 1972, Palmieri et al 1971). An interesting experiment by McCammon et al (1971) who failed to measure the absorption of these soft X-rays through the magellanic clouds appears to confirm this.

(5):-

Figure 1.16 shows (Silk 1970) shows the estimates of X-ray background in comparison to the flux of electromagnetic radiation in different spectral regions. The estimates are

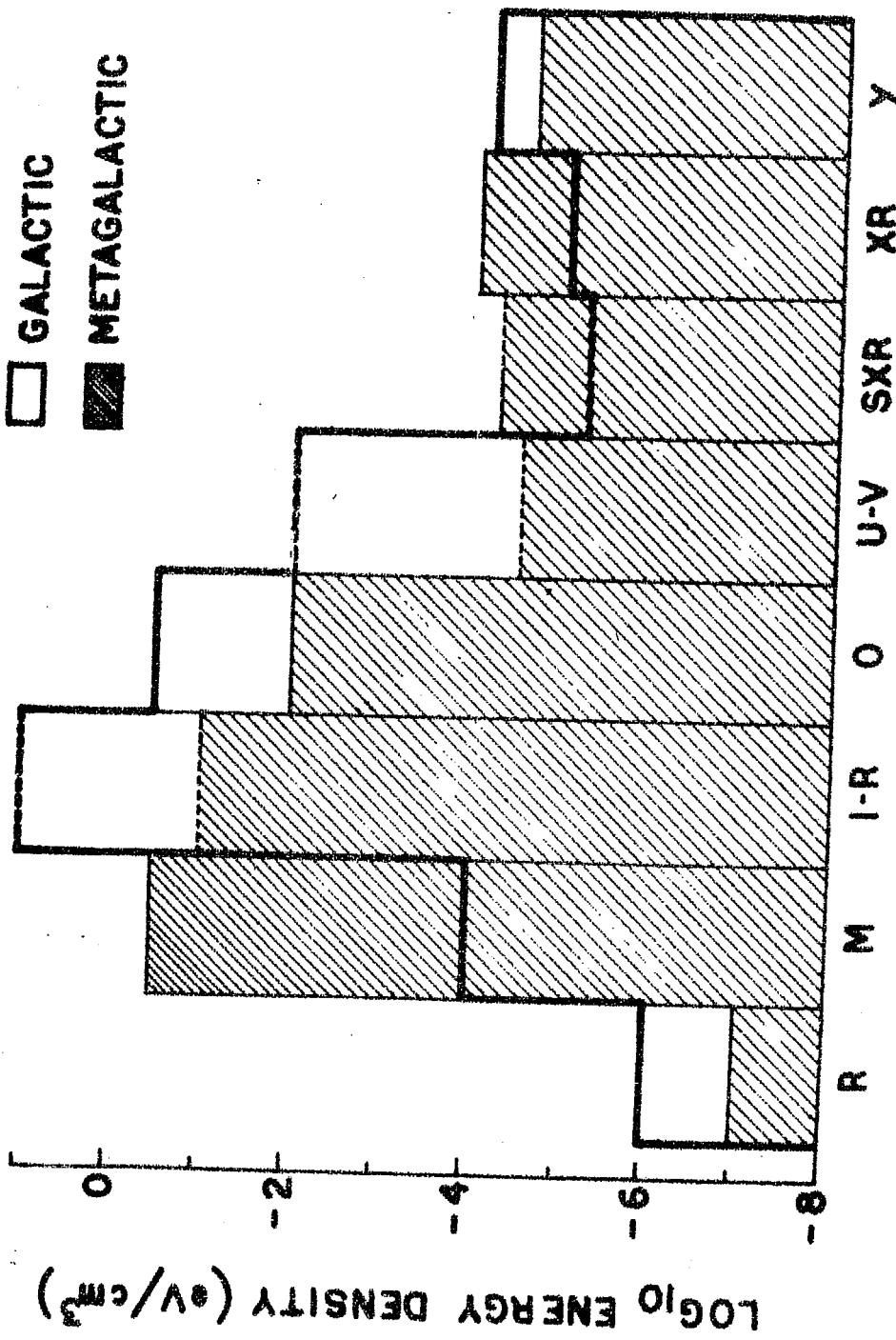


FIG.1.16: THE DISTRIBUTION OF COSMIC PHOTONS (SILK 1970). R = RADIO, M = MICROWAVE, I-R = INFRARED, O = OPTICAL, U-V = ULTRAVIOLET, SXR = SOFT X-RAY, XR = X-RAY, γ = GAMMA RAY.

:1.48:

plotted in units of photon energy density (eV.cm^{-3}). The unshaded columns denote the average photon density produced by our own galaxy evaluated for the solar neighbourhood. This is compared with the mean photon density in the metagalaxy (denoted by the shaded regions), where only contributions from distant sources are included. It can be noted that in most of the spectral regions, the galactic contribution dominates, just as one might expect, the star light from the Milky Way is some two orders of magnitude more intense than the optical flux from distant galaxies.

(6):-

No conclusive evidence of any line features in the diffuse component has been obtained so far from observations in different energy intervals (Shulman et al 1971, Boldt et al 1971, Toor et al 1971).

(7):-

Detailed observations of Davidson et al 1972^b, Kato 1972 and Bunner et al 1971^c, show that the emission of the amount of diffuse soft X-ray flux is well correlated with the distribution of hydrogen column density derived from measurements at 21 cm radio wavelength (see figure 1.15; Davidson et al 1972^b).

1.6.0. MODELS FOR DIFFUSE X-RAY BACKGROUND:

Any model for the origin of diffuse radiation should explain its intensity which is having an energy density of $\approx 6 \times 10^{-5} \text{ eV.cm}^{-3}$ in the 2-1 MeV energy range and its high degree of isotropy within 5%. Besides the spectral shape another important parameter which should be accounted for is the spectral index. The spectral index in the energy range 2-20 keV is observed to be $\alpha \approx -1.8$ and steepens to $\alpha \approx -2.5$ above 20 keV. Broadly all the models can be classified in two categories as described below:

- (a): Those where the background is interpreted as the integrated effect of discrete sources.
- (b): Those models where the emission mechanisms are assumed to operate throughout the intergalactic space, or atleast in very extended diffuse regions.

Both of these types of models can be further divided into those not involving cosmological evolution and those involving it.

1.6.1. MODELS NOT INVOLVING COSMOLOGY:

(a) Gold and Burbidge (1963) were the first to propose a theory based on the superposition to account for the diffuse X-ray background. The superposed X-ray energy from all galaxies, like ours, with average density of $.03 \text{ Mpc}^{-3}$ or 10^{-75} cm^{-3} within the Hubble distance ($= 10^{28} \text{ cm}$) and having an average flux similar to our galaxy i.e.

$\sim 10^{39}$ ergs.sec $^{-1}$ is estimated at $\approx 2 \times 10^{-6}$ eV.cm $^{-3}$ (Oda 1965, Sciama 1969 and Silk 1970). This estimate falls short by a factor of ≈ 50 to account for the observed diffuse intensity. To fulfil the requirement for the observed flux, galaxies with intense emission ($\sim 10^{43}$ ergs.sec $^{-1}$) such as M-87 or quasars have been invoked. However, in view of the low spatial density of these objects ($\approx 10^{-6}$ Mpc $^{-3}$; Schmidt, 1968), the superposition model has difficulty in accounting for the observed intensity of cosmic background.

(b) Felton and Morrison (1966) have proposed that the X-ray background can be explained as due to Compton collisions between the high energy metagalactic electrons. However, the electrons needed to produce X-ray background can produce radio emission far in excess of the observed radio emission through synchrotron mechanism. If both X-ray and radio background have to be explained simultaneously then one has to invoke very low magnetic fields ($\approx 2 \times 10^{-8}$ G; Kawabata et al 1969). Such low fields are untenable even in the extended radio sources. In their theory they have been able to link the spectral index of electrons (≈ 2.6) leaking from radio galaxies to produce Compton scattered X-rays of photon index ≈ 1.8 . However, the intensity estimates fall short by a factor of ≈ 100 . Brecher and Morrison (1969) on the other hand, have considered that ordinary galaxies might provide the electron source. However, in this case normal galaxies are required to produce $\approx 10^{41}$ ergs.sec $^{-1}$ in GeV electrons; consequently, if the leakage time were $\approx 10^6$ yr,

the average cosmic ray density would exceed that in our own galaxy by an order of magnitude. Thus in view of the energy requirements this hypothesis does not seem to be plausible (Setti and Rees, 1970; Silk, 1970).

In addition to the inverse Compton effect, other processes like thermal and non-thermal bremsstrahlung over extended regions have also been considered. Although the super thermal electrons with different exponents can explain the observed spectrum through non-thermal bremsstrahlung process the energy requirements are severe due to the low efficiency ($\approx 1\%$) of this process (Setti and Rees 1970, Silk 1970). On the other hand, thermal bremsstrahlung process cannot be accepted since observed spectrum above ~ 2 keV does not fit the shape of the spectrum expected from such a process, without postulating temperature gradients. Although, the extragalactic component at the soft X-ray energies (≤ 1 keV) can in principle be explained as due to emission from hot dense intergalactic medium (Gorenstein and Tucker 1972, Hayakawa S. 1973), the observational data of X-ray spectrum in this energy range presently available is still meagre to draw any definitive conclusions.

1.6.2. MODELS INVOLVING COSMOLOGY:

a) In evolutionary cosmologies, the intergalactic gas is assumed to have been denser in the past, and the primeval radiation field more intense. Moreover, there is evidence both from the distribution of quasars (Schmidt 1968, Rowan Robinson 1968) and from radio source counts (Ryle 1968)

that violent events were more frequent at earlier epochs, which, if cosmology is introduced makes the energy problem less embarrassing (Setti and Rees 1970). This being a common problem to all the earlier mentioned models proposed to explain the origin of cosmic background X-radiation, all of these models have been extended to incorporate evolutionary effects. As a result of inclusion of evolutionary effects, the energy requirements for unit volume are increased in proportion to the mean redshift factor $(1 + \bar{z})$. The observed photons would of course have been generated with energies higher by the same factor $(1 + \bar{z})$. The expansion time scale t_{exp} for the universe would have been shorter in the past depending on the models adopted (except in Lemaitre-type models). These two effects require that the power output in the X-rays would need to have been much greater in the past in order to have the red shift be responsible for the dominant contribution.

Silk (1969,1970) has treated the discrete source models by including the evolutionary cosmological effects. He has pointed out that subject to sufficient increase in the X-ray luminosity of individual galaxies with large red shift, one can account for the observed diffuse background by counting normal galaxies. However, the large red shifts ($\bar{z} = 15$) invoked in this model are not compatible with the cosmological time scales. Moreover, the same evolution, if true, should increase the radio power much beyond the presently observed extragalactic radio background (Setti and Reess 1970).

While in the case of radio galaxies strong evolution cannot be considered because of the limit set by the radio background considerations of evolutionary factors only in the case of quasars leads to an intensity which is inadequate by almost a factor of 10.

Bergamini et al (1967) showed that when the evolution of temperature and radiation are considered, the observed background X-ray flux could be explained by Compton interactions of thermal radiation with electrons leaking from radio galaxies. In an evolutionary universe, the temperature of the blackbody radiation is proportional to $(1 + \bar{z})$, where \bar{z} is the red shift, owing to the adiabatic cooling. The photon energy density, will be,

$$W_{ph} \propto (1 + \bar{z})^4$$

This means that at large red shifts the energy of relativistic electrons can be converted more rapidly into X-rays.

Consequently the permitted magnetic field to fit the radio data can be increased in proportion to W_{ph} . The observed X-rays can be explained by applying a cut-off at $\bar{z} = 5$ since beyond $\bar{z} > 5$, the electrons responsible for radio emission have their half lives reduced considerably. Similar conclusions have been reached by Brecher and Morrisson (1967).

Silk and McCray (1969) attempted to fit the observed spectrum using a non-thermal model in an evolving universe. This process is more efficient at large red shifts due to

the higher density of intergalactic gas. The authors have postulated that the subrelativistic electrons with suitable spectrum are injected at a red shift ≈ 10 . The break in the electron spectrum is explained as a result of Coulomb losses, which flatten the electron spectrum at low energies. The source of electron spectrum is chosen in an ad hoc fashion and besides there is a possibility of the electron spectrum getting modified as they escape into the intergalactic space.

Even though both types of models i.e. the superposition of discrete sources and the radiation from intergalactic space, can explain the observed intensity of X-ray background and their spectral characteristics under certain circumstances, the restrictions are less severe in the case of the model based on Compton scattering. The bounds on the break at 3 GeV in the electron spectrum of the sources, will vanish in the light of the present finding of the absence of a break in the diffuse spectrum beyond 20 keV.

The recent discovery of NGC 1275, a Seyfert galaxy as an intense extragalactic X-ray object, leads us to believe that significant contribution to the observed diffuse background comes from extragalactic objects. If all the Seyfert galaxies which form 1% of the population of all spiral galaxies emit X-rays at the intensity of NGC 1275 ($\approx 3 \times 10^{44}$ ergs.sec⁻¹; Fritz et al 1971), the estimated superposed energy will be much more than the observed background intensity even without the consideration of evolutionary effects. However, the intensity of other Seyfert galaxies such as NGC 4157 and NGC 1018 falls far short of the required average

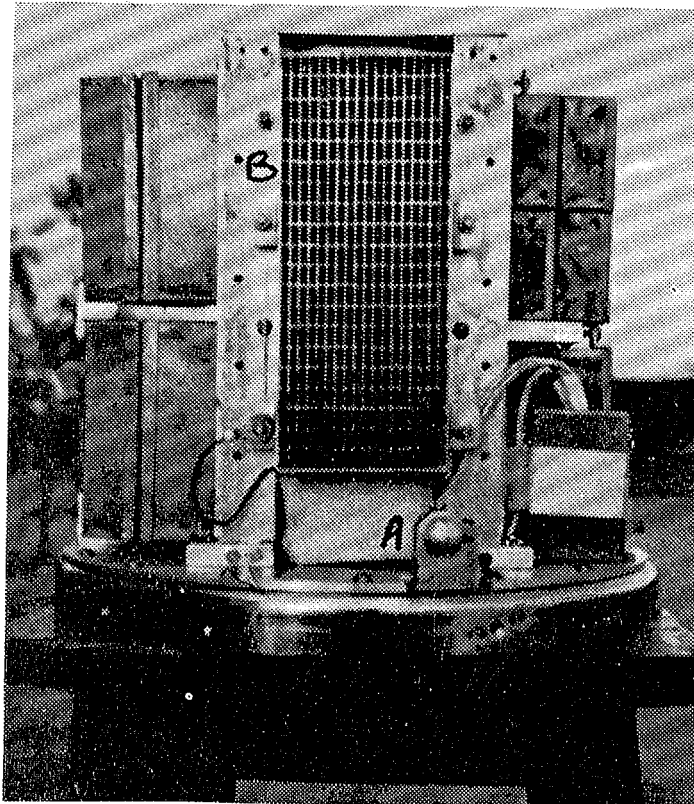
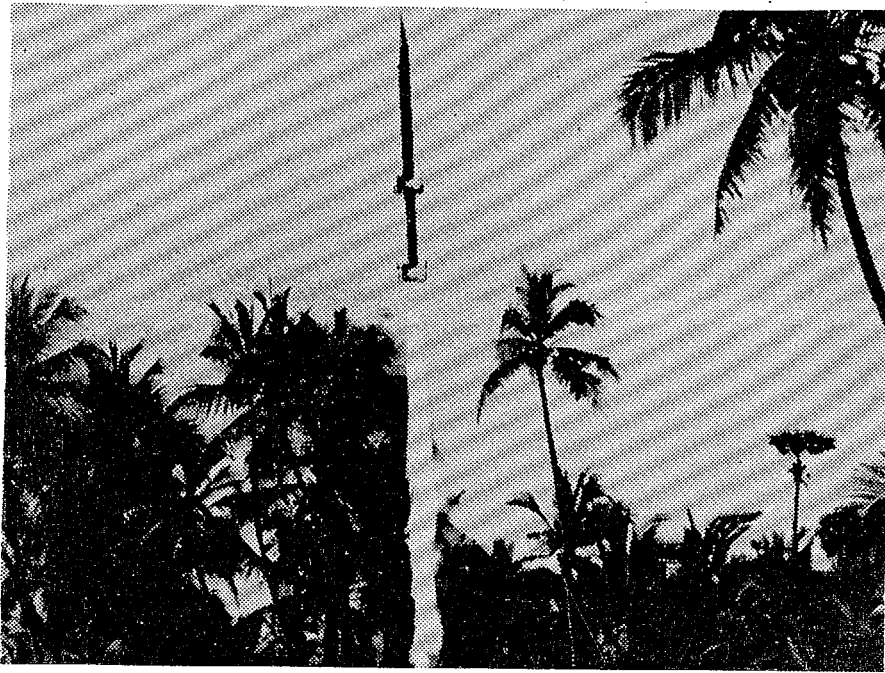
CHAPTER II

THE ROCKET EXPERIMENT

2.1. BRIEF DESCRIPTION OF THE ROCKET PAYLOAD:

The rocket payload primarily designed to study the new born X-ray source Cen X-4 was launched on a Centaure rocket from Thumba Equatorial Rocket Launching Station (TERLS) on December 7, 1969. The experiment was conducted during the declining phase of this spectacular source which erupted into a prominent X-ray star on August 9, 1969 and attained full brightness within a matter of 3 days and decayed back into its original status in about 100 days. In addition to the above mentioned source, observations were recorded on a few other sources viz Nor X-2, Cen X-1 and Cen X-2 which were in the field of view of the detector during the same flights. In this chapter we give a brief description of the payload, the associated electronics and also discuss the results obtained from these experiments. The photograph on the next page shows the payload prior to launch and the rocket after launch.

In the present experiment the detector used was a proportional counter filled with 90% Xenon and 10% methane at one atmospheric pressure. The detector which had a depth of 25 mm had a 100 micron thick beryllium entrance window. The body of the proportional counter was made of welded stainless steel. A slat collimator made of stainless steel was mounted in front of the detector which defined the field of view of the detector as $6.5^\circ \times 15^\circ$ FWHM in the perpendicular and parallel directions



The picture shows the Centaure Rocket Payload and Rocket after Launch. A is the Solar Sensor, B is the Collimator and other boxes contain Electronics.

: 2 : 3 :

BLOCK SKETCH OF X-RAY PAYLOAD

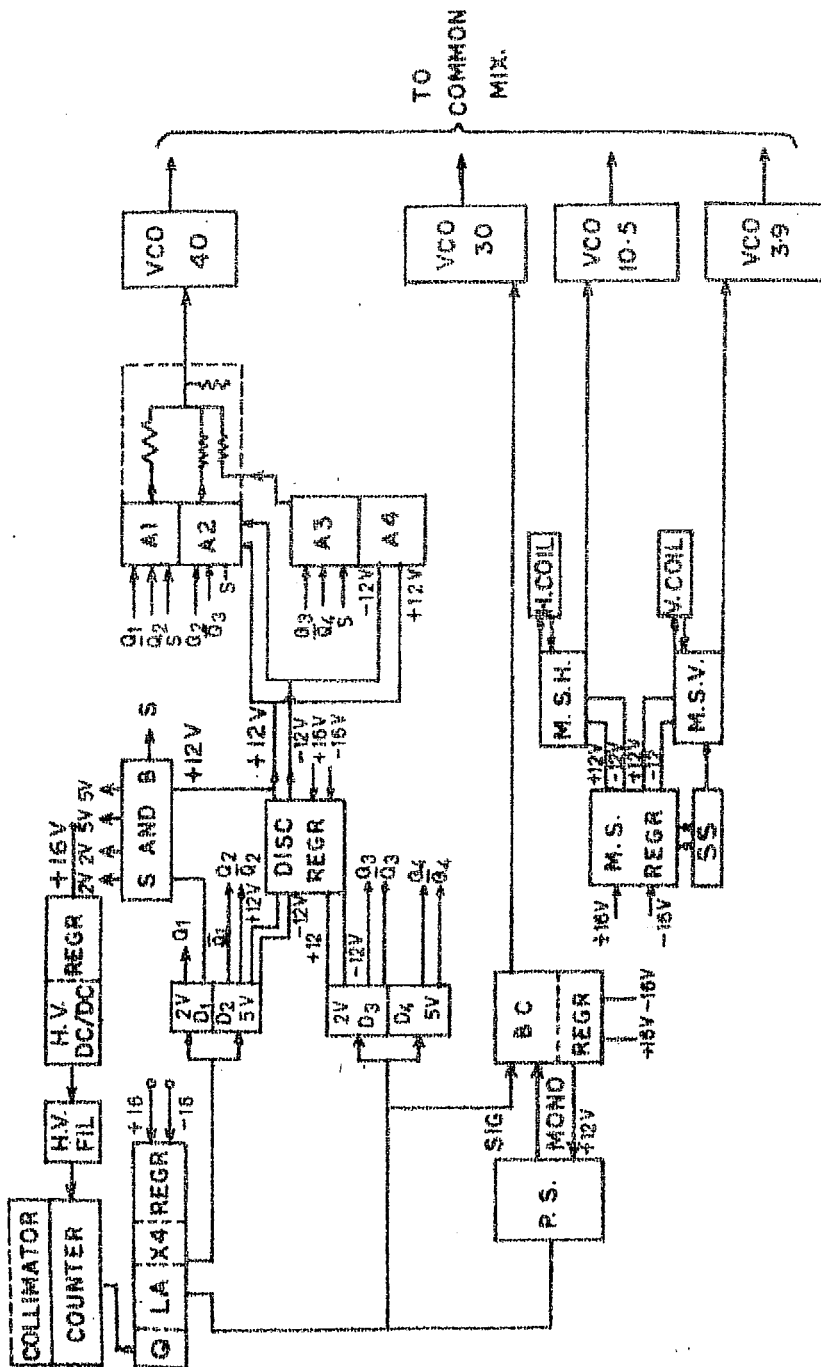


FIG:2.1 THE BLOCK DIAGRAM OF X-RAY EXPERIMENT OF DECEMBER 9, 1969.

to the spin axis. The detector had an effective area $\approx 55 \text{ cm}^2$.

Figure 2.1 gives the block diagram of the conventional electronics used in association with the detector for energy discrimination. The output of the FET pre-amplifier was further amplified and fed to a "box-car" circuit in parallel with a three stage difference amplifier type discriminator to separate the individual X-ray pulses into three energy ranges viz. 2.1-5.1 keV, 5.1-8.7 keV, 8.7-18.0 keV. The parallel input to the "box-car" circuit (Seshadri et al 1971) provided a redundant analog output corresponding to the 2-10 keV interval, the output being proportional to the energy of the incident X-rays. Both outputs were then fed to conventional voltage controlled oscillators and were transmitted to the ground using standard FM/FM Telemetry system,

The calibration of the "box car" as well as the pulse height analyser were achieved by monitoring the pulse height when the counter was irradiated by various radioactive sources such as Fe^{55} (5.8 keV), Zn^{65} (8.05 keV) and Cd^{109} (22 keV). The linearity as well as the frequency response of the linear amplifier and of the "box car" circuit were checked thoroughly before the flight.

Inflight calibration of the detector was carried out till the rocket reached an altitude of 60 kms using a Fe^{55} radio active source fixed on the inside of a door on the rocket nose cone. At about 60 km altitude this door was

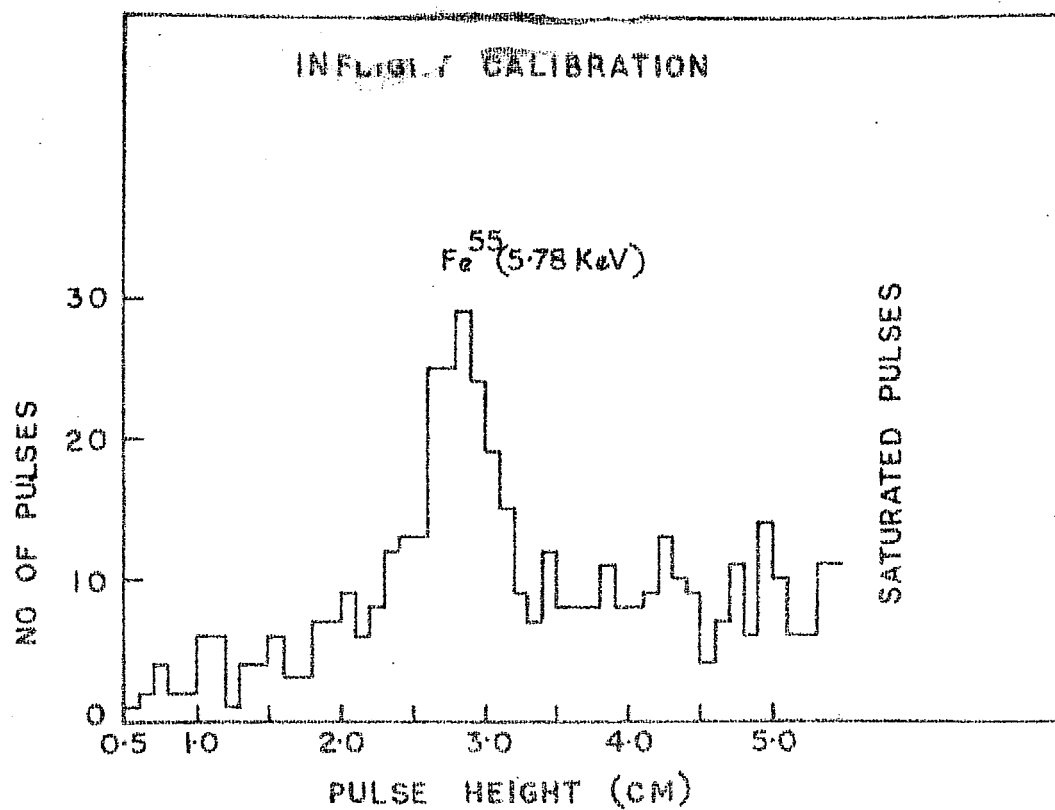


FIG. 2.2- THE FIGURE SHOWS THE INFLIGHT CALIBRATION OF THE PROPORTIONAL COUNTER BY ^{55}Fe SOURCE.

ejected explosively, after which the counter was exposed to the celestial sky for receiving useful data. Figure 2.2 shows the inflight calibration where the observed count rate is plotted as a function of the pulse height.

The details of the rocket trajectory required for attitude analysis were obtained from the data received from radar tracking of the transponder. The attitude of the rocket as a function of time were derived by using horizontal and vertical flux gate magnetometers and solar sensors. Figure 2.3a shows the rocket altitude as a function of time.

The method of rocket attitude determination is described in Appendix A-2 and results are summarised in table 2.1.

2.2.1. RESULTS AND DISCUSSION:

Even though our rocket experiment was primarily designed to conduct observations on the nova like X-ray source, Cen X-4 the same flight also provided some significant results on Cen X-1, Cen X-2 & Nor X-2. Further, the data from this experiment were also utilized to derive information on the intensity and spectral characteristics of the cosmic X-ray background in the energy range 2-10 keV, using the earth as a shutter. The region of the sky scanned by the detector is shown in figure 2.3b. The region of the sky utilized to derive the background X-ray spectra is also shown by shaded area.

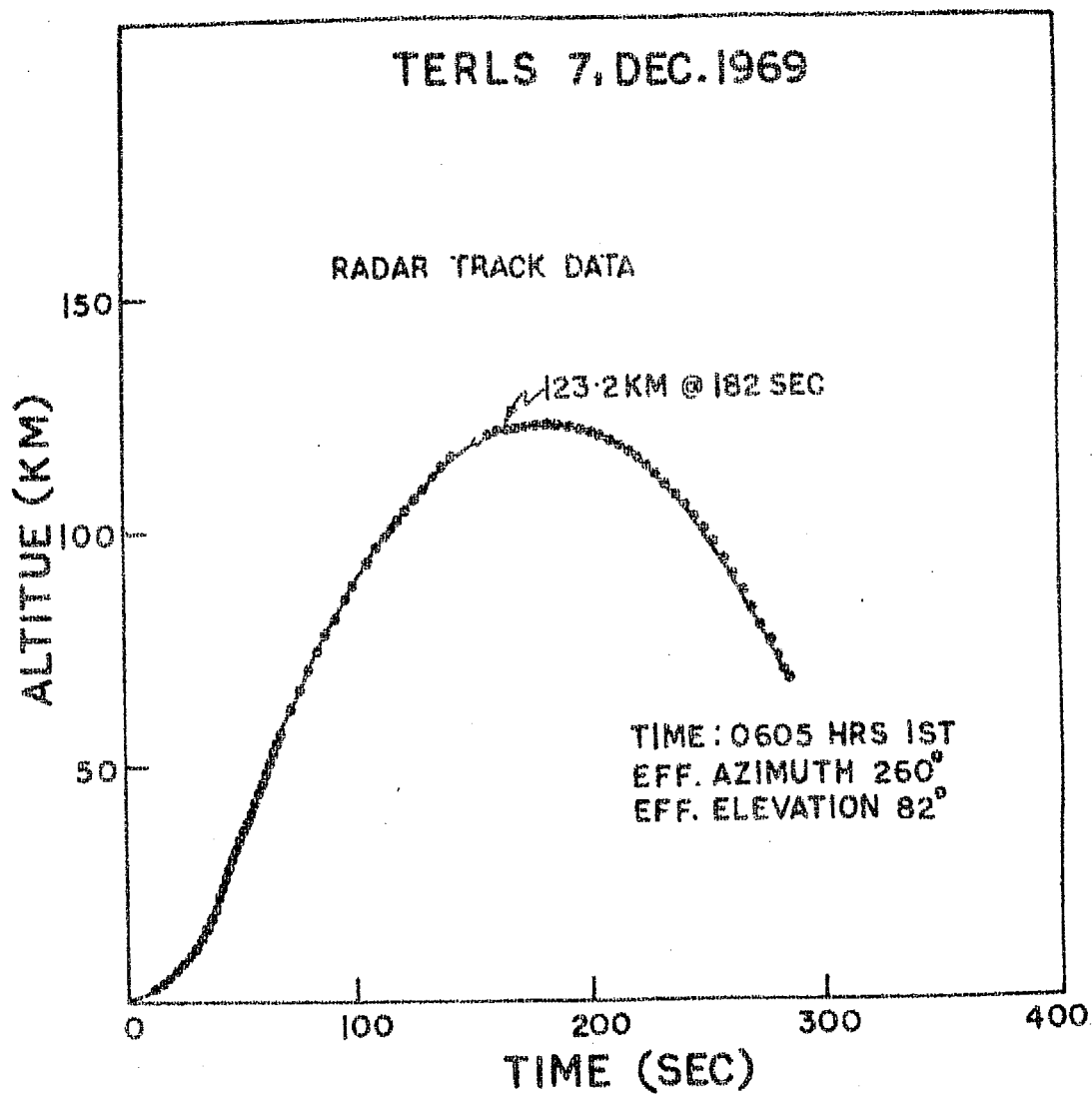


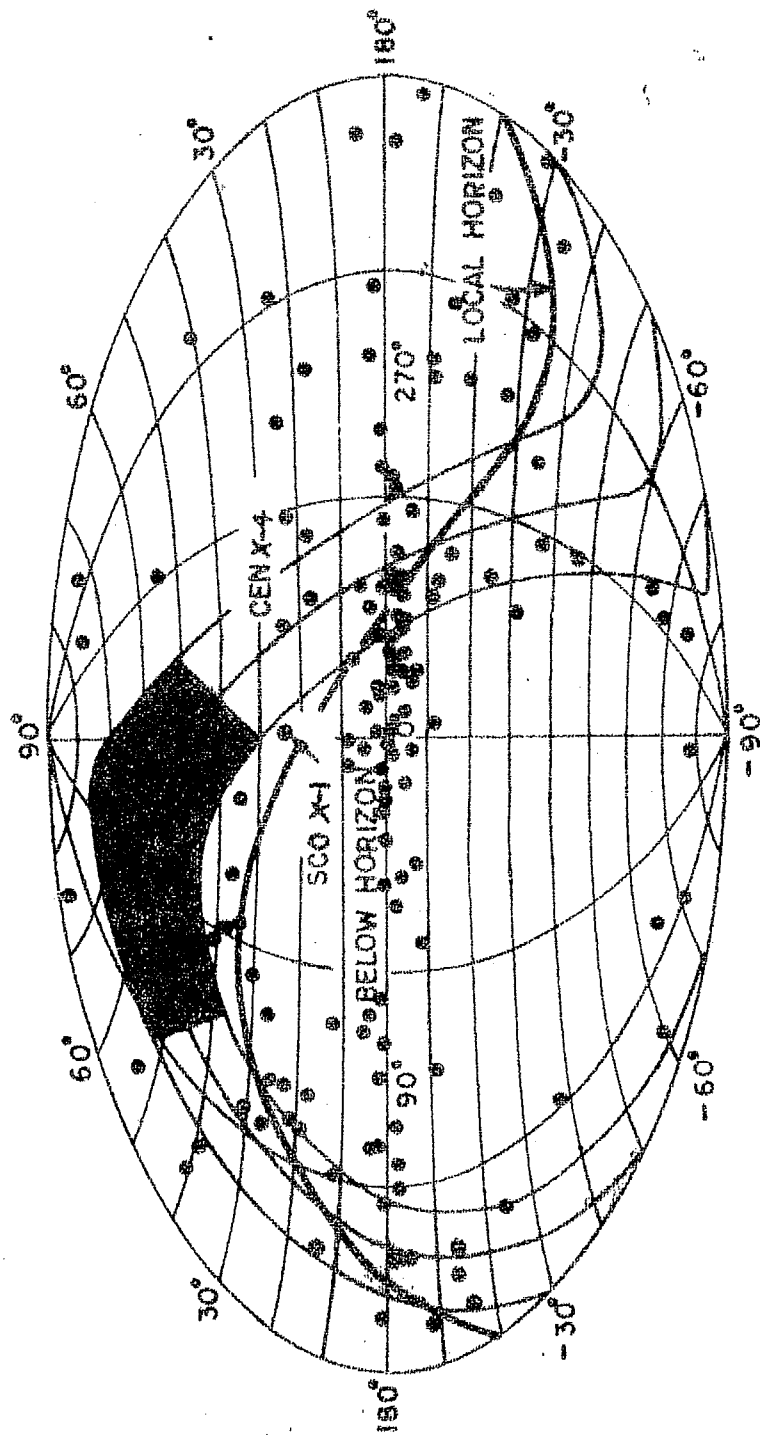
FIG:2.3a TIME Vs ALTITUDE HISTORY OF ROCKET FLIGHT ON
DECEMBER 7, 0035 UT, 1969.

:2.8:

Table 2.1

Summary of Rocket Experiment

1. Date of experiment	.. December 7, 1969, 0035 UT
2. Maximum altitude of rocket	.. 123 km
3. Detector	.. Xe + CH ₄ counter with effective area $\approx 55 \text{ cm}^2$, window: 100 micron beryllium.
4. Collimation angles (FWHM)	.. $6.5^\circ \times 15^\circ$
5. Sources in the field of view	.. Nor X-2, Cen X-1, Cen X-2, Cen X-4
6. Aspect parameters:-	
R.A. of sun	.. $253^\circ 24'$
Declination of sun	.. $-22^\circ 34'$
R.A. of precession axis	.. 134°
Declination of precession axis	.. 3°
Precession period	.. $78 \times .1893 = 14.7654 \text{ sec.}$
Spin period	.. $.1893 \text{ sec.}$
Precession cone angle	.. 3°
R.A. of Magnetic field	.. $00^h 42^m$
Declination of Magnetic field	.. $81^\circ 54'$



NEW GALACTIC COORDINATES

FIG. 2.3b: SHOWS THE BELT SCANNED DURING THE ROCKET FLIGHT ON DEC. 7, 1969. THE DARK REGION SHOWS THE AREA ABOVE HORIZON SELECTED FOR BACKGROUND ESTIMATES. THE OUTER LINES OF THE THREE SHOW THE BOUNDRIES OF MINIMUM COLLIMATOR TRANSMISSION AND CENTRAL LINE SHOWS THE DETECTOR NORMAL.

2.2.1. CEN X-4:

This nova like source was first discovered by Conner et al (1969) through their observations using instruments on board vela satellites. The source became visible when it dramatically erupted into a bright X-ray star between $23^{\text{h}} 30^{\text{m}}$ UT, July 6, and $04^{\text{h}} 30^{\text{m}}$ UT July 9, 1969, in the constellation of Centaurus. Initially the source strength increased rapidly reaching a maximum around July 11, 1969. It remained almost constant at its peak brightness for the next four days and then gradually began to decline. At its peak this source was almost twice as bright as Sco X-1.

Since the early experiments provided information only in two energy channels, only limited spectral information on the source could be obtained. The hardness ratio (flux in the 6-12 keV band/flux in 3-6 keV band) calculated from the observations, however, clearly indicated that the spectrum of the source softened considerably after the first two days of its eruption, the hardness ratio changing from ≈ 1.08 to $\approx .45$. The ratio remained constant there after till almost the last stages of its decline, thus suggesting that the source was an isothermal one behaving very similar to an optical nova. On August 7, 1969, Kitamura et al (1969), observed the same source during a rocket flight and found that the observations were consistent with an exponential spectrum similar to that of Sco X-1 with a flux of ≈ 44 photons. cm^{-2} . sec^{-1} in the 2-25 keV energy band. Balloon

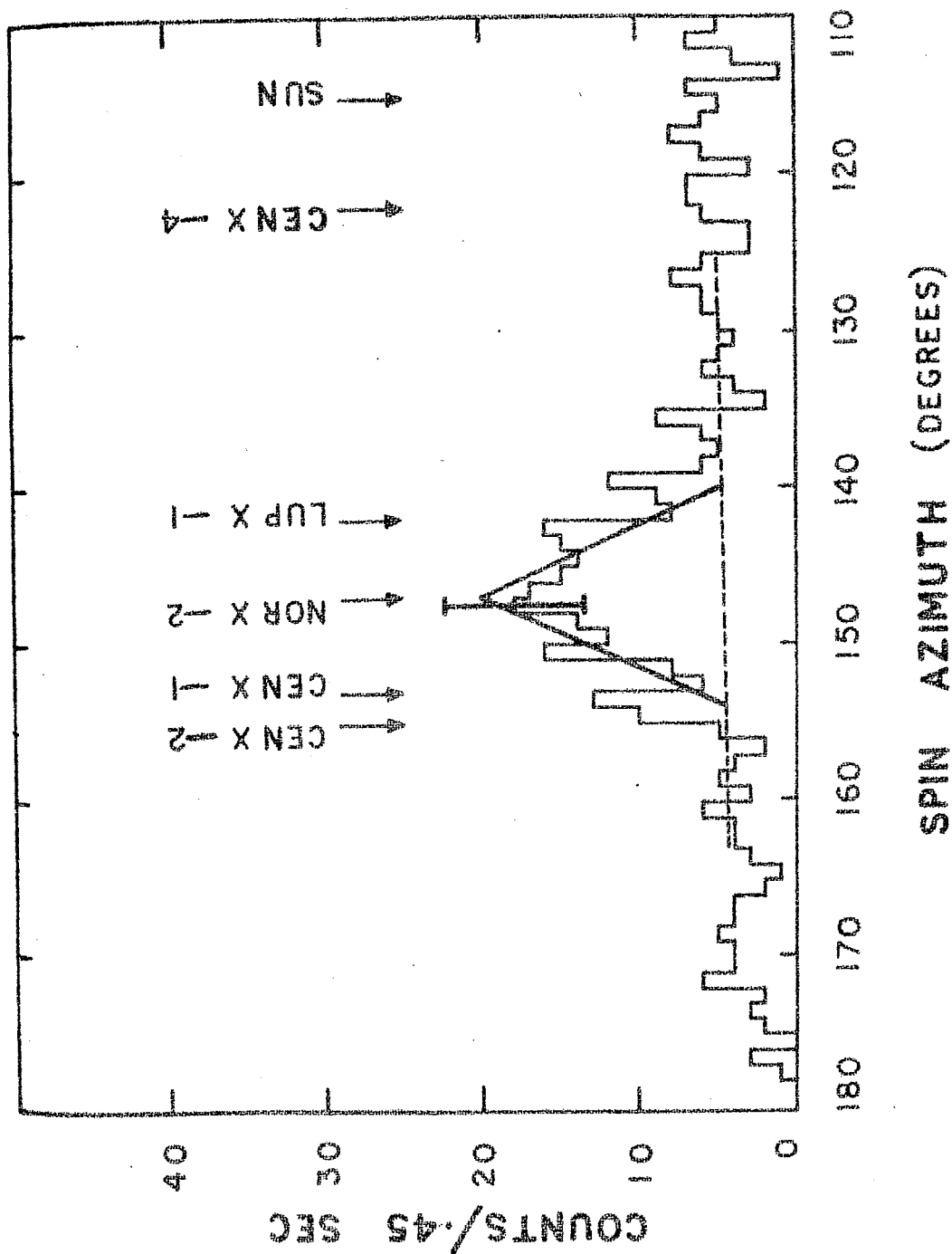


FIG.2.4a: ACCUMULATED COUNTS AS A FUNCTION OF SPIN AZIMUTH. THE POSITION OF VARIOUS SOURCES WHICH WERE IN THE FIELD OF VIEW OF THE DETECTOR ARE MARKED IN THE FIGURE. THE TRIANGULAR RESPONSE OF THE COLLIMATOR IS ALSO INDICATED.

212

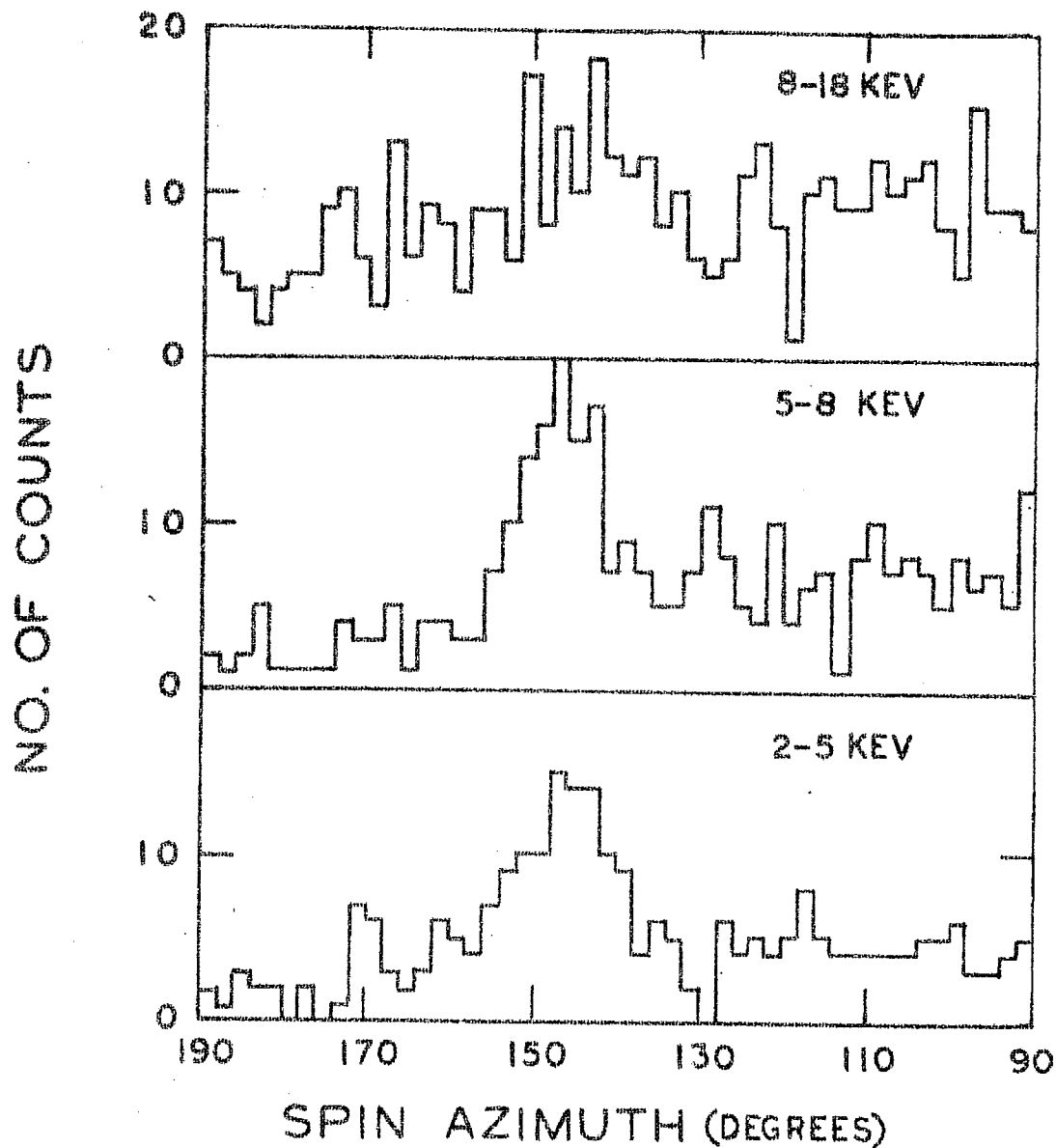


FIG:24b THE AZIMUTHAL DISTRIBUTION OF THE COUNTS DEPOSITED IN THE DETECTOR. ONLY THE SOURCE REGION IS SHOWN.

observation by Thomas et al (1969) 18 days later, on August 25, 1969 showed that the intensity of the source had decreased by factor ≈ 6 in 10.8-19.7 keV band as compared to the intensity of August 7, 1969 when extrapolated using Kitamura et al's observation.

As a continuation of the above observations and in order to investigate the decay characteristics and detailed spectral features of this interesting source, a proportional counter X-ray payload was launched from the Thumba Equatorial Rocket Launching Station, India on December 7, 1969 at 0035 UT. The launch time was chosen so as to have the Cen X-4 source well above the horizon (30° elevation) and close to the center of the field of view of the detector. Figure 2.4a and b show the raw counting rate data plotted as a function of spin azimuth where the positions of various sources (figure 2.4a) which were within the field of view of the detector are marked. As is evident from the figure, the detector did not record any significant count rate above the background level from the direction of Cen X-4 indicating that the source had declined below the limit of detection of the present experiment by December 7, 1969. Our observation on December 7, 1969 shows that in the energy range 2-18 keV the source strength had decreased at least by a factor of ≈ 800 over a period of ~ 150 days from the peak emission. Consequently, we can only provide upper limits with the present data (2σ level, see table 2.2) in the various energy ranges.

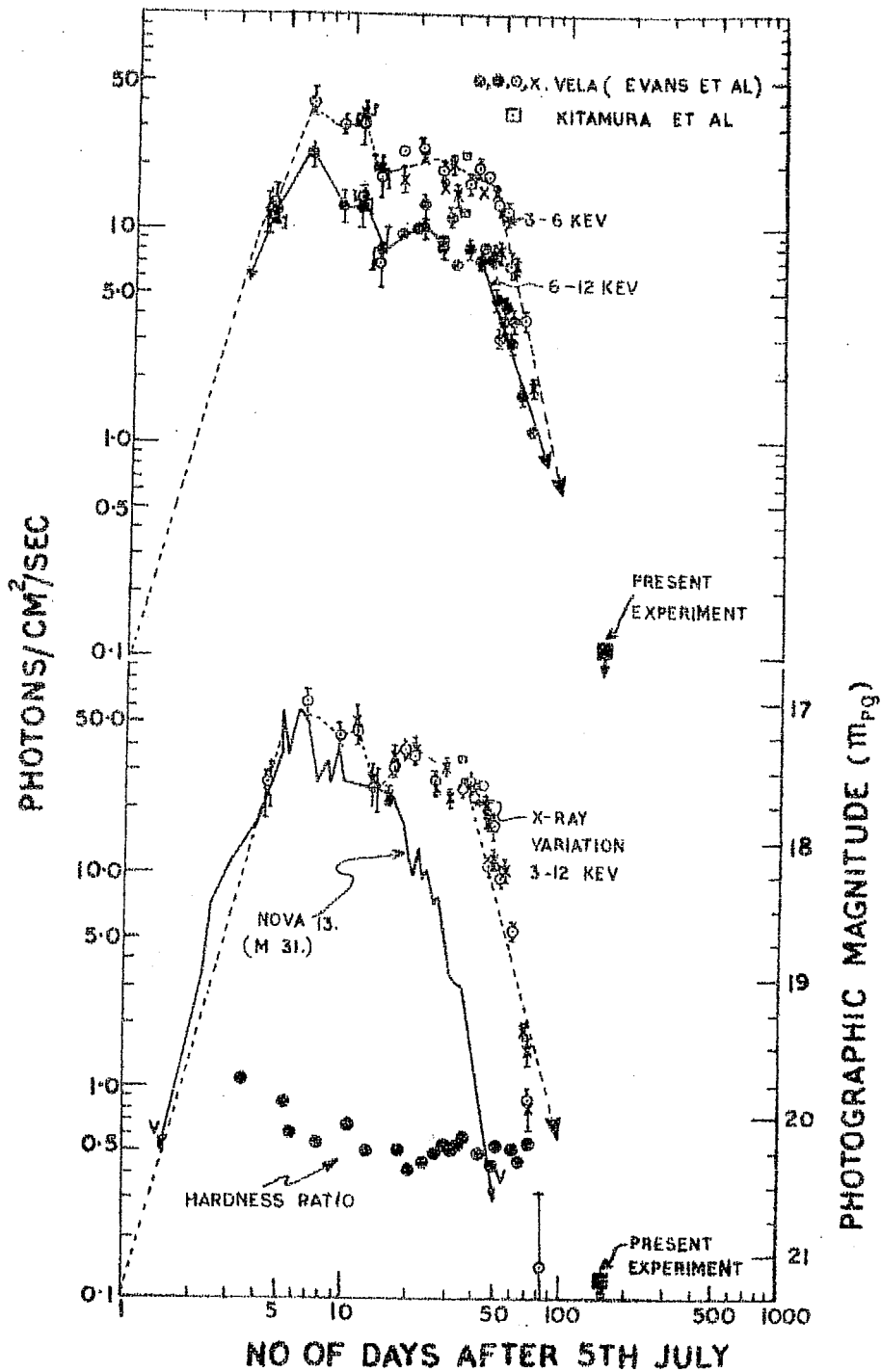


FIG.2.5; FIGURE SHOWING THE TIME PROFILE OF THE X-RAY FLUX FROM CEN X-R. THE SOLID CURVE DEPICTS THE LIGHT CURVE OF A NOVA (SEE TEXT).

Table 2.2 : Upper Limits of Flux of Cen X-4
(at 2 σ level)

Energy Range (keV)	Upper Limits (photons $\text{cm}^{-2}.\text{sec}^{-1}.\text{keV}^{-1}$)
2.1 - 5.1	1.50×10^{-2}
5.1 - 8.7	1.00×10^{-2}
8.7 - 18.0	0.55×10^{-2}

In figure 2.5 are plotted the totality of all epochal measurements of X-ray flux from Cen X-4 as a function of time. The data points from Vela satellites (Evans et al 1970) plotted in the graph have been corrected for transmission through .005 inch thick beryllium window in front of the NaI (Tl) detector. The figure clearly shows the rapid build up within about two days followed by an exponential decay with a time constant of ~ 10 days. The flux recorded at the end of 80 days on September 24, 1969, was less than 0.5% of its peak intensity. On December 7, 1969 after ~ 150 days, the present experiment shows that the flux was ≤ 0.13 photons $\text{cm}^{-2}.\text{sec}^{-1}$ (at 2 σ level) in the energy range 2-18 keV.

The spectacular time variation observed in the X-ray flux of Cen X-4 has many similarities with the normally observed time variation of the optical luminosity of a nova.

H.Arps has studied in detail the various characteristics of optical novae from M-31 galaxy which have been published in a catalog form (Arp 1956). From an examination of the data published, a definite relationship between the maximum optical intensity attained by novae and their total duration has been established. According to this relationship, lesser the magnitude of a nova at its peak intensity lesser will be the duration. This means brighter the nova at its peak intensity shorter will be its duration. An optical nova with a duration similar to Cen X-4 should have a maximum optical intensity corresponding to an optical magnitude ~ 17 . We observe that Nova 13 in M-31 galaxy was of magnitude ~ 17 . Since M-31 is quite similar to our own galaxy, we can compare the characteristics of this optical nova with the rise and decay characteristics of Cen X-4. In figure 2.5 the luminosity characteristics of nova 13 in Arps's catalog has also been plotted for easy comparison with the corresponding X-ray flux profile of Cen X-4. The striking similarity between the optical luminosity observation of nova 13 and X-ray flux variation of Cen X-4 is quite evident from the figure. The general similarity between the concentration of X-ray sources and optical novae along the galactic plane discussed by Gratton (1969) adds further support to our observation. Further, the recent observation of Belian et al (1972) of occurrence of a short duration intense X-ray pulse (~ 10 minutes) on July 7, 1969 from the same general region of Cen X-4 is also in agreement with our hypothesis.

2.2.3 CEN X-1:

Since, Cen X-1 was also at the center of field of view of our instrument, attempt has been made to determine the flux of this source in various energy bands. This source which was discovered by Friedman et al (1967) was reported to have an intensity of $0.17 \text{ counts cm}^{-2} \cdot \text{sec}^{-1}$ in the 1.5-3 keV band. Several attempts by various workers to observe this source (Peterson et al 1968, Lewin et al 1968, MacGregor et al 1970) subsequently did not meet with success. The data obtained by us, as can be seen from figure 2.4a, also indicates that this source was not observable above the background level, thus yielding only upper limits for this source in various energy bands (see table 2.3). All the observations indicate that Cen X-1 also belongs to the same class of transient sources as Cen X-2 and Cen X-4. If this is true we wish to draw the attention to the fact that Centaurus Constellation has been the scene of at least three major transient nova-like X-tars.

Table 2.3 : Upper Limits of flux from Cen X-1
(at 2σ level)

Energy Range (keV)	Upper limits (Photons $\cdot \text{cm}^{-2} \cdot \text{sec}^{-1} \cdot \text{keV}^{-1}$)
2.1 - 5.1	1.40×10^{-2}
5.1 - 8.7	0.95×10^{-2}
8.7 - 18.0	0.52×10^{-2}

2.2.4. CEN X-2:

Even though Cen X-2 was the first reported spectacular transient X-ray source with a nova like character, it is one of the least understood. This source was first discovered on April 4, 1967 by Harries et al (1967) when it had an intensity of ≈ 0.8 times that of Sco X-1 in the energy band 2-8 keV. It presumably reached its peak intensity around April 10, after which it decayed to about a quarter of its peak value by 25th April 1967, within a period of about 15 days. On September 28, 1967 Chodil et al (1968) were unable to detect this X-tar above the background level which fact was confirmed by a rocket flight on July 12, 1968 by Pounds et al (1969). Subsequently, rocket flights by Rao et al (1969) on November 3 and 7, 1968 showed a resurgence of this source indicating that the source had a recurring nova type character. However, MacGregor et al (1970) who had a flight barely 24 hours after the PRL flight could not confirm this.

Cen X-2 was also in the detector field of view of the present flight. The data (figure 2.4a) shows that on December 7, 1969 the intensity of the source was definitely below the limit of detection of the present instrument which is consistent with the results obtained from Uhuru survey (Giacconi et al 1973a). Consequently, we can again derive only the upper limits for this source which is given in Table 2.4.

Table 2.4 : Upper limits of X-ray flux from Cen X-2 in different energy bands (at 2 σ level)

Energy range (keV)	Upper limits (Photons $\text{cm}^{-2} \text{sec}^{-1} \text{keV}^{-1}$)
2.1 - 5.1	3.6×10^{-2}
5.1 - 8.7	2.4×10^{-2}
8.7 - 18.0	1.3×10^{-2}

The low energy observations of this source made at different times are tabulated in table 2.5.

Table 2.5 : Low energy observations of Cen X-2

Flight Date	Energy, 2-5 keV ($\times 10^{-8} \text{ erg.cm}^{-2}.\text{sec}^{-1}$)	Reference
October 8, 1965	< 0.25	Grader et al (1966)
April 4, 1967	11.0 ± 1.0	Harries et al (1967)
April 10, 1967	16.0 ± 1.0	Cooke et al (1967)
April 20, 1967	7.5 ± 1.0	Francey et al (1967)
May 28, 1967	2.6 ± 0.4	Chodil et al (1967)
September 28, 1967	< 0.3	Chodil et al (1968)
June 12, 1968	< 0.1	Pounds (1969)
November 3, 1968	$0.68 \pm .08$	Rao et al (1969)
November 7, 1968	$0.23 \pm .14$	Rao et al (1969)
December 7, 1969	$< .07$	Present experiment

2.2.5. DISCUSSION:

Out of the total number of about 170 X-ray sources discovered so far, possibly six of these can be included in the category of nova like X-ray sources. Table 2.6 lists these sources along with their position coordinates and main properties. Out of these five sources, Cen X-2, Cen X-4 and Lup X-2 have been studied in detail by various workers (Francey et al 1967, Rao et al 1969, Evans et al 1970, Rao et al 1971, Matilsky et al 1971, Giacconi et al 1973a and Ulmer et al 1973b). The X-ray source Cet X-2 which was first reported by Shukla and Wilson (1970) has not been observed since then. Since, the continuous Uhuru survey which started later, did not report any source at the position of Cet X-2, the observation of Shukla and Wilson, if accepted, leads us to the conclusion that this source should have also been a transient source. Recognising that the source position was quite favourable to have an observable effect on lower ionosphere, the VLF data at Ahmedabad was searched to confirm the hypothesis. The details of this ground based method are described in Chapter IV. The VLF records clearly indicate the signature of such an effect due to presence of Cet X-2 source coincident with the time of rocket observation of Shukla and Wilson. A careful observation of subsequent records show that the strength of the source steadily decreased with time decaying to $\leq 1/15$ th of Sco X-1 brightness approximately two months after its first sighting. From an extrapolation of the decay curve we estimate that the

TABLE 2.6 - TRANSIENT X-RAY SOURCES

Source	R.A. Decln.	l II, b II	Spectral Character	Peak intensity (2-10 keV) and eruption date ergs. $\text{cm}^{-2} \cdot \text{sec}^{-1}$)	Duration
1. Cen X-2	$13^{\text{h}} 56.0^{\text{m}}$; $-62^{\circ} .5$	$306^{\circ} .0$; 0.0	Exponential with $KT \sim 3.6 \text{ keV}$, $T \sim 4.6 \times 10^7 \text{ K}$ or power law with $\alpha = 1.4$	1.8×10^{-7} on 20-30 March 1967 (extrapolated)	Seen for ~ 50 days but not scanned for 17 months prior to first observation. Extrapolation shows a life time ~ 100 days.
2. Cen X-4	$14^{\text{h}} 56^{\text{m}}$; $-32^{\circ} .2$	$332^{\circ} .0$; $23^{\circ} .1$	Exponential Spectra. On Aug. 7, it was having $KT \sim 7 \text{ keV}$ or $T \sim 8 \times 10^7 \text{ K}$	5.0×10^{-7} erupted on 6-9th July 1969	Seen for ~ 80 days
3. Cet X-2	$2^{\text{h}} 14^{\text{m}}$; $4^{\circ} .55$	$159^{\circ} .10$ $-52^{\circ} .5$	Exponential, KT $\sim 7 \text{ keV}$, $T \sim 8$ $\times 10^7 \text{ K}$	1.4×10^{-7} erupted some where around 30 Nov. 1969	Seen only in one experiment. Ionospheric data shows that it had an intensity 1/15th of Sco X-1 for ~ 90 days.
4. 3U 1543-47 (\neq Lup X-2)	$15^{\text{h}} 43^{\text{m}}$; $-47^{\circ} .6$	$330^{\circ} .94$; $5^{\circ} .37$	Power law with $\alpha = 3.0$ or exponential with $T \sim 2 \times 10^7 \text{ K}$	3×10^{-8} erupted around 17 Aug. 1971 $\sim 10^{-8}$	Seen for ~ 200 days
5. 3U 1735-28	$17^{\text{h}} 35.8^{\text{m}}$; $1^{\circ} .56$	$359^{\circ} .57$; $1^{\circ} .56$	--	$\sim 10^{-9}$ (in 7-20 keV)	Observed for one week during March 1971. Not seen in April with upper limit of $10^{-9} \text{ ergs. cm}^{-2} \cdot \text{sec}^{-1}$ Observed for ~ 20 days.
6. Ceph X-4	$21^{\text{h}} 37^{\text{m}}$ $56^{\circ} .78$	$98^{\circ} .96$ $3^{\circ} .4$	Exponential or blackbody with $KT = 3.87$ & 195 keV respectively	$\sim 10^{-9}$ (in 7-20 keV)	

: 2.22

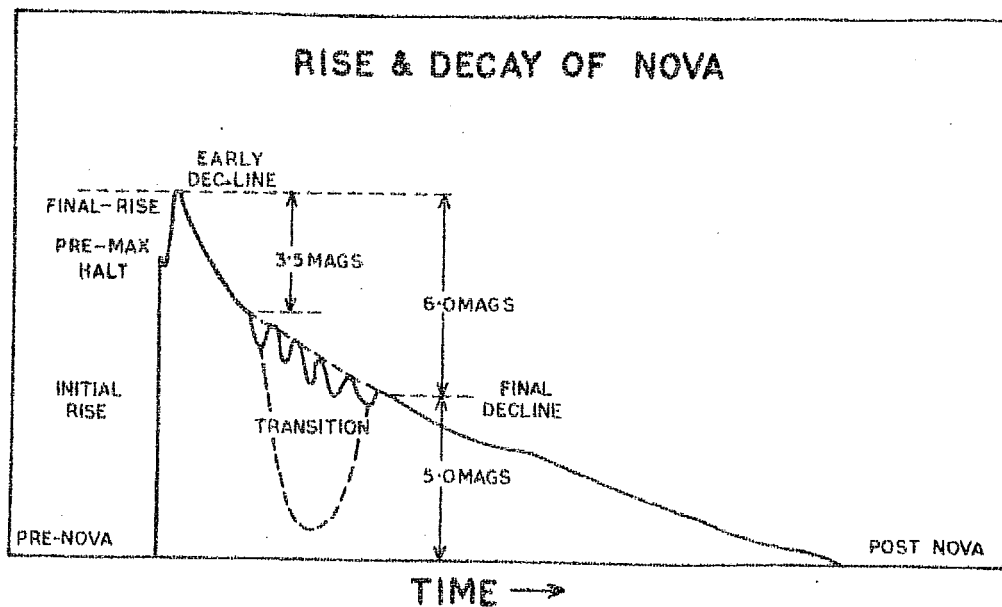


FIG. 2.6. THE FIGURE SHOWS THE SCHEMATIC TIME PROFILE OF OPTICAL LUMINOSITY OF A NOVA. THE X-RAY TIME PROFILE SEEN IN CASE OF X-RAY SOURCE CEN X-4 (HORIZONTAL SCALE IS EXPANDED) IS VERY SIMILAR TO THE OPTICAL PROFILE.

total duration of the source was ~ 90 days when the source strength decreased to $\leq 10^{-9}$ ergs.cm $^{-2}$.sec $^{-1}$ in the 2-8 keV region. The fifth source in the table i.e. 3U 1735-28 was also discovered by Uhuru (Kellogg et al 1971, Giacconi et al 1973a) and was observed for about a week during March, 1971. Even though very little observational data exists for this source, available evidence (Giacconi et al 1973a) points out that the source must have decayed to $\leq 8.5 \times 10^{-10}$ ergs.cm $^{-2}$ sec $^{-1}$ in April 1971. The last source included in the table was first reported by Ulmer et al (1973b) from observations using the detectors on board OSO-7 satellite. The observations of the source have been reported only above 7 keV. However, since the X-ray light curve observed by them indicates that it may be a binary source, further observations are necessary to establish the true nature of this source.

In spite of the nonavailability of detailed data for most of the sources (see table 2.6) some broad features of this class of sources can be listed.

- 1) The most significant characteristic of these sources is that they erupt into sudden brightness, reach a maximum in a few days and then decay more or less exponentially. One often observes short period fluctuations superimposed on the smooth decay profile. The general behaviour of such sources is very much comparable to the typical optical nova whose characteristic light curve is shown schematically in figure 2.6.

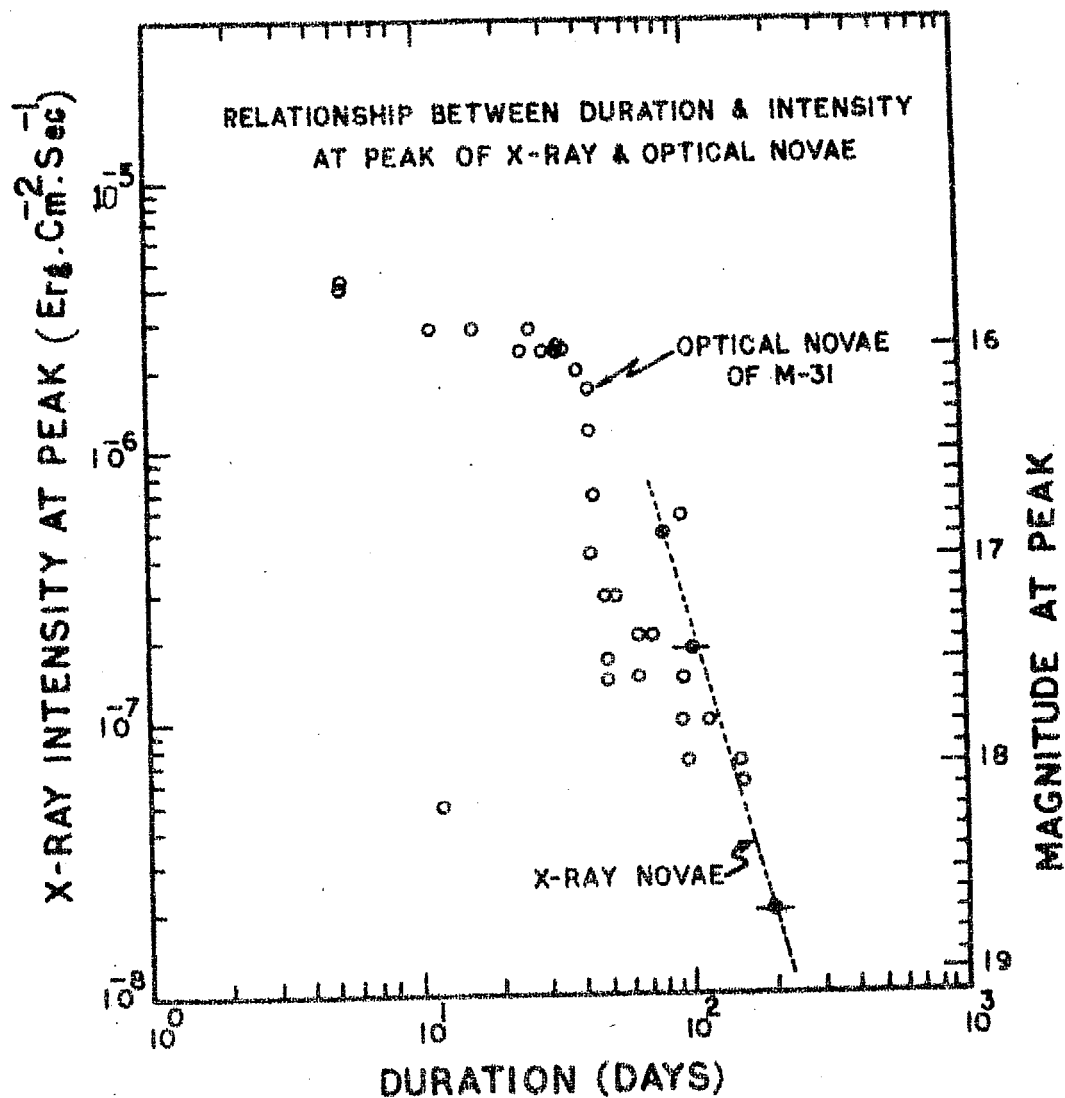


FIG.2.7: COMPARISON OF DURATION VS PEAK INTENSITY OF X-RAY NOVAE IS MADE WITH THOSE OF OPTICAL NOVAE IN M-31.

The detailed comparison of the rise and decay characteristics of the X-ray novae with those of optical novae may be seen in figures 2.7 and 2.8. It is quite well established that in case of optical novae, the brighter the novae (i.e. lesser the magnitude) at the peak, the slower is the rise time and the period of the decay. Examination of figure 2.8 shows that the same qualitative feature holds good for X-ray nova also. The peak brightness of Lup X-2 is much less than that of Cen X-2 and Cen X-4 whereas it shows a much longer time of decay. For a quantitative comparison we define the decay time as the time required to decay from maximum brightness to $\leq 10^{-9} \text{ ergs.cm}^{-2}.\text{sec}^{-1}$ (2-10 keV). The limit of $10^{-9} \text{ ergs.cm}^{-2}.\text{sec}^{-1}$ being the practical limit of detection of X-ray source above the cosmic background level. In figure 2.7 the decay time of optical novae is plotted against the peak X-ray intensity which clearly shows that lesser the peak magnitude (or brighter the novae) shorter is decay time. For comparison the observed brightness of optical novae (Arp, H. 1956) is also plotted. The similarity between the two kinds of sources for the relationship between emission at peak and decay time is remarkable.

2) Almost all the sources of the category seems to exhibit basically an exponential spectra. Assuming the X-ray source to be isothermally hot thin plasma, the temperature of the source can be deduced from

$$\epsilon(E) = A. e^{-E/kT} \text{ ergs. cm}^{-2}.\text{sec}^{-1}$$

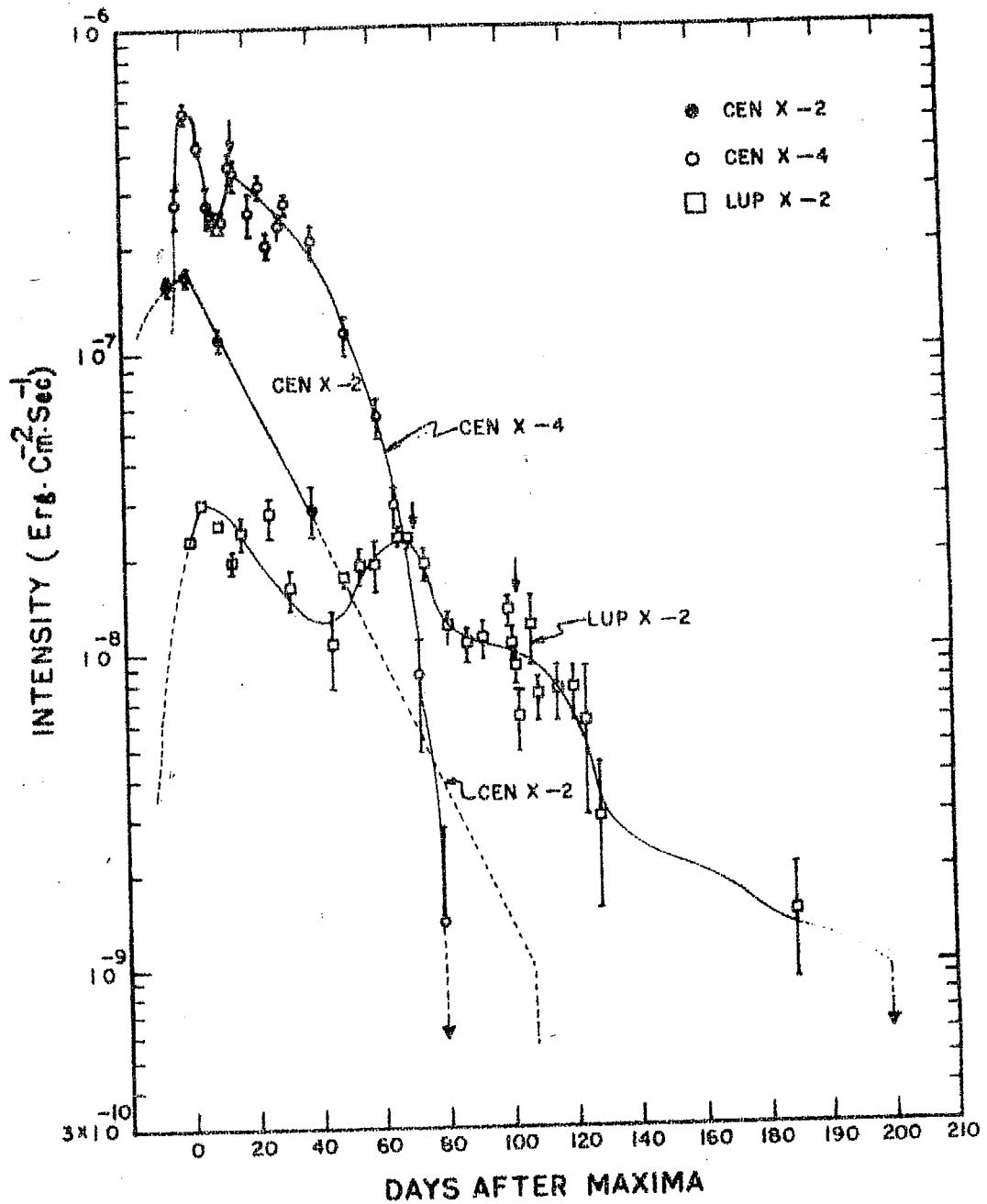


FIG.2.8: COMPARISON OF LIFE HISTORY OF X-RAY EMISSION OF NOVA LIKE X-RAY SOURCES.

Figure 2.9 shows the temperatures observed for Cen X-2 and Cen X-4 sources derived using the above method and utilizing the available observations (Evans et al 1970). It is clear from the figure that Cen X-2 showed a steady decline in temperature during the decay indicating a monotonic cooling of the plasma from ≈ 4.2 to $.6 \times 10^7$ °K (Chodil et al 1968) in about 44 days. During the corresponding period the intensity in the 2-8 keV region also declined by a factor of five. Cen X-4 source, on the other hand, showed sharp decrease in temperature from $>16 \times 10^7$ °K to $\approx 5 \times 10^7$ °K from eruption to ~ 6 days in the decline phase after the maximum. During the decay, whereas the energy flux steadily declined the temperature seems to remain practically constant. The behaviour of Lup X-2 also seems to be more or less similar to that shown by Cen X-4 in that no change in the spectral index or temperature were observed (Matilsky et al 1971) except during short periods of time.

3) Superimposed on the steady decay, irregular fluctuations in both intensity and spectrum are **often** observed for short periods of time. This feature is clearly seen in figure 2.8 in which we have compiled a number of observations. The short period fluctuations in the life time of the source are clearly observed from figure 2.5 where detailed spectral observation of Cen X-4 are plotted. The hardness ratio which is a measure of the change in spectral shape also changes quite considerably during the periods when the source exhibits short duration fluctuations (Evans et al 1970). As for example

the temperature of the emitting plasma on August 20, 1969 went upto $kT \approx 10$ keV as compared to the normally observed value of $kT \approx 6$ keV during steady period. This conclusion is further supported by Uhuru observations on Lup X-2 which show a positive indication of the changes in the temperature of the emitting region (Matilsky et al 1972) on October 25, 1971; and November 25, 1971. These short period excursions are indicated by arrows in figure 2.8.

(4) None of the X-ray nova discovered so far have been identified with any optical counterpart.

Due to the incomplete X-ray data and solely negative optical information available at the present time a meaningful detailed interpretation of the physical nature of these sources is difficult. However some rough estimates of the size of the source and such other physical parameters can still be made. The fact that the sources of this type show fluctuations typically having a time scale of the order of ≈ 1 hour in their emission, can be used to estimate their sizes. Generally speaking the time scale of fluctuations can be estimated by

$$P \geq (G \cdot \bar{\rho})^{-\frac{1}{2}}$$

where G is the gravitational constant and $\bar{\rho}$ the mean density of the object. Substituting 1 hour for P we find that $\bar{\rho} \geq 1.5 \text{ gm.cm}^{-3}$ which is equivalent to that observed in the sun. In other words sources of this type probably have dimensions of the same order as that of the sun.

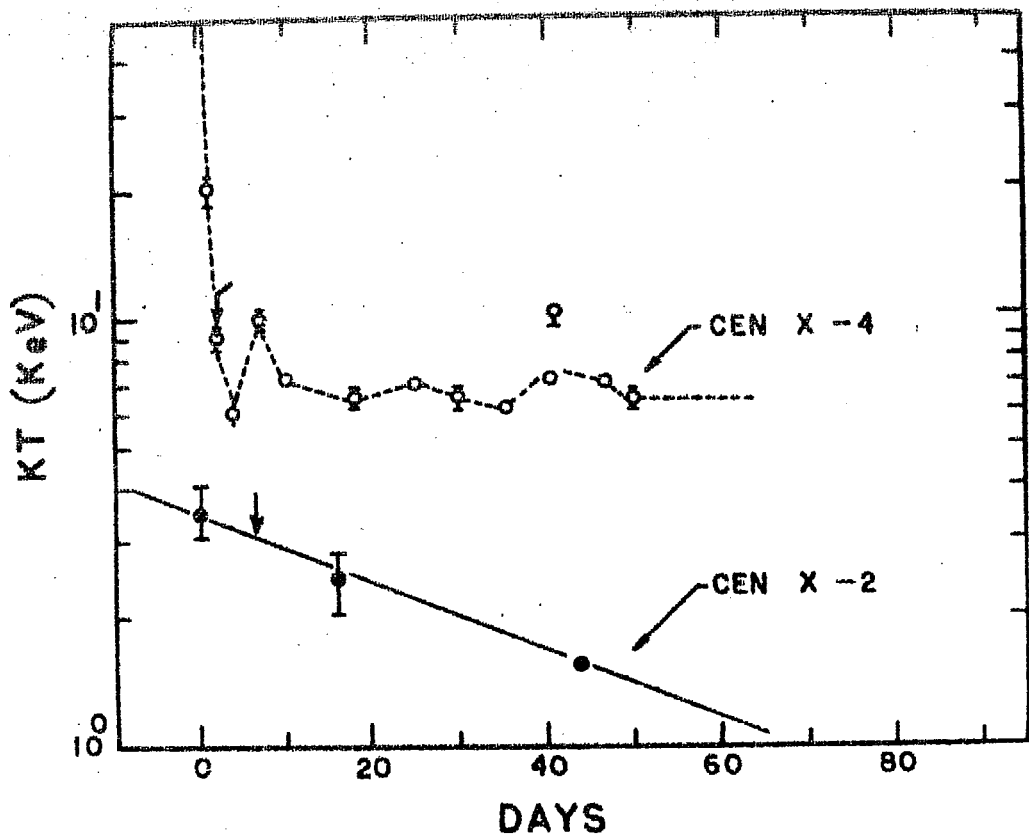


FIG.2.9. VARIATION OF TEMPERATURE OF EMITTING PLASMA OF NOVA LIKE SOURCES CEN X-4 AND CEN X-2.

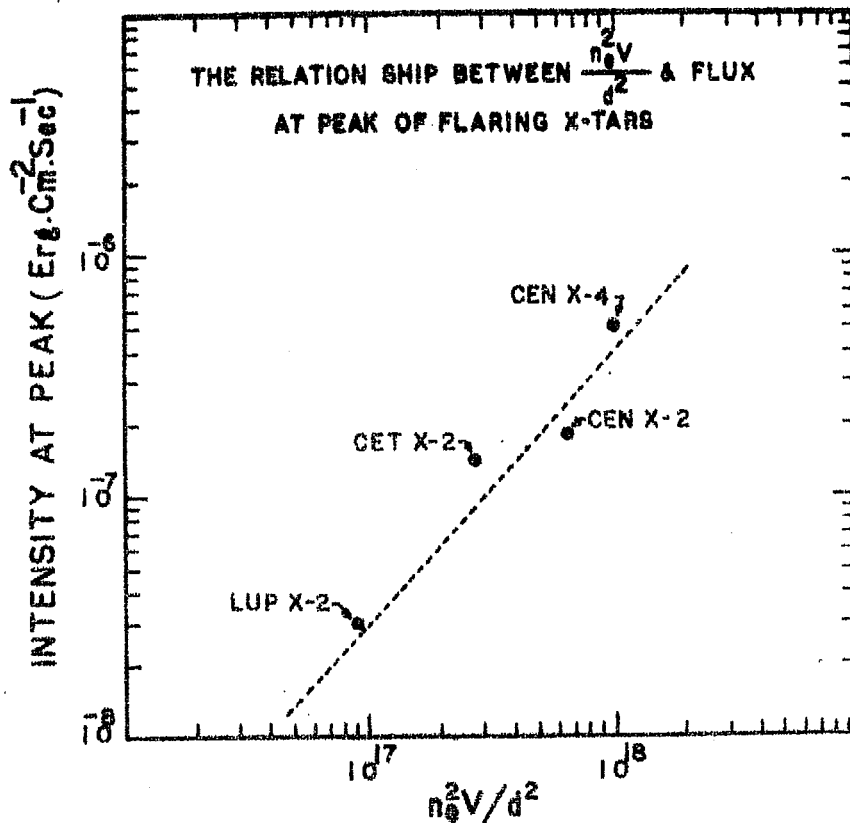


FIG.2.10. SHOWS THE RELATIONSHIP BETWEEN $n_e^2 V / d^2$ AND FLUX

The exponential nature of the energy spectra of X-ray emission observed for these nova like X-tars, leads us to believe that the X-ray emission in these stars is due to an isothermal thin plasma in which case the flux radiated could be represented by:

$$j(E) \cdot dE \text{ (keV)} \approx 10^{-28} \cdot \frac{N_e^2 \cdot V}{d^2} \cdot \sqrt{T} \cdot \frac{e^{-E/kT}}{kT} dE \text{ ergs.cm}^{-2} \cdot \text{sec}^{-1}$$

where the terms have usual meaning. The estimates of $\frac{N_e^2 \cdot V}{d^2}$ for average energy interval dE of 2-10 keV at the peak intensity are shown in table 2.7 and figure 2.10. It can be seen that $\frac{N_e^2 \cdot V}{d^2}$ is larger if larger is the intensity at peak. Since none of these stars have been identified with an optical candidate, for our rough estimates we may assume that the failure in tracking these stars optically is essentially dictated by the limit of optical intensity observable from the earth (max magnitude observable = +5 absolute magnitude) which means that the distance of these sources is at least of the order of ≈ 1 kpc. Using the distance $d = 1$ kpc, values of N_e have been calculated which are also shown in table 2.7.

The striking similarity between the optical time profiles of novae and the X-ray time profiles of this class of transient sources suggest that the theories which have been evolved to explain the optical novae outburst may contain a significant clue to the mechanism of X-ray production, emission and time profile of the transient X-ray sources.

Table 2.7- The parameter $\frac{Ne^{2.V}}{d^2}$ for various flaring stars at their peak intensity are shown

Source	Peak intensity $\text{ergs.cm}^{-2} \text{ sec}^{-1}(2-10 \text{ keV})$	$\frac{Ne^{2.V}}{d^2}$	Ne^* (cm^{-3})
Cen X-2	1.8×10^{-7}	6.5×10^{17}	1.65×10^9
Cen X-4	5×10^{-6}	1×10^{18}	3.6×10^7
Cet X-2	1.4×10^{-7}	2.7×10^{17}	1.9×10^7
Lup X-2	3×10^{-8}	9×10^{16}	1.1×10^7

* A typical distance of $d \approx 1 \text{ kpc}$ and $R \approx 7 \times 10^{10} \text{ cm}$ are assumed.

Even though the model tries to explain some of the detailed features observed in the time profile of the transient X-tars, it is still very qualitative and speculative. Without further detailed observations on the behaviour of such sources it is clearly not possible to propose elaborate and more qualitative models. Edwards (1967) proposed a model as early as 1967, just to explain the decay phase which assumes the emission as due to an adiabatic shock wave propagating outward. Even though this model qualitatively accounts for the time profile of Cen X-2, it is neither complete nor can explain the detailed features such as oscillations and change of spectra observed for this class of sources. With the discovery of a larger number of these sources and further observation, it is now possible to at least think of more elaborate models. It is now generally believed that these

X-tars accrete hydrogen rich mass at a constant rate from the red component of a close binary system (e.g. Rose, 1968). The constant addition of hydrogen to the envelope of the star results in the enhancement of energy generation due to the increased hydrogen burning which takes place in a thin, non-degenerate shell and at this stage the X-ray emission may start. When the burning reaches a luminosity $L \geq 15 M_{\odot}$ the hydrogen shell source probably becomes thermally unstable and at this stage the burning continues to rise independent of mass accretion with a folding time of ≈ 2 days. This may be compared with the build up time ≈ 2 days observed for Cen X-4. Due to the very high rate of nuclear energy generation the star becomes pulsationally unstable and the outer envelope starts expanding which might ultimately result in an explosion and consequent emission of a large amount of energy ($\sim 10^{42-44}$ ergs.sec⁻¹). The fluctuations often observed during the declining phase of these sources may be due to the side lobes in the decay of pulsations.

2.3. SOURCE IN NORMA/LUPUS CONSTELLATION:

The broad peak shown in figure 2.4a around the spin azimuth 140° - 160° is identified with the sources Nor X-2 and Lup X-1. The separation between these two sources is not clear from the records due to the larger field of view of our collimator ($6.5^{\circ} \times 15^{\circ}$ FWHM perpendicular and along the rocket axis) and the close azimuthal proximity of the sources, the separation between them being $\approx 4.5^{\circ}$. The two sources

: 2.33:

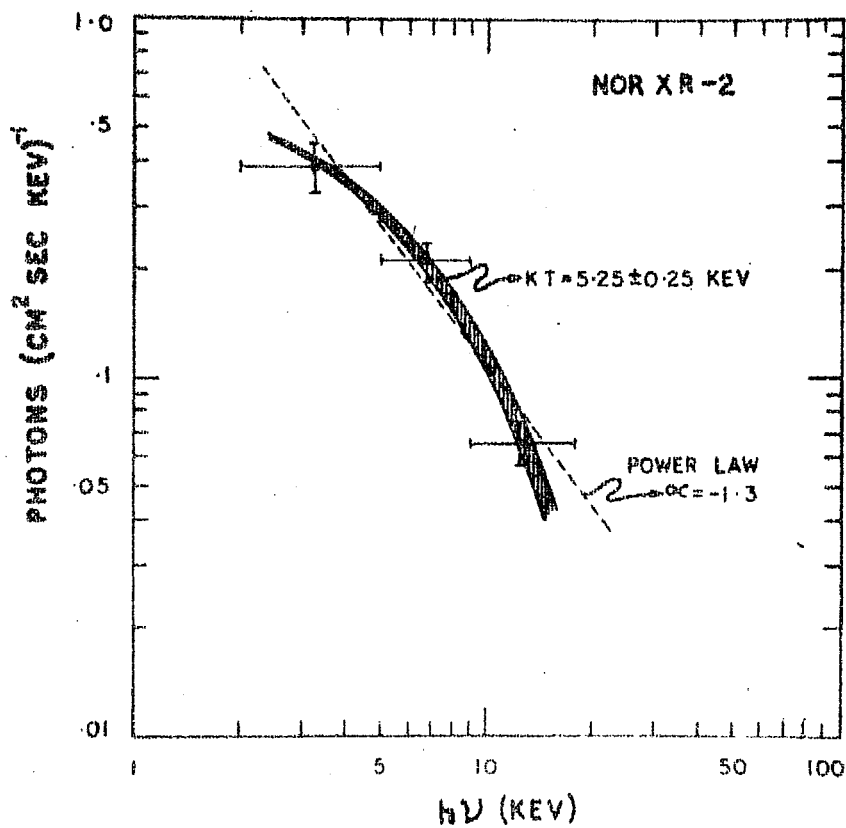


FIG. 211 - THE SPECTRUM OF THE X-RAY SOURCE NOR X R-2. THE EXPONENTIAL FIT AS WELL AS THE POWER LAW FIT ARE SHOWN.

Nor X-2 and Lup X-1, at the time of our observation were situated away from the detector normal at a distance of 8° and 3° respectively. Thus we are in a more favourable position to observe Lup X-1. However, as can be seen from figure 2.4a the observed peak is shifted towards Nor X-2. Since the azimuthal position of any source could be determined in our experiment to an accuracy better than $\approx .5^\circ$, we are led to attribute the peak intensity to mainly the X-ray source Nor X-2. Regarding source Lup X-1 the data indicates that either it is absent or, being a variable source, its intensity is in its low phase at the time of our observation.

By convoluting with the triangular response of the collimator, the source flux in the various energy bands have been calculated to derive the spectral characteristics of the source. The best fit spectra for Nor X-2 is found to be an exponential which can be expressed as:

$$\frac{dN}{dE} = 0.75 \exp(-E/5.25) \text{ photons cm}^{-2} \cdot \text{sec}^{-1} \cdot \text{keV}^{-1}$$

Implying a temperature of about 6×10^7 °K. Figure 2.11 shows the observed data points with the best fit exponential spectrum. The poor statistics however do not preclude the possibility of the spectrum being a power law with a spectral index of $\alpha \approx -1.3$ which is also shown in the same figure. The number of photons emitted in the 2-10 keV region is

$$\approx 2.0 \text{ photons cm}^{-2} \cdot \text{sec}^{-1} \text{ corresponding to an intensity } 1.75 \times 10^{-8} \text{ ergs.cm}^{-2} \cdot \text{sec}^{-1}.$$

2.3.1. DISCUSSION:

All the low energy observations of Nor X-2 made at different epochs are summarised in table 2.8 and plotted in figure 2.12. Figure 2.13 also includes the observations made at hard X-ray energies. From the low energy observations one can notice that the source spectrum as well as the intensity (figure 2.14) show large variability (Cooke et al 1971, Harries et al 1971, Cruddace et al 1972 etc.). Whereas the X-ray flux changes by factors as large as ≈ 6 , the temperature of the source derived under the assumption of an exponential spectrum shows variations from $kT \approx 4$ keV to $kT \approx 11$ keV. The existence of such a large variability has also been confirmed by Uhuru observations (Giacconi et al 1973a) which have shown intensity variations in the 2-6 keV energy band by as much as factor of ≈ 36 in extreme cases. Further OSO-7 observations (Peterson, private communication) indicates that the high degree of variability is not confined to only low energies but also extends to higher energies all the way from few keV to 100 keV.

In addition to the highly variable and complex behaviour of the source the possible existence of short time periodicities have also been reported by Margon et al(1971). However, the lack of continued, systematic and well calibrated observations make it extremely difficult to make quantitative inferences on the nature of the source. Nevertheless, the presently available observations clearly indicate the need to make detailed study and observations of these variable sources in order to understand the complex mechanisms that operate

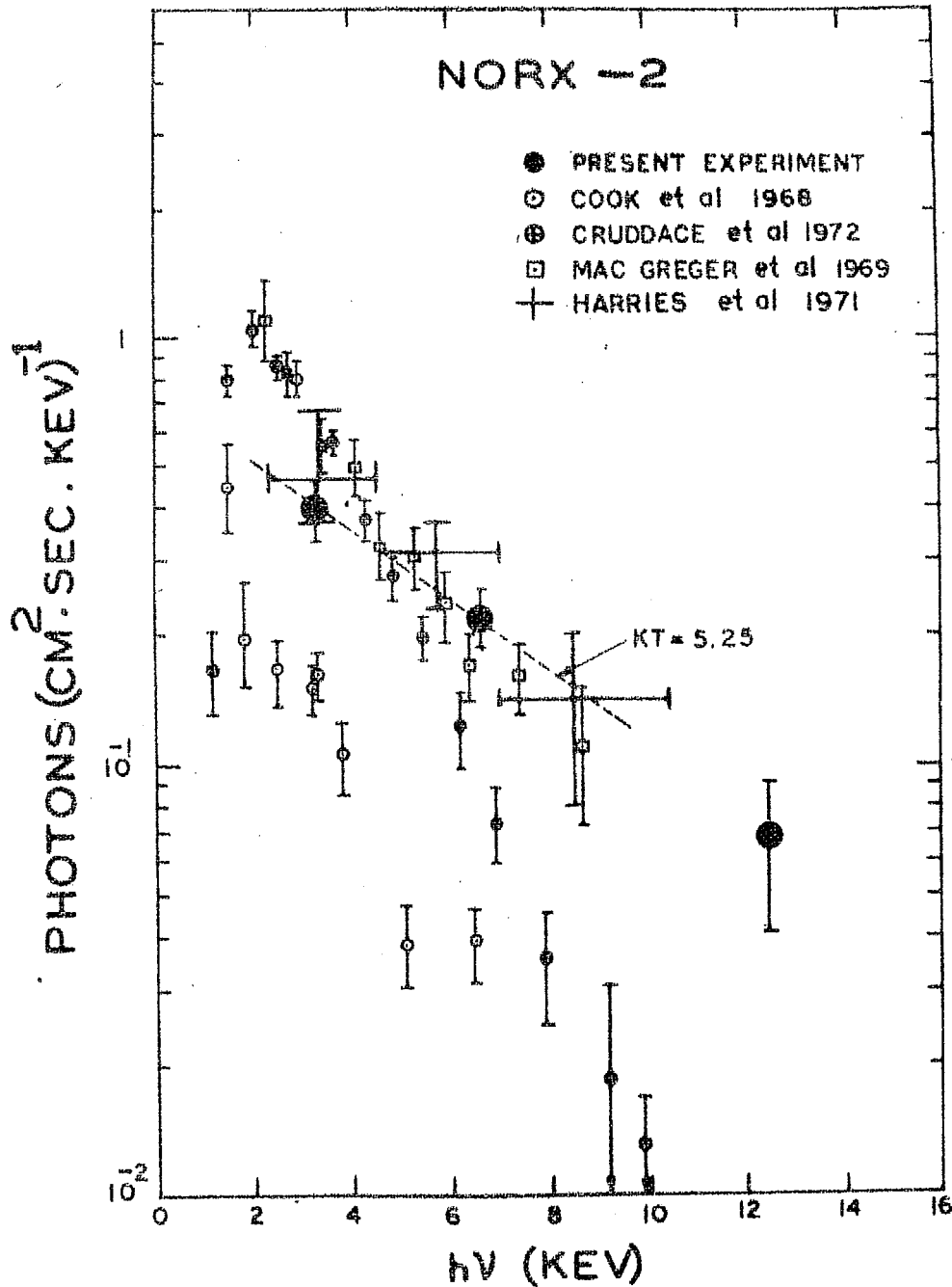


FIG.2.12: THE MEASUREMENT OF PHOTON SPECTRUM OF NOR X-2 IN LOW ENERGY REGION BY VARIOUS WORKERS.

Table 2.8 - Low energy measurements of Nor X-2(420 keV)

Date of observation	Field of view	Flux (2-10 keV) eigs.cm ⁻² .sec ⁻¹	Spectral parameters	Reference
April 25, 1965	8° FWHM	0.5×10^{-8}	--	Friedman et al (1967)
June 12, 1968	4° x 27.5°	$(3.5 \pm .64) \times 10^{-9}$	--	Cooke et al (1971)
Nov. 3, 1968	3° FWHM	$(2 \pm 0.3) \times 10^{-8}$	kT \approx 5 keV	MacGregor et al (1969)
April 1, 1969	4° x 27° .5	$(3.5 \pm .64) \times 10^{-9}$	kT \approx 11.9 keV	Cooke et al (1971)
June 14, 1969	$\theta_1 = 3^\circ \times 12^\circ$ $\theta_2 = 1.6^\circ$ FWHM (two collimators)	$(1.0 \pm .06) \times 10^{-8}$	kT \approx 4.0 keV	Craddock et al (1972)
Dec. 7, 1969	6.5° x 15°	$(1.75 \pm .16) \times 10^{-8}$	kT \approx 5.25 keV	Present experiment
July 10, 1971	3.4° x 35°	$(1.7 \pm .20) \times 10^{-8}$	kT \approx 11 keV	Harries et al (1971)

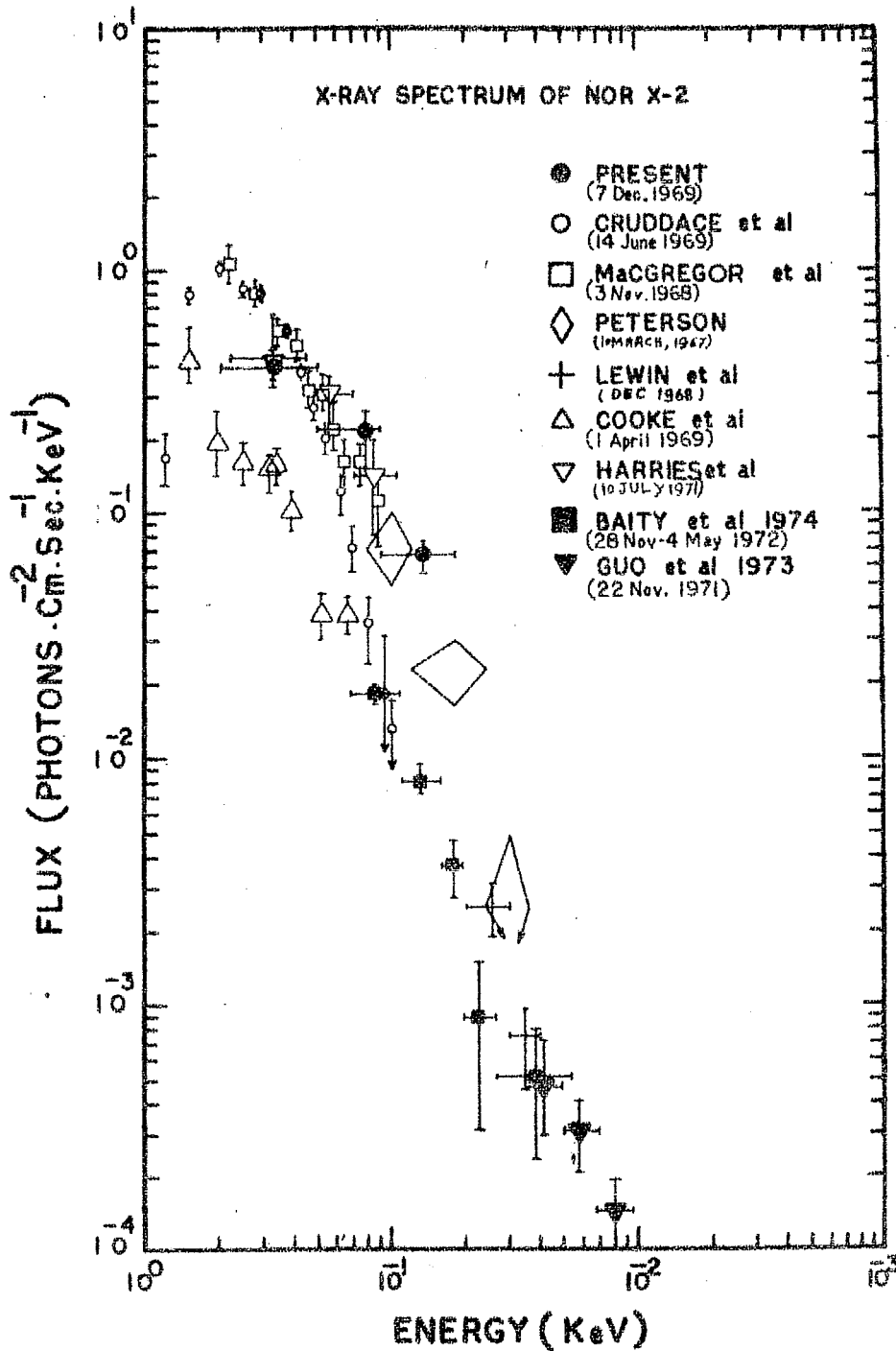


FIG.2.13: THE COMPILATION OF OBSERVATIONS ON NOR X-2.

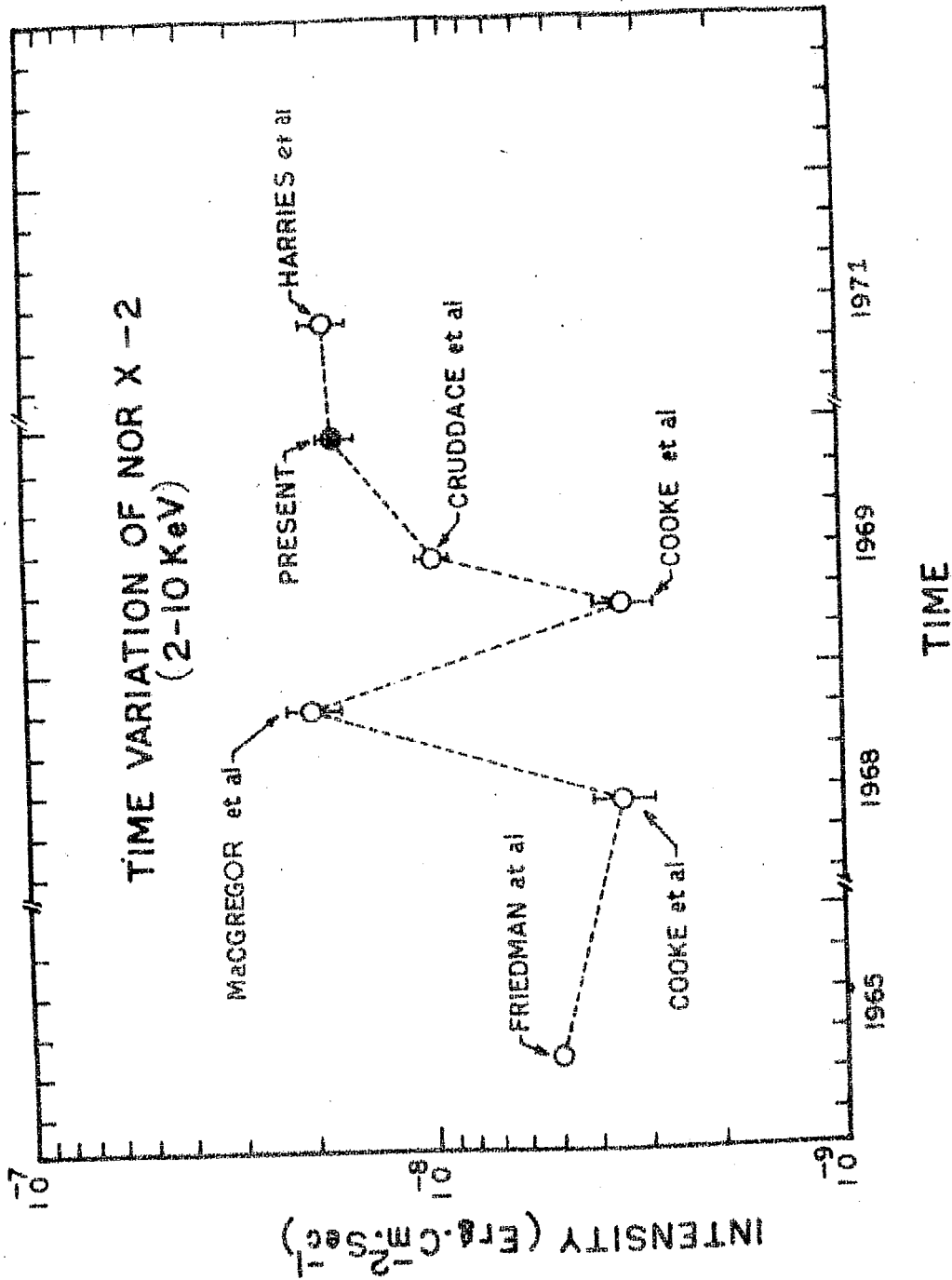


FIG.2.14: THE TIME VARIATION OF INTENSITY OF NOR X-2 IN THE ENERGY RANGE 2-10 KEV.

2.4. DERIVATION OF BACKGROUND SPECTRUM:

A brief description of various methods is presented in table 1.2 in chapter I. The background spectrum for the first time was derived by using earth as the occulting body. The details are presented below:

The earth and its atmosphere will play the role of a shutter blocking the celestial X-rays, whenever the detector views the earth during any part of the rocket spin. The detector registers counts both due to charged particles as well as diffuse X-ray background when it views the celestial sky. The count rate when the detector is facing towards the earth (in ideal cases $Z = 180^\circ$) is only due to the charged particle background. Consequently a comparison of count rate when the detector looks at the earth with the rate when it looks at the sky should provide a reliable estimate of the diffuse X-ray background flux.

The above simple situation exists for rocket observations where small opening angles of the telescope are used. In practice, however, when the zenith angle is not very far from 90° and the detectors have fairly large opening angles, intermediate situations exist. Larger the deviation of zenith angle of the rocket from 90° more complete will be the blocking effect of the earth as a shutter and more reliable will be the estimate of the diffuse background. Hence the effective solid angle has to be evaluated for different portions of the spin azimuth to estimate the background flux.

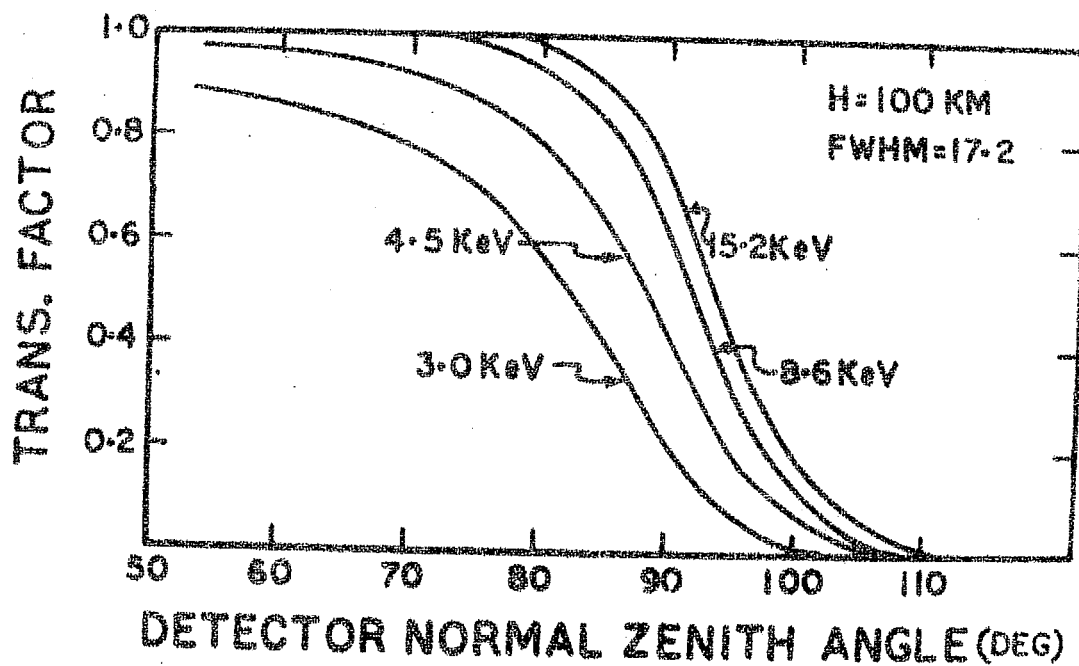


FIG.2.15. THE TRANSMISSION FACTOR CALCULATED FOR THE COLLIMATC OF FLIGHT ON NOV.3, 1968 IS SHOWN.

The geometrical sensitivity of an element of the detector between zenith angle θ and $\theta + d\theta$ is given by,

$$G.F. = \left[1 - \frac{\tan(|Z| - \theta)}{\tan \phi_0} \right] \frac{d\theta}{\phi_0}$$

where Z is the zenith angle of the detector normal and ϕ_0 is the half cone opening angle of the collimator in the vertical plane. The transmission factor through the atmosphere along the line of sight of this element is given by

$$\text{Transs. (Air)} = \exp \left[-\mu(E) \cdot g(\theta) \right]$$

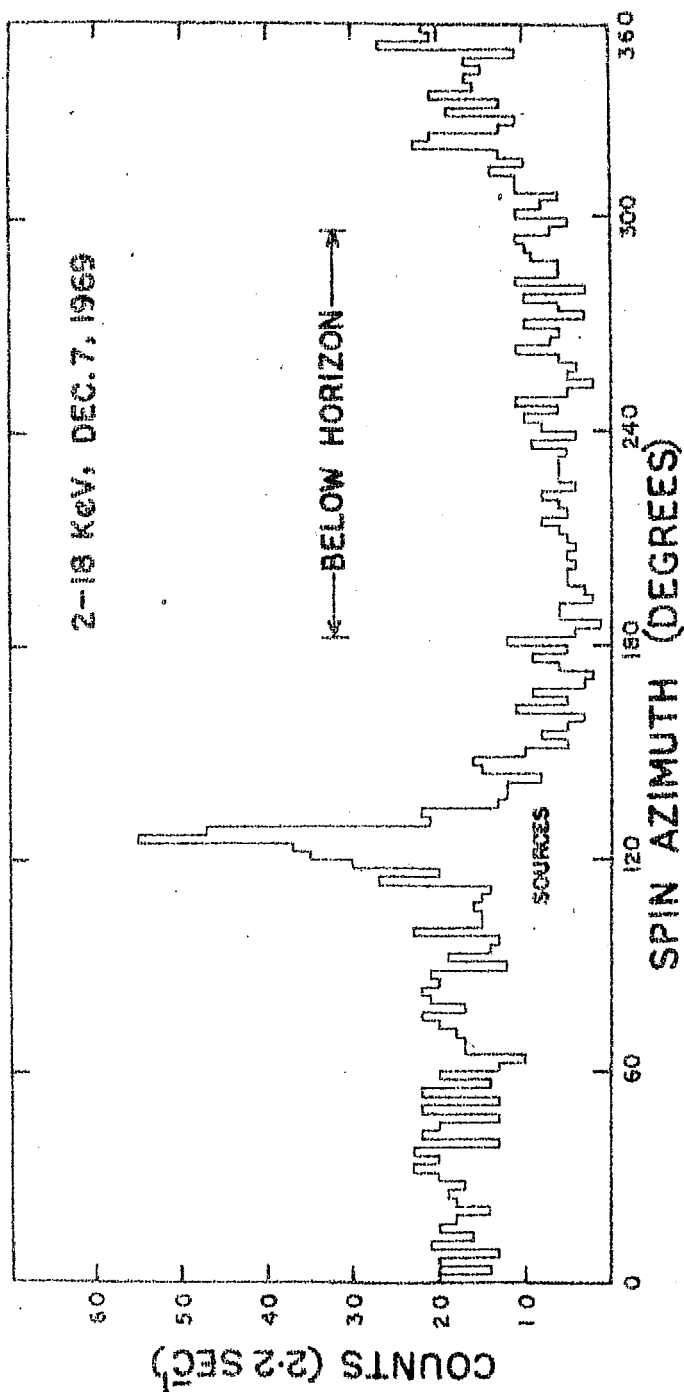
where $\mu(E)$ is the absorption coefficient of air at energy E and $g(\theta)$ is the grammage of air at zenith angle θ . The effective transmission factor of the detector at zenith angle (Z) is then given by equation

$$\text{Transs. (coll.)} = \int_{Z-\phi_0}^{Z+\phi_0} \left[1 - \frac{\tan(|Z-\theta|)}{\tan \phi_0} \right] \cdot \frac{1}{\phi_0} \left\{ \exp(-\mu(E) \cdot g(\theta)) \right\} d\theta$$

The effective transmission factors for different energies have been evaluated using the above formula and are shown for some specific energies in figure 2.15 at a height of 100 kms.

To derive the background spectra the data from the two centaure rocket flights (November 3, 1968 and December 7, 1969) have been used, the elevation of the rocket in two cases being 73° and 64° respectively. The geometrical factors for the detector for isotropic radiation (Kane and Rao 1958) for the two rocket experiments were 2.88 and $1.67 \text{ cm}^2, \text{sr.}$ respectively.

:243:



216a
FIG: COUNTS DEPOSITED IN THE COUNTER WHEN IT SPINNED 360° . THE DATA IS SUPERPOSED FOR A NUMBER OF SPINS AFTER PROPER CORRECTION

1244:

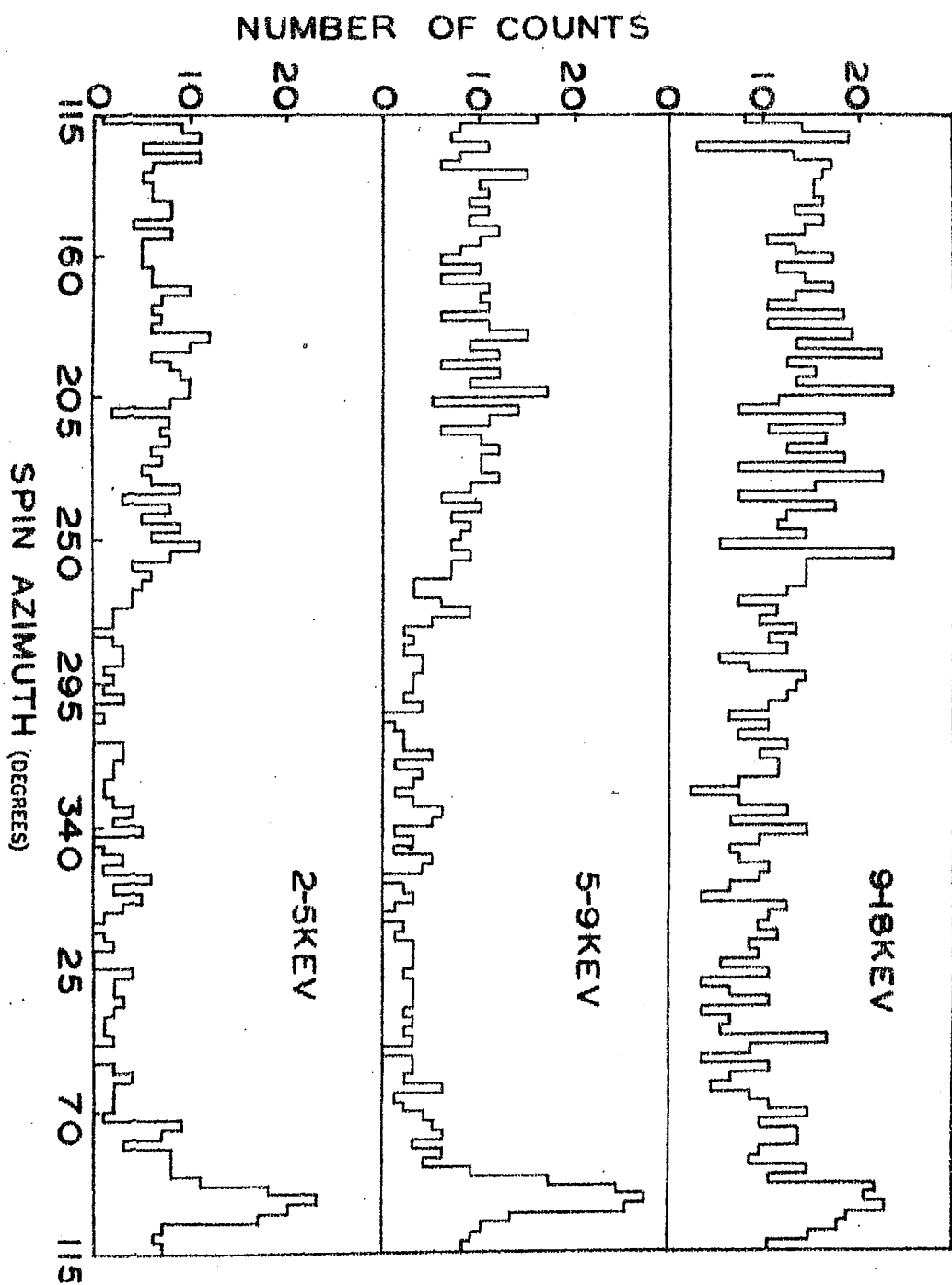


FIG. 2.16. THE COUNTS DEPOSITED IN THE COUNTER IN VARIOUS AZIMUTHAL DIRECTIONS ARE

Figure 2.16a,b show the plot of the count rate versus spin azimuth during the rocket flight on December 7, 1969. The difference in the counting rate when it goes from below horizon to above horizon is clearly seen. The absolute photon flux in each differential energy channel after various corrections was derived by the technique described in Appendix A3.

The region of the celestial sky plotted in galactic co-ordinates has already been shown in figure 2.3b. The area for which the background is derived is shaded in that figure. The data from the regions 20° on each side of sun in the azimuthal scan were rejected to avoid any contribution from the albedo flux due to the scattering of solar X-rays. It can also be seen that the area is almost free from contamination due to any strong X-ray source.

The diffuse X-ray background obtained from the data of these two rocket flights are plotted in figure 2.17. The data have been fitted to a power law photon spectrum. The best fit spectrum for the results in the energy range 2-18 keV for the flight November 3, 1968 is given by,

$$\frac{dN}{dE} = 9.0 \pm 2.3 E^{-1.57 \pm 0.13} \text{ photons. cm}^{-2} \cdot \text{sec}^{-1} \cdot \text{sr}^{-1} \cdot \text{keV}^{-1}.$$

A similar fit for the data for flight on December 7, 1969 is given by,

$$\frac{dN}{dE} = 17.5 \pm 3.5 E^{-1.84 \pm .24} \text{ photons.cm}^{-2} \cdot \text{sec}^{-1} \cdot \text{sr}^{-1} \cdot \text{keV}^{-1}.$$

Since the results are derived by the same technique and are almost from the same region of sky. the data from both flights

:2'46:

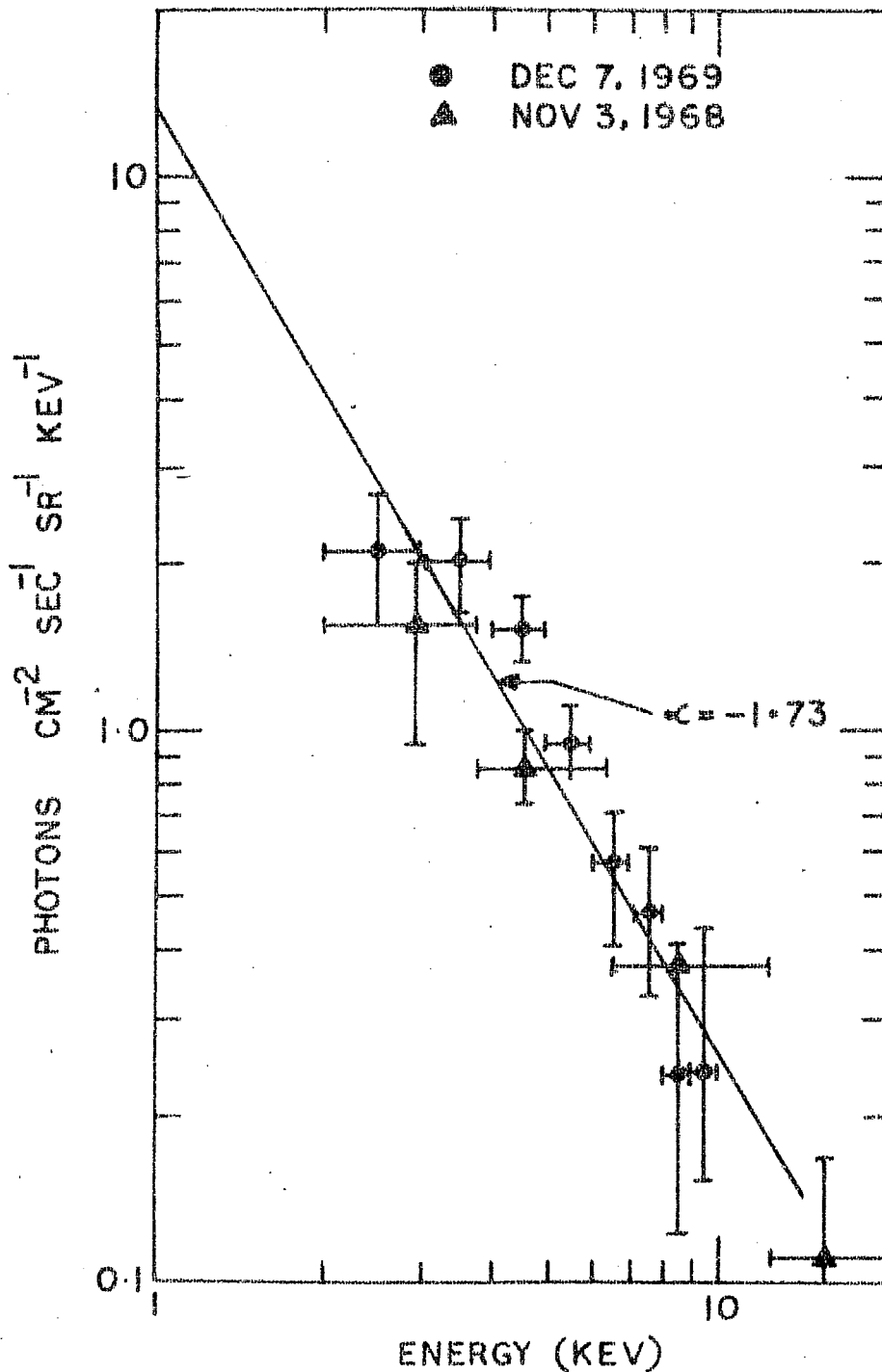


FIG:217 THE PHOTON SPECTRUM MEASURED DURING TWO ROCKET FLIGHTS. THE BACKGROUND X-RAYS ARE OBTAINED BY USING EARTH AS THE OCCULTING BODY. THE SPECTRA FITS AN INDEX = -1.7.

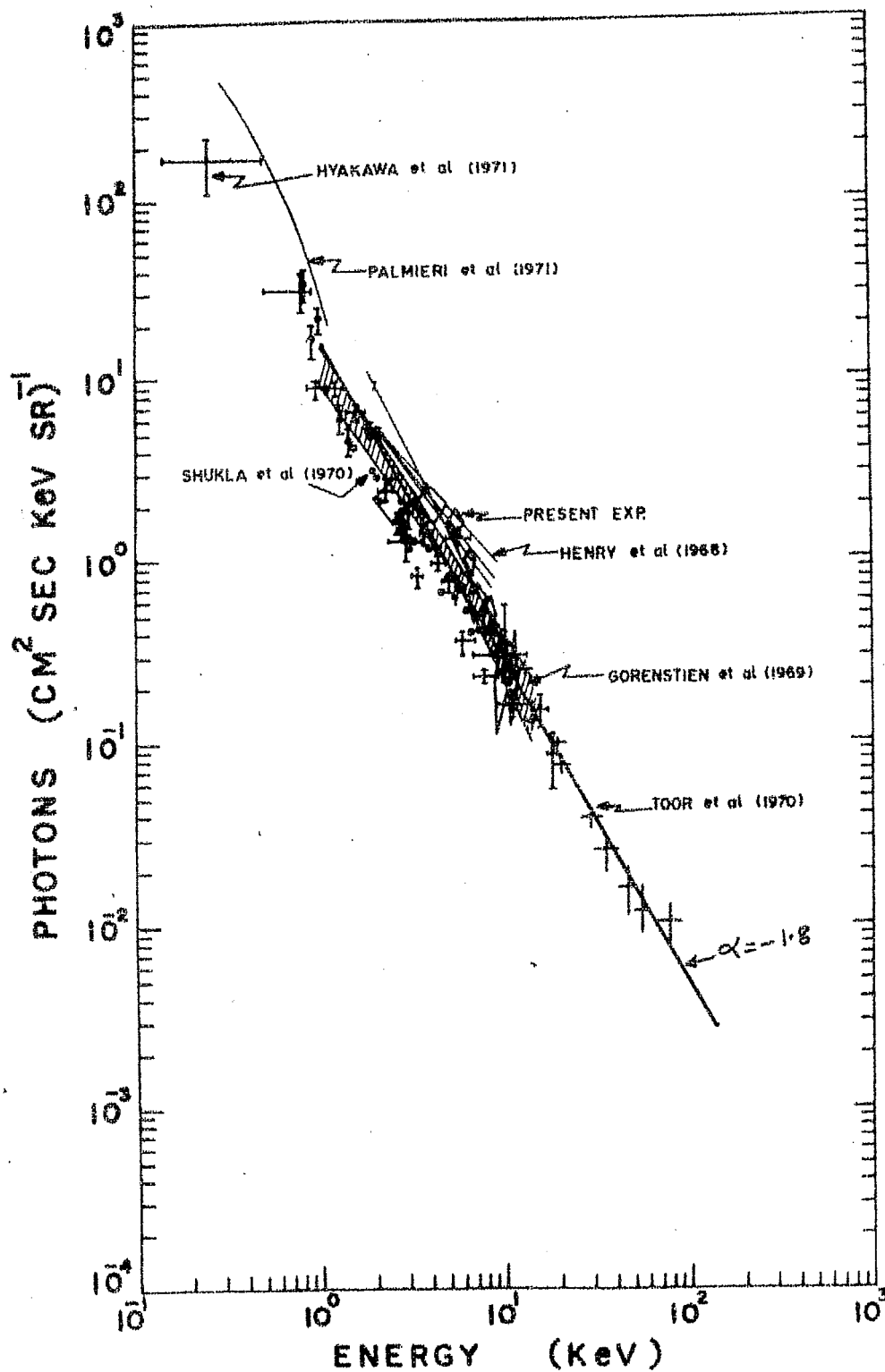


FIG.2.18. THE BACKGROUND X-RAY SPECTRUM OBSERVED UPTO ~ 100 KEV. A SINGLE SPECTRUM WITH $\alpha = -1.8$ REPRESENTS THE SPECTRUM FROM 2 TO 100 KEV.

have been fitted to obtain to give the spectrum,

$$\frac{dN}{dE} = 13.6 \pm 3.8 E^{-1.73 \pm .15} \text{ photon cm}^{-2} \cdot \text{sec}^{-1} \cdot \text{sr}^{-1} \cdot \text{keV}^{-1}$$

These results are consistent with the results obtained by other techniques (see figure 2.18).

The results clearly indicate the effectiveness of the method using the earth as a shutter for deriving the diffuse background flux. With larger area counters used in conjunction with the secondary background rejection techniques, such as the veto counters and pulse shape discrimination, this method of analysis can be very powerful for obtaining an accurate estimation of the diffuse background.

CHAPTER III

BALLOON EXPERIMENT

3.1. INTRODUCTION:

A balloon payload was designed and fabricated with the intention of carrying out some detailed studies on the pulsating X-ray binary Her X-1 and spectroscopic binary Cyg X-1. Cyg X-1 was studied in two balloon flights one on March 29, 1972 and the second on January 18, 1973. The Cyg X-1 source was tracked for about 1 hour and 15 minutes in the first flight and for about 1 hour in second flight. A brief description of all the flights is given in table 3.1. The study of high energy X-ray emission from Her X-1 was conducted on December 28, 1972 and January 18, 1973 and were the first observations of this kind. We give a brief description of the payload and then follow it up with an account of the results obtained and their interpretation.

3.2. X-RAY TELESCOPE

3.2.1. THE DETECTOR:

Figure 3.1 shows the schematic diagram of the detector used in the present balloon flights. The basic sensor used was a 4 mm thick NaI(Tl) crystal having a diameter of 10 cms and an aluminium entrance window of thickness 0.9 mm. The crystal was coupled to the photomultiplier through a pyrex optical window of thickness 10 mms which in addition to reducing the effect of non-uniformity of the photocathode and reduction in background also served as a shield for the beta, gamma radiation from K^{40} . It may be noted that K^{40} is usually

Table 3.1 - Details of various experiments

Date of experiment	Launch vehicle	Place	Max. Altitude	Detector & Area	Collimator FWHM (degree)	Studies made on
7 December 1969 00 35 UT	Centaure Rocket	TERLS	123 km	55 cm ² xenon filled counter with 100 μ thick Be window	6.5 x 15	Cen X-4, Nor X-2 and Diffuse background
29 March 1972 0500 UT	3 million cu. feet balloon	Hyderabad	6.5 gm.cm ⁻² of residual atmosphere	75 cm ² NaI(Tl) with .032" Al window, plastic anti-coincidence shield	18	Cyg X-1 Tracked for 1 hour & 15 minutes
28 December 1972 0510 UT	-do-	-do-	5 gm.cm ⁻²	81 cm ² -do-	13.5	Her X-1 seen for ~11 mts.
18 January 1973 0500 UT	-do-	-do-	4.5 gm.cm ⁻²	-do-	13.5	Her X-1 and Cyg X-1. Her X-1 was tracked for ~15 mts. and Cyg X-1 for ~1 hr.

:3.3:

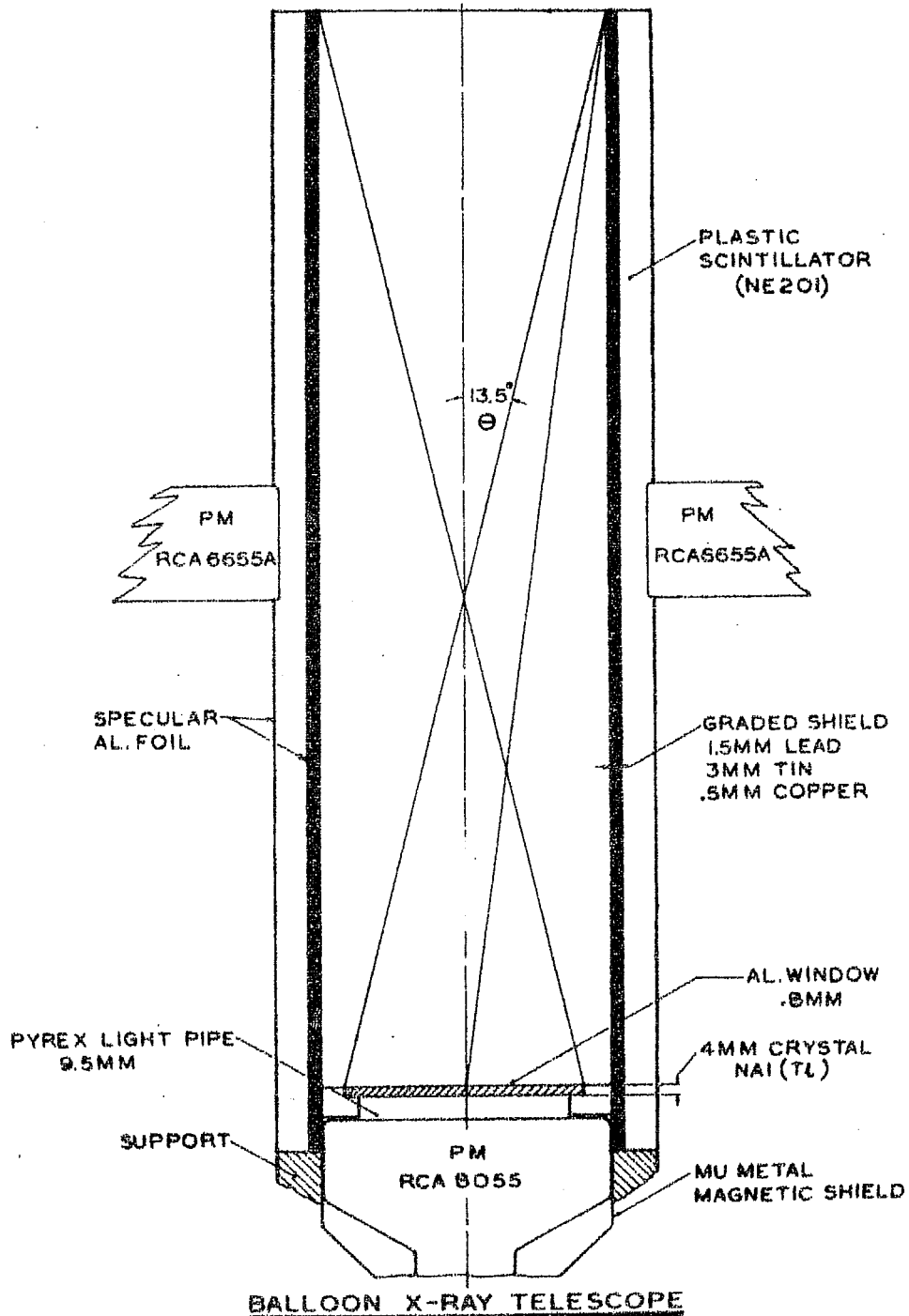


FIG.3.1: THE FIGURE SHOWS THE SCHEMATICS OF THE DETECTOR, COLLIMATOR AND ANTICOINCIDENCE DETECTOR.

contained as an impurity in the photocathode glass. The crystal assembly was coupled with the cathode of the RCA 8055 photomultiplier tube with Dow Corning cement 20-0057. The entire assembly of crystal phototube was enclosed by a magnetic shield of high permeability mu-metal to reduce the effect of the earth's magnetic field. The detector assembly was further enclosed in a graded shield collimator consisting of 1.5 mm thick lead followed by 3 mm thick tin and 0.5 mm thick copper cylinders. The lead shield had adequate thickness to provide $\sim 100\%$ collimation to gamma rays upto about 200 keV. The characteristic X-rays of lead (~ 88 keV) are absorbed by the tin shield, the K-X-ray radiation from which (~ 24.8 keV) is further absorbed by the copper cylinder. Since the energy of K-fluorescence from copper (~ 8.1 keV) lies well below the threshold, they do not vitiate our observations. The collimator had a field of view of 18° FWHM in the first flight and 13.5° FWHM in the other two flights.

As shown in figure 3.1 the cylindrical collimator along with the crystal phototube assembly was further enclosed in a 1.5 cm thick cylinder made of NE 102 plastic scintillator which acts as the veto counter for the detector assembly. Aluminium foil wrapped round the plastic scintillator acts as a specular reflector thereby increasing the light collection efficiency. Two 2" photomultiplier tubes (RCA 6655 A) viewing from the centre of the plastic cylinder were used to collect the light output from the veto counter. The detection

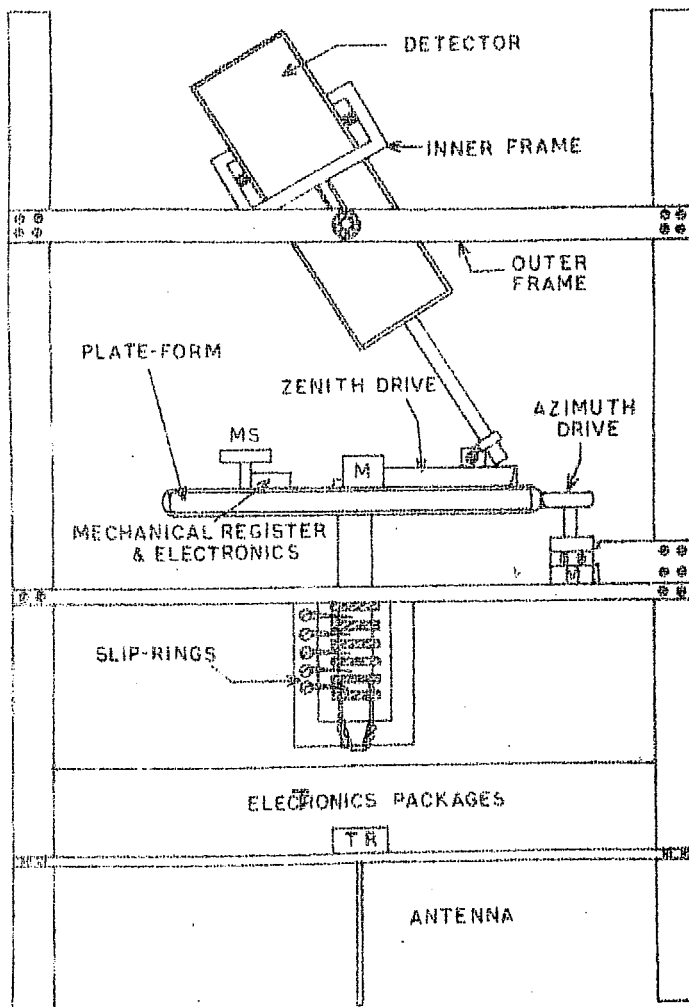


FIG.32 - THE WHOLE DETECTOR SYSTEM

efficiency of the guard scintillators was determined experimentally with the standard method of using relativistic cosmic ray muons. Except at the remote edges, the detection efficiency of the veto counters for relativistic muons was found to be $\geq 98\%$.

The efficiency, resolution and the method of calculating the energy spectrum are described in appendix A3.

3.3. ORIENTATION SYSTEM AND MAGNETIC SENSORS:

In order to detect the high energy X-ray radiation from selected celestial sources with improved statistics and reduction in the background the payload was mounted on an oriented platform. The X-ray telescope was oriented with respect to the earth's magnetic field using a flux gate magnetometer which had a peak pointing accuracy of $\pm 1.5^\circ$. Figure 3.2 shows the schematic of the orientation system used in the balloon experiments. The magnetic sensor was fixed on the rotating platform, the orientation of which would be changed by the radially mounted preprogrammed D.C. motor. The detector which was fixed on this platform rotated around the vertical axis at a fixed angle as the platform rotated.

The block diagram of the orientation device is shown in figure 3.3 when the output of the magnetic sensor (see figure 3.4) is positive (i.e. indicating the telescope pointing north) it gives a positive voltage to the D.C. motor and vice versa. The polarity of the motor for pointing the detector in different directions was controlled by a timer motor, which

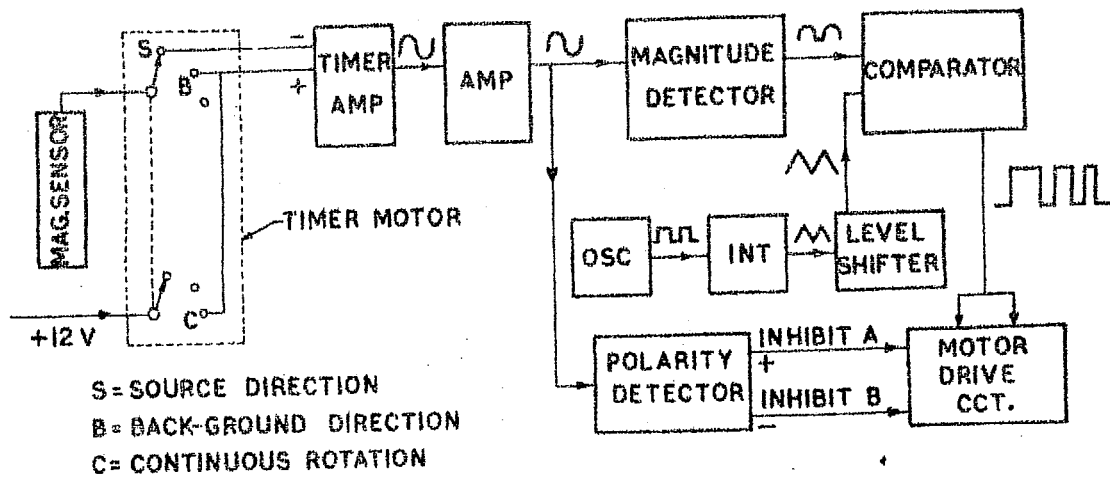


Fig. 3.3: ORIENTATION CIRCUIT FOR TELESCOPE

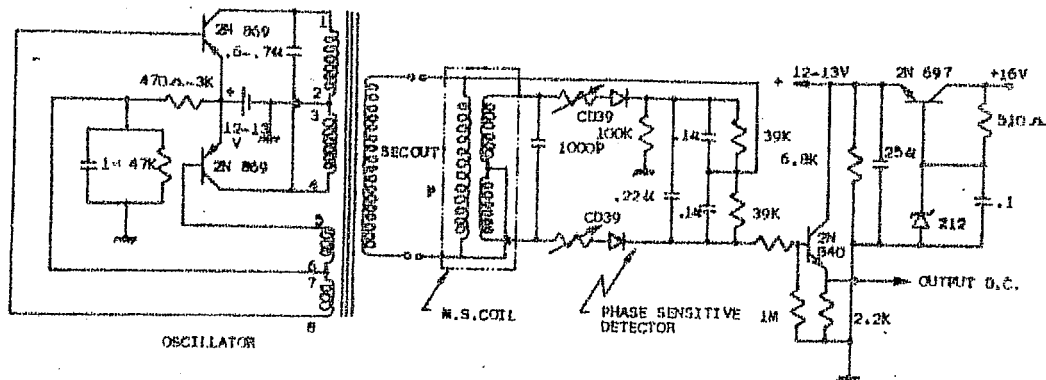


Fig. 3.4: MAGNETIC SENSOR



The picture shows the balloon payload before packing for launch. The clocks seen are used as timers for starting the tracking controls at proper times.

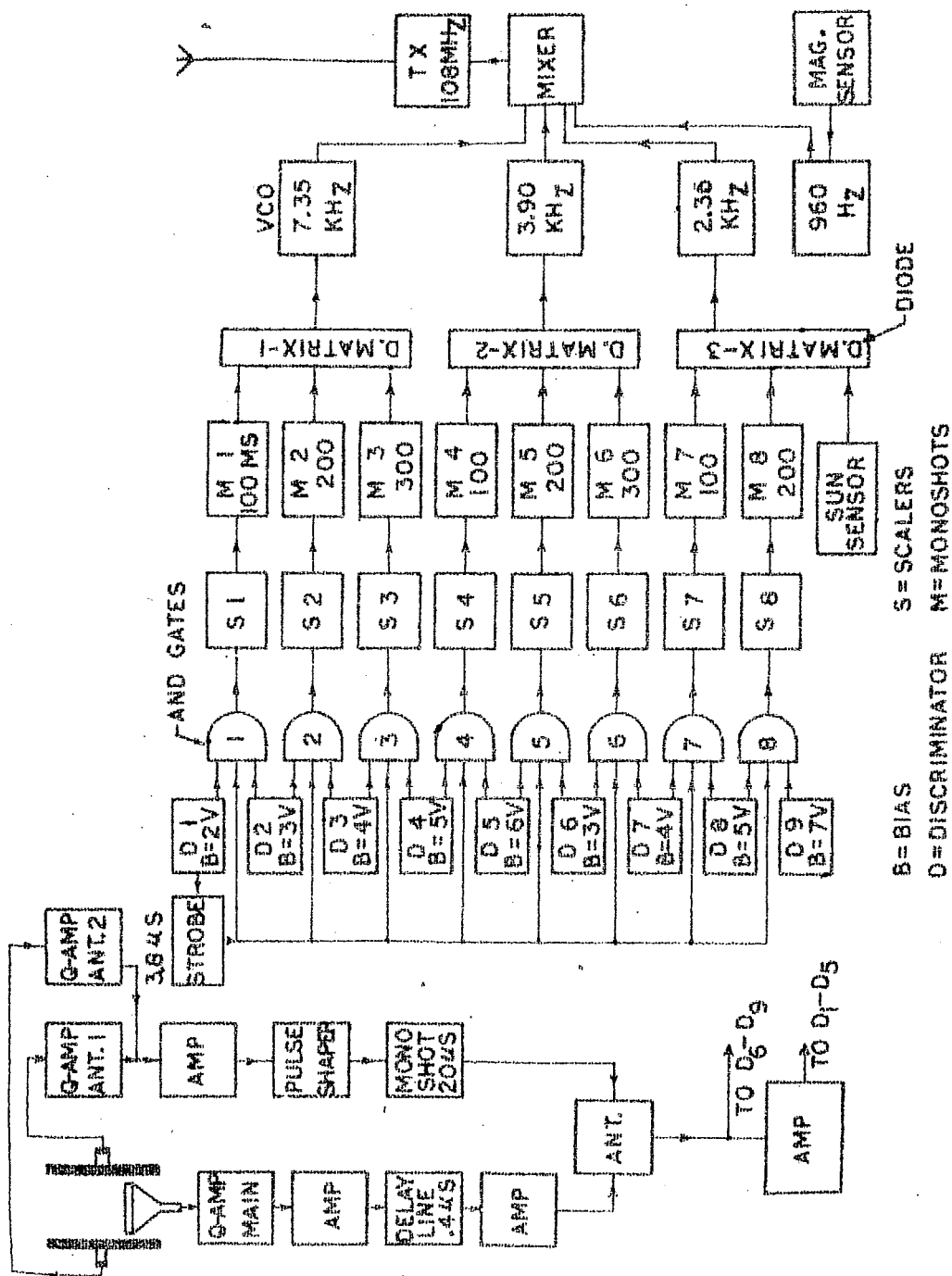
also worked as a programmer. The programming sequence of the observation usually involved three different modes. The first mode beginning with the detector pointed towards the source to be observed for four minutes, the second mode, when the detector pointed towards the background for almost an equal time and the third mode, when the detector was in continuous rotation for about half a minute during which inflight calibration with radioactive source was carried out. The output from the detector as well as other house keeping information were all taken through slip rings as shown in the figure 3.2 and then telemetered to the ground.

3.4. TRACKING THE X-RAY SOURCE:

The selected sources (Cyg X-1 and Her X-1) were tracked both in zenith and azimuth. Whereas the azimuthal tracking was accomplished by changing the orientation of magnetic axis by an appropriate rate ($6^\circ/\text{minute}$), the change in the zenith angle orientation of the detector, for these sources, during the flight was accomplished with the help of a timer and changing the detector axis with respect to the normal. With this technique it was possible to observe both Cyg X-1 and Her X-1 in the same balloon flight.

3.5. ELECTRONICS AND ASSOCIATED INSTRUMENTATION:

The block diagram of the electronics used is shown in figure 3.5. Pulses from the anode of main photomultiplier were amplified by a preamplifier mounted close to the tube



BLOCK DIAGRAM OF PAYLOAD ELECTRONICS

FIG. 3-5 THE BLOCK DIAGRAM OF COMPLETE X-RAY PAYLOAD

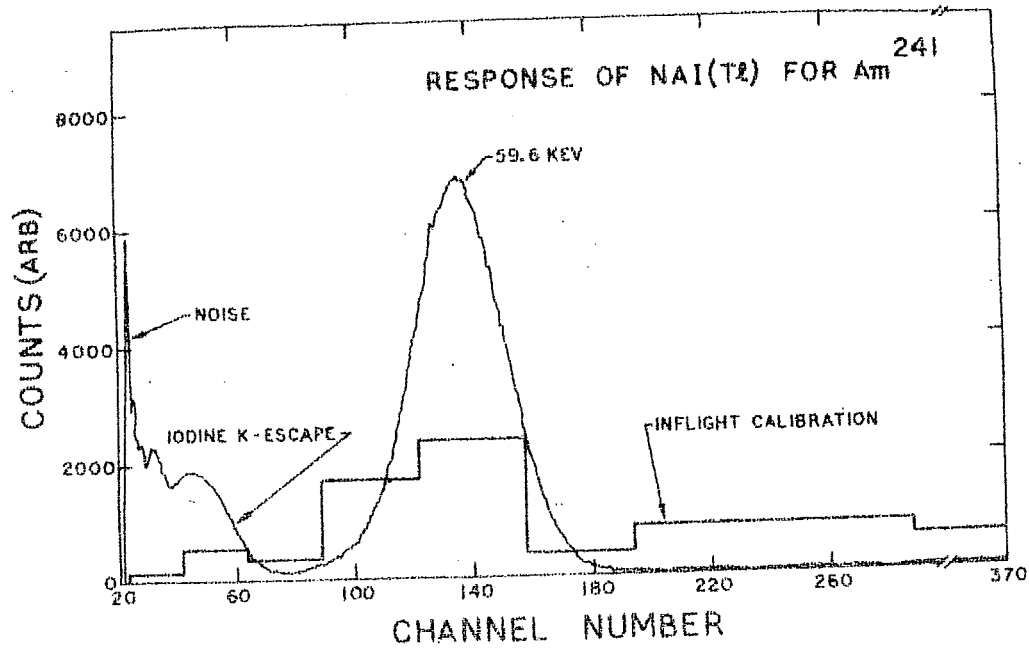


FIG. 3.6 - THE FIGURE SHOWS THE RESPONSE OF THE NaI (TL) CRYSTAL

and then further amplified by a chain of amplifiers. The output of the linear amplifier was fed to the discriminators to obtain spectral information from eight contiguous energy channels viz. 20-30, 30-40, 40-50, 50-60, 60-75, 75-90, 90-120 and 120-150 keV. The preflight calibration of the detector was accomplished using an Am^{241} radioactive source and the corresponding calibration curve is shown in figure 3.6. The outputs from the discriminators were given to scalers and then through conventional Voltage controlled oscillators fed to an FM/FM transmitter at 110 MHz. A photograph of the flight record is shown in figure 3.7 where along with photon pulses, the magnetic sensor output and the output of the solar sensor are also recorded.

Regulated power supply for the entire payload was derived from the primary source of silver-zinc accumulators which were charged prior to the flight. Two additional DC-DC convertors supplied the high voltage required for the photomultiplier tubes. The high voltage output from the convertors was regulated using conventional corona tubes.

3.6. INFLIGHT CALIBRATION AND ALTITUDE MEASUREMENTS:

Inflight calibration was accomplished using an Am^{241} radioactive source (59.5 keV), which was mounted on a moving arm and was brought into the field of view of the detector periodically as described earlier (figure 3.6).

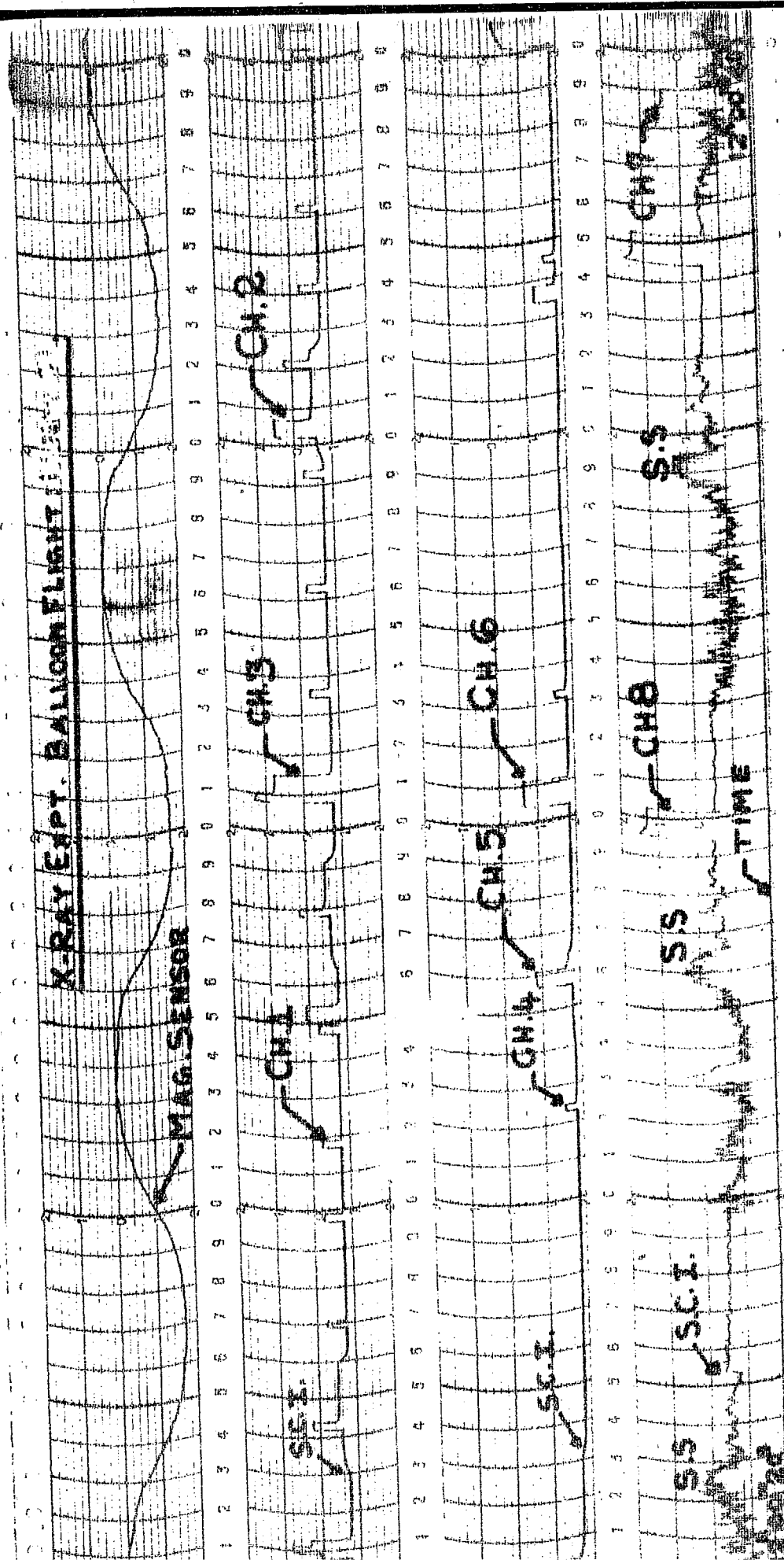
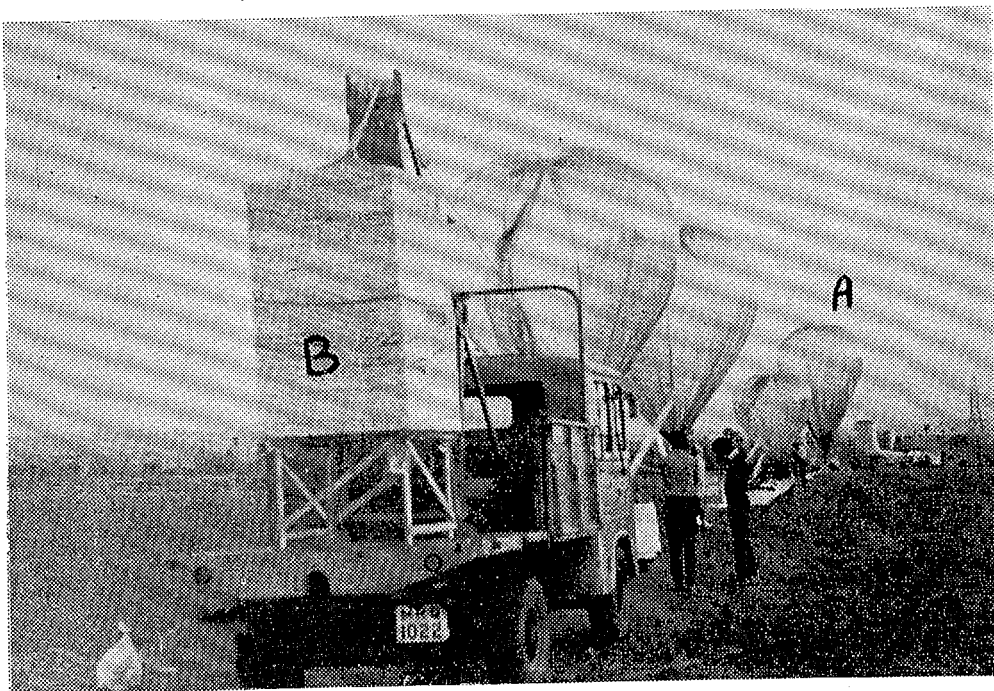
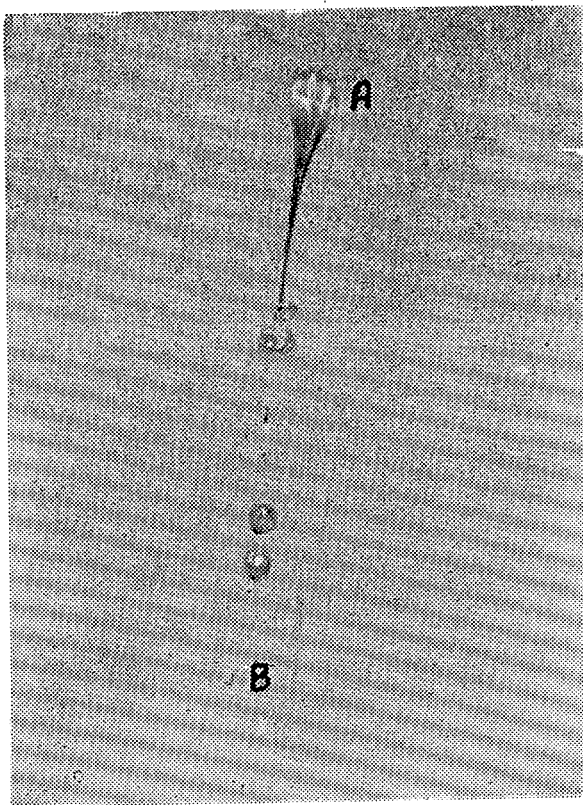


FIG. 37 - SAMPLE OF CHART RECORD OF TELEMETRY OF BALLOON FLIGHT
 CH = CHANNEL, SS = SOLAR SENSOR,
 SCI = JECTOR CHANGE INFORMATION.



The picture shows the balloon during launching operation and during the initial phase of flight. B shows the payload and A the main balloon.

The balloon altitude was determined by three independent methods, by radio sonde, radar and by recording on a photobarograph onboard the balloon. Onboard photobarograph was a Wallace and Tiernnan dial type pressure guage sensitive in the range of 0-65 milibars and which can be read to an accuracy of about 0.2 mb. A thermograph was also mounted in the payload gondola to record inflight temperature of the X-ray payload.

3.7. THE DETAILS OF THE BALLOON FLIGHTS:

The first payload to study Her X-1 was launched on a three million cubic feet balloon on December 28, 1972 which reached a ceiling altitude of 4.9 mb at 0945 IST. The second payload was launched on a similar balloon on January 18, 1973, which reached a ceiling altitude of 4.5 mb at 1000 IST (Table 3.1). A picture of the launch is shown on preceding page. The altitude time history for both the flights are shown in figure 3.8.

The observation on Her X-1, in the first flight could be carried out only for 15 minutes owing to the failure of the zenith drive mechanism. The observation on Her X-1 and Cyg X-1 was carried out as planned during the second flight and the entire system behaved properly throughout the complete duration of the flight.

A typical counting rate profile for the detectors used here during the ascent phase is shown in figure 3.9.

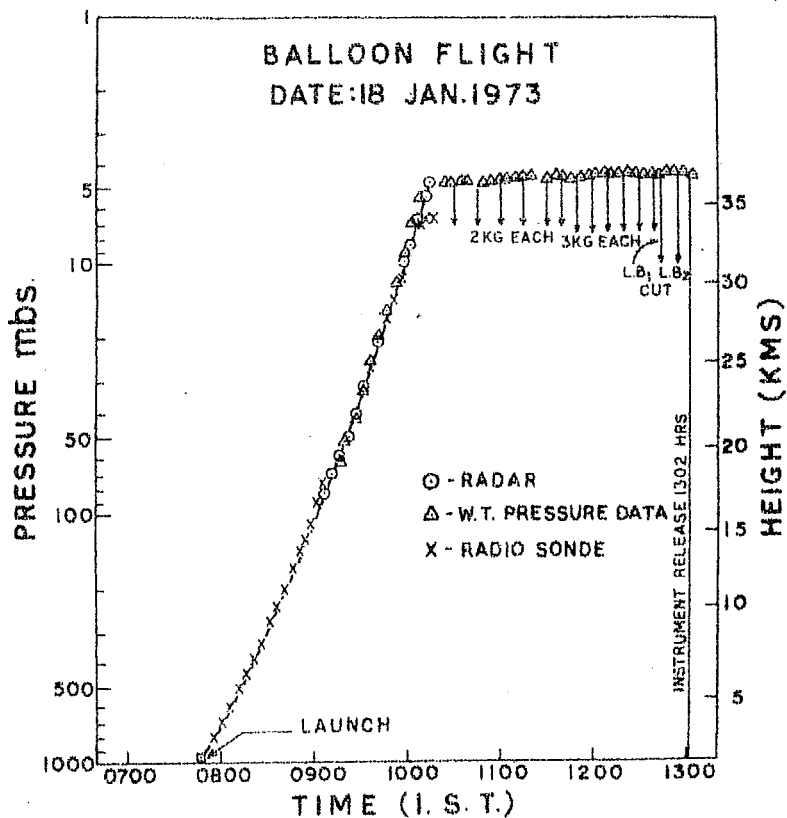
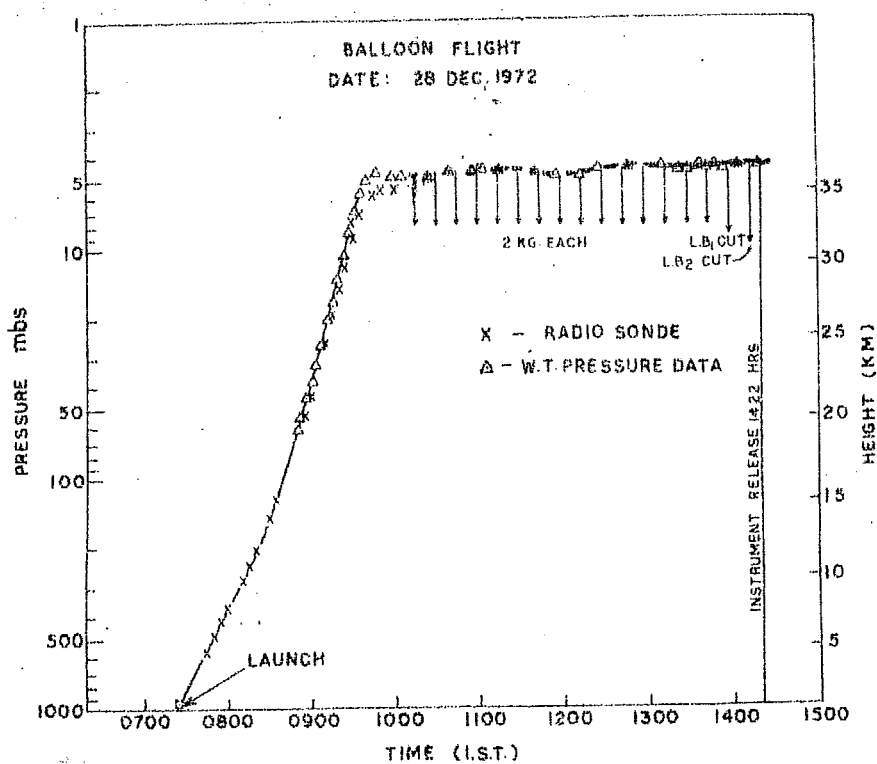


FIG. 3.8 - TIME-PRESSURE-HEIGHT CURVE OF BALLOON FLIGHT CONDUCTED ON 28TH DEC., 1972 AND 18TH JAN., 1973.

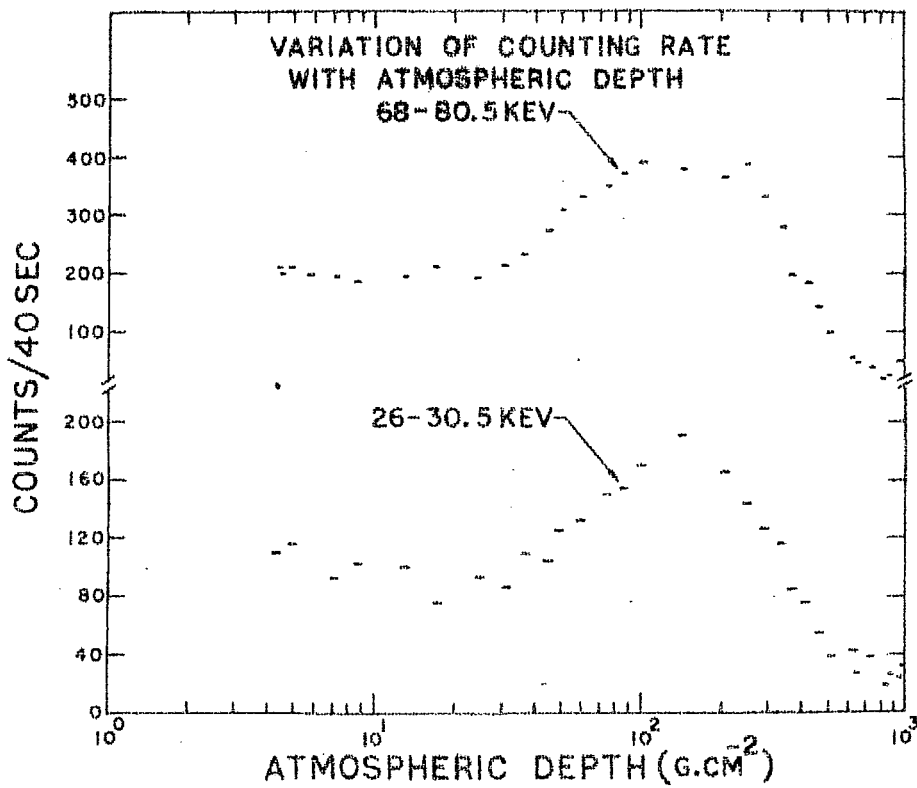


FIG. 3.9- THE COUNT RATE DEPOSITED IN THE DETECTOR WITH RESPECT TO HEIGHT.

It can be seen that the count rate decreases upto a height of about 1000 feet immediately after the balloon leaves the ground which is due to the decrease in the terrestrial radioactivity. The count rate then increases due to the effect of secondary cosmic rays in the atmosphere till the Pfotzer maximum which is normally at $\sim 120 \text{ gm. cm}^{-2}$ at these latitudes. After reaching the maximum the count rate again shows a decrease which continues to an altitude of $\sim 25 \text{ gm. cm}^{-2}$. Beyond these altitudes, the effect of diffuse celestial cosmic X-rays results in an upward turn in the counting rate, and the count rate shows a steady increase with altitude. The effect of diffuse background is particularly prominent at low latitude stations like Hyderabad, where the cosmic ray induced background is minimal. In figure 3.9 where the observed features of intensity profile in the two energy ranges of 26-30.5 keV and 68-80 keV observed on January 18, 1973 are shown, the effect of diffuse X-ray background particularly in the lower energy interval is very conspicuous. This is in conformity with the exponential nature of the energy spectrum of the diffuse background.

3.8.0. OBSERVATIONS ON BINARY X-TARS:

A. HER X-1:

3.8.1. PROGRAMME OF OBSERVATION:

From the observational data presented in chapter I, it is clear that there exists very meagre information on the source Her X-1 particularly at energies above 20 keV.

OBSERVATIONS OF HER X-1

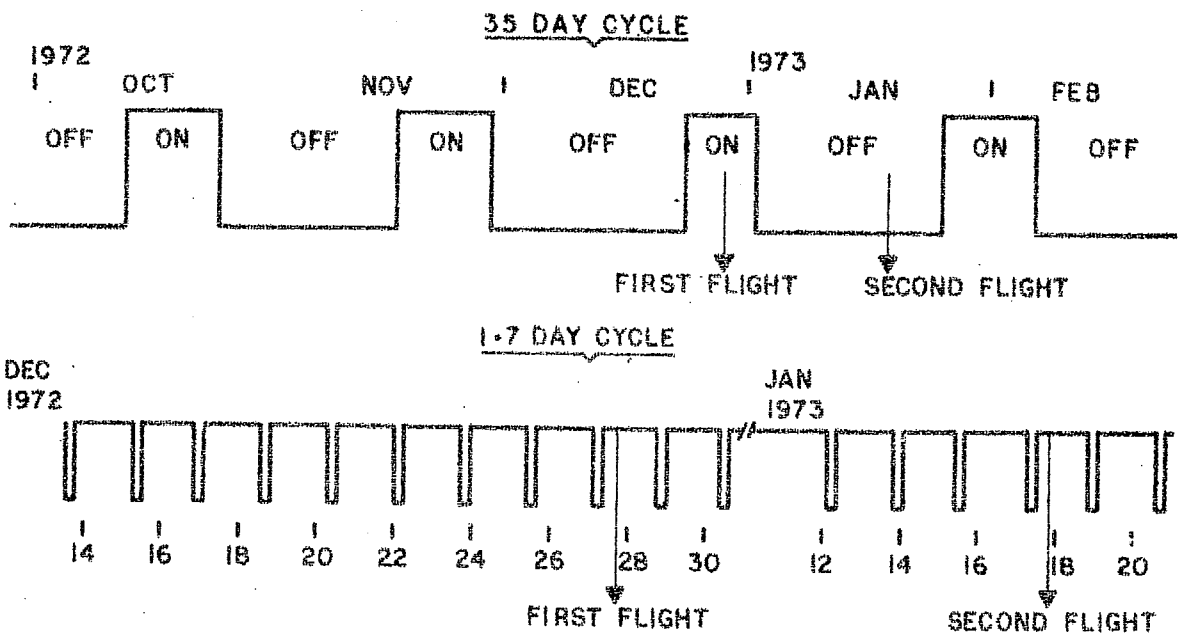


FIG.3.9a: THE FIGURE SHOWS THE TIME OF OBSERVATIONS OF HER X-1.

The source exhibits a number of prominent periodicities such as 1.24 second corresponding to the spin motion of the star and 1.7 days corresponding to the orbital motion of the binary system, in addition to the 35 day periodicity whose origin is still being debated.

It has also been established that the X-ray source is under eclipse for ~ 0.24 days in the 1.7 day cycle and for about 23 days in the 35 day cycle (OFF state). The origin of the 35 day cycle being still clouded in mystery, it is essential to monitor the behaviour of the source during the OFF state (23 days) as well as during the ON state (12 days) in order to infer the nature of mechanism that is responsible for the extraordinary behaviour of this source.

With the aim of monitoring this X-ray source in the high energy region in ON and OFF states, two balloon flights were conducted from Hyderabad which provided the first significant observation on Her X-1 in the energy range 20-100 keV. Figure 3.9a shows the time of observation in relation to the occurrence of ON and OFF states as well as in relation to the phase of the binary 1.7 day period. As is evident from the figure the first balloon flight was conducted (December 28, 1972), during the middle of the ON state and coincided with the maximum brightness of the 1.7 day cycle (phase ~ 0.3). The second balloon observation was conducted (January 18, 1973) during the middle of the OFF state but again coincident with the maxima of 1.7 day binary (phase $\sim .2$) period. The later observation was well before (~ 5 days) the onset of the

12 day ON state. The X-tar was observed for ~ 11 minutes during its transit over the detector during the first balloon flight corresponding to Collimator transmission efficiency $\geq 40\%$. During the second flight Her X-1 was tracked for ~ 15 minutes corresponding to Collimator transmission efficiency $\geq 95\%$.

3.8.2. RESULTS

3.8.2a. OBSERVATION DURING ON STATE:

The observed count rate of X-rays at different energies in the energy range 20-100 keV from the direction of X-ray source Her X-1 are presented in the figure 3.10a. The count rate presented in the diagram have been corrected for detector efficiency taking into account the effect of escape radiation in the detector, collimator transmission and also the transmission coefficient in the atmosphere above the detector. The procedural details for applying these corrections to the basic data obtained from the flight and the details of the method of analysis are described in detail in appendix A-3. It may be also noted that the photon flux distribution with energy shown in the figure has been obtained after subtracting the background counts as described in section A 3.6.

After trials with various spectral fits, the best fit spectrum for the energy dependence of the X-ray source was obtained using minimum χ^2 method. The details of the procedure adopted are also described in Appendix A-3. The best spectrum for Her X-1 is found to obey a power law distribution with an

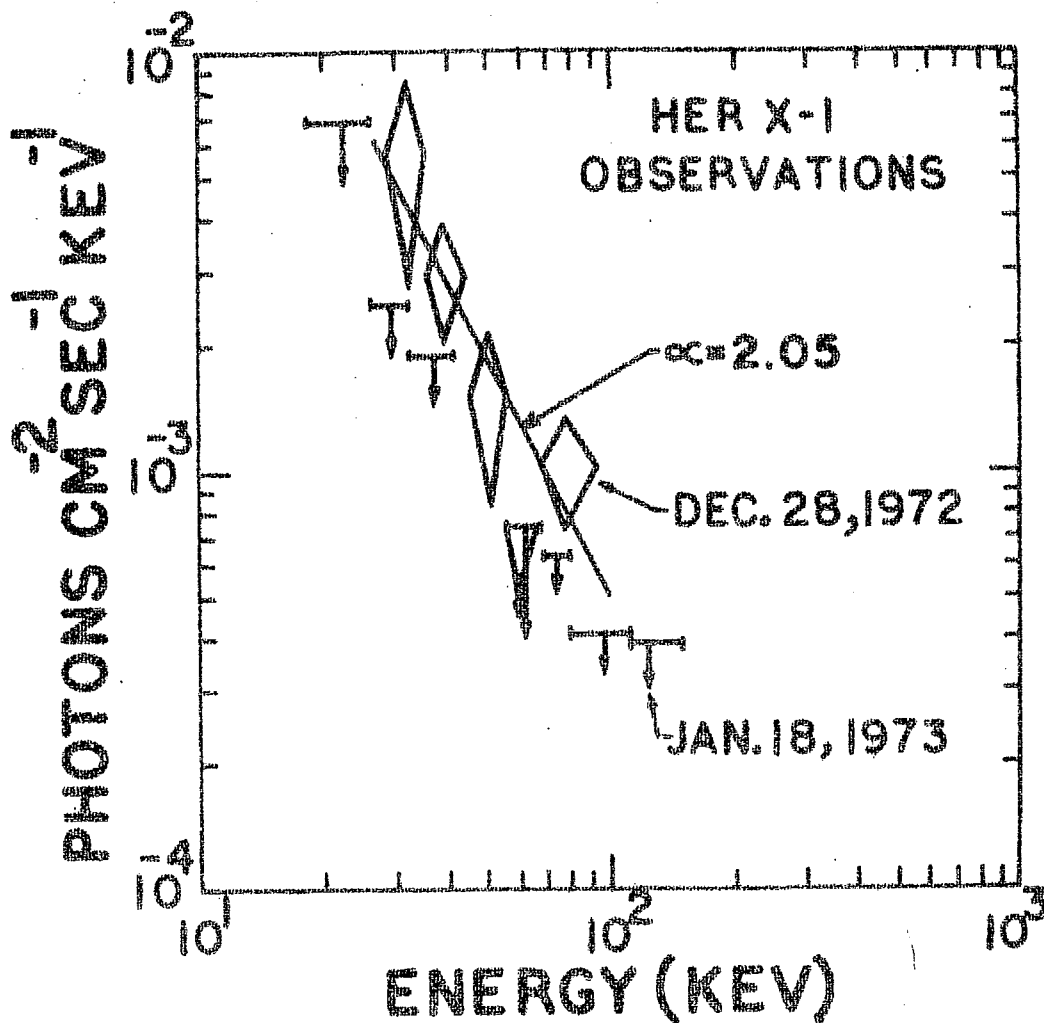


FIG. 3.10a. THE FIGURE SHOWS THE TWO OBSERVATIONS OF HER X-1 MADE IN EXTENDED LOW PHASE (JAN 18, 1973) AND BRIGHT PHASE OF THE 35 DAY PERIOD ON DECEMBER 18, 1973

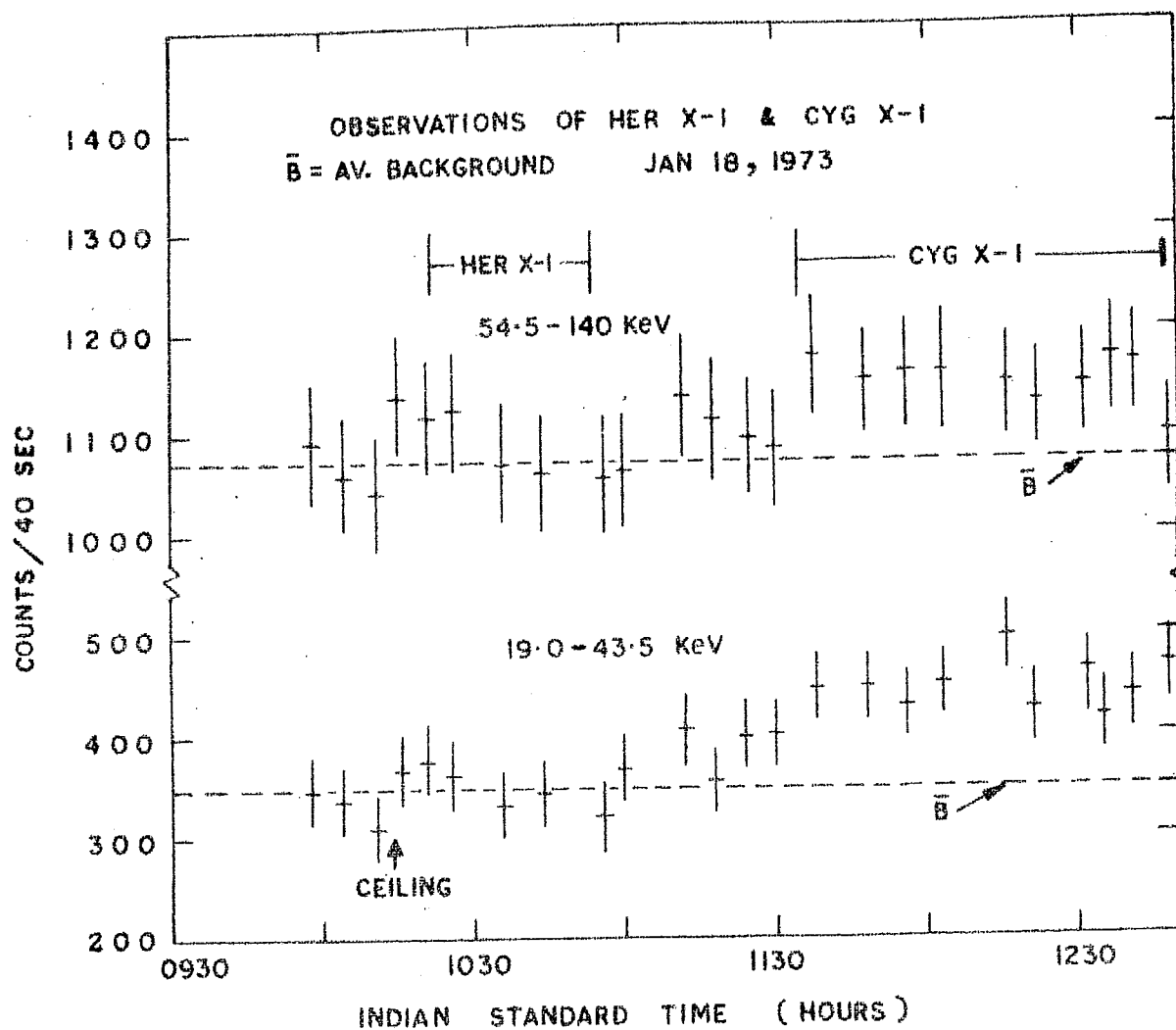


FIG.3.10b: THE COUNTS DEPOSITED IN THE DETECTOR ON JAN.18, 1973 WHEN HER X-1 AND CYG X-1 WERE TRACKED. THE VERTICAL BARS SHOW ONE SIGMA LEVEL STATISTICAL FLUCTUATIONS.

index of $\alpha \approx -2.05$ in the energy range 20-100 keV. The best fit spectrum, also marked in figure 3.10a can be represented by,

$$\frac{dN}{dE} = 2.65 E^{-2.05 \pm .33} \text{ photons. cm}^{-2}.\text{sec}^{-1}.\text{keV}^{-1}.$$

The differential flux of X-ray photons in the energy range 20-100 keV observed during this flight was $\approx 1.73 \times 10^{-2}$ photons $\text{cm}^{-2}.\text{sec}^{-1}.\text{keV}^{-1}$. The level at which Her X-1 emission was detected in the present flight was significant at 2σ level. It may be noted that our observation constitute the first set of published results on the high energy spectral characteristics of Her X-1.

3.8.2b. OBSERVATION IN OFF STATE:

Her X-1 was also monitored in the same manner as described above and the X-ray photon flux is computed after necessary corrections during the time when it was tracked. It is found that the source during the OFF state does not contribute any significant counts within statistical limits (see figure 3.10b). Therefore, it has been possible to obtain only 1σ upper limits during its OFF state. The differential photon flux emitted by the source in the energy range 20-100 keV was $\approx 0.9 \times 10^{-2}$ photons $\text{cm}^{-2}.\text{sec}^{-1}.\text{keV}^{-1}$. Figure 3.10a also shows the upper limits for the photon flux in the various energy bands during its OFF state. It may be seen from the figure that intensity in ON state is atleast a factor of ≈ 2 greater than the intensity in OFF state.

Table 3.2 - Observations of Her X-1

Date of observation	Energy range (keV)	Spectral parameters		Phase of 1.7 day period	State ON or OFF	Reference
		A	α			
January to June 1972	2-20	-	1.0	$\sim .5$	ON	Giacconi et al(1973b)
Dec.6-12, 1971	1-30	.58 \pm .06	1.6 \pm .15	$\sim .5$	ON	Clark et al (1972)
Nov.14-24, 1972	1-40	-	1.3-1.5 $\pm .2$	Max	ON	McClintock et al(1974)
May 29, 1972	7-26	.076	.96 \pm .5	$\sim .5$	ON	Ulmer et al (1973)
	7-40	.46	1.7 \pm .7			
Dec.8-10, 1971	7-26	.11	.89 \pm .6	$\sim .5$	ON	Ulmer et al (1973)
	7-40	.80	1.7 \pm .6			
Dec.28, 1972	20-100	2.65	2.07 \pm .33	$\sim .3$	ON	Present
Jan.18, 1973	20-120	Only upper limits		.25	OFF	-do-
March 9, 1973	20-90	6.3	2.4 \pm .2	-	ON	Manchanda et al(1973)
Dec.12, 1973	20-90	-	2.7	$\sim .25$	ON	Iyengar et al(1974)

3.8.2c. COMPARISON WITH THE RESULTS OF OTHER EXPERIMENTERS:

All the available observations extending from a few keV to ~ 100 keV including the results obtained in the present flight are presented in figure 3.11. The relevant details including the time of each observation, the corresponding phase of 1.7 day binary period and other relevant parameters are tabulated in table 3.2.

It is evident from the figure 3.11 that the spectral shape of the X-ray flux at higher energies is completely different from that at lower energies. Whereas the power law spectral index below ~ 20 keV can be approximated to $\alpha \approx -1.0$, it steepens considerably at energies above ~ 20 keV. Ulmer et al (1972, 73^a) have also reported the same phenomena and found that the spectral index changes from $\alpha \approx -1.0$ to $\alpha \approx -2.5$ which is consistent with our observations. As can be seen from the table all the observations at high energies consistently show a steep energy spectrum varying between $\alpha \approx -2$ to 2.5 .

Figure 3.11 shows a large scatter between various observations which is possibly indicative of the existence of large time variations in intensity at different phases or with different cycles of 35 day period. This fact is well established below 20 keV (Giacconi et al 1973b). The present observations bring out the fact that large fluctuations in intensity by factors as large as 2 to 3 are present even at high energies.

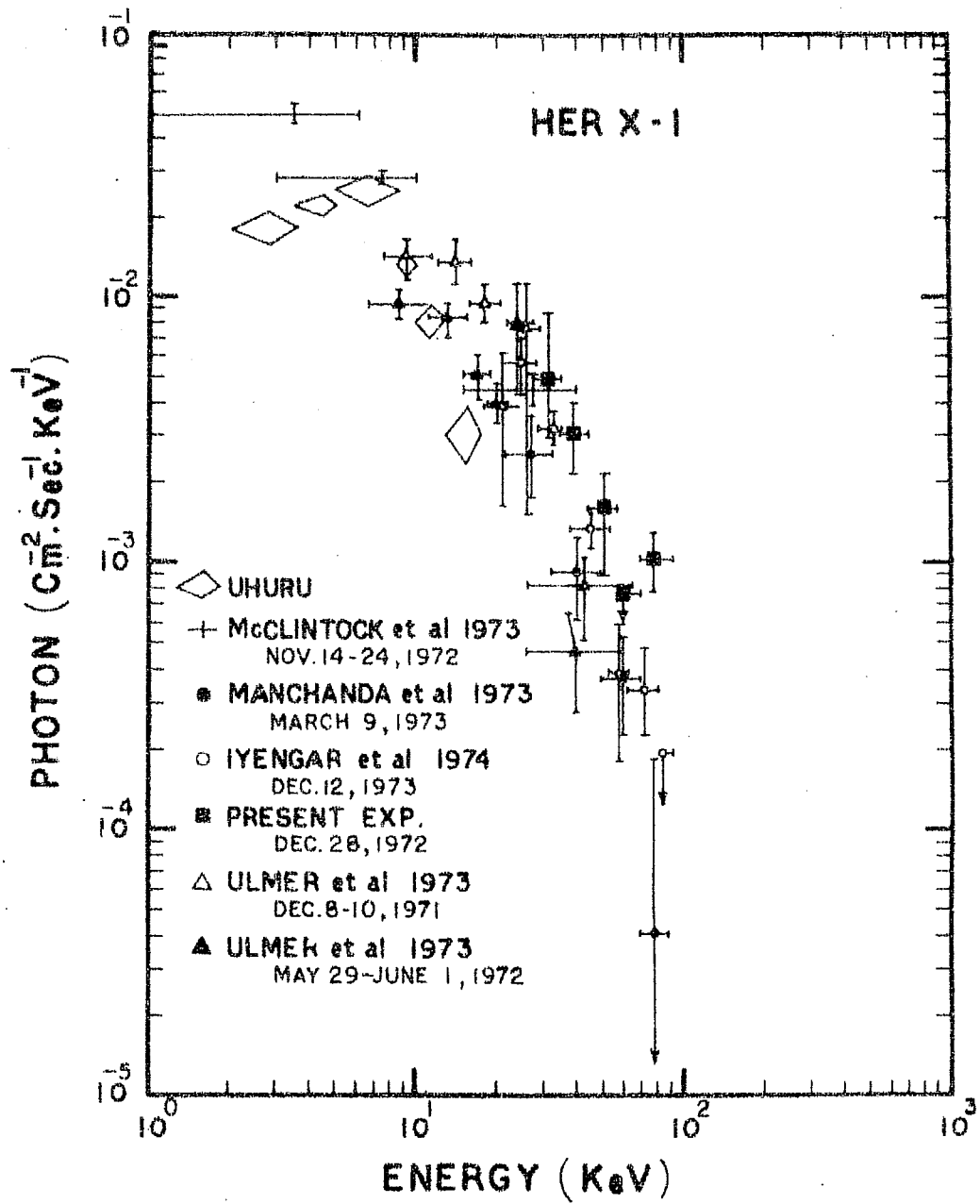


FIG.3.11: THE FIGURE SHOWS THE COMPILATION OF DATA ON HER X-1 IN LOW AND HIGH ENERGY REGIONS.

TIFR results (Iyengar et al 1974) showing an increase in the intensity by a factor of two within 70 minutes are consistent with the above conclusion. From the same figure it can also be noted that the intensity beyond 70-80 keV is observed to fall very sharply.

Except for the present flight results, there are no other high energy observations of Her X-1 reported in the OFF state. The present experiment in the OFF state does not show any emission from Her X-1, similar to the behaviour of the source exhibited at lower energies (Giacconi et al 1973b).

3.8.3. DISCUSSION:

3.8.3a. BRIEF INTRODUCTION:

From our own observations and the brief review presented in Chapter I the following salient features of Her X-1 can be listed which should be considered in formulating any theoretical model for this type of sources.

(1):- Her X-1 emission shows that there exist following three periodicities in the flux received from this source, 1.24 second, 1.7 day and 35 days. At higher energies (≥ 20 keV) 1.24 second pulsation period is not detected.

(2):- The X-ray spectrum during ON state can be best fitted with a power law in the energy region extending from a few keV to ~ 100 keV. The spectrum is observed to steepen considerably above 20 keV, the power law index changing from ~ -1.0 to ~ -2.5 .

(3):- No substantial X-ray emission is detected during the OFF state. The luminosity observed during ON state is $\approx 10^{37}$ ergs.sec⁻¹.

(4):- The Her X-1 X-ray source is associated with the optical binary Hz Hercules which is a ~ 13 th magnitude star. In optical region the pulsations of 1.24 second are seen only when the X-ray source is in ON state. On the other hand, the 1.7 day periodicity is observed all the time that is no 35 day periodicity is observed at optical wavelengths.

3.8.3b. DISCUSSION ON SOURCE MODELS:

The discovery of three major periodicities of 1.24 second 1.7 day and 35 day must necessarily form the basis of any model one proposes. From the constancy of the frequency of 1.24 second pulses it is evident that this periodicity can arise only due to the spinning of the X-ray emitting object. The Doppler shift observed in the 1.24 second period positively indicates that the X-ray emitting object is rotating in a orbit and the eclipse observed in the emission reveals that the X-ray source is rotating around a larger companion with a period of 1.7 days. The 35 day periodicity has been suggested to be due to precession of the orbit of the X-ray due to which the emission goes out of the line of sight periodically.

The short duration (≈ 1.24 second) pulsation observed in the emission indicate that the emitting source is a compact body. In general the pulsation period is related to the physical parameter of the source through the relation,

$$P \geq (G \cdot \bar{\rho})^{-\frac{1}{2}}$$

where P is the period of pulsation, G is the gravitational constant and $\bar{\rho}$ is the average density of the compact body. Substituting the above values we observe that Her X-1 should have a density, $\bar{\rho} \geq 10^6 \text{ gm.cm}^{-3}$, which suggests that this source falls under the category of degenerate white dwarf, neutron star, or a black hole.

The possibility of rotating black hole is ruled out because the non-axisymmetric black hole can have only a transient existence (Davidson and Ostriker 1973), which leaves a choice between a rotating degenerate white dwarf and a rotating neutron star. The power law of the X-ray spectrum for the emission of Her X-1 being indicative of the synchrotron process suggests, in addition, that the source is likely to be associated with a large magnetic field. In other words, from the observation it is seen that Her X-1 is either a rotating magnetic white dwarf or a rotating magnetic neutron star.

Assuming that the loss of rotational energy is responsible for the X-ray emission, one would expect a gradual increase in the 1.24 second rotation period which is contrary to the observational fact (Giacconi et al 1973b) which clearly indicates a decrease in the time period of the order of ~ 4.5 micro-second over a period of six months. Therefore, in order to satisfactorily account for the change in the time period and the luminosity, accretion of mass on to the compact star from the companion has been invoked. The thermal heating of

the matter due to the acceleration during the process of accretion can provide the necessary input for the X-ray emission.

Based on these considerations most of the models suggested can be broadly classified under two categories:

a) Models based on white dwarf being the X-ray star (Gribben 1971, Henricksen 1971, Brecher and Morrison 1973, Chau 1973 etc.). The most important consideration in proposing these models seems to be based on the fact that neutron stars are generally found only in supernova remnants (e.g. Crab nebula, Vela) and none of these neutron stars have so far been discovered in binary systems. Brecher and Morrison have argued against the hypothesis of neutron star on the basis that the ejection of large amount of mass during a supernova outburst would decouple any binary system. On the other hand, the main objection to the white dwarf theory stems from the observed fast rotational period of ~ 1.24 second (Lamb et al 1973). In addition, the observed periodicity of 35 day and the high temperatures cannot be explained satisfactorily using white dwarf model and makes such models very unattractive for explaining the X-ray emission from Her X-1 and hence for further discussions we confine ourselves to the neutron star models.

Detailed models based on neutron stars as the X-ray source and different mechanisms of accretion of matter have been proposed by a number of authors, for example, accretion from stellar wind emanating from larger star (Davidson and Ostriker 1973), disk model (Pringle and Rees 1972, Lamb et al 1973)

and the slaved disk model (Roberts 1974). Some of these are also based on evolution of close binary systems which at some stage of their evolution explode as supernovae and the lighter star in the remnant becomes the fast spinning neutron star (Van den Heuvel 1972, 1973a,b).

Knowing that the X-ray emission is due to the heating of accreted matter and that X-ray luminosity of Her X-1 is $\sim 10^{37}$ ergs.sec $^{-1}$ we can calculate the accretion rate which is given by the equation,

$$L_x \approx \frac{dM}{dt} \cdot \frac{G.M.}{R} \text{ ergs.sec}^{-1}$$

where $\frac{dM}{dt}$ is the accretion rate on to an object of mass M and radius R . For Her X-1, assuming the mass $1 M_{\odot}$, accretion rate of $\sim 10^{-9} M_{\odot} \text{ yr}^{-1}$ is required. This accretion of mass on the neutron star can be obtained by the following processes (Davidson and Ostriker 1973):

1) If the companion fills its Roche lobe, material will be gravitationally pulled out of the cusp of the lobe and may be partially accumulated by the neutron star. This material on it gets accelerated during accretion and may release some of its energy as X-rays.

2) If the larger star is sufficiently massive, it may have a strong stellar wind of the type normally observed along the upper main sequence (Morton 1967, 1969; Carruthers 1968). Some of this mass outflow can be accreted by the rotating neutron star. This case may not be applicable to the case

of Her X-1 because the estimated mass of the companion is $\sim 2 M_{\odot}$ (Giacconi et al 1973b, Jones et al 1973b).

3) If the presence of a luminous X-ray source in a nearly grazing orbit heats and evaporates material from outer layers of the star, the wind so produced, self consistently can help to fuel the accretion process. This hypothesis requires assumptions regarding the luminous X-ray source which seem to be quite artificial.

In view of the objections raised for second and third alternatives, at present, the first alternative seems to be the best alternative. However much more information is needed before finally deciding between different accretion mechanisms.

3.8.4. THE 35 DAY PERIOD OF HER X-1:

The 35 day period was first suggested to be due to free precession of the X-ray star (Brecher 1972, Brecher and Morrison 1973) where the rotating pencil beam of the X-ray pulsar misses the earth periodically. But this model does not explain many aspects, such as the actual cause responsible for the precession of the neutron star with a 35 day period. Moreover, the large duty cycle of the 1.24 second pulse suggests a rather wide opening angle for the X-ray beam. If the beam has horizontal symmetry about the magnetic pole, it is difficult to understand the profile of the 11-12 day active phase of the 35 day cycle. The precession hypothesis encounters further difficulty with the observation that the 35 day cycle is not strictly periodic (Giacconi et al 1973b)

and the rapid onset of the active phase is observed to fluctuate by a few days. To overcome this further, Pringle 1973 and McCray 1973, have proposed new hypothesis which involves the regulation of variation of mass transfer.

The above hypothesis assumes that there is a minimum mass flux that rotating magnetized neutron star can accrete. Infalling material is unaffected by the field until it reaches the 'Alfven Radius' R_m , where the magnetic energy density is roughly equal to the kinetic energy density of the infalling material. Within this radius, the material, which is highly conducting attaches itself to field lines and can then fall along the field lines on to the star's magnetic polar caps. If, however, centrifugal force dominates over gravity at Alfven radius, matter attaching to the field lines cannot be accreted and is expelled by the star. Centrifugal force balances gravity at the "Corotation radius or Synchronous radius", R_{Ω} . As the incoming mass flux slowly increases, matter builds up outside the Alfven radius until sufficient material has accumulated to crush the field, reducing R_m within R_{Ω} . At that point accretion to the neutron star surface begins and the pulsed X-rays are turned on. The material accumulated at R_m along the line of sight to the neutron star may be optically thick initially to the X-ray radiation. As accretion proceeds, the X-ray intensity increases, and the amount of accumulated matter declines until the line of sight suddenly becomes optically thin. This is the turn on of 35 day period. The spectral information does seem

to support the hypothesis of absorption effect and plays important role in the turn on. Even if the mass transfer rate from the large star varies in a regular fashion, the turn on depends critically on the density of the material along the line of sight and on the enhancement in X-ray intensity and consequently one does not necessarily expect the turn on to be strictly periodic.

Although, in this model also the mechanisms suggested for the variation of mass transfer are not very convincing, nevertheless, the model presents a good picture.

From the results and discussion presented above, it is clear that much more information particularly at higher energies is needed both to understand the spectral behaviour of the source, its dependence on both energy and the time variation of the source.

B. CYG X-1

3.9.1. OBSERVATIONAL PROGRAMME:

From the observational data presented in chapter I, it is clear that Cyg X-1 is most powerful X-ray source above 20 keV. The observations clearly indicate that this source exhibits short duration non-periodic fluctuations in intensity at all energies extending from a few keV to ≈ 200 keV. Further, the source has also been identified with a ~ 9 th magnitude optical spectroscopic binary HDE 226868. However, it has not yet been possible to establish conclusively the presence of any

periodicity in the X-ray flux from this source. Since the binary period of the optical counter-part is 5.60009 days, it is clearly necessary to carry out large amount of observations of this source both in the X-rays and in the optical region for extended periods of time to establish the correlation between the optical binary and the X-ray star. In addition, it is also essential to monitor both, the time variation of the X-ray flux as well as the spectral nature of the source for understanding the mechanism of production of X-rays in the source as well as its physical nature.

In view of the importance of these measurements two balloon flights were planned from Hyderabad ($\Delta_m \approx 8^\circ$) to obtain longest possible exposure of the source Cyg X-1. The first observation was made on March 29, 1972 during which the source was tracked for about one hour and 15 minutes corresponding to collimator transmission efficiency of $\geq 45\%$. The field of view of the collimator in this flight was $18^\circ.0$ FWHM. The second flight was conducted on January 18, 1973 during which the source was tracked for about 1 hour corresponding to the collimator transmission efficiency of $\geq 95\%$. The field of view of the collimator in this flight was 13.5° FWHM. The balloon reached a ceiling altitude of ~ 5 mbars in the first flight and an altitude of ~ 4.8 mbars in the latter flight.

3.9.2. RESULTS:3.9.2a. OBSERVATIONS OF CYG X-1 DURING FIRST FLIGHT:

In figures 3.12a and 3.12b, the normalised excess counting rates observed in the first balloon flight from the direction of Cyg X-1 are plotted as function of time. Figure 3.12a represents the counting rate averaged over 5 minutes and 3.12b, represents the same counting rate averaged over 10 minutes and represented in two energy ranges 29-60 keV and 87.5-160 keV respectively. The statistical error at 1 σ level in the counting rate is also shown and is indicated by vertical bars. In computing the statistical error, the possible error due to the swing of the detector ($\pm .5^\circ$) while orienting, is also taken into account. The excess counting rate is plotted in these figures after subtracting the background due to both diffuse X-rays as well as other atmospheric effects as described in section A 3.3. In addition the count rate derived has been normalised after applying corrections for both, atmospheric effects as well as for the detector exposure efficiency, the details of the procedure are described in appendix A-3.

From both the figures it is quite evident that the source Cyg X-1 contributed significant counting rates from 1000 IST to 1100 IST. The observed counting rate from the source was more or less constant from approximately 1000 IST to 1040 IST, at which time the counting rate showed a significant enhancement almost by a factor of two, for approximately 10 minutes.

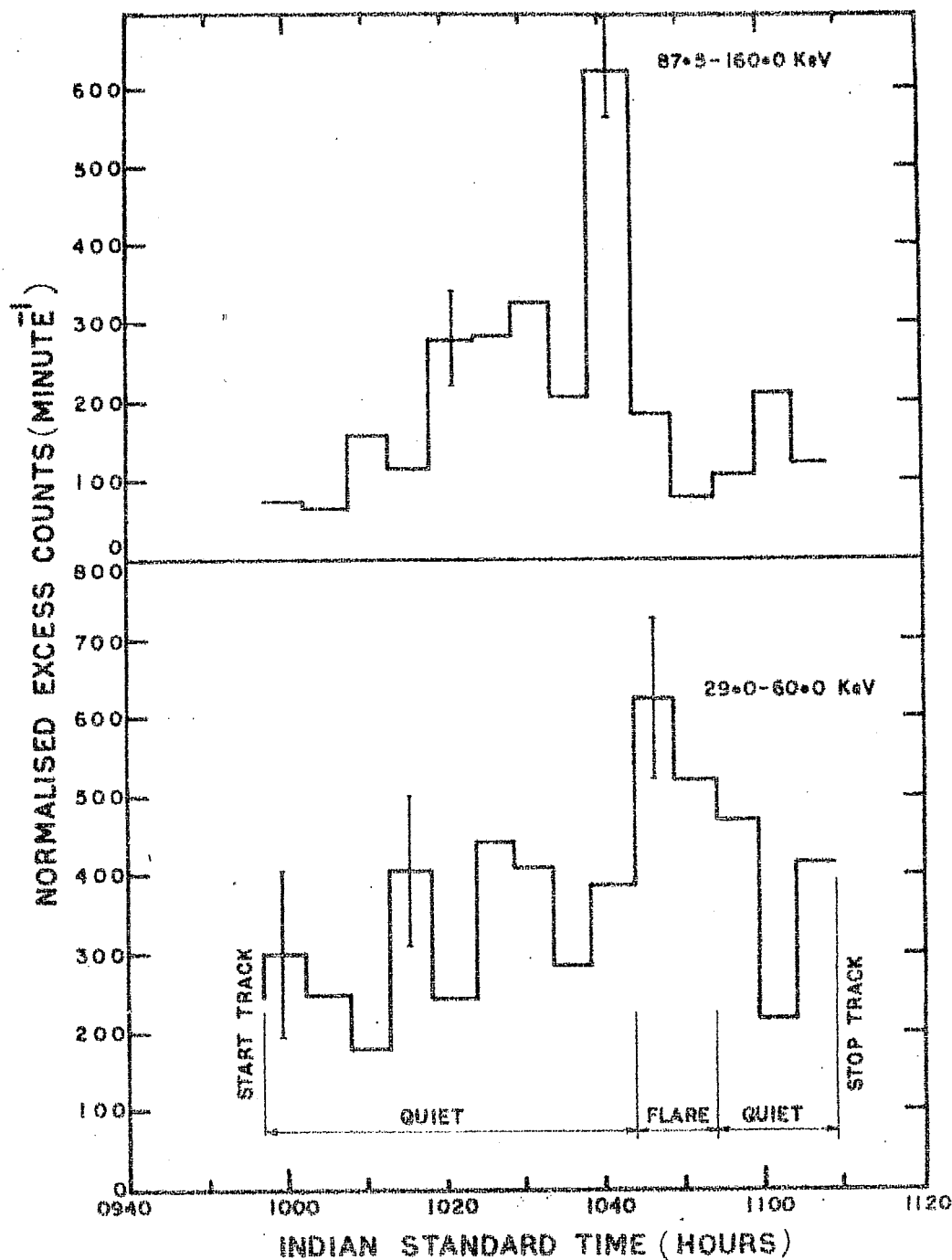


FIG.3.12a: THE COUNTS DEPOSITED IN THE DETECTOR DURING THE TRACKING OF CYG X-1 ON MARCH 29, 1972 AND CORRECTED FOR TRANSMISSION EFFICIENCY THROUGH ATMOSPHERE AND COLLIMATOR, SHOWN OVER THE BACKGROUND. THE DATA IS AVERAGED OVER 5 MINUTES TIME SCALE.

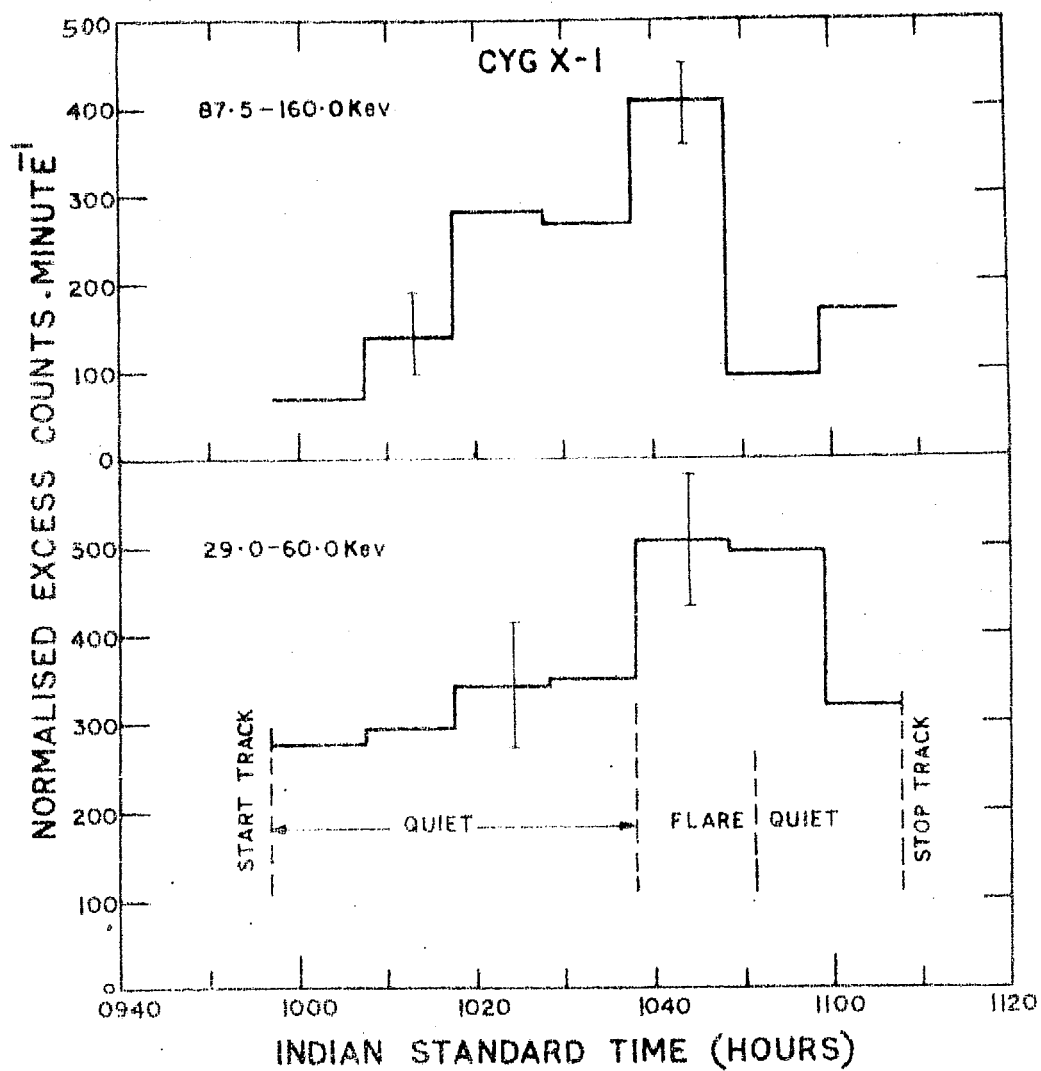


FIG.3.12b: SAME AS FIGURE 3.12a. BUT DATA AVERAGED OVER 10 MINUTES TIME SCALE.

Following the enhancement the counting rate dropped again to its normal original value till 1100 IST beyond which time the source would not be tracked. The figure 3.12 shows the two distinct phases of Cyg X-1 which were observed during the flight, (i) 'quiet condition': Observed both at the beginning as well as at the end of the observation and (ii) the short period 'flaring condition' in the emission of the Cyg X-1 when the source emitted greatly enhanced intensity compared to that during 'quiet' condition.

In figure 3.13 the observed photon counting rate from Cyg X-1 during 'quiet' as well during 'flare' condition plotted separately is represented as a function of energy. The best fit spectrum based on the observations are also shown in the figure. The best fit spectrum for Cyg X-1 in the energy range 20-160 keV during the quiet condition is consistent with a power law which can be conveniently represented by the eqn.

$$\frac{dN}{dE} = 6.10 E^{-1.90 \pm .10} \text{ photons cm}^{-2} \cdot \text{sec}^{-1} \cdot \text{keV}^{-1}$$

The average integrated intensity in the energy range 20-100 keV during this flight in the 'quiet' condition observed is,
 $\approx 1.86 \times 10^{-8} \text{ ergs} \cdot \text{cm}^{-2} \cdot \text{sec}^{-1}$.

As noticed earlier, around 1040 IST the X-ray flux from the same source showed an abrupt increase in all the energy bands in the range 20-160 keV. This flaring lasted for about 10 minutes during which period our detector registered approximately twice the flux from the same source as observed during

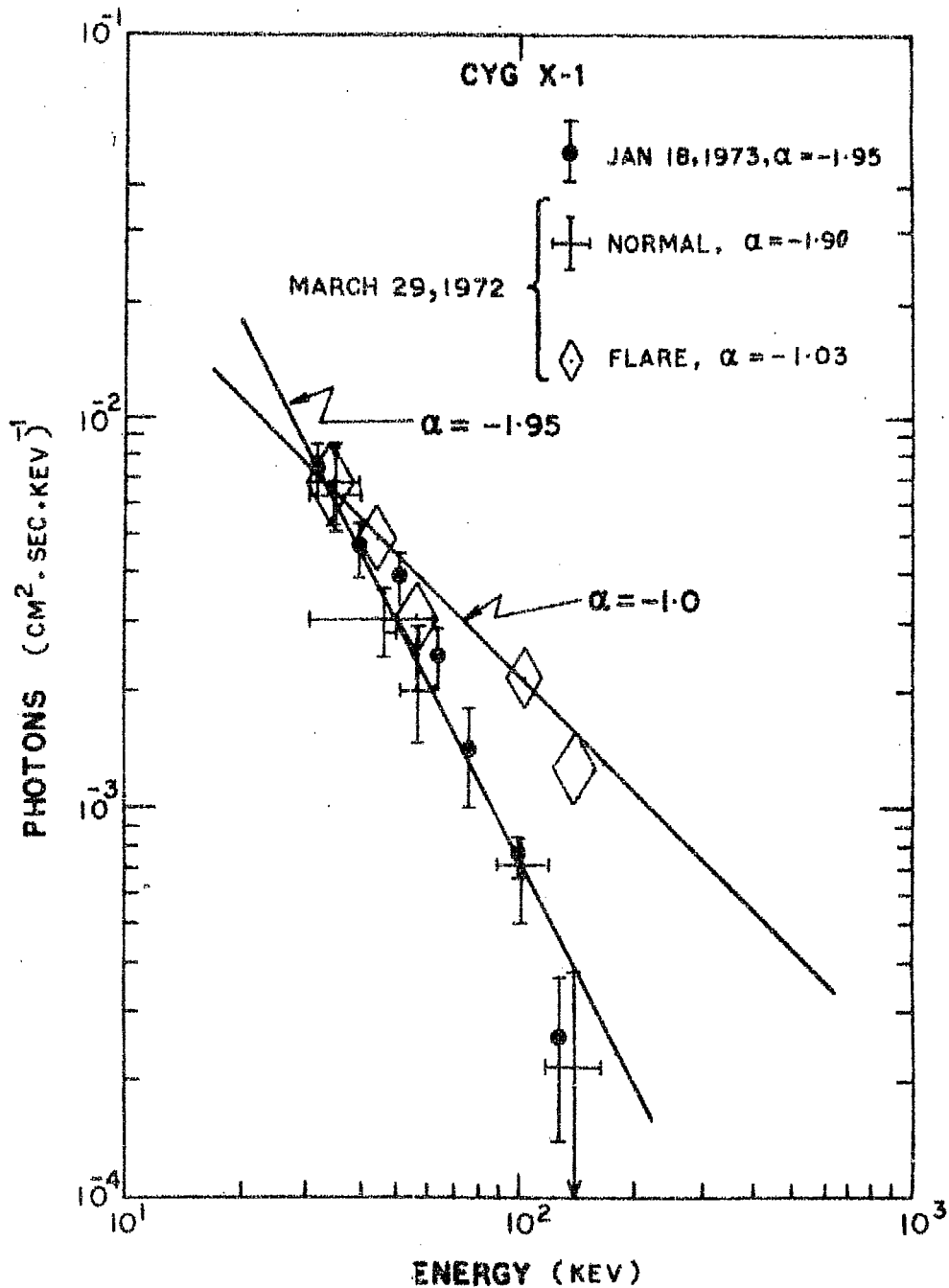


FIG.3.13: THE SPECTRA OF CYG X-1 OBSERVED DURING THE TWO BALLOON FLIGHTS. IN JAN. 1973 FLIGHT NO FLARING WAS OBSERVED BUT ON MARCH 29, 1972 THE SOURCE FLARED FOR ABOUT 10 MINUTES DURING WHICH SPECTRA HARDENED. THE POINTS DURING QUIET AND FLARE CONDITIONS ARE BEST FITTED BY POWER LAW SPECTRUM WITH EXPONENTS $\alpha = -1.9$ AND -1.0 RESPECTIVELY.

the quiet condition. After the completion of the flare the source flux decreased abruptly and returned to the normal preflare condition.

Close examination of figure 3.12a,b immediately reveal some distinct features which are characteristic of the flaring condition:

(1):- Observations indicate that during flare, the rise time to reach the peak intensity is slow i.e. takes about 10 minutes. On the other hand the decay to the normal condition is very abrupt. Whereas the statistical significance of the data is not sufficient to precisely quantify this characteristic, nonetheless the observation strongly points to the difference in rise and decay times of the flare.

(2):- A close examination of figure 3.12a indicates clearly that there is distinct time delay between low and high energies when the source is in the flare condition. The observations indicate that flaring at high energies (87.5 - 160.0 keV) starts about 5 minutes earlier to that at low energy (29.0 - 60.0 keV), a behaviour which is quite contrary to the normal expectation. To check the validity of this result we have very carefully examined the behaviour of each energy channel in the calibration mode when the entire detector is subjected to periodic calibration using a radioactive source. We conclude that the observed delay of approximately 5 minutes in the rise in intensity in lower energy channel compared to the rise at high energies is a phenomena which must have its origin in the X-ray source itself.

(3):- The best fit spectrum during the flare when compared with the preflare spectrum shows that source spectrum hardens quite considerably during the flare condition. The best fit power law spectrum in 19-160 keV range can be represented by,

$$\frac{dN}{dE} = 4.5 E^{-1.0 \pm .05} \text{ photons.cm}^{-2}.\text{sec}^{-1}.\text{keV}^{-1}$$

The average integrated intensity in the 20-100 keV energy band is $\approx 2.86 \times 10^{-8} \text{ ergs.cm}^{-2}.\text{sec}^{-1}$ which is 1.5 times higher than the quiet conditions.

3.9.2b. THE RESULTS OF SECOND FLIGHT:

The observed counting rate from Cyg X-1 during the flight on January 18, 1973 is shown in figure 3.10b and after applying all the necessary corrections for transmission through air, collimator transmission efficiency and detector efficiency as described earlier, is shown in the figure 3.13 for ease of comparison with the results of first flight. The observations are also plotted separately in figure 3.14. The observations during this flight which lasted for about an hour of time, did not show any indication of the presence of fluctuation in the source intensity. In other words, the source was essentially in the 'quiet' condition and the best fit power law spectrum consistent with the observations, in 19-160 keV range, can be represented by,

$$\frac{dN}{dE} = 6.6 E^{-1.95 \pm .11} \text{ photons.cm}^{-2}.\text{sec}^{-1}.\text{keV}^{-1}$$

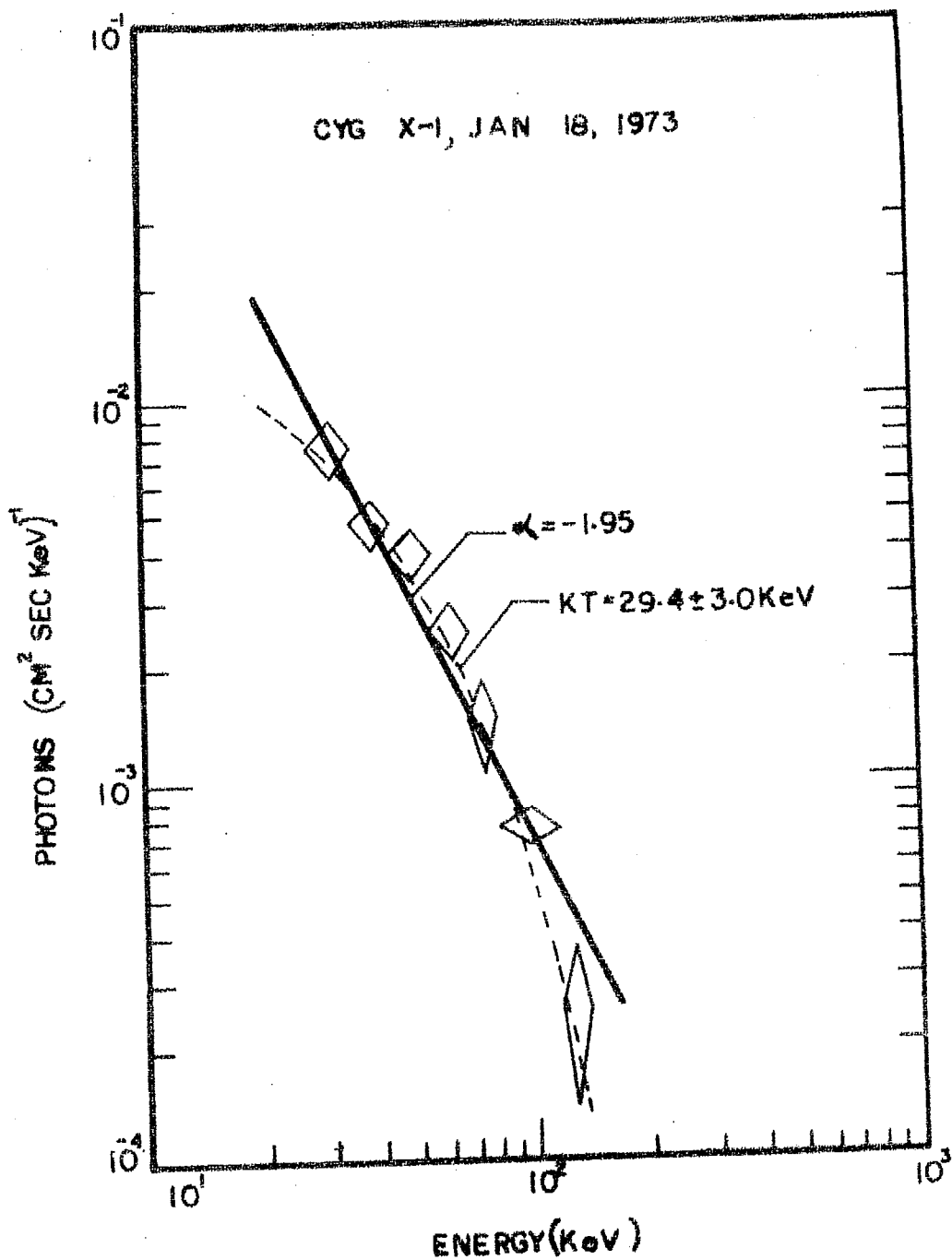


FIG.3.14: THE X-RAY SPECTRUM OF CYG X-1 OBSERVED ON JAN.18, 1973. THE EXPONENTIAL AND POWER LAW FITS ARE ALSO SHOWN.

Figure 3.14 also shows the best fit power law spectrum fitted to the observations. It may be noted that the power law index is consistent with spectral behaviour observed during the quiet condition of first flight within statistical errors.

The average integrated intensity in 20-100 keV energy range is observed to be $\sim (1.8 \pm .2) \times 10^{-8}$ ergs.cm⁻².sec⁻¹ which also agrees reasonably well with the quiet time observations of first flight. Owing to the rather poor statistics of the data obtained during the short period of observation during this flight, the data could also be fitted equally well to an exponential spectrum with a hot thin plasma temperature given by $kT \approx 29.4$ keV corresponding to $T \approx 8 \times 10^8$ °K.

3.9.2c. CONTRIBUTION DUE TO CYG X-3:

Due to the large field of view of the collimator used during the first flight on March 29, 1972 it is necessary to assess the contribution to the observed countrate, due to Cyg X-3 X-ray source which is situated very close to Cyg X-1. Further, such an assessment becomes important due to the detection of radio flare observed in September 1972, when the radio intensity of Cyg X-3 went up by a factor of ~ 2000 in the radio region and the fact that Cyg X-3 could in principle have contributed $\sim 40\%$ during the present (first flight) experiment, if there was any flare like activity associated with Cyg X-3 at the time of our observation. However, since no correlated enhancement in the X-ray emission from Cyg X-3

were detected at the time of radio flare of 1972 (Parsignault et al 1972, Conner et al 1972), we can rule out the possibility of Cyg X-3 as a cause of intensity enhancement observed during the first flight. Although, the intensity of Cyg X-3 at low energies (≤ 20 keV) is reported to change by as much as a factor of ≈ 60 during its binary period of 4.8 hours, the maximum flux observed from Cyg X-3 is still a factor of ≈ 6 lower than the quiet intensity of Cyg X-1 (Giacconi et al 1973a). Long term monitoring of Cyg X-3 above 20 keV (OSO-7 results, L.E. Peterson, private communication) seems to indicate that this source does not show flare type variation. In view of the fact that the intensity of Cyg X-3 is lower at least by a factor of ≈ 3 compared to that of Cyg X-1 (Matteson 1971) in the energy range of our interest, we conclude that Cyg X-3 could ~~not~~ have contributed $\leq 1/9$ th of the counts registered during our flight, which is too low to effect our basic conclusion regarding the flare type behaviour of Cyg X-1. Based on similar arguments we estimate the possible contribution due to Cyg X-3 in the second flight (collimator field of view $\sim 13.5^\circ$ FWHM) to be also less than 5%.

3.9.3. DISCUSSION:

3.9.3a. FLARE PHENOMENA IN CYG X-1:

The flare like enhancement of the flux observed during the first flight is undoubtedly a very unusual phenomena observed in the emission of Cyg X-1 at hard X-ray energies.

The fact that no such enhancements have been reported to date at energies less than 20 keV (Uhuru results, Schreier et al 1971, Tananbaum et al 1972b, Giacconi et al 1973a), further substantiates our observation which indicates a hardening of the spectrum during the flare.

Table 3.3 contains all the observations where 'flare' like enhancements in the Cyg X-1 emission are observed. The table includes the details of the detector system, balloon altitude, time of observation and the observational characteristics. The table also includes the phase of the optical binary corresponding to the time of the flare observed.

Examination of the table reveals the following important points regarding the flare phenomena.

(1):- The X-ray intensity in the 20-100 keV range from Cyg X-1 shows abrupt increase by factors ranging from 1.5 to 4 during the flare condition.

(2):- Considering the totality of all observations, the source is found to be in the flaring condition for $\approx 10\%$ of the total observation time. Even though the statistics is rather poor for drawing very significant conclusions, the observations do indicate that the flaring phenomena is quite an important characteristic of the source. The fact that Cyg X-1 was observed in flaring condition for ~ 10 minutes in our total observation of ~ 1 hour 15 minutes is consistent with the statistics of occurrence of flare in Cyg X-1.

Date of observation	Flight duration	Altitude Gm	Phase corresponding to optical binary	Field of view of detector and contribution from Cyg X-3(FWHM)	Observation	Spectrum	Detector	Reference
June 10 1969 0926 UT	The source was observed for ~1 hour during the transit over the detector	3.2	.430	5.9° no contribution from Cyg X-3	Fluctuation in the intensity by as large as factor of two on time scales of five minutes were observed in 17-31 keV range. At higher energies the fluctuations are not in phase. One minute data does not show any fluctuations at high energies & at low energies the statistics are poor.	In the 17 to 93 keV region (13E)-1.03 DE and 79-203 keV range the spectrum is $\frac{dN}{dE} \approx 5.E$ (-2.37). A break in the spectrum at ~83 keV is observed	NaI(Tl)+ CsI(Tl) in phos-witch mode. The total area was 54.2 cm ²	Matteson (1972)
April 4, 1971 0058 UT	The source was observed for 1 h 25 m with the help of two detectors	5.5	.11	18° Cyg X-3 contributed ~10% at the time of observation. Otherwise more than ~20% found. The intensity during the flare shot up by a factor of ~2.3.	Flare observed upto 88 keV lasting for about 3 mts. The rise and fall lasted for 9 min. Sudden drop in intensity after the flare was found. The intensity during the flare shot up by a factor of ~2.3.	No change in the spectrum was noticed on 8 mt. average basis. The flare & pre-flare spectra showed aspect-total effective area index of 1.74±.2&1.71±.25 respectively.	NaI(Tl) crystal with plastic scintillator anticoincidence shield. The area of the detector was 90 cm ²	Agrawal (1972)2

:2:

March 29 1972 0530 UT	The source was observed for 1 hour and 15 minutes	5.5 .22	18° Cyg X-3 contributed 30-40%	The flare was observed in 19-150 keV range. During flare the flux is 6.5E(-1.9) and hardens during flare to have a spectrum of the form 4.5E(-1.0)	Before flare the spectrum is 6.5E(-1.9) and hardens during flare to have a spectrum of the form 4.5E(-1.0)	NaI(Tl) crystal surrounded by plastic scintillator anti-coincidence shield. Total area ~81 cm ²	Present experiment
-----------------------	---	---------	--------------------------------	--	--	--	--------------------

The data show very large fluctuations. The data on 5 minute averaging also show same fluctuations but not in phase with that observed at high energies. The intensity during decay of flare goes down very fast.

3.47:

June 30, 1972 0046 UT	2 ^h 25 ^m	6.0 .22	18° Cyg X-3 contributed ~30%
-----------------------	--------------------------------	---------	------------------------------

The intensity during the flare goes up by a factor of ~1.8 and the flare lasted for about 10 minutes. The observation of flare is mainly below 100keV

The spectra during the flare softened to spectral index $\alpha = 2.5 \pm .2$ from an index $\alpha = 1.8 \pm .07$

NaI(Tl) detector with thickness of $\frac{1}{2}$ inch. Total area was ~280 cm²

Fulgini et al (1973)

October 7, 1972 1010UT	3 hours	5 (38km)	.45 4° x 20°
------------------------	---------	----------	--------------

The flux during the flare went up by a factor of ~4. The flare lasted for about 25 minutes. The flare had a rise time of 15 minutes and decay time of 10 minutes.

Preflare spectra was represented with an index of ~1.7 and during flare softened to ~3.9.

NaI(Tl) with plastic anticoincidence shield.

Nakagawa et al (1973)

(3):- The spectral characteristics of the source during the flare condition is usually observed to be substantially different from that during the quiet conditions. The various observations, however do not reveal a consistent picture regarding the type of spectral change the source undergoes during the flaring condition. Whereas our own observations indicate that the spectrum becomes harder during the flare, the observations of Nakagawa et al (1973) and Fulgini et al (1973) indicate a softening in the spectrum. On the other hand Agrawal et al (1972) have not been able to observe any change in the spectral characteristics during the flare conditions.

(4):- Our observation clearly indicates a time difference in the enhancement of intensity at low energy channels which seems to be delayed as compared to that in the high energy channels. Subsequently, the observations of Brinkman et al (1974) (Uhuru results) and also of Matteson (1971) also show similar type of time difference. From the body of various independent observations presented, we strongly believe that the early enhancement in the X-ray flux in high energy is an important feature of the source itself which must have its origin in the very mechanism of the production of emission and its acceleration. It is very important for any model which tries to explain the production of X-rays to take into account this property.

(5):- It is obvious from the table that out of the five observations listed here four observations (present experiment, Matteson et al 1971, Fulgini et al 1973 and Nakagawa et al 1973) show abrupt enhancements in the intensity to be at phase $.5 \pm .2$ i.e. very close to the maximum intensity of the optical binary. This indicates that the 'flare' phenomena is usually associated with the maximum light emission of the optical counter part. Our own observations of Cyg X-1 conducted at times corresponding to the optical phase ≈ 0.22 and ≈ 0.1 also support this view since the flare condition was observed only when the optical counterpart was brighter. It is interesting to note that the recent satellite observations (Li et al 1974, Sanford et al 1974) at energies ≤ 40 keV have also indicated that the variation in X-ray emission is well correlated with the optical luminosity.

3.9.3b. TIME VARIATION OF FLUX FROM CYG X-1:

As already mentioned earlier, Cyg X-1 emission shows large fluctuations in its emission at all X-ray energies. In fact the emission is observed to be in the form of pulse trains having durations from a few milli seconds to several seconds. Not only short duration pulse trains are reflected in its emission but the source also shows a long term time variation in its intensity. All the observations of Cyg X-1 conducted at energies above 20 keV are collected in table 3.3 where along with the date of observation, the energy range of measurement and the observed spectral characteristics are given. The flux at 30 keV is also given in the same table.

Table 3.4 - SUMMARY OF OBSERVATION OF CYG X-1 (HIGH ENERGY)

Date of observation	Observer	Energy range (keV)	Flux at 30 keV ergs.cm ⁻² .sec ⁻¹ x 10 ⁻⁹	Spectral data
April 4, 1965	McCracken (1966)	20-58	.24	-
April 13, 1965	Brini et al (1965)	20-200	.36 ± .05	-2
October 28, 1965	Grader et al (1966)	1-40	.335 ± .15	-2
January 13, 1966	Boidt et al (1966)	20-100	.33 ± .10	-1.5 ± 0.2
April 5, 1966	Bleeker et al (1967)	20-130	.43 ± .09	16
April 27, 1966	Reigler (1969)	20-60	.38 ± .07	-2.2 ± .8
July 19, 1966	Clark et al (1968)	20-100	.28 ± .04	7.47
September 13, 1966	Peterson et al (1968)	20-200	.24 ± .04	-2.0 ± .3
September 19, 1966	Overbeck et al (1967)	23-97	.25 ± .02	-
February 13, 1967	Lewin et al (1968)	20-100	.36 ± .10	3.58
April 20, 1967	Rocchia et al (1969)	18-130	.29 ± .05	4
April 29, 1967	Chodil et al (1968)	23-80	.51 ± .09	-1.6
May 3, 1967	Bingham et al (1969)	20-130	.575 ± .085	-
May 3, 1967	Reinert (1969)	20-100 100-200	.57 ± .05	3.05
May 16, 1967	Overbeck et al (1968)	23-101	.6 ± .04	-1.83 ± .15
May 25, 1967	Overbeck et al (1968)	23-101	.48 ± .05	-

:3.50:

60±4.4

-2.5±.6

3.45

-1.71±.1

9.50

-3.1±1.5

-1.7

-1.7

June 27, 1967	Overbeck et al (1968)	23-101	$.36 \pm .04$	-	-1.7
August 29, 1967	Haymes et al (1968)	25-123	$.35 \pm .03$	$3.42 \pm .58$	$-1.8 \pm .04$
October 2, 1967	Glass (1969)	20-70	$.39 \pm .05$	3.36	-1.780
January 15, 1968	Metzger et al (1968)	20-33	$.16 \pm .04$	-	-
October 25, 1968	McClinktock et al (1969)	15-65	$.27 \pm .10$	10.5 ± 1.2	-2.0
December 22, 1968	Agrawal et al (1972)	30-119	$.56 \pm .06$	-	-
April 16, 1969	Agrawal et al (1972)	25-150	$.38 \pm .16$	3.54	$-1.89 \pm .22$
May 10, 1969	Webber et al (1970)	25-150	$.28 \pm .035$	-	-2
June 5, 1969	Haymes et al (1970)	34-124	$.19 \pm .07$	$4.57 \pm .61$	$-1.91 \pm .03$
June 10, 1969	Matteson (1969)	17-93 79-203	$.335 \pm .025$	$.134 \pm .006$ 5.0 ± 3.1	$-1.03 \pm .12$ $-2.37 \pm .29$
July 17, 1969	Matteson (1969)	24-159	$.1 \pm .05$	1.8×10^{-2}	-1.03
April 6, 1971	Agrawal et al (1972)	22-154	$.385 \pm .03$	5.41	$-1.92 \pm .10$
December 17-24, 1971	Baity et al (1973)	7-150	$.34 \pm .03$.81	$-54 \pm .24$
March 29, 1972	Present	20-160	during flare normal	4.5 6.1	-1.0 -1.90
June 30, 1972	Fuligni F & Frontera F (1973)	20-200	during flare normal	- -	$-2.5 \pm .2$ $-1.8 \pm .07$
October 7, 1972	Nakagawa et al (1973)	20-100	normal flare	- -	-1.8 -3.9
January 18, 1973	Present	20-160	$.36 \pm .07$	6.6	-1.95

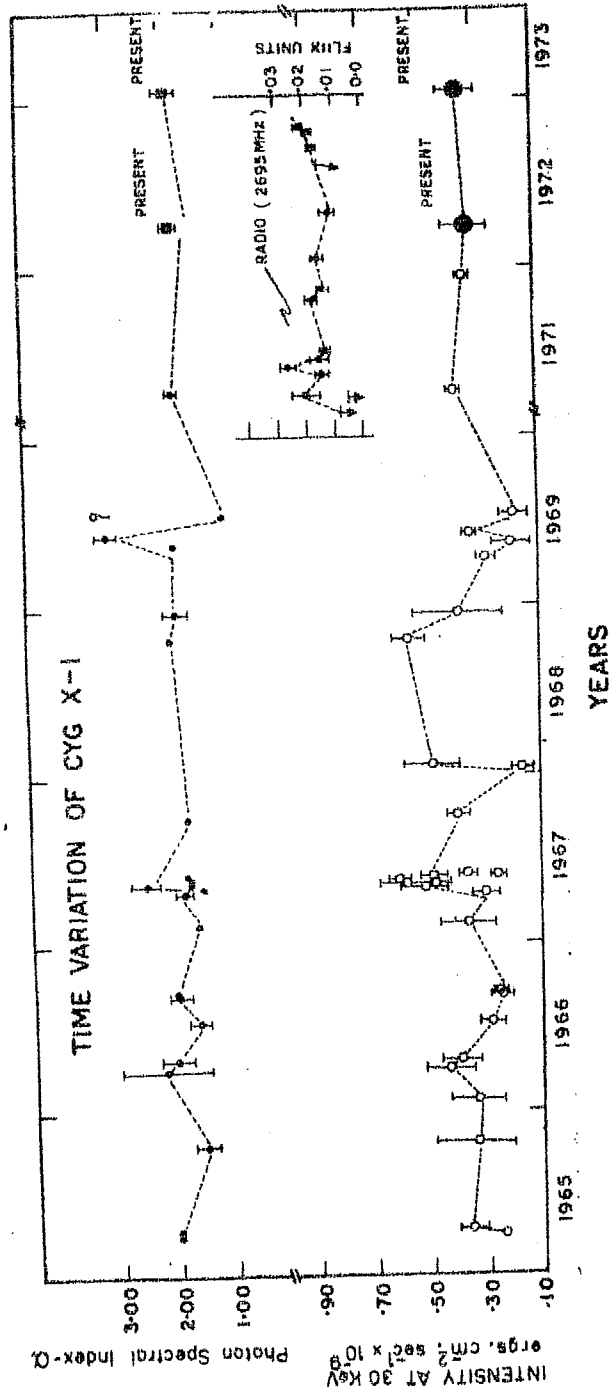


FIG.3.15: THE TIME VARIATION OF INTENSITY OF CYG X-1 AT 30 KEV.

All the observations listed in table 3.4 are plotted in the figure 3.15. Plotted in the same figure are also the simultaneous radio flux measurement at 2695 MHz wherever available in addition to spectral index and intensity at 30 keV. The observations during the flare condition are not plotted. It can be seen from this figure that spectral index remains very close to ≈ 1.90 .

In addition to the flare like enhancements in the emission of Cyg X-1, figure 3.15 indicates that the X-ray flux even during quiet conditions does show variation of flux from epoch to epoch, intensity showing variations by as large as factors of two. However, it is very interesting to note that the spectral indices except in one or two doubtful observations, have shown almost a constant value over a period of almost 8 years spanning from 1965 to 1973.

3.9.4. MODELS FOR CYG X-1:

Before we proceed to describe a suitable model for Cyg X-1 some salient features based on our own observations and the introduction presented in chapter I can be listed as follows:

(1):- The present balloon observations and the experiments performed by other experimenters at low energies as well as at high energies show that the spectrum follows a power law. However, our observation of January 18, 1973 and of Haymes et al (1968)

show that they can also be fitted with an exponential spectrum with a plasma temperature of $\approx 10^9$ °K.

(2):- The emission at all the energies is characterised by short duration non-periodic pulsations.

(3):- At balloon energies (i.e. ≥ 20 keV) short duration flares are observed during which the intensity goes up by several factors and then drops in a very abrupt manner. The spectrum observed during these flares is different than that observed at quiet times.

(4):- Cyg X-1 has been identified with a spectroscopic optical binary HDE 226868.

(5):- So far no conclusive measurements exist indicating a correlation between the quiet time X-ray emission at hard energies with the optical binary cycle. At low energies (≤ 20 keV), however, evidence exists for a considerable change in X-ray luminosity coincident with optical minima and maxima (Li et al 1974, Sanford et al 1974).

(6):- A weak variable radio source of average intensity ≈ 0.15 f.u. is identified with the X-ray source.

The short duration fluctuations (few seconds to few minutes) show that the X-ray source should be of compact nature with a mean density $\geq 10^6$ gm. cm⁻³. Thus there are only three types of objects which can be considered as the possible source of X-rays viz. white dwarf, neutron star or black hole.

Bolton by solving the optical light curve of HDE 226868 on the light velocity diagram, has derived the various parameters of this binary and calculated that the mass of star, so derived ($\approx 14.5 M_{\odot}$) rules out the possibility of it being either a neutron star or a white dwarf. This leads us to conclude that the unseen X-tar is a black hole and the X-ray emission is due to the matter being accreted on to this star from the massive companion, part of which is liberated as X-ray emission which is detected at the earth. Recent observation of short period fluctuation on time scales of the order of ≈ 1 ms by Rothschild et al (1974), if interpreted in terms of turbulence in the disc accretion at the innermost orbits, leads us to conclude that the radius of the star must be $\approx 10^2$ km again indicating that Cyg X-1 must be a black hole.

The X-ray emission takes place when the accreted mass while approaching towards the Schwartzchild radius gets heated during its acceleration. In such a case one would expect to observe a distinctive signature of low energy absorption as the matter accretes on to the star. The delay in the enhancement of low energy X-rays during flaring condition observed in our present experiment as well as by other similar experiments can be considered as an evidence signifying the above hypothesis. The emission from the mass spilling towards the compact companion is further confirmed by the observation of He II, λ_{4686} in the optical region whose radial velocity is in antiphase to the radial velocity of absorption indicating

that the mass giving rise to this line is intimately associated with the compact, unseen companion of giant star HDE 226868.

Having established that the emission in Cyg X-1 is due to the accretion of mass on to a black hole one has to explain the absence of the correlated emission throughout the X-ray spectrum and at optical wavelengths. To explain this we suggest the following hypothesis:

(1):- The radiating mass being accreted on to the radius of light circle is always out of the field of view of the observer. This situation can be justified by favourable orientation of the orbit of the black hole around the giant star.

(2):- Alternately, we propose that the giant star is also a major contributor to the X-rays observed and emits mainly towards high energy. Moreover, the absence of variation in X-ray intensity (at hard X-ray energies) correlated with the optical emission in the binary cycle indicates that either the emission due to accretion is too weak or the emission is mainly at soft X-ray energies.

We favour the second case as more suited to explain the observed data. If the smaller star is responsible for only soft X-ray production, the emission of hard X-rays by the giant star will not allow any modulation due to the orbital motion at these energies, even though, modulation should still be observable at relatively soft X-ray energies.

The fact that the existence of such modulation is confirmed by Li et al (1974) and Sanford et al (1974) adds further credence to this model.

The calculations of luminosity and frequency of spectrum from the interstellar gas being accreted on to a black hole in spherically symmetric steady state accretion for the case when black hole is non rotating and is at rest in the interstellar space, are made by Stuart Shapiro (1973). The principal radiation mechanisms considered by him are electron photon and electron electron bremsstrahlung. The results for a black hole of $1 M_{\odot}$ show that the spectrum should have an exponential shape with a temperature $\approx 10^9$ °K. The results from present flight (second flight) and other workers (Haymes et al 1968), which show that the data from this source can be fitted by an exponential spectrum having a plasma temperature $\approx 10^9$ °K, seem to support the above hypothesis.

Recently, Brecher and Morrison (1973) have pointed out that there is no need to invoke black hole to explain the X-ray emission from Cyg X-1. They have shown that the observed emission could be explained by assuming the X-tar to be a magnetic, differentially rotating white dwarf. Their theory does not explain how the large mass of X-tar could be stabilized in this condition. Nor does it explain the observation of flares.

Jackson (1972) has suggested a model which explains the production of X-rays at high energies assuming the unseen X-ray star to be a source of relativistic electrons. These

electrons presumably convert the ultra violet photons from the X-tar into hard X-rays by inverse Compton scattering which can account for the observed power law spectrum. According to this model the intensity modulation would arise due to X-ray photons at maximum intensity originating from ultra violet photons suffering a head on collision with electrons whereas the intensity at minimum arising from tail on collisions. The model is plausible only if the relativistic electrons are contained within a small region, not significantly longer than the component spectrum.

So far no satisfactory model exists which can explain all the observed properties. The important points that emerge from the studies described so far are summarised below:

- (1):- At hard X-ray energies, Cyg X-1 shows flare like enhancements in intensity lasting for several minutes and which probably have some relationship with the phase of the optical binary.
- (2):- The spectral index in flare condition is different from that observed during normal condition.
- (3):- The spectrum at high energies is also consistent with an exponential spectrum.
- (4):- Simultaneous observations in X-ray, radio and optical region should be carried out to gain a better understanding of the physical nature of the system.

CHAPTER - IV

MONITORING OF X-TARS THROUGH IONOSPHERE

4.1. INTRODUCTION:

Extensive investigations by Kreplin (1961) at NRL using rocket borne proportional counters led to the preliminary conclusion that the sun emits X-rays in the wavelength range 0-60Å more or less continuously. Subsequently satellite observations (Kreplin, Chupp and Friedman 1962, Lindsay 1963) have established a quiet time energy flux of about 10^{-4} ergs. cm^{-2} . sec^{-1} that could increase by an order of magnitude during disturbed periods. These solar X-rays in their propagation through the atmosphere are absorbed at different altitudes depending on their energy thus providing a source of ionization (Swider 1969).

The possible significance of X-radiation in the formation of the D-region was suggested many years ago by Muller (1935) and again by Rawer (1952) and more recently by Chamberlain (1961). Using the data obtained during solar maxima, Poppoff and Whitten (1962) demonstrated the significance of X-radiation in the lower D-region. Owing to the fact that VLF propagation should be affected by the changes in the D-region ionization, Anathakrishnan (1969) investigated the VLF field strength variation associated with the changes in the solar X-ray emission and came to the conclusion that there is a positive correlation between the two. This confirmed the earlier prediction that solar X-rays comprise a significant

energy input at D-region altitudes from the standpoint of ionization.

These considerations led us to suspect that strong non-solar X-ray sources may also significantly influence the VLF propagation especially during the night time when the effect of solar X-rays is virtually absent. A search of the VLF data recorded at Ahmedabad corresponding to the 164 KHz transmission from Tashkent, was made to look for the effects associated with the transit of Sco X-1. The choice of this source for looking for the VLF effect was made on the consideration of its strength in the 1-10 keV range which is about 5×10^{-7} ergs. cm^{-2} . sec^{-1} . The genuineness of this effect was convincingly demonstrated by the apparent shift in the peak absorption on a day to day basis arising from the sidereal effects.

Investigation by Edwards et al (1969) and Kaufman et al (1970) further confirmed the observability of this effect in relation to Cen X-2 and Cen X-4 besides Sco X-1. Burgues and Jones (1969) in their search of the data corresponding to the Omega navigational system, however, could not find positive evidence for ionospheric detection of X-ray sources. From the theoretical standpoint, Whitten and Poppoff (1969) questioned the effectiveness of the extrasolar X-ray sources in providing significant electron density perturbations at D-region altitudes. They computed contributions from the ambient ionization against such as Ly α radiation, galactic cosmic rays and

celestial X-ray background and compared the resultant total effect with that expected from discrete celestial sources thus demonstrating the insignificant role of the latter. Further, they objected to the interpretation by Ananthakrishnan and Ramanathan (1969) on the basis of observed time profile. From a more detailed analysis, Francey (1970) questioned the analysis by Whitten and Poppoff and showed that the relative importance of the contributions from the discrete cosmic X-ray sources to the electron production rates in the night time D-region critically depend upon the value of the concentration of NO (which is ionized by $Ly\alpha$) in the 80-90 km region, used in the calculation. Thus the observability of the effect of the celestial sources on the ionosphere depends on the magnitude of their ionizing effect compared to that from all other sources and in particular to the magnitude of ionization due to $Ly\alpha$.

Considerable uncertainties exist in the experimentally observed values of the different parameters responsible for the night time D-region ionization. Nevertheless, in view of the strong experimental evidence obtained at Ahmedabad and elsewhere in favour of the detectability of the ionospheric effects of the discrete X-ray sources, a reappraisal of the role played by different ionization agencies seems to be highly desirable. Such an investigation, in addition to resulting in a better understanding of the night time D-region processes could also be in principle the first step towards

evolving a simple and relatively inexpensive ground based technique for the long term monitoring of the X-ray sources. With these considerations, the role of the different ionization agencies in having a significant impact on the night time D-region processes with particular reference to the effects of celestial X-ray sources is re-examined in this thesis. First, a critical assessment is made of the relative importance of the various agencies to the ionization of the night time D-region. The computations have been made using the most recent values available of the relevant parameters. Secondly, the effects of the transit of strong X-ray sources Sco X-1 and Tau X-1, are evaluated in terms of the electron density enhancements. The contribution expected due to X-rays from the galactic centre is also estimated. The calculation of electron densities is made by a direct comparison of the electron production rates by different ambient ionization agencies with the experimentally measured electron densities. Towards the end of the chapter, the observed VLF absorption of the 164 KHz signal from Tashkent recorded at Ahmedabad has been shown quantitatively to be related to the computed ionization effects of the X-ray sources and thus the satisfactory agreement between the observations and the theoretical calculations of the magnitude and time profile of VLF absorption is demonstrated.

4.2. IONIZATION DUE TO CELESTIAL X-RAY SOURCES:

It has been shown by a number of authors (Whitten et al 1965, Swider 1969, Francey 1970) that the X-rays in the energy range 1-10 keV impinging on the top of the atmosphere produce ionization mainly in the 80-90 km height interval. At lower altitudes, the effect of X-rays becomes relatively unimportant due to severe exponential absorption they undergo in the atmosphere during their passage downwards. In addition, whereas X-rays below 1 keV are absorbed considerably even at altitudes of 100 km, those above 10 keV for normal power law spectrum of the type E^{-2} , contribute very little to the ionization due to their low flux at altitudes below 70 km.

The energy absorption per unit volume from a monoenergetic beam of X-rays of intensity $I(\text{keV} \cdot \text{cm}^{-2} \cdot \text{sec}^{-1})$ passing through a path dx (cm) of the absorber is given by

$$\frac{dI}{dx} = \rho \mu(E) \cdot I \text{ keV} \cdot \text{cm}^{-3} \cdot \text{sec}^{-1}$$

where ρ = density of the absorber ($\text{gm} \cdot \text{cm}^{-3}$)

$\mu(E)$ = mass absorption coefficient (Photoelectric linear attenuation coefficient, $\text{cm}^2 \cdot \text{gm}^{-1}$) and is a function of energy.

The electron production rate in a volume element at altitude h km is correspondingly given by

$$q(h) = \frac{\mu(E) \rho(h) \cdot I(h)}{Q} \text{ electrons} \cdot \text{cm}^{-3} \cdot \text{sec}^{-1} \quad \dots (4.2)$$

where $Q = 0.035$ keV is the average energy for the production of an ion pair, $I(h)$ is the intensity of the X-ray source

at height h and is related to its primary intensity I_0 , by

$$I(h) = I_0 \exp \left[- \mu(E) \int_h^{\infty} \left(\frac{\rho(H)}{\cos Z} \right) dH \right] = F \text{ (say)} \quad \dots(4.3)$$

where Z is the 'Local' zenith angle at h. Using a reasonable approximation for the curved atmosphere (for $H \geq h$ and actual zenith angle $z < 90^\circ$) Z is obtained using the relationship

$$\cos Z = \left[1 - \left\{ \frac{R + h}{R + H} \cdot \sin z \right\}^2 \right]^{-\frac{1}{2}} \quad \dots (4.4)$$

where R = Earth's radius = 6371 kms.

Thus, if a source has a spectrum of the form

$$J(E) \cdot dE = K \cdot f(E) \cdot dE \cdot \text{keV} \cdot \text{cm}^{-2} \cdot \text{sec}^{-1} \quad \dots (4.5)$$

The electron production rate due to X-rays having energy in the band E_1 to E_2 keV, at height h and zenith angle z is calculated from

$$\begin{aligned}
q(h) &= \frac{1}{Q} \cdot \rho(h) \cdot I(h) \\
&= \frac{\rho(h)}{Q} \int_{E_1}^{E_2} \mu(E) \cdot K f(E) \cdot dE \cdot \exp \left[-\mu(E) \int_h^{h'} \rho(H) \cdot \left\{ 1 - \left(\frac{R+H}{R+H} \cdot \sin^2 z \right)^{\frac{1}{2}} \right\} dH \right] \\
&= \frac{\rho(h)}{Q} K \cdot \int_{E_1}^{E_2} \mu(E) dE f(E) \cdot \exp \left[-\mu(E) \int_h^{h'} \rho(H) \cdot \left\{ 1 - \left(\frac{R+H}{R+H} \sin^2 z \right)^{\frac{1}{2}} \right\} dH \right]
\end{aligned}$$

electrons.cm⁻³. sec⁻¹ ... (4.8)

The electron production due to isotropic background X-rays whose spectrum can be described by

$$J(E).dE. d\Omega = K.f(E).dE. d\Omega \text{ keV. cm}^{-2}. \text{sec}^{-1}. \text{sr}^{-1}$$

is obtained by integrating the contribution over all energy elements for the solid angle $d\Omega$ over the zenith angle z and azimuths from 0 to 2π .

Since,

$$d\Omega = \sin z. d\theta. dz$$

we get

$$q(h) = \frac{2\pi \cdot \rho(h)}{Q} \cdot K. \int_{E_1}^{E_2} \mu(E). f(E). \int_0^{89} \sin z. \exp \left\{ -\mu(E) \int_h^{h'} \rho(H) \left[1 - \left(\frac{R+h}{R+H} \cdot \sin z \right)^2 \right]^{-\frac{1}{2}} dH \right\} dz. dE. \text{electrons. cm}^{-3}. \text{sec}^{-1} \dots (4.7)$$

The values of $\mu(E)$ are taken from the tables computed by Victoreen (1949) and Henke et al (1967). The densities of the atmosphere at various heights used in these calculations are obtained from the 1965 CIRA model. The above equation is then integrated using the appropriate values for the various parameters and the electron production rates are then calculated for different X-ray sources. The X-ray data corresponding to Sco X-1 and Tau X-1 are taken from Gorenstein et al (1969) Chodil et al (1969), Reigler et al (1971). The calculated electron production rates for Sco X-1, galactic center and Tau X-1 are shown in figure 4.1 for two zenith angles, $X = 0^\circ$ and $X = \theta$, where θ is the effective zenith angle at the point corresponding to the single hop reflection for VLF transmission between Tashkent and Ahmedabad.

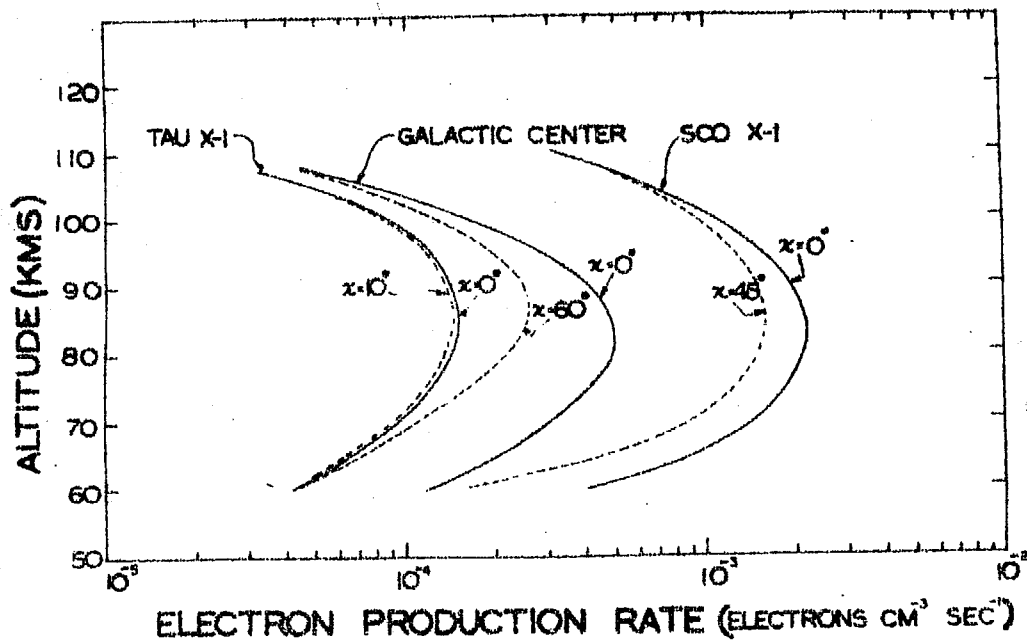


FIG. 41 - THE FIGURE SHOWS THE ELECTRON PRODUCTION RATES PRODUCED DURING THE TRANSIT OF TAU X-1, SCO X-1 AND GALACTIC CENTER. THE CURVES ARE SHOWN BOTH FOR 0° ZENITH AND THAT CORRESPONDING TO MID OF SINGLE HOP POINT OF REFLECTION BETWEEN TASKENT AND AHMEDABAD.

4.3. IONIZATION DUE TO OTHER SOURCES IN THE NIGHT TIME D-REGION:

As the effect due to X-rays from celestial sources depends on the magnitude of their ionization relative to that arising from other ionizing agencies in the night time ionosphere, a critical study of the role of the latter becomes necessary. The various ambient ionizing agencies responsible for the production of electrons in the nocturnal D-region are now identified to be

1. Diffuse cosmic X-rays
2. Galactic cosmic radiation
3. Ly α radiation
4. Ly β radiation
5. Meteors.

In addition to the above, possible role of soft electron fluxes at D-region altitudes has been pointed out by Tulinov et al (1969) and Potemra and Zmuda (1970). Precipitation effects from Van Allen belts have been advocated as a source of these low energy electrons by Thomas (1971) and Aikin (1971). However, owing to the inconclusive nature of the evidence of the importance of these fluxes as a source of night time D-region ionization, especially at lower latitudes ($L \approx 1$ to 2) from where all the positive VLF observations of the celestial X-ray effect have been reported, this effect is left out of the present consideration.

In what follows, the effects of the above agencies are described one by one.

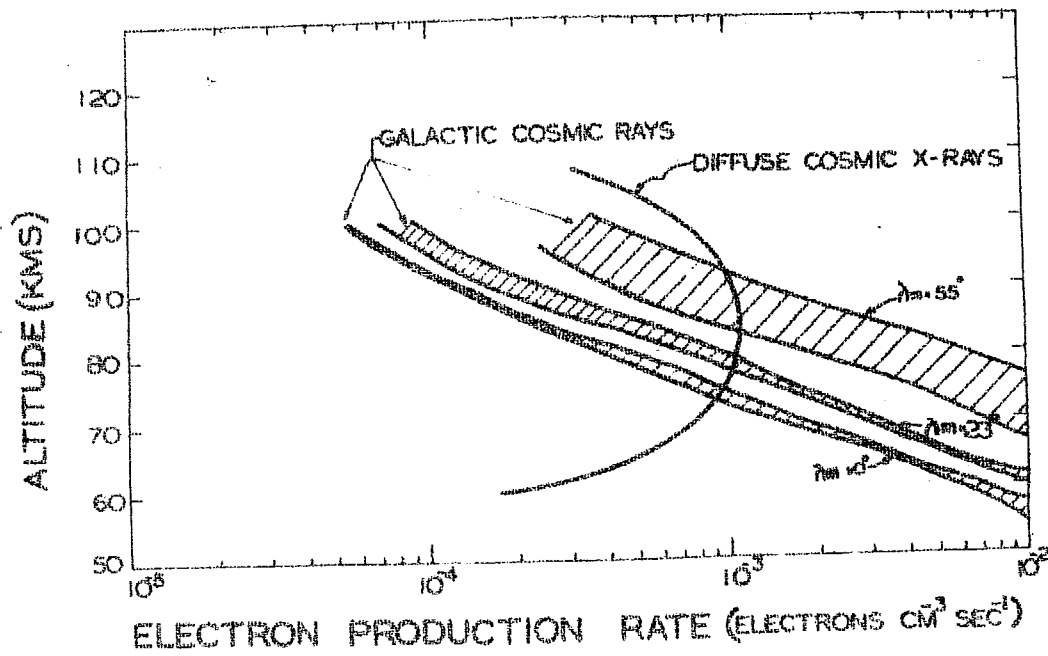


FIG. 4.2- THE FIGURE SHOWS THE ELECTRON PRODUCTION RATES DUE TO DIFFUSE BACK GROUND X-RAYS AND ARE COMPARED TO THOSE PRODUCED BY GALACTIC COSMIC RAYS AT VARIOUS LATITUDES.

4.4. IONIZATION DUE TO THE DIFFUSE COSMIC X-RAYS:

The ionization due to the diffuse cosmic X-ray background in the energy range 1-10 keV can be estimated fairly accurately because of the reasonable accuracy of the available rocket observations in this energy range (Prakasarao et al 1971, Gorenstein et al 1969 and Boldt et al 1969). The electron production rate due to the diffuse cosmic X-ray flux is calculated on the basis of equation 4.7, assuming a spectral distribution of the type,

$$\frac{dN}{dE} = 13.6 E^{-1.7} \text{ photons. cm}^{-2} \cdot \text{sec}^{-1} \cdot \text{keV}^{-1} \quad \dots(4.8)$$

Such a spectral function is also consistent with that evaluated by Kasturirangan and Rao (1972) who have critically examined all the available data on the background X-ray flux. The resulting electron production rate is shown in figure 4.2. Since the effect due to difference between different atmospheric models is completely negligible below 100 kms (Francey 1970), the CIRA 1965 model of the atmosphere has been used in these calculations.

4.5. IONIZATION DUE TO GALACTIC COSMIC RAYS:

The role of the galactic cosmic radiation on the D-region ionization process was initially investigated by Webber (1962) in some detail. A more thorough analysis including the ionization effects of particles of higher charge numbers has been recently made by Velinov (1968) for locations corresponding to four different geomagnetic latitudes $\lambda_m = 0^\circ, 30^\circ, 41^\circ$

and 55° for both solar maximum and solar minimum periods. The analysis shows that the electron production due to primary cosmic X-ray flux besides being dependent on the geomagnetic latitude and the degree of solar activity also exhibits seasonal variations due to changes in the density of the atmosphere at any particular altitude. Taking into account the observations of annual variations of the atmospheric density (Spencer et al 1964, Stroud and Nordberg, 1963) and the eleven year variation of the cosmic ray intensity, the calculations indicate that cosmic rays produce minimum ionization during winter of maximum solar activity period and maximum ionization in the summer of minimum activity period. The electron production rates by cosmic rays at geomagnetic latitudes 0° , 23° and 55° in the 60-100 kms range based on the calculation of Velinov (1968) are shown in figure 4.2. The extent of variation in the production rates resulting from the solar modulation effects of the cosmic radiation and the seasonal variation of the atmospheric densities are shown by the shaded areas.

4.6. IONIZATION FROM NIGHT TIME $Ly\alpha$:

4.6.1. NIGHT TIME $Ly\alpha$:

Another important and crucial source of night time D-region ionization, on which considerable uncertainty still exists, is the ionization due to $Ly\alpha$ radiation. It is generally believed that 85% of the night time $Ly\alpha$ emission originates from scattering of solar $Ly\alpha$ by hydrogen in the

geocorona. The rest probably comes from galactic sources such as emission from gaseous nebulae (Tinsley 1969). The $\text{Ly}\alpha$ radiation produces ionization in the atmosphere through photo-ionization of nitric oxide (Nicolet and Aikin 1969). Hence a realistic evaluation of ionization due to $\text{Ly}\alpha$ requires an accurate knowledge of the night time $\text{Ly}\alpha$ intensity as well as the concentration of nitric oxide.

Available observational data on "scattered" $\text{Ly}\alpha$ intensity at the top of the atmosphere from various spacecrafts such as OGO III, OGO IV and OSO IV show the existence of a diurnal variation in the intensity of this component from 20 kR at noon down to about 1.1 kR at midnight (Meier, 1970). Over a solar cycle, a change by almost a factor of two in the solar $\text{Ly}\alpha$ intensity has also been reported by Hinteregger (1965). In the present case $\text{Ly}\alpha$ intensity of 1.1 kR ($\approx 1.5 \times 10^{-3}$ ergs. cm^{-2} . sec^{-1} . sr^{-1}) for the solar minimum period and 2.7 kR ($\approx 3 \times 10^{-3}$ ergs. cm^{-2} . sec^{-1} . sr^{-1}) for the solar maximum period are taken at the top of the atmosphere for the estimation of night time ionization in the D-region.

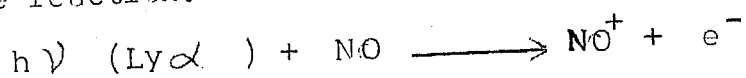
4.6.2. MOLECULAR OXYGEN DENSITY:

For the determination of the $\text{Ly}\alpha$ intensity in the 70-90 km altitude range, it is necessary to fold into calculations the absorption cross-section of O_2 10^{-20} cm^2 in the narrow band around 1216 \AA (Watanabe 1958), i.e. the intensity of $\text{Ly}\alpha$ at any depth is essentially determined by the total molecular

oxygen concentration above that height in the atmosphere. Even though the estimation of molecular oxygen density at higher levels is dependent on the assumed model of the atmosphere, below 120 km altitude, where most of the $\text{Ly}\alpha$ absorption takes place, all atmospheric models (CIRA 1965, US Standard 1966, Jacchia, 1970) essentially predict the same value. Further, direct experimental observations of molecular oxygen (Carver et al 1964, Wildman et al 1969, Brannon and Hoffman 1971) are found in good agreement (within 20%) with the molecular oxygen predicted by CIRA model, particularly at altitudes below 110 kms. The recent results measured using rocket borne $\text{Ly}\alpha$ detectors in the height range 70-100 km by Subbaraya et al (1972) near geomagnetic equator are also in good agreement with the CIRA model. A diurnal variation of less than about 20% is indicated from the existing measurements (Weeks and Smith 1968) on the density of molecular oxygen.

4.6.3. NITRIC OXIDE DENSITY:

The principal difficulty in the estimation of the $\text{Ly}\alpha$ ionization stems from the uncertainties in our knowledge of the NO density profile. $\text{Ly}\alpha$ flux attenuated through absorption by molecular oxygen ionizes NO to produce electrons in the D-region ionosphere (Nicolet and Aikin 1960) according to the reaction.



The cross section for the above reaction is $2 \times 10^{-18} \text{ cm}^2$ (Watanabe 1958). Owing to the fact that a realistic evaluation of the extent of contribution to the electron concentration in the night time D-region made through this reaction is most crucial to the present problem, an appraisal of the present status of our knowledge on NO density altitude profile appears to be appropriate.

The information on the NO concentration in the mesosphere has been derived by direct rocket observations of its resonance fluorescence day glow in the gamma bands [$\gamma(1,0)$ band ; Barth 1966, Pearce 1969, Meira 1971] and from the diurnal and solar cycle variations of the electron density in the D-region (Mitra 1966, Mitra 1968) as well as through photochemical considerations (Nicolet 1965, Wagner 1966). The day glow observations using rocket borne spectroscopic techniques have yielded results which seem to be conflicting with each other at altitudes below 90 km. The recent values of Meira are considerably lower than those from earlier measurements of Barth and Pearce. Revised values of Pearce (Thomas 1971) are, however, close to Meira's results. The major difficulty of interpreting the NO day glow measurements stems from complicated correction from the background radiation resulting from Rayleigh scattering. Meira's results show the NO density to be a minimum around 85 km and gives a value $\approx 10^7 \text{ cm}^{-3}$ for this altitude.

By identifying the atmospheric level at which the $\text{Ly}\alpha$ ionization predominates from an examination of the diurnal variation of the electron density profile, Mitra (1969) concludes that the NO density at 75 km should be around $7 \times 10^6 \text{ cm}^{-3}$. Study of solar cycle variations in the electron density yields about $8 \times 10^5 \text{ cm}^{-3}$ for NO concentration at 70 kms (Mitra 1966). Adopting other ionospheric methods such as the use of measured NO^+ and O_2^+ concentrations together with the relevant rate coefficients (Wagner 1966) or zenith angle variation in absorption (Parthasarathy and Larfald 1965) the NO density has been estimated to be in the range of $1-2 \times 10^6 \text{ cm}^{-3}$ between 75 and 80 kms. These values are also consistent with those expected from photochemical considerations (Mitra 1969) although they are much higher than the earlier estimates of Nicolet and Aikin (1965). In table 4.1 we summarise the values of NO density estimated by different methods at heights around 75 km. It is seen from the table that the NO concentration estimates around this altitude, even though derived from different methods are all in fair agreement with each other, the mean value at 75 kms being $\approx 2 \times 10^6 \text{ cm}^{-3}$.

In addition, some of the altitude profiles of NO concentration obtained by experimental observations and theoretical calculations are shown in figure 4.3. It is seen from this figure that considerable discrepancy exists in the existing data on the value of NO density at different

Table 4.1

Height (kms)	NO concentration (cm^{-3})	Method of estimate	Reference
70	8×10^5	From solar cycle variation in electron density	Mitra (1966)
75	2×10^6	From diurnal variation in electron density	Mitra (1968)
75	2×10^6	From NO^+ , O_2^+ measurements	Mitra (1968)
75	1.8×10^6	From laboratory measurements of rate coefficients	Kistiakowsky and Volpi (1957)
75	2×10^6	Same as above	Mavo rayannis and Winckler (1961)
75	3.5×10^6	Same as above	Clyne and Thrush(1959)
75	3×10^7	NO Air glow by rocket	Meira (1971)
80	1×10^6	Zenith angle variation in absorption	Parthasarathy and Larfald (1965)
80	6×10^7	NO Air glow by rocket	Barth (1966)
80	1.7×10^7	Same as above	Meira (1971)
84-100	10^6	From NO^+ , O_2^+ measurements	Wagner (1966)
85	6×10^7	NO Air glow by rocket	Barth (1966)
85	1.3×10^7	Same as above	Meira (1971)

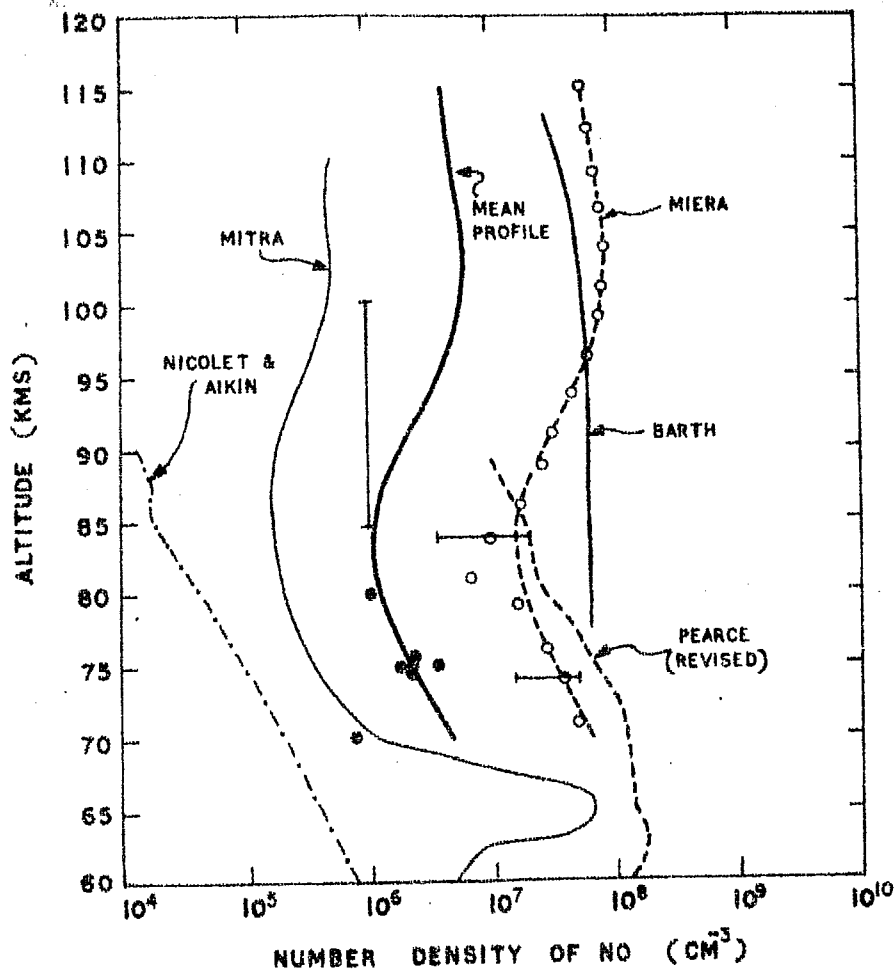


FIG. 4.3 - THE FIGURE SHOWS THE VARIOUS PROFILES OF N_O IN D-REGION. THE MEAN PROFILE IS PREDICTED ON THE BASIS OF VARIOUS ESTIMATES SHOWN BY POINTS. THE VALUE FITS THE ABSORPTION IN VLF TRANSMISSION SEEN DUE TO TRANSIT OF X-RAY SOURCES.

altitudes. We have therefore used a profile similar to that of Meira but with the value of NO density normalised to $2 \times 10^6 \text{ cm}^{-3}$ at 75 kms, at which altitude as explained earlier, the agreement between different independent observations is quite good. Besides, the resulting profile of NO yields densities at other altitudes which are in satisfactory agreement with the corresponding values given in table 4.1. This is further justified by recent theoretical calculations of Strobel (1972a,b) who also has suggested a similar value of NO.

4.6.4. IONIZATION CALCULATIONS:

Ionization rate due to $\text{Ly}\alpha$ of intensity I photons $\text{cm}^{-2} \text{ sec}^{-1} \text{ sr}^{-1}$ can be computed using the equation,

$$q_{\text{Ly}\alpha}(h) = 2\pi N_{\text{NO}}(h) \cdot \sigma_i \cdot I \int_0^{89} \exp\left[-\sigma_a \cdot \sec Z \cdot \int_h^\infty N_{\text{O}_2}(h) \cdot dh\right] \cdot \sin Z \cdot dZ \quad \dots(4.24)$$

where $N_{\text{NO}}(h)$, $N_{\text{O}_2}(h)$ are the number density of NO and O_2 as a function of h . σ_i is the ionization cross-section of NO at 1216 \AA (taken to be $2 \times 10^{-18} \text{ cm}^2$) σ_a is the absorption cross section of O_2 at 1216 \AA (taken to be 10^{-20} cm^2) and Z is the effective zenith angle. In figure 4.4 the electron production rates as a function of altitude are shown for the NO distribution discussed earlier in the cases when $\text{Ly}\alpha$ intensities are determined by the molecular oxygen distribution as defined by CIRA 1965 model and by Brannon and Hoffman (1971) measurements. The effect of $\text{Ly}\alpha$ intensity variation with

solar cycle is also shown in this figure. The maximum difference in electron production rates due to different molecular oxygen distributions is found to be less than $\approx 20\%$.

4.7. IONIZATION DUE TO $\text{Ly}\beta$:

Besides $\text{Ly}\alpha$, $\text{Ly}\beta$ component could also cause some degree of ionization. But the high absorption cross section of molecular oxygen, $\approx 1.5 \times 10^{-18} \text{ cm}^2$, for this radiation (Young et al 1968) results in the flux of $\text{Ly}\beta$ at depths below 90 kms to be too negligible to cause significant ionization.

4.8. IONIZATION DUE TO METEORS:

Unlike the first three agencies, the ionization effect from meteors is sporadic. Considerable uncertainties exist about the degree of ionization from meteors. However, it is believed that the effect should be much less than $10^{-3} \text{ cm}^{-2} \text{ sec}^{-1}$ electrons (Thomas 1971). Owing to the highly infrequent nature of this source, it is not considered in the present work.

4.9. THE ELECTRON DENSITY PROFILES:

Equilibrium density of electrons N_e from the electron production rate $\sum q_j$ is calculated using the well known continuity equation

$$\frac{dN_e}{dt} = \frac{q_j}{1 + \lambda} - (\alpha_e + \lambda \alpha_i) \cdot N_e^2 \quad \dots (4.10)$$

where α_e is the ion electron recombination coefficient, α_i is the ion-ion recombination coefficient and λ is the

:4.21:

ratio of ion density to electron density. The above equation under equilibrium conditions reduces to

$$\frac{dN_e}{dt} = 0 \quad \dots(4.11)$$

$$\begin{aligned} \text{or } \frac{\sum q_j}{N_e^2} &= (1 + \lambda) \cdot (\alpha_e + \lambda \alpha_i) \\ &= (1 + \lambda) \alpha_{\text{eff}} \\ &= \psi \text{ (say)} \quad \dots(4.12) \end{aligned}$$

where α_{eff} is the effective recombination coefficient.

When $\lambda \ll 1$,

$$\psi = \alpha_{\text{eff}}$$

and equation for the equilibrium becomes

$$\frac{\sum q_j}{N_e^2} = \psi \quad \dots(4.13)$$

Owing to the large uncertainties in the value of the recombination coefficient for the night time D-region, the exact evaluation of the night time electron density profile from the known electron production rates is rendered difficult. Therefore, an attempt has been made to obtain a quantitative estimate of the electron density increase for the transit of a X-ray source such as Sco X-1 in the night time ionosphere by comparing the directly measured electron density profile with the calculated electron production rates.

The experimental observations of the night time D-region electron density profile are rather meagre. In figure 4.5,

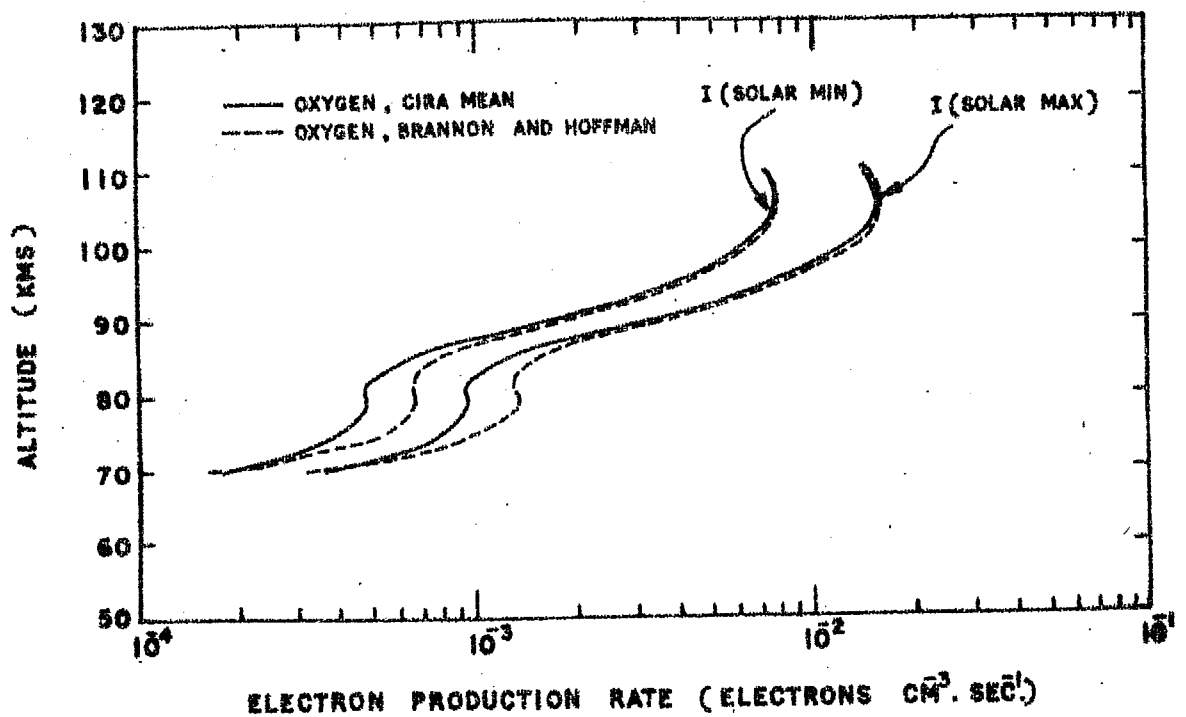


FIG. 4.4 - THE FIGURE SHOWS THE ELECTRON PRODUCTION RATE DUE TO NIGHT TIME L_y α DURING SOLAR MINIMA AND MAXIMA

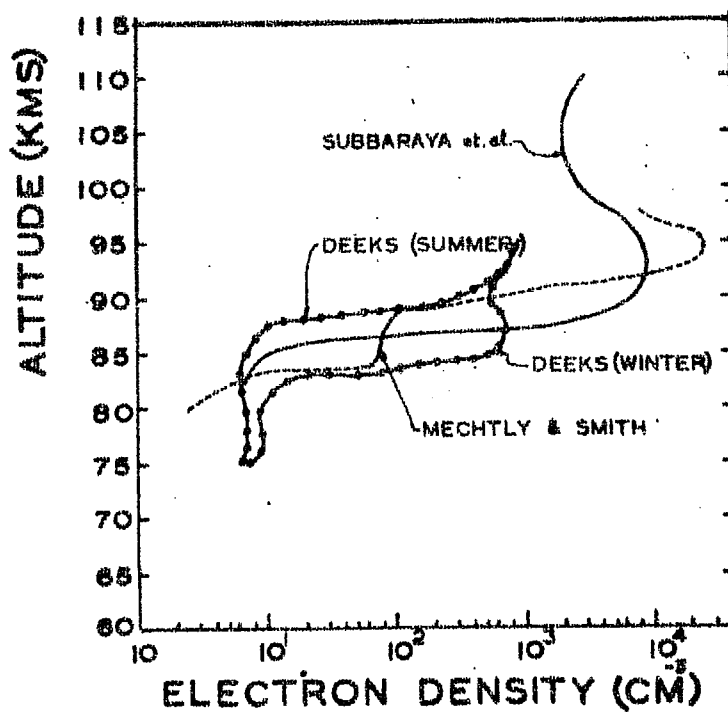


FIG. 4.5 - THE FIGURE SHOWS A COMPILATION OF NIGHT TIME ELECTRON DENSITY.

some of the available measurements of night time electron density profiles are compiled. The results of Deeks (1966) are obtained from ground based measurements at mid latitudes using VLF propagation technique and are representative of the electron density during the low solar activity. The measurement of Mechtly and Smith (1968) correspond to rocket borne probe techniques. The results of the rocket observations of night time ionosphere over the geomagnetic equator in India by Subbaraya et al (1971) using Langmuir probes are also plotted in this figure.

It is apparent from figure 4.5 that the existing measurements are grossly inadequate for resolving the nature of long term variations of the night time D-region electron density which is controlled principally by varying solar activity. Such changes are expected because of the intensity variations of $Ly\alpha$ and galactic cosmic rays over a solar cycle as pointed out earlier. The difficulty could be partially explained by the uncertainties in the normalisation of the different experimental results obtained by using a variety of techniques. Under these circumstances the rocket results of Subbaraya et al (1971) have been used down to 80 kms and summer values of Deeks (1966) have been used between altitudes 75 and 80 kms as representative of the electron density distribution over low and mid-latitudes in computations involving Sco X-1 and galactic center group of sources.

The specific choice of the former results is owing to the fact that the measurement was done in August 1971, around which period of the year, the night time observations on Sco X-1 and galactic center are possible from Ahmedabad. For calculations of the Tau X-1 effects, the winter profile of Deeks (1966) is used for the same reason. Using these observed values of N_e and the computed value of q_j corresponding to ambient ionizing agents $\left[\sum q_j (\text{ambient}) \right]$, the values of recombination coefficient (ψ) for different altitudes are calculated by

$$\psi = \frac{\sum q_j (\text{ambient})}{N_e^2 (\text{ambient})} \quad \dots(4.14)$$

The altitude dependence of q_j for different stable sources of ionization are shown together with $q_j (\text{ambient})$ in figure 4.6 and are representative of the quiet conditions. The galactic cosmic ray effect, corresponds to $\lambda_m = 23^\circ$ that of Gulmarg, India. All the subsequent discussions will be in relation to this location as the point of single hop reflection of the 164 KHz VLF waves transmitted from Tashkent and received at Ahmedabad should be situated above this place, which is midway between these two stations.

The electron density enhancements due to X-rays from Sco X-1, Galactic Centre and Tau X-1 sources at 10° , 45° and 60° zenith angles respectively, correspond to meridian transit of these sources over Gulmarg. These have been calculated using the values for the recombination coefficients at different

Table 4.2

Height (kms)	Ambient production rate ($q_1+q_2+q_3$) $\text{cm}^{-3}\text{sec}^{-1}$	Electron density increase due to Sco X-1 and galactic center (G.C.)				Electron density increase due to Tau X-1			
		Ambient electron density* $=N_e \text{ cm}^{-3}$	$q(h)$ Sco X-1 $\text{cm}^{-3} \text{ sec}^{-1}$	G.C. $\text{cm}^{-3} \text{ sec}^{-1}$	ΔN Sco X-1 cm^{-3}	Ambient electron density** $=N_e \text{ cm}^{-3}$	$q(h)$ $\text{cm}^{-3} \text{ sec}^{-1}$	ΔN cm^{-3}	
75.0	2.995×10^{-3}	6.4	1.210×10^{-3}	1.65×10^{-4}	1.134	0.175	7.0	1.15×10^{-4}	0.133
77.5	2.675×10^{-3}	7.0	1.365×10^{-3}	1.95×10^{-4}	1.603	0.251	9.6	1.25×10^{-4}	0.223
80.0	2.413×10^{-3}	7.0	1.500×10^{-3}	2.20×10^{-4}	1.915	0.313	9.4	1.36×10^{-4}	0.263
82.5	2.287×10^{-3}	7.0	1.565×10^{-3}	2.42×10^{-4}	2.085	0.361	15.0	1.43×10^{-4}	0.470
85.0	2.284×10^{-3}	10.0	1.600×10^{-3}	2.55×10^{-4}	3.040	0.540	600.0	1.42×10^{-4}	18.300
87.5	2.674×10^{-3}	2.0×10^3	1.580×10^{-3}	2.60×10^{-4}	523.0	95.0	700.0	1.40×10^{-4}	18.100
90.0	3.458×10^{-3}	8.0×10^3	1.480×10^{-3}	2.45×10^{-4}	1560.0	278.0	500.0	1.35×10^{-4}	9.700

* N_e taken from Subbarya et al and Deeks (summer)** N_e taken from Deeks (winter)

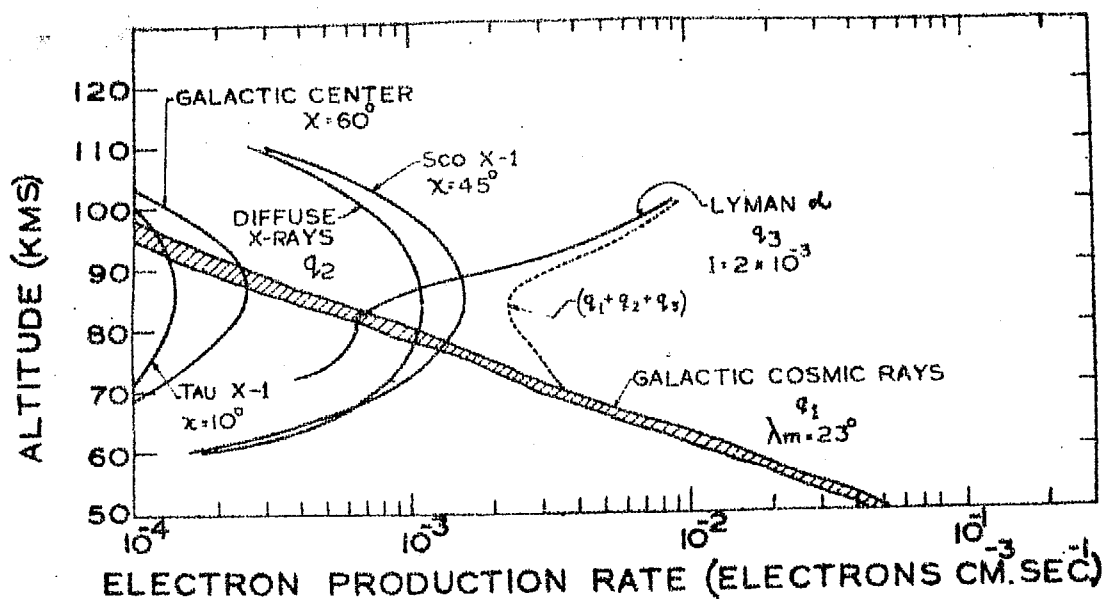


FIG. 4.6 - THE FIGURE SHOWS THE ELECTRON PRODUCTION RATE DUE TO ALL QUIET TIME AGENCIES AND COMPARES TO THOSE OF SCO X-1, TAU X-1 AND G.C.

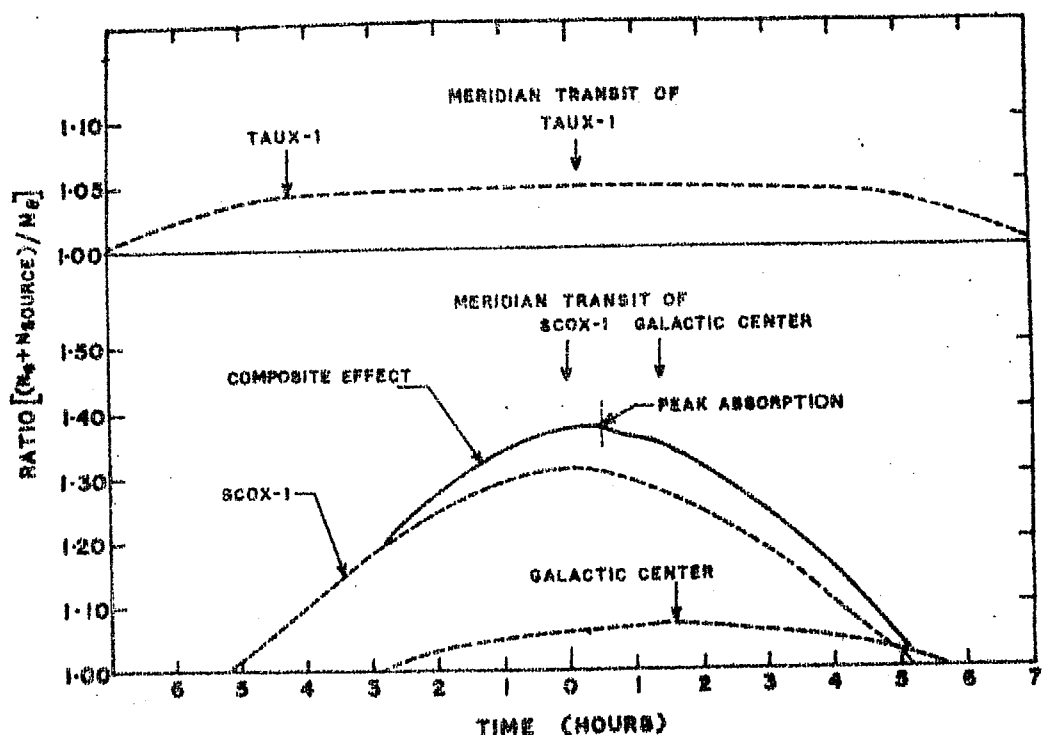


FIG. 4.7 - THE FIGURE SHOWS THE RATIO $\frac{N_{\text{quiet}} + N_{\text{source}}}{N_{\text{quiet}}}$ FOR TAU X-1 AND SCO X-1 FOR THEIR TRANSIT OVER 31° LATITUDE.

altitudes derived from equation 4.14.

The estimates of ambient $\sum q_j$ and the q_j (source), due to both Sco X-1 and Tau X-1 X-ray sources are shown in table 4.2. The table also tabulates the electron density increases at different altitudes for these sources. As the relative absorption effect due to celestial X-ray sources such as Sco X-1 depends only on the relative contribution compared to the ambient ionization, uncertainties in the values of the ambient electron density should have little effect on the final result. The electron density increases over the ambient values at 85 kms altitude as a function of time, around the time of the meridional transit of these sources are shown in figure 4.7.

4.10. 164 KHz VLF OBSERVATIONS AT AHMEDABAD:

In this section, attempt is made to explain the observed attenuation of the VLF radio waves, correlated with the time of transit of Sco X-1, galactic centre and Tau X-1, in terms of the electron density enhancements estimated in the previous section. Typical records showing the variations of the field strength as a function of time for the 164 KHz radio waves from Tashkent registered at Ahmedabad, associated with the passage of these X-ray sources are presented in figure 4.8. On an average basis, the nature of the effect is shown in figure 4.9 and is deduced by superposed epoch analysis of the daily records over a large number of days. In what follows, a brief outline of the main considerations relevant

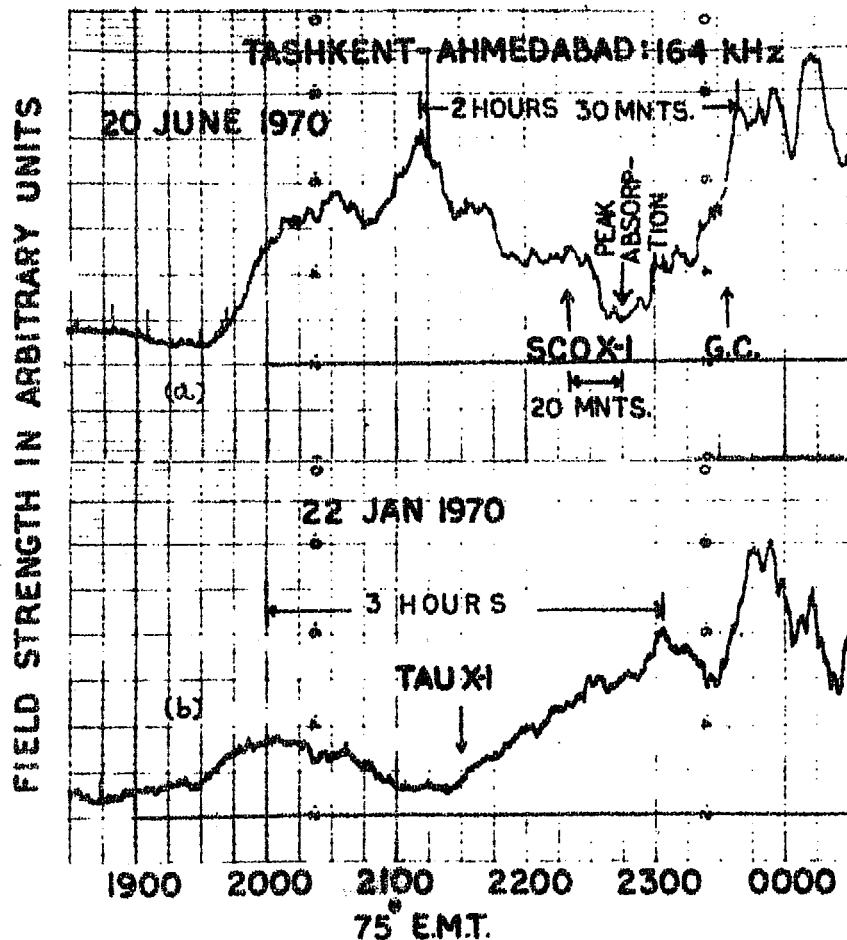


Fig 4.8 - FIGURE SHOWS THE ACTUAL RECORD OF VLF TRANSMISSION AT 164 KHZ AT THE TIME OF (UPPER) SCOX-1 (LOWER) TAU X-1. EACH VERTICAL LINE REPRESENT 15 MINUTE.

to the calculations are given. The complete details of the calculations are published elsewhere (Chakravarty, 1971).

Calculation of absorption is made by deriving the values of complex reflection coefficients of the D-region for the propagation of low frequency waves. Considering the electric field components parallel and perpendicular to the plane of incidence, two reflection coefficients ${}_{||}R_{||}$ (Parallel R Parallel) and ${}_{||}R_{\perp}$ (Parallel R Perpendicular) are defined to represent the reflected wave, with the first subscript representing the direction of the electric field in the incident wave and the second one that for the reflected wave. In the case of 164 KHz Tashkent signal received at Ahmedabad, the angle of incidence works out to be $80-85^{\circ}$ for the single hop geometry. The signal intensity measured will correspond to the reflection coefficient as the receiving antenna system is directed so that its main lobe lies in the plane of incidence. Also from a series of long wave radio observations by Bracewell et al (1951) and Belrose (1957) it has been concluded that the reflection coefficient ${}_{||}R_{||}$ in the day time is few orders of magnitude higher than that of ${}_{||}R_{\perp}$ for long transmitter receiver distances. However, in the night time, these two quantities may be of the same order (Belrose 1968). Since we register only the ${}_{||}R_{||}$ in our measurements, the present calculations are limited to ${}_{||}R_{||}$ only, and should, to a good approximation, represent the waves received at Ahmedabad.

For a realistic treatment of the long wave propagation through the ionosphere at oblique incidence, it is necessary to consider the partial reflections from a range of heights rather than the sharp reflection from a particular height. The wave admittance method developed by Barron and Budden (1955) which deals with the problem of such a nature is therefore used here to compute the reflection coefficients. The initial value of the coefficient is determined by considering a height well above that of reflection using the sharply bound model of Sheddy (1968) and involves the solutions of Booker's quartic equations (1938). Final value of admittance is obtained by numerically integrating the differential equations representing the variation of admittance with altitude resulting from the changes in electron density and collision frequency. A modified Runge-Kutta method given by Gill (1951) has been used for such an integration. The numerical integration is stopped at a height where the electron density is practically zero. The final value of the wave admittance for the radio waves leaving the ionosphere so calculated gives the final effective value of $||R||$. This in turn can give the total absorption in decibels using the formula

$$L = -20 \log ||R|| \quad \dots (4.15)$$

The collision frequency profile used in these calculations is taken from the experimental results of Deeks (1966). This profile is also in good agreement with that derived from the theoretical calculations of Sen and Wyler (1960).

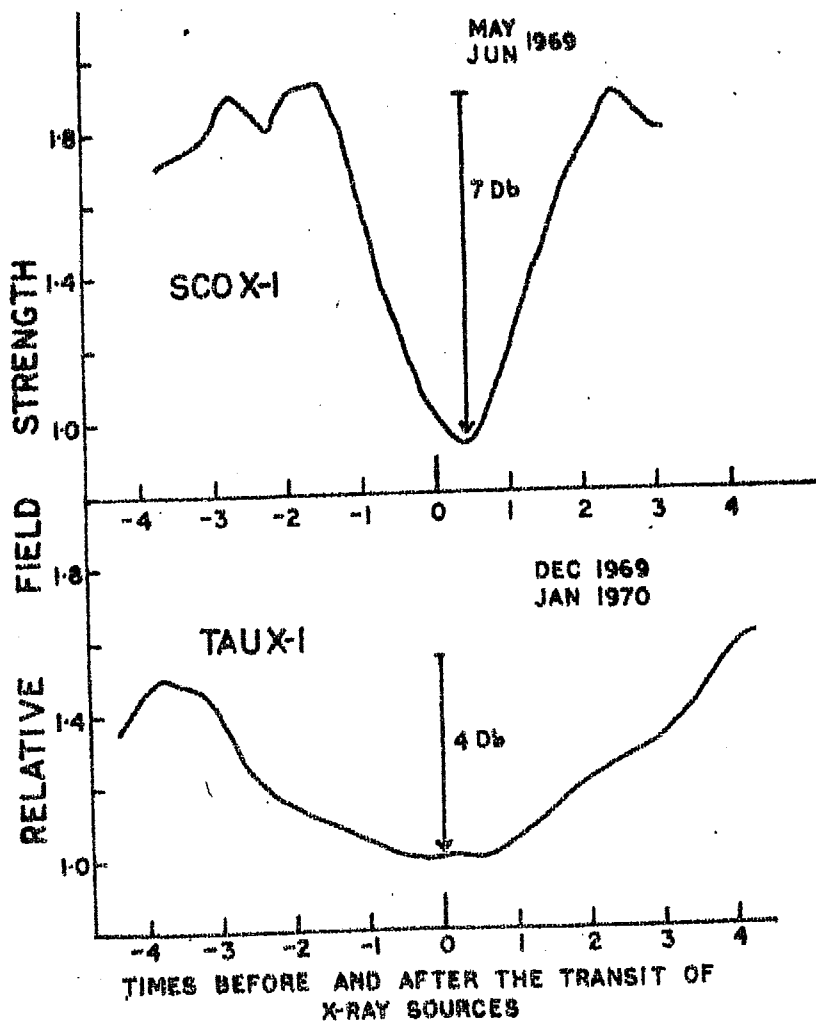


FIG. 4.9 - THE FIGURE SHOWS THE CHREE ANALYSIS OF LARGE NUMBER OF DAYS (SUPERPOSED ON EACH OTHER AFTER CORRECTION OF TRANSIT TIME OF SOURCES) FOR SCO X-1 AND TAU X-1. THE EFFECT IN CASE OF SCO X-1 LOOKS TO BE SHIFTED LATER AND IS EXPLAINED IN TEXT DUE TO G.C.

Table 4.3

Source	Calculated excess peak absorption (dB)	Observed excess peak absorption (dB)
Sco X-1	4.2	--
Galactic center	1.5	--
Sco X-1 + Galactic center	4.4	7
Tau X-1	1.2	4

Determination of the magnitudes of absorption for the 164 KHz radio waves are made both for the normal electron density profiles when there is no irradiation of the ionosphere by the cosmic X-ray sources as well as for the enhanced electron density conditions arising from the passage of these sources. The effect of the transit of these sources on the VLF propagation is then evaluated as the difference in the absorption values for the enhanced and normal conditions of electron density. In table 4.3, values so obtained are shown together with those of direct observations for Sco X-1, Galactic center and Tau X-1.

As is evident from the theoretically computed time profile of the effect shown in figure 4.7 and its observational counterpart in figure 4.8, the density enhancements should be present for about 2-3 hours on either side of the meridian transit of these sources. In addition, owing to the fact that the galactic center meridian transit takes place 1 hour 25 minutes after the transit ^{of} Sco X-1, in the records

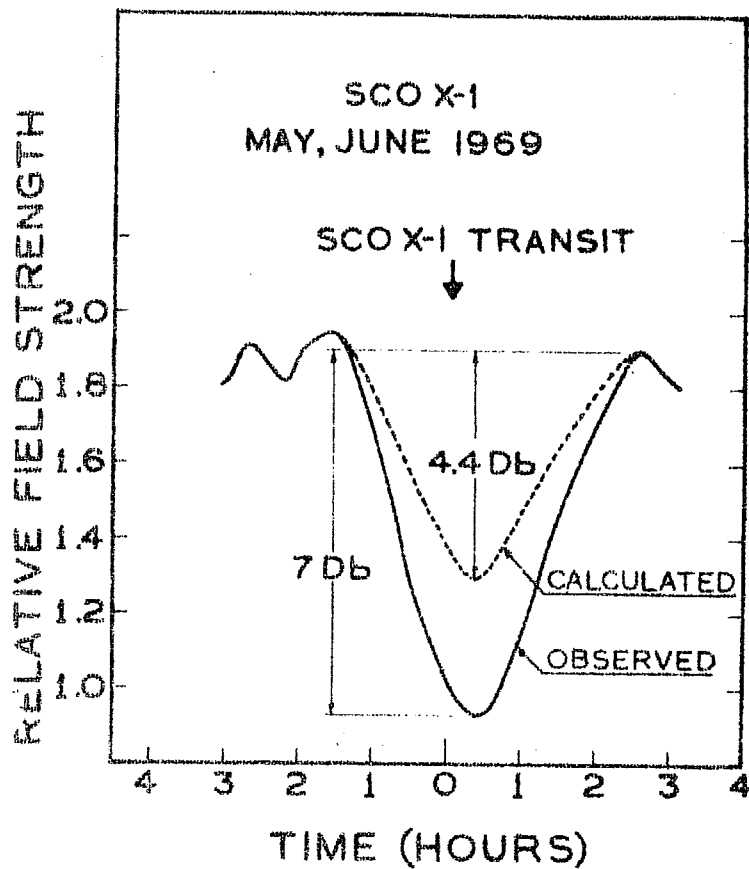


FIG. 4.10 - THE PROFILE OF THE FIELD STRENGTH VARIATION DUE TO TRANSIT OF SCO X-1. THE OBSERVED PROFILE IS COMPARED WITH CALCULATED.

such as that presented in figure 4.8, the effects from these two sources are seen as a composite one. Further, it may be noted that this composite effect is seen as a shift in the time of peak absorption, by 20-30 minutes, subsequent to the time of transit of ~~Sco X-1~~, in the registered 164 KHz data and agrees reasonably well with the computed time profile of electron density at 85 kms shown in figure 4.10. The calculated peak absorption for the resultant effects is 4.4 dB and compares favourably with the observed absorption of 6 to 7 dB in the case of Sco X-1 and galactic center.

In the case of Tau X-1, the agreement between the calculated and observed peak absorption values is less striking. Nevertheless the result of the computation shown in figure 4.7 leads to the conclusion that the expected duration of the effect should be longer for Tau X-1 compared to that for Sco X-1. On an average basis, this aspect is also conspicuous in the observational results presented in figure 4.8 and 4.9.

4.11. DETECTION OF FLARE STARS:

As already pointed out, there exists a class of sources that could be characterized as 'X-ray Novae'. These sources have the property of sudden appearance, sharp intensity increases going through a maximum and disappearance like optical novae. For most of such known sources like Cen X-4, Cen X-2 the intensity at the peak is comparable to or more than that of Sco X-1. Foregoing considerations with regard

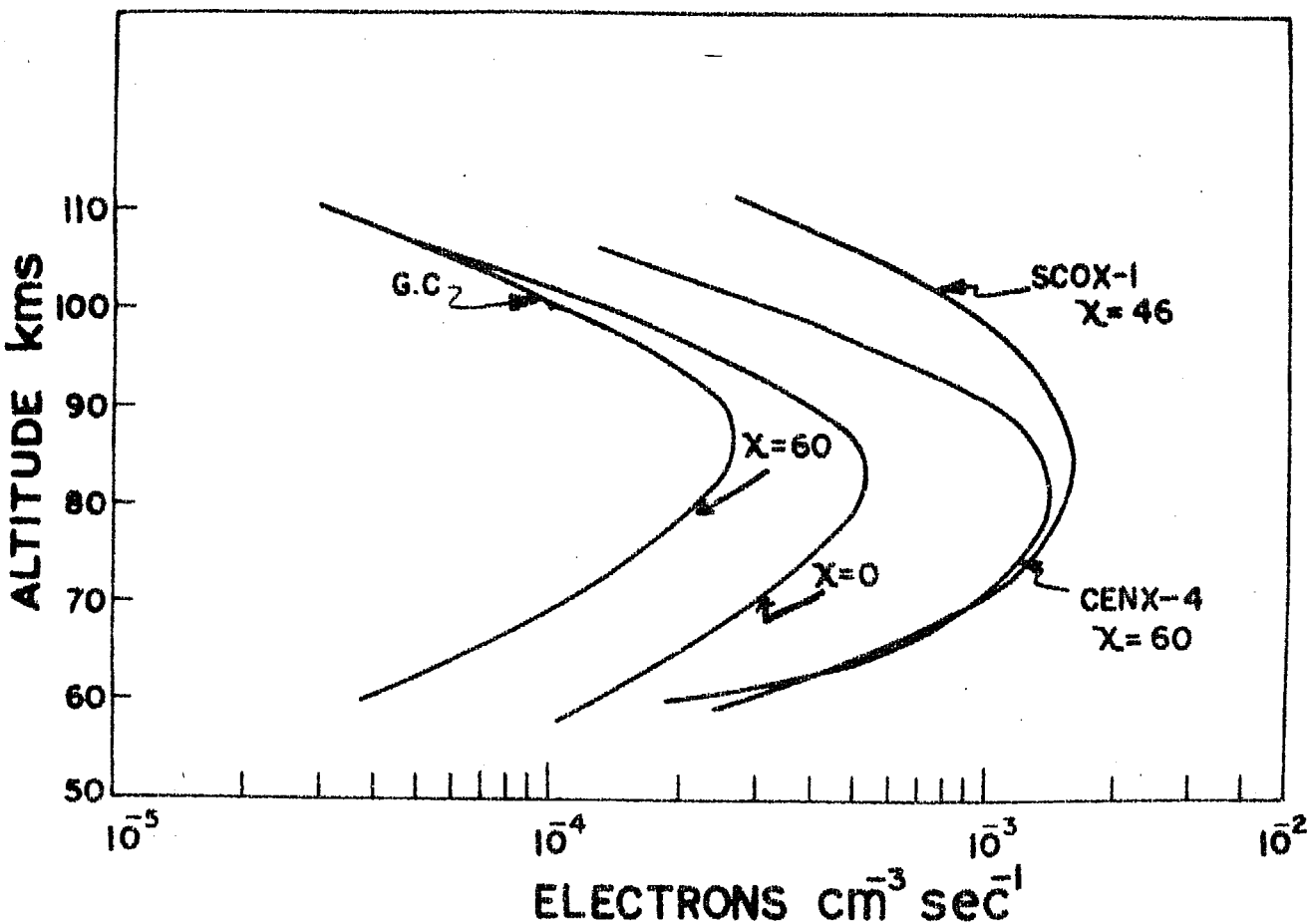


FIG. 4.11 - IN THIS FIGURE THE ELECTRON PRODUCTION RATE DUE TO TRANSIT OF CEN XR-4 AND SCO X-1 AND GALACTIC CENTER ARE COMPARED. $\chi = 60$, $\chi = 46$ CORRESPONDS TO TRANSIT OVER LATITUDE 31°N .

to the ionospheric effect of X-ray sources clearly indicate the possibility that the nova like X-ray sources could be detectable through their effects on the D-region ionosphere. Figure 4.11 shows the results of the calculation of the electron production rate arising due to X-rays from Cen X-4 corresponding to the peak of its emission for $\chi = 60^\circ$. For comparison, the production rates due to Sco X-1 are also shown from which it is clear that the effects from these two sources are comparable. The VLF data for the corresponding period available at Ahmedabad however did not reveal any positive indications. However, it may be noted that the quality of the available data at this time was rather poor and hence definite conclusions could not be drawn. For the same source, there is atleast one report of successful ionospheric detection (Kaufman et al 1972).

A similar analysis was made in connection with Cet X-2 (intensity 0.8 of Sco X-1) which because of its low zenith angle at the meridional transit point over Gulmarg could produce almost the same electron density perturbations as Sco X-1 (figure 4.12). Search of the corresponding VLF data revealed the associated field strength variations demonstrating significant electron density fluctuations. Figure 4.12 shows the results of the superposed/epoch analysis of the VLF data corresponding to the transit of Cet X-2 for a number of successive days around the time of its maximum X-ray emission. Evidence as obtained from this analysis is again quite strong for the possible ionospheric detection of X-ray sources. It is also

: 4.36 :

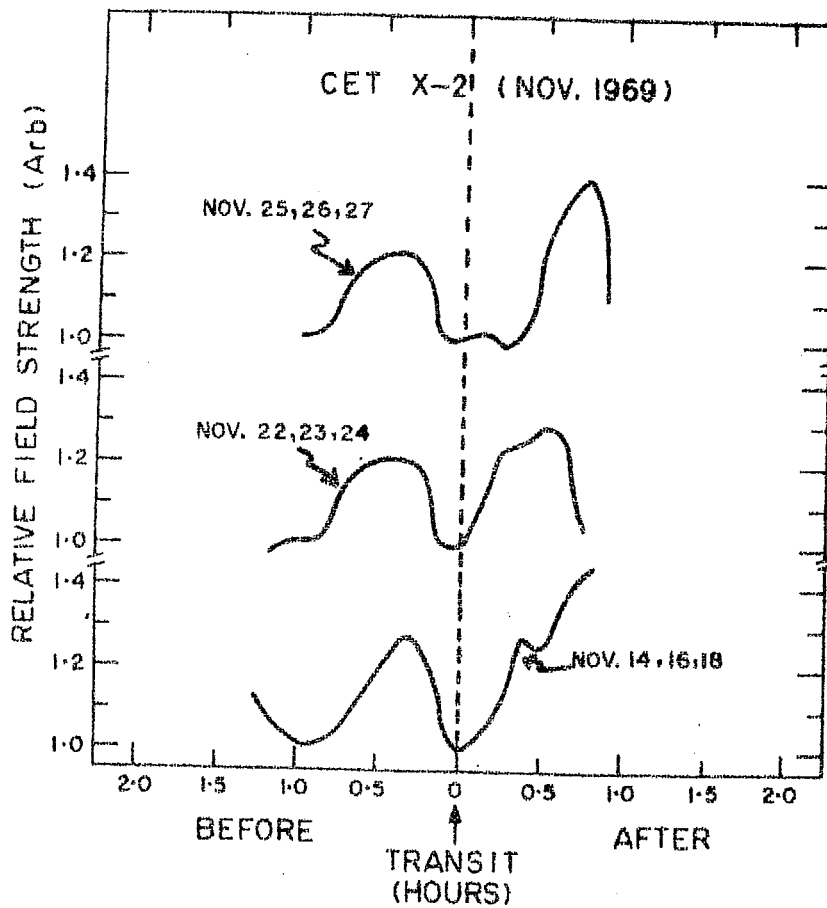


FIG.4.12). THE FIGURE SHOWS THE SUPERPOSED EPOCH ANALYSIS OF THE VLF DATA CORRESPONDING TO THE TIME OF TRANSIT OF CET X-2 X-RAY SOURCE.

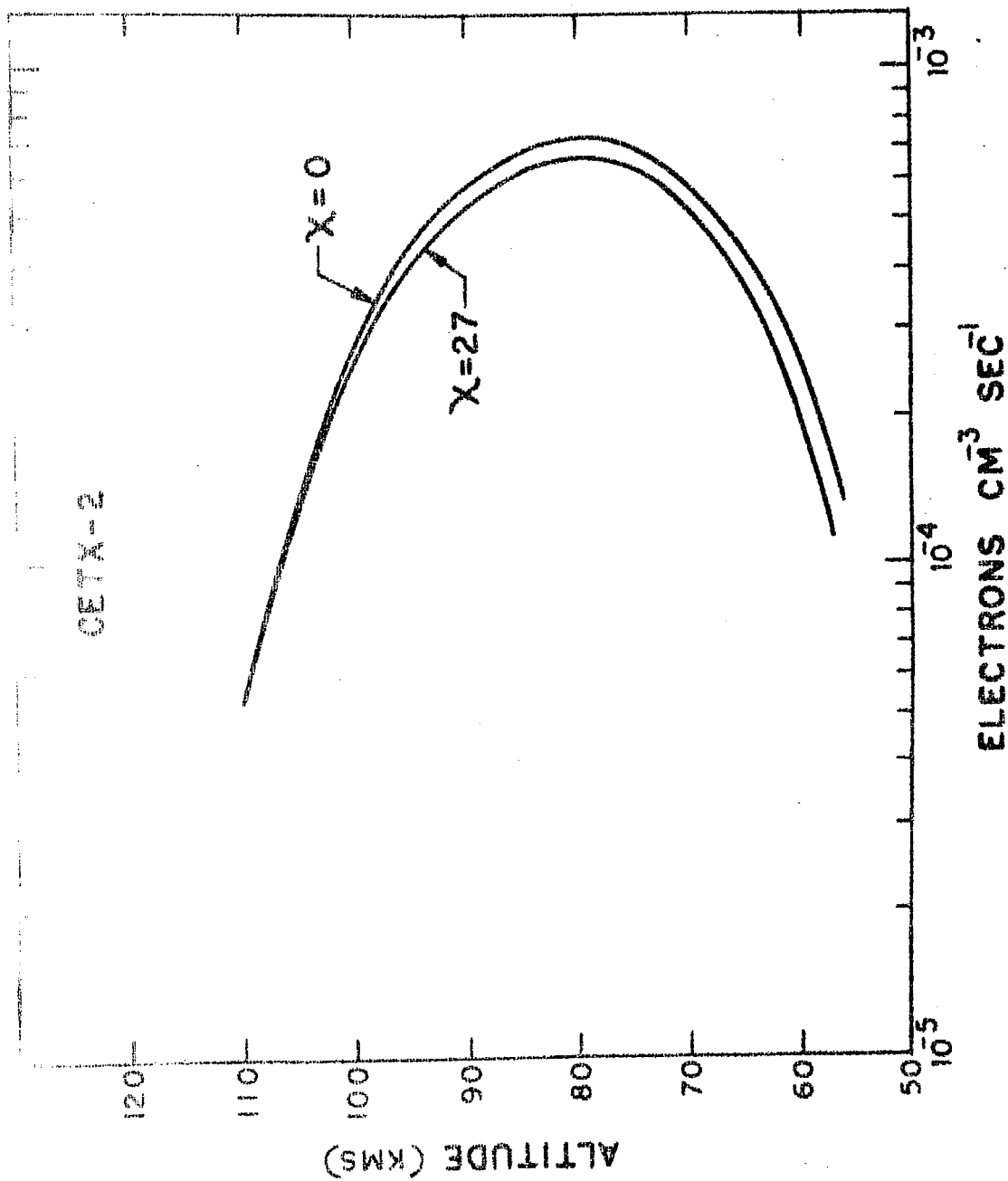


FIG. 4/3 THE ELECTRON PRODUCTION RATE FOR NOVA LIKE SOURCE CET X-2 IS SHOWN. CALCULATIONS CORRESPONDS TO $\chi = 0$ AND $\chi = 27^\circ$ OF SOURCE TRANSIT.

interesting to note that this is the only alternate evidence for Cet X-2 other than the rocket detection by Shukla and Wilson (1971).

4.12. DETECTION OF GAMMA RAY BURSTS:

Detection of gamma ray bursts of cosmic origin by detectors on board Vela, OGO, IMP-6 and OSO-7 satellites (Kelobesadal et al 1973, Cline et al 1973, L' Heuneux et al 1974) is one of the major surprises of observational astronomy in the recent times. Dictated by the response characteristics of these satellite detectors, the bursts were observed over the energy range 7 keV to 1.5 MeV and further, were found to have the time durations ranging from less than a second to about 80 seconds with integrated flux density lying between a few times 10^{-5} and 3×10^{-4} ergs. $\text{sec}^{-1}.\text{cm}^{-2}$ for different events. Even though their spectra at high energies can be grossly represented by an exponential function the complex time structure with a time scale as short as 16 milisecond seen in their time profiles show the similarity with impulsive X-ray emission often observed during solar flares. Coincidences between spatially separated satellite observations have served to identify genuine events from spurious ones. From the twenty events that have been thus detected so far from data accumulated over 5 years, it is found that these events are distributed almost isotropically on the celestial sphere and occur at a frequency of about five per year, at the level of sensitivity of vela satellite instrumentation. A number of

theories have been proposed, none of which is entirely satisfactory due to the nature of insufficient observations that exist today. In view of the fact that so far no positive associations could be established with other well known transient phenomena (Klebesdal et al 1973, Cline et al 1973b) such as super novae, galactic noise spikes, rapid atmospheric fluorescence increases, Cyg X-3 flare type of events or even with gravitational radiation events, continuous patrol for detecting these events is very important to understand the nature of their origin. Further the importance of carrying out such a patrol through as many independent techniques as possible needs hardly any emphasis from the standpoint of increasing the efficiency of sky coverage and establishing the genuineness of each of these events.

We have, therefore, searched effects on the VLF propagation characteristics in the D-region of ionosphere which is already described in earlier sections. Besides providing a simple ground based technique for monitoring these transient celestial events, such detection, could give valuable information on the source position, if data from different propagation paths could be related. Moreover, the monitoring by this method could establish the frequency of these bursts at the energies to which D-region (2-10 keV) is most sensitive and where no meaningful spacecraft data exists.

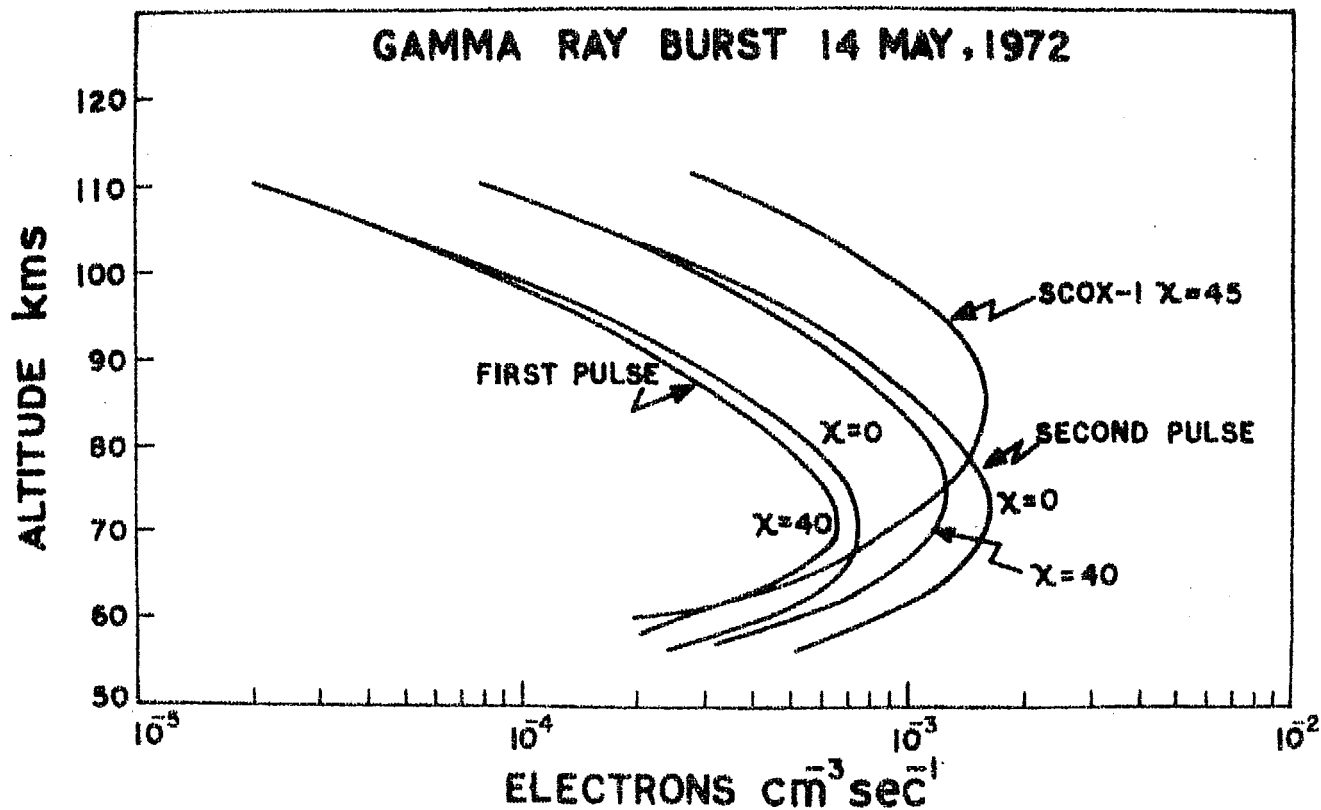


FIG. 4.14 - THE FIGURE SHOWS THE ELECTRON PRODUCTION RATE DUE TO γ -RAY BURST OF 14 MAY 1972 CORRESPONDING TO THE ZENITH OF THE SOURCE AT 0° AND 40° . THE ELECTRON PRODUCTION RATE DUE TO SCO X-1 ARE ALSO SHOWN FOR COMPARISON.

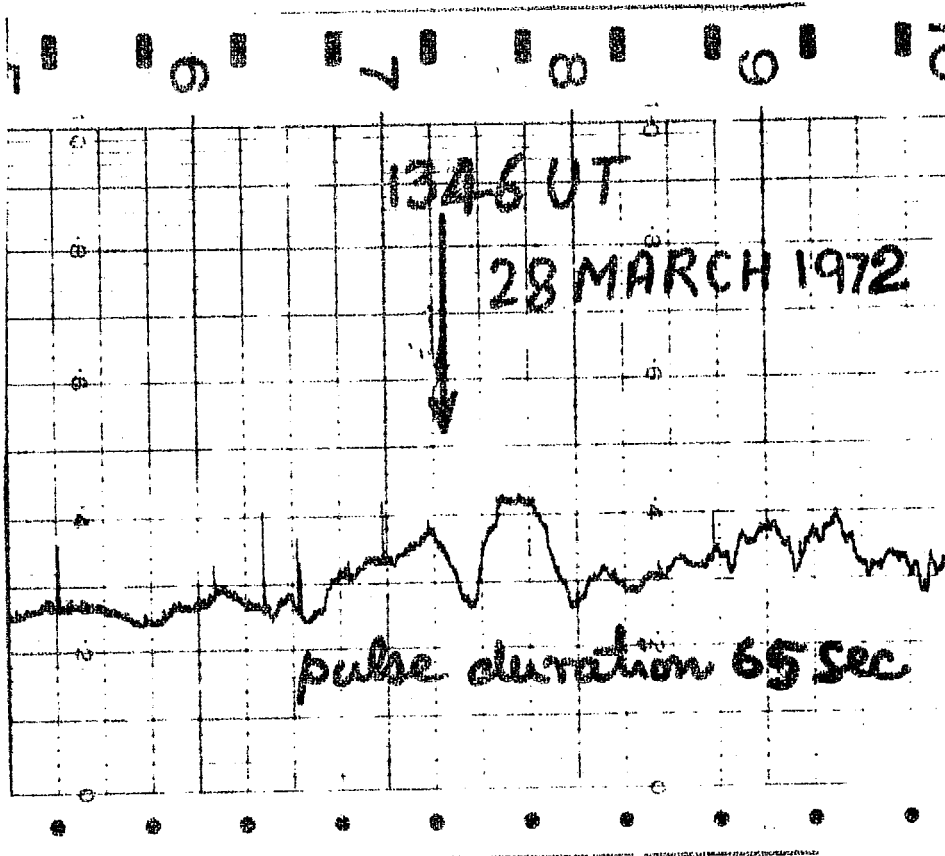


FIG.4.15 - SHOWS THE CHART ON WHICH VLF SIGNAL FROM TASHKENT IS RECORDED. THE ARROW POINTS TO THE TIME OF OCCURRENCE OF GAMMA RAY BURST ON 28TH MARCH 1972.

To investigate the effects of these bursts on VLF propagation the records taken during the night time between 1900 hours LMT and 0700 hours LMT were searched corresponding to those events which occurred during this period. This is because they could be identified unambiguously in the absence of solar effect. Table 4.4 summarises the results of such a search for a number of bursts selected on the above criterion. From the table it can be seen that there was no observable field strength variations associated with any of the above events. Figure 4.14 shows the relevant position of a typical field strength recorded at Ahmedabad corresponding to the time of occurrence of the event dated March 28, 1971. The hatched portion shows the expected time profile of the VLF field strength, if the X-ray burst event under consideration had an observable effect on the lower D-region ionosphere.

The absence of a sharp fall in the field strength corresponding to the time scale of the event shows that the X-rays from this event did not have any observable influence on the ionization of the D-region and hence all these events which are not detected through their effect on ionosphere do not sufficiently influence the D-region. This can be understood from the estimated electron production rates in the D-region for a typical event such as of May 14, 1972 for which detailed spectral data (Wheaton et al 1973) are available above 7 keV. Owing to the fact that the atmospheric region between 70 and 90 kms altitude is most responsive to X-rays between 1-10 keV

Table 4.4

Vela event No.	Date of observation	U.T. Hr.Mt.	Duration Sec.	Position coordinates for 3 S/C coincidences Position 1 Posi. 2	Circle of position for 2S/C coincidences	Estimated flux (ergs.cm ⁻²)	Observability of the event from the reflect-ion point	Whether effect is seen
69-4	17-10-1969	21 42	1.5	α δ α δ	156 1	4×10^{-5}	Uncertain	No
70-2	22-8-1970	16 50	10	143 65 205 25	- +	1×10^{-4}	Not visible	No
70-3	1-12-1971	20 01	-		91 -30	4×10^{-5}	Visible	No
71-1	2-1-1971	19 11	10	Poor intersatellite timings		1×10^{-4}	Uncertain	No
71-3	18-3-1971	15 28	30	75 -5 100 -60		1×10^{-4}	Uncertain	No
72-1	17-1-1972	17 39	30	104 +9 136 -29		7×10^{-5}	Visible	No
72-2	12-3-1972	15 53	-	277 +1 298 +35		5×10^{-5}	Not visible	No
72-3	28-3-1972	13 46	-		283 22	1×10^{-4}	Uncertain	No
72-5	1-11-1972	18 57	-	11 +19 309	-56	7×10^{-6}	Uncertain	No
73-2	10-5-1973		-		25 -36	1×10^{-4}	Uncertain	No

α and δ are right ascension and declination respectively in degrees.

(Swider, 1969) we have extrapolated the observed power law number spectrum down to 1 keV for this calculation. Recent observations down to about 2 keV by Appollo 16 justify such an extrapolation (Peterson, LE; private communication). The electron production rates are shown in figure 4.15 for two zenith angles viz. $\chi = 0^\circ$ and $\chi = 40^\circ$ together with that of Sco X-1 at $\chi = 45^\circ$ for comparison. Even though the second peak of the burst appears to be comparable to that from Sco X-1, the average production integrated over the duration of burst (≈ 65 sec) is found to be atleast a factor of two lower and the altitude of maximum production is at ≈ 70 km compared to 85 km due to Sco X-1. An important consequence of such a profile is that the peak electron production rate for these type of bursts results in low equilibrium electron densities owing to the high value of recombination coefficients. The value of recombination coefficients at 70 kms is orders of magnitude higher than that at 85 kms where X-rays from Sco X-1 have maximum influence and where much higher equilibrium electron densities could be produced. Estimates show that the electron density enhancements arising from this burst is insignificant at 70 kms and is much less than 5% over the ambient value at 85 kms. Because of the fact that the burst under consideration is one of the strongest recorded so far, it is clear that the effects to be expected from the bursts listed in table 4.4 should be many magnitudes lower and this explains why it is not possible to detect them by their effect on D-region ionosphere.

In summary, following main conclusions emerge from the present investigation on the ionospheric effects of nonsolar X-ray and gamma emission from the astronomical standpoint:

1) Evidence is quite strong both from the observational and theoretical standpoint for the detection of ionospheric effect due to strong celestial X-ray sources especially from observations at low latitudes. Presently available evidence shows that the contribution to night time ionization of equatorial D-region ionosphere from cosmic X-rays, cosmic rays and $Ly\alpha$ are comparable with each other. There is also reasonable agreement between the theoretically expected nature of the effect and the experimental observations of VLF propagation.

2) The effect of these sources persists for about 2-3 h on either side of the time corresponding to the peak effect, the extent of spread depending on the declination of the source, as well as the nature of its energy spectrum. Also the effect of all the sources clustered in intervals of an hour or so in right ascension is seen as a composite one, with the time of peak absorption suitably shifted with respect to the time of expected peak effect from individual sources. In other words, the ionosphere behaves as an X-ray telescope with a large opening angle so far as the transit of celestial sources are concerned.

3) In general, since the contribution from $Ly\alpha$ can become significant during disturbed periods, the effect of celestial X-ray sources should be more frequently observed during solar quiet periods.

4) On an average basis, it should be possible to study systematic long term variations of the intensity of strong X-ray sources, in the time scales of a few months to a few years, using the data on VLF propagation. Study of the systematic day to day variations, however, may be difficult owing to our insufficient knowledge of the variabilities of the corresponding D-region processes.

5) There now exists a real possibility for the detection of such rare celestial events as flaring X-ray stars or supernovae through their transient ionospheric effects using ground based VLF observations.

6) The recently detected cosmic gamma ray bursts however appear to be incapable of producing significant electron density perturbation at D-region altitudes so as to modify VLF propagation characteristics.

7) The controlled irradiation of the ionosphere provided by the discrete celestial X-ray sources, should be of immense value towards understanding the physical processes in the night time D-region. One could, for example, reverse some of the previous calculations and derive the night time

recombination coefficient at D-region altitudes by relating the observed excess absorption of VLF waves due to X-ray sources with the corresponding computed electron production rate profile.

8) Owing to the fact that NO is a very important minor constituent at D-region altitudes for deciding the ambient electron density, accurate knowledge of its altitude ion-concentration profile is very vital. It is interesting to note that the detectability of X-ray sources implies a concentration of NO atleast a factor of 5-10 lower than that determined by the direct experiments.

APPENDIX A-I

In this section we will discuss the importance of conducting X-ray experiments on equatorial latitudes where the geomagnetic cut off rigidity is maximum. The sensitivity of any instrument to a given signal will ultimately depend upon the signal to noise ratio i.e. background level of radiation present at any place. Therefore, a quantitative estimate and analysis of the background problem at any place is very important, particularly ~~when~~ study of weak sources such as Her X-1 is involved. Main sources of background for the X-ray astronomy experiments can be summarised as follows:

- a) Cosmic ray induced background
- b) Atmospheric X-ray background
- c) The background produced in the material surrounding the detector due to interaction of high energy particles and gamma rays.
- d) The presence of low energy electrons which penetrate the detector and produce X-ray like events.

The last contributes mainly in the low energy region and is a major source of background at rocket altitudes. The distribution of electron fluxes below 100 keV obtained from satellite data (Seward 1974) shows that TERLS, Thumba is the best launching station judged from the lowest background level.

The first three constitute the major source of the background at balloon altitudes. Figure A 1.1a,b show the background rates due to atmospheric X-rays and that induced

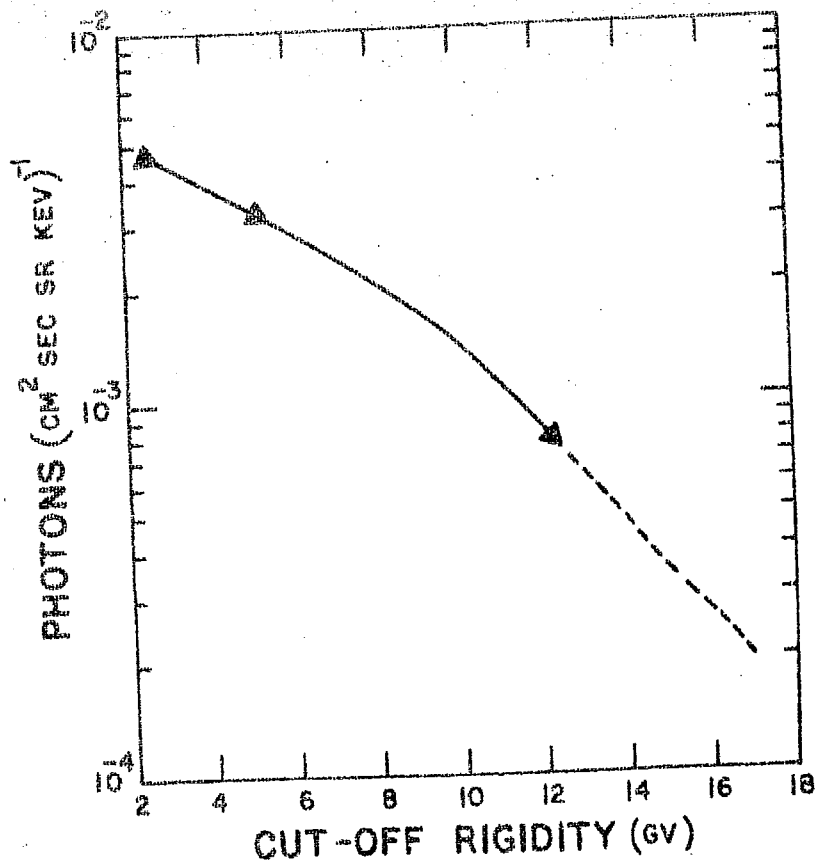


FIG. 11b - THE FIGURE SHOWS THE INTENSITY OF ATMOSPHERIC X-RAYS VERSUS CUTOFF RIGIDITY EXTRAPOLATED TO 16.9 GeV FOR HYDERABAD.

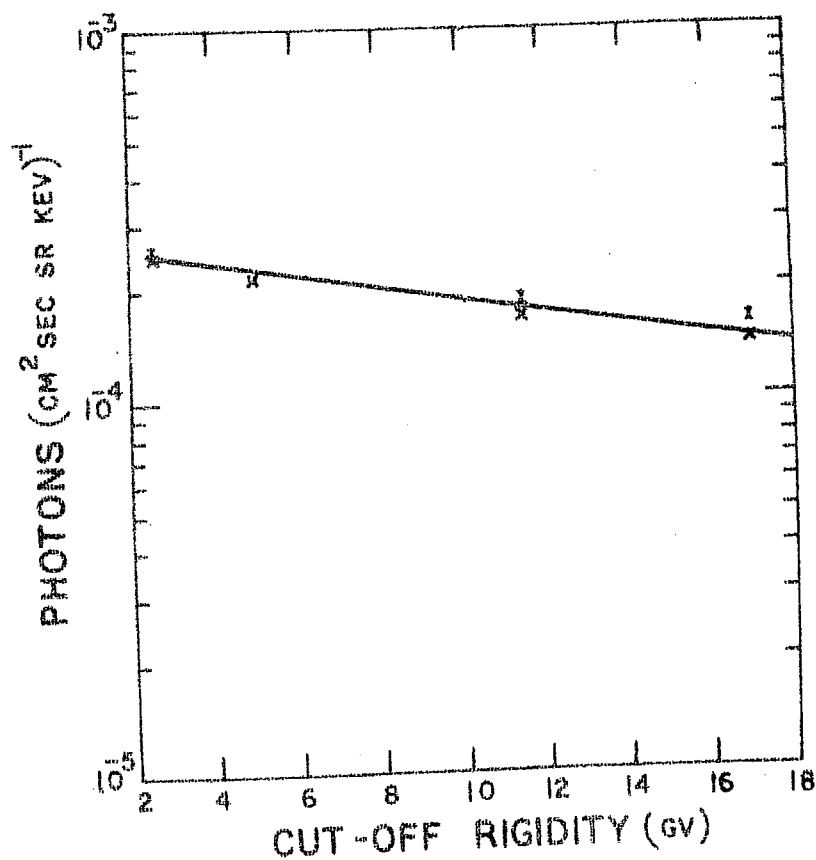


FIG. 11a - THE FIGURE SHOWS THE VARIATION OF COSMIC RAY INTENSITY WITH CUTOFF RIGIDITY.

:A 1.3:

Table A 1.1 - The table give the details of backgrounds shown in figure A 1.2.

Experimenter	Sym- bol	Place of observat- ion	Cut- off Rig. (GV)	Detector			
				FWHM (Deg)	Solid Angle (Sr.cm ⁻²)	Thick- ness (mm)	Alti- tude (gms.cm ⁻²)
Harris (1968)	1	Woomera	5.0	35x10	-	25	
Matsuoka et al (1968)	2	Kagoshima	14.0	38x6	0.0175	47	
Palmieri et al (1971)	3	Kauai (Hawai)	13.0	20x1	0.008	-	
Chodil et al (1968)	4	-do-	13.0	15x5	-	-	
Present	5	Thumba	17.5	32x10	0.014	25	
Present	▲	Hyderabad	17.5	14	0.05	12.5	5.0
Kasturirangan (1971)	□	-do-	17.5	20	0.44	12.7	7.8
Agrawal (1972)	●	-do-	17.5	12	0.45	4	6.3
Reigler et al (1968)	○	Palestine (Texas)	4.0	11	0.17	2	3.2
Webber & Rein ert(1970)	△	-do-	4.0	6x20	-	25	3
Lewin et al (1968)	×	Mildura	4.0	13	-	-	3
Bleeker & Deerenberg (1970)	■	Aire-sur L'Adour	5.0	35	0.4	12.5	4

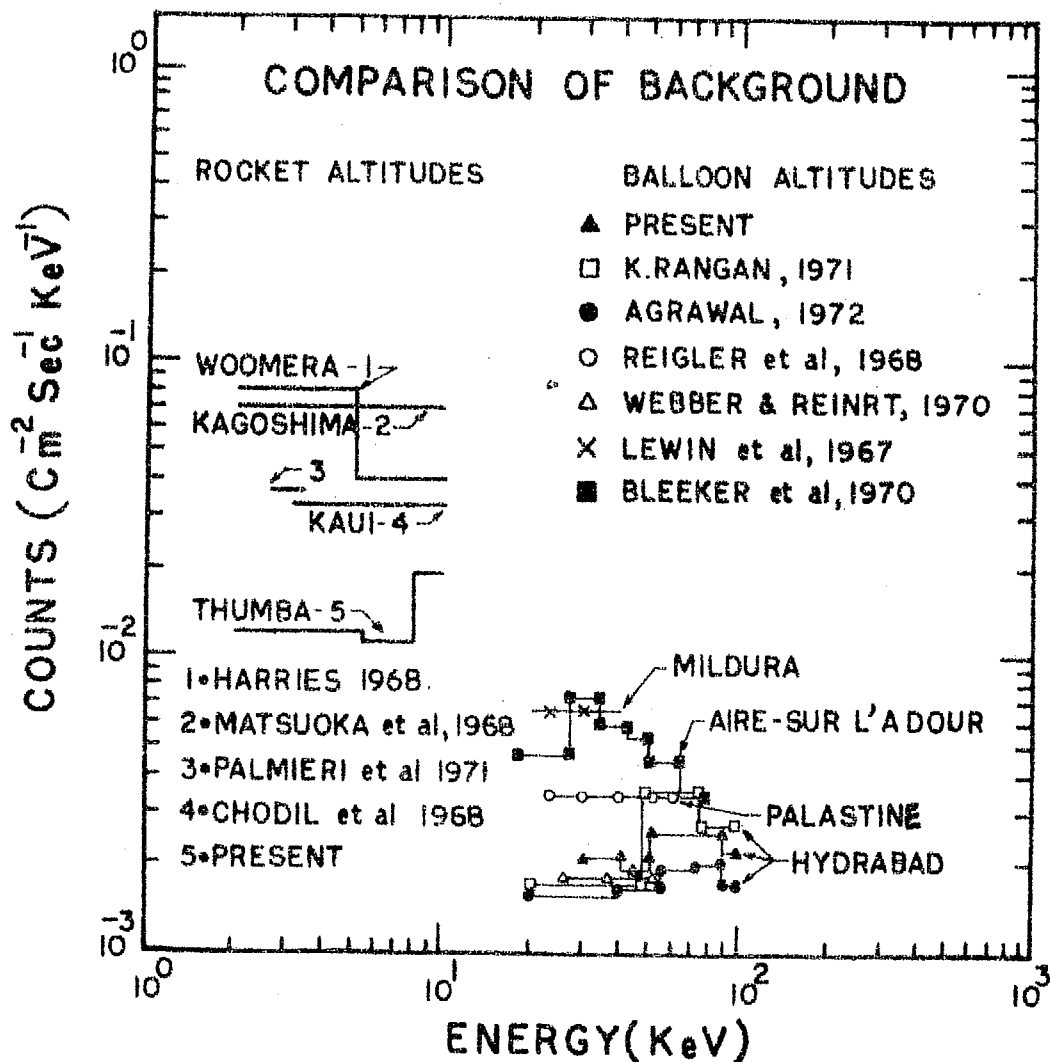


FIG.A 1.2: THE COMPILATION OF NON-X-RAY BACKGROUND OBSERVED AT VARIOUS LAUNCHING SITES OF BALLOONS AND ROCKETS WHICH ARE TABULATED IN TABLE A 1.1.

:A 1.5:

by cosmic rays and their variation with cut off rigidity. The cosmic ray induced background reduces by a factor ≈ 1.5 while going from stations like Palastine (cut off rigidity ≈ 4 GeV) to stations like Hyderabad (≈ 17.5 GeV). It is also noted from figure A 1.1b that the atmospheric X-ray background reduces by a factor of ≈ 10 at stations with high cut off rigidity compared to those of low cut off rigidity stations. Thus the sensitivity of the detectors also increases correspondingly and hence weaker sources like Her X-1 could easily be monitored.

Figure A 1.2 and table A 1.1 present the background monitored at various experimental sites for rockets and balloons. It can be noted from the figure A 1.2 that TERLS and HYDERABAD are the stations which have minimum background and are thus the best suited launching stations for cosmic X-ray sources and X-ray background experiments. In the table A 1.1 no attempt has been made to take into account the detector thickness.

APPENDIX A 2

A 2.1. ATTITUDE DETERMINATION OF ROCKET:

Since the methods of determination of attitude for a spin stabilized rocket are now well established (Giacconi et al 1965). We present here only a brief description of the methodology adopted. The Centaure rocket which was used in the present investigation initially had a spin rate of about 5.5 revolutions per second which remained practically constant above 80 kms altitude. Since only a very small window in front of the counter was ejected at 60 kms, the precession cone angle was quite small ($< 3^\circ$). The motion of a spinning rocket above the atmosphere is equivalent to a rigid body in which case rocket axis is the symmetry axis and also the minor axis of inertia. Assuming the rocket spin rate to be Ω_s along the minor axis of inertia and precession rate to be Ω_p along a direction fixed in space, the two will be related by the formula,

$$\cos \theta = \Omega_s / \Omega_p \cdot I_1 / (I_2 - I_1) \quad \dots (A 2.1)$$

where θ is the half cone precession angle and I_1 and I_2 are the moments of inertia of the rocket with respect to spin axis and a direction perpendicular to it. The above equation however, assumes that the rocket behaves as a perfect rigid body which in practice is not actually true. The practical problems of departure from perfect rigidity can be overcome by modifying the equation to,

$$\Omega_s + \dot{\Omega}_p = \Omega_0 + At + Bt^2 + \dots \quad (A 2.2)$$

where Ω_0 , A and B are the constants which can be determined from the actual measure of the spin period. Figure A 2.1 shows the actually observed change in the spin period during the

A2.2

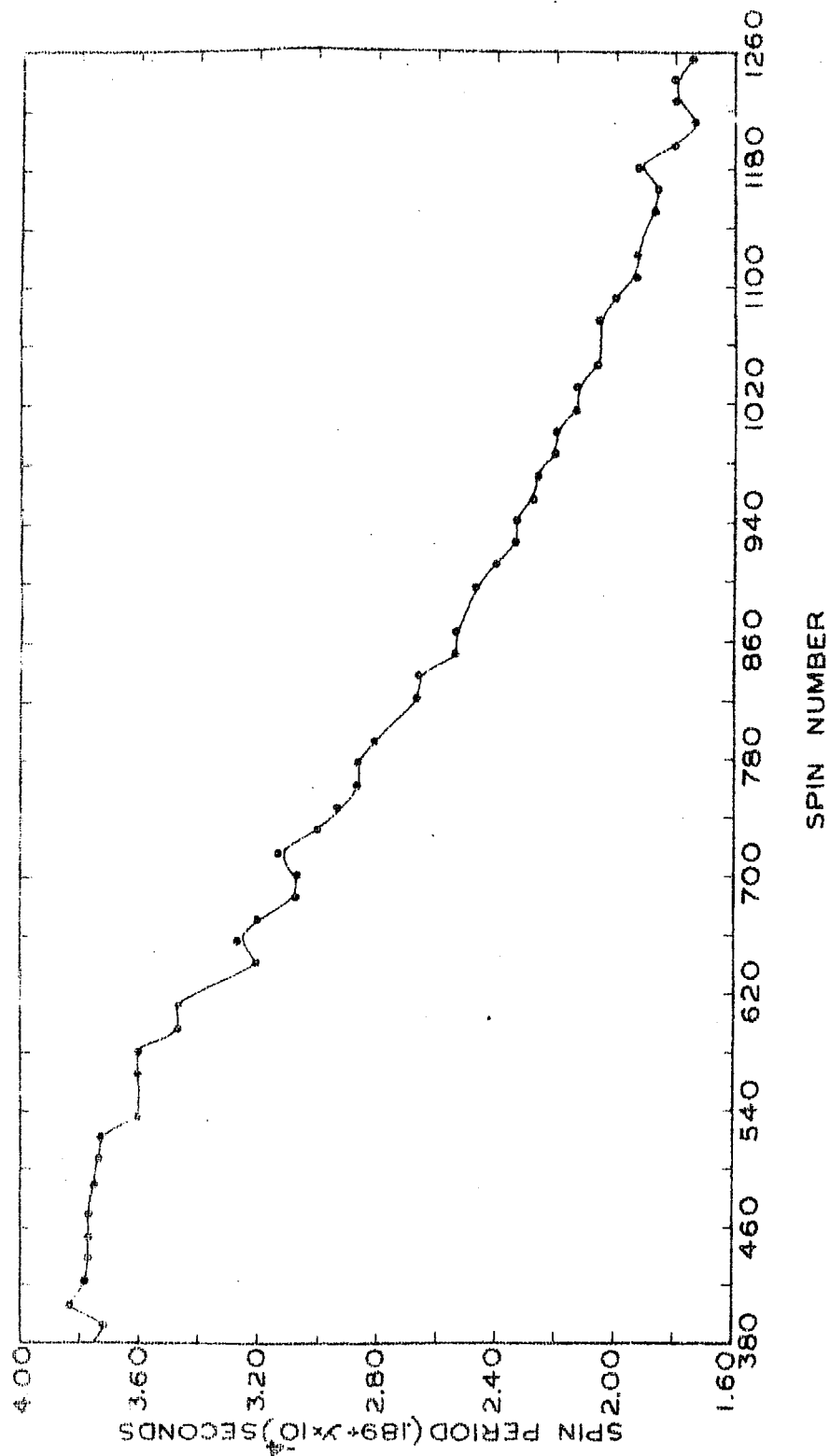


FIG: A2.1 THE SPIN PERIOD FOR THE WHOLE FLIGHT IS SHOWN AS IT CHANGES FROM BEGINNING TO END.

present flight which was approximated to a polynomial of the type,

$$\Omega_s = 0.18932 + A x + Bx^2 + Cx^3 \quad \dots$$

The path of the detector normal on the celestial sphere during the flight was analytically determined by using the method adopted by Giacconi et al (1965) and Harries (1967).

Let X_k , Y_k and Z_k be a fixed coordinate system in the sky and let X_p , Y_p and Z_p describe the precession system of co-ordinates (i.e. precession frame of reference). OZ is the precession axis which coincides with OZ_k and OZ_p (see figure A 2.2). Let X_p and Y_p make an angle ϕ with respect to X_k and Y_k . The coordinates X_p , Y_p and Z_p of any point P in terms of fixed coordinates X_k , Y_k and Z_k are given by,

$$\begin{vmatrix} X_p \\ Y_p \\ Z_p \end{vmatrix} = \begin{vmatrix} \cos \phi & \sin \phi & 0 \\ -\sin \phi & \cos \phi & 0 \\ 0 & 0 & 0 \end{vmatrix} \begin{vmatrix} X_k \\ Y_k \\ Z_k \end{vmatrix} \quad (\text{A } 2.3)$$

The spin axis of the rocket is at an angle θ to the OZ_p axis i.e. θ , the half cone angle of precession is given in this figure as,

$$\theta = \pi/2 - \lambda_p^{(s)} ; \Delta \phi = \phi_p^{(s)}, \psi = \phi_s \quad (\text{A } 2.4)$$

X_s , Y_s and Z_s is the spin frame of reference where OZ_s is the spin axis and $X_s = Z_s + Z_p$. That is, X_s lies in the plane of X_p and Y_p . Thus,

$$\begin{vmatrix} X_s \\ Y_s \\ Z_s \end{vmatrix} = \begin{vmatrix} 1 & 0 & 0 \\ 0 & \cos \theta & \sin \theta \\ 0 & -\sin \theta & \cos \theta \end{vmatrix} \begin{vmatrix} X_p \\ Y_p \\ Z_p \end{vmatrix} \quad (\text{A } 2.5)$$

Since the rocket spin axis coincides with its own axis (i.e. $OZ_s = OZ_r$), we can write,

$$\begin{vmatrix} X_r \\ Y_r \\ Z_r \end{vmatrix} = \begin{vmatrix} \cos \psi & -\sin \psi & 0 \\ \sin \psi & \cos \psi & 0 \\ 0 & 0 & 1 \end{vmatrix} \begin{vmatrix} X_s \\ Y_s \\ Z_s \end{vmatrix} \quad (A 2.6)$$

The angles ϕ and ψ (angle between X_s and X_r) in the rocket frame of reference (X_r, Y_r, Z_r), in the above equation vary smoothly with time as,

$$\begin{aligned} \phi &= \phi_0 + \Omega_p (t - t_0) \\ \psi &= \psi_0 + \Omega_s (t - t_0) \end{aligned} \quad (A 2.7)$$

where t is the time and ϕ_0 and ψ_0 are the values of ϕ and ψ at $t = t_0$. If the detector axis forms an angle $\lambda_r(d)$ ($\equiv \lambda_s(d)$) with the equatorial X_r, Y_r plane of the rocket, the elevation of the detector in the precession frame will oscillate between $\lambda_r(d) + \Theta$ and $\lambda_r(d) - \Theta$ during each spin on a rectangular grid. Its representative point will describe a nearly sinusoidal curve with an amplitude equal to Θ and phase that changes gradually from one spin to the next.

Using the three coordinate conversion as described earlier, the following equation is obtained,

$$\begin{vmatrix} X_r \\ Y_r \\ Z_r \end{vmatrix} = T \begin{vmatrix} X_k \\ Y_k \\ Z_k \end{vmatrix} \quad (A 2.8)$$

where T is the product of three matrices of the three conversions in sequence. Since the above matrices are orthogonal we can write,

$$\begin{vmatrix} X_k \\ Y_k \\ Z_k \end{vmatrix} = \bar{T} \begin{vmatrix} X_r \\ Y_r \\ Z_r \end{vmatrix} \quad \text{.. (A 2.9)}$$

where \bar{T} is inverse of matrix T i.e. $T \cdot \bar{T} = 1$. Hence the above matrix system can be re-written as,

$$\begin{vmatrix} X_k \\ Y_k \\ Z_k \end{vmatrix} = \begin{vmatrix} \cos \phi & \sin \phi & 0 \\ \sin \phi & \cos \phi & 0 \\ 0 & 0 & 0 \end{vmatrix} \begin{vmatrix} 1 & 0 & 0 \\ 0 & \cos \theta & \sin \theta \\ 0 & -\sin \theta & \cos \theta \end{vmatrix} \begin{vmatrix} \cos \psi & -\sin \psi & 0 \\ \sin \psi & \cos \psi & 0 \\ 0 & 0 & 1 \end{vmatrix} \begin{vmatrix} X_r \\ Y_r \\ Z_r \end{vmatrix} \quad \text{..(A 2.10)}$$

In the present experiment the detector was mounted along the rocket axis OX_r . The motion of OX_r can then be represented by the matrix,

$$\begin{vmatrix} X_k \\ Y_k \\ Z_k \end{vmatrix} = \begin{vmatrix} \cos \phi \cdot \cos \psi & -\sin \phi \cdot \cos \theta & \sin \psi \\ \sin \phi \cdot \cos \psi & -\cos \phi \cdot \cos \theta & \sin \psi \\ \sin \theta \cdot \sin \psi \end{vmatrix} \quad \text{(A 2.11)}$$

In the celestial frame of reference X_c , Y_c and Z_c (with Z_c aligned along the North pole and X_c coinciding with Vernal equinox), if OX_k is assigned the southern direction, it can be shown that X_k makes an angle with X_c which is equal to the Right ascension (R.A.) of the precession axis. In this case, Z_k makes an angle δ with Z_c which represents the declination of the precession axis (figure A 2.5). It can then be shown,

$$\begin{vmatrix} X_c \\ Y_c \\ Z_c \end{vmatrix} = \begin{vmatrix} \cos \alpha \cdot \sin \delta & -\sin \alpha \cdot \cos \alpha & \sin \delta \\ \sin \alpha \cdot \sin \delta & \cos \alpha \cdot \sin \alpha & \sin \delta \\ -\cos \delta & 0 & \sin \delta \end{vmatrix} \begin{vmatrix} X_k \\ Y_k \\ Z_k \end{vmatrix} \quad \text{(A 2.12)}$$

and,

$$\alpha = \arcsin \left[\frac{Z}{\sqrt{X_c^2 + Y_c^2 + Z_c^2}} \right] \quad \text{(A 2.13)}$$

With the help of the above transformations, the trajectory of the detector axis in the celestial coordinates was obtained. The constants ϕ_0 and ψ_0 and t_0 used in the equations were derived from equations,

$$\begin{aligned}\phi &= \phi_0 + \Omega_p (t - t_0) \\ \psi &= \psi_0 + \Omega_s (t - t_0)\end{aligned}\tag{A 2.14}$$

A 2.2. MAGNETOMETER DATA REDUCTION:

Two flux gate magnetic sensors, one mounted along and the other perpendicular to the rocket axis (VMS and HMS) were used to derive the preliminary information of Ω_s , Ω_p and α_p , δ_p . An independent check of these parameters was also obtained from the solar sensor data. During each spin scan the output of HMS exhibited a sinusoidal amplitude variation due to the change in horizontal component of the geomagnetic field. The peak to peak amplitude during successive spins itself exhibited a sinusoidal variation, the magnitude of variation depending on the precession cone angle. The VMS on the other hand executed only one cycle of variation during each precession, the amplitude being greater for larger precession cone angle.

Dividing the rocket motion into two components as shown in figure A 2.4 where OX represents the spin axis and OP the precession axis, it is seen that OX will rotate about OP.

$\theta = \angle POX$, the half cone angle of precession, is expected to be constant during the flight. Since OP and OA are assumed to be fixed in inertial space, the angle between OA and OP will also

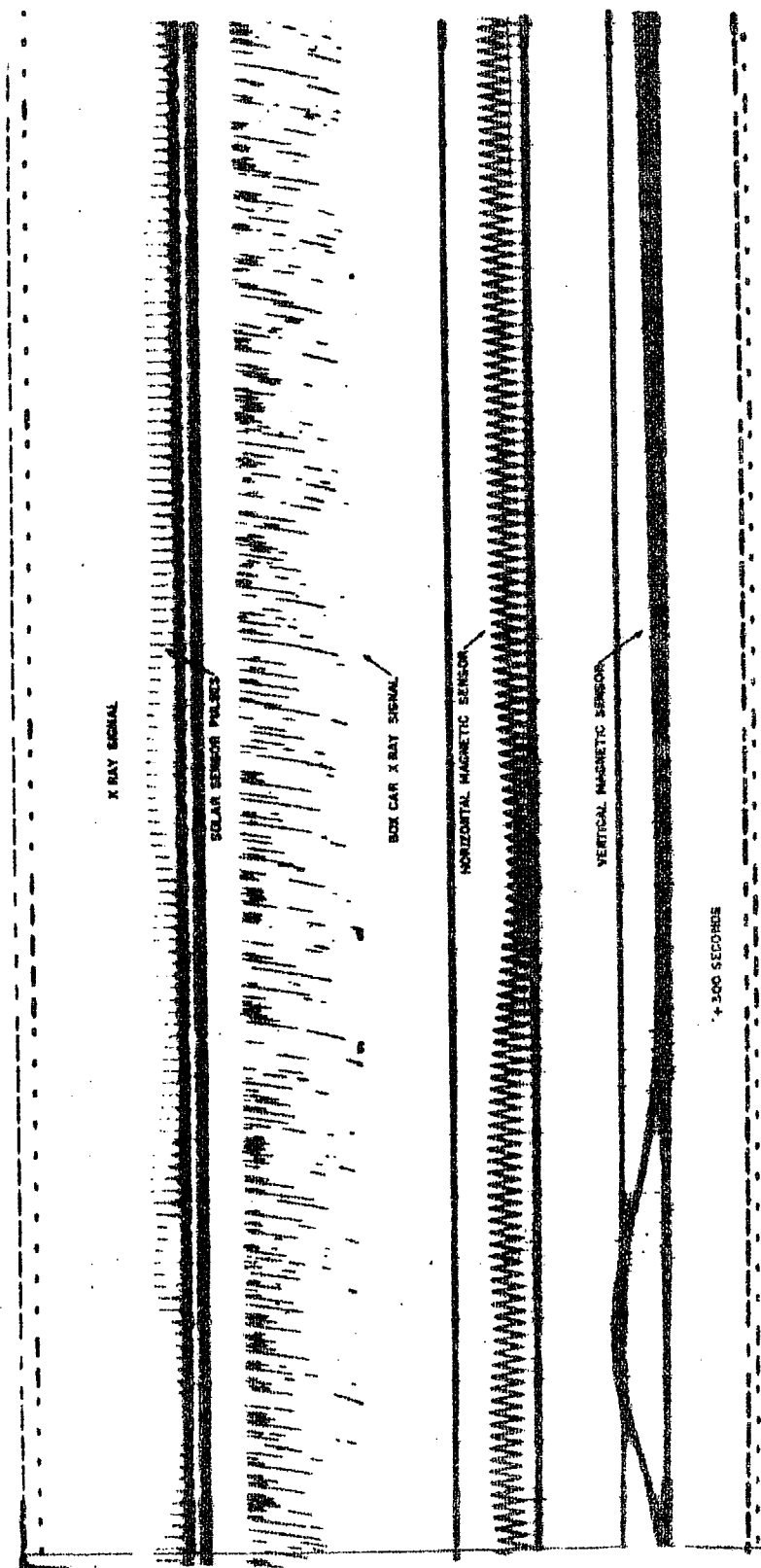


FIG: 123 THE ACTUAL DATA CHART OF THE FLIGHT RUN AT 1°/SEC IS SHOWN WHEN ROCKET RE-ENTERS THE ATMOSPHERE. THE EFFECT OF LARGE PRECESSION (OR TUMBLING) CAN BE SEEN ON MAGNETIC SENSORS AND SOLAR SENSOR OUTPUT.

be constant (say ξ) during each precession and the angle XPA (say χ) will increase monotonically as,

$$\chi = \Omega_p \cdot t + \phi \quad (\text{A 2.15})$$

Using spherical trigonometry it can be seen that,

$$\begin{aligned} \cos XOA &= \cos \theta \cos \xi + \sin \theta \sin \xi \cos (\Omega_p \cdot t + \phi) \\ &= A + B \cdot \cos (\Omega_p t + \phi) \end{aligned} \quad (\text{A 2.16})$$

where the constant A and B are given by,

$$A = \cos \theta \cdot \cos \xi$$

$$B = \sin \theta \cdot \sin \xi$$

Once A and B are determined, the value of θ and ξ can be found

$$\begin{aligned} (\theta + \xi) &= \arccos [\cos (A-B)] \\ (\theta - \xi) &= \arccos [\cos (A+B)] \end{aligned} \quad (\text{A 2.17})$$

It may be seen that if A coincides with zenith, the angle XOA will vary between the limits $\xi - \theta$ and $\xi + \theta$ if the zenith angle lies outside the precession cone. If on the other hand, it lies inside the precession cone the limits on angle XOA will be between $\theta - \xi$ and $\theta + \xi$. Provided, the magnetic sensors are well calibrated and the influence of other material in the rocket are kept to an absolute minimum, the magnetic field at any height can be calculated. In order to make an accurate estimate of the field value as a function of altitude, Finch and Leaton (1957) simulation of the geomagnetic field has been used. The field value was calculated using the equation,

$$M = M_0 (1 - 5.05 \times 10^{-4} h)$$

The necessary magnetic data were obtained from the magnetic observatory at Trivandrum.

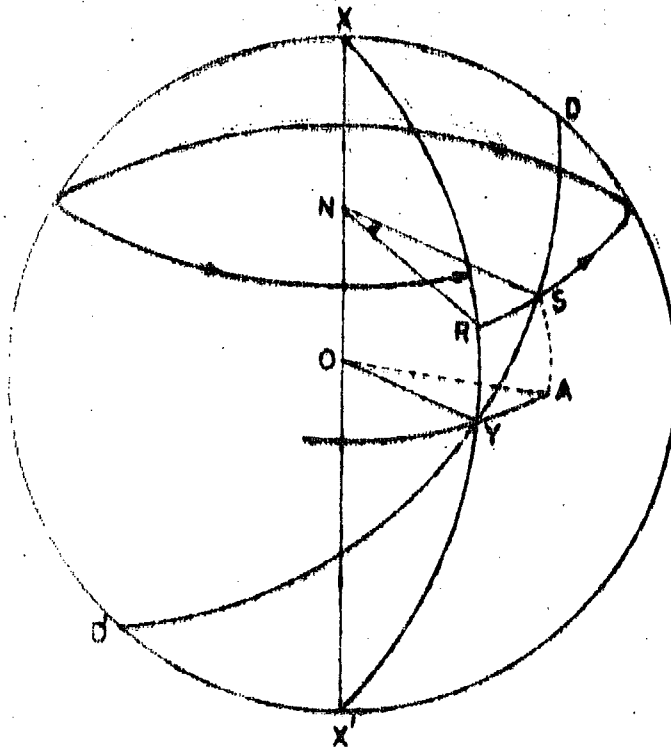
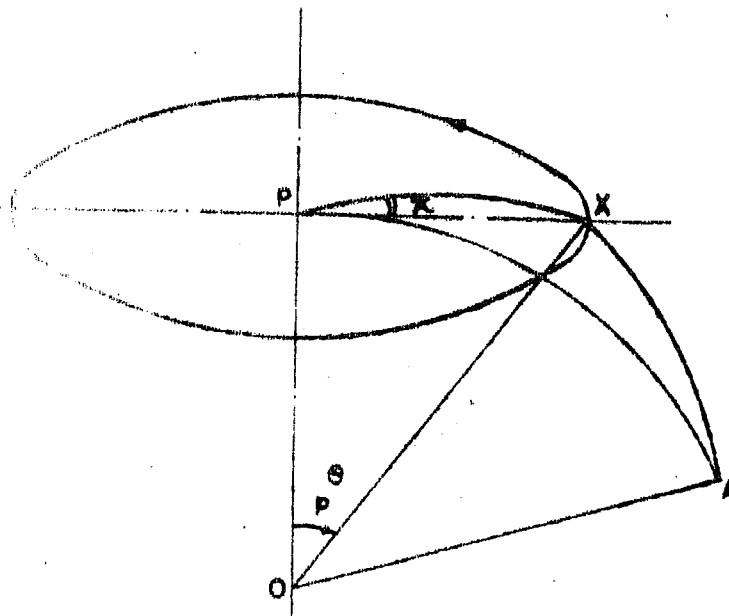


FIG. A25- GEOMETRY OF THE SOLAR SENSOR

FIG. A24- GEOMETRY TO THE THEORY OF
MAGNETIC SENSOR.

A 2.11

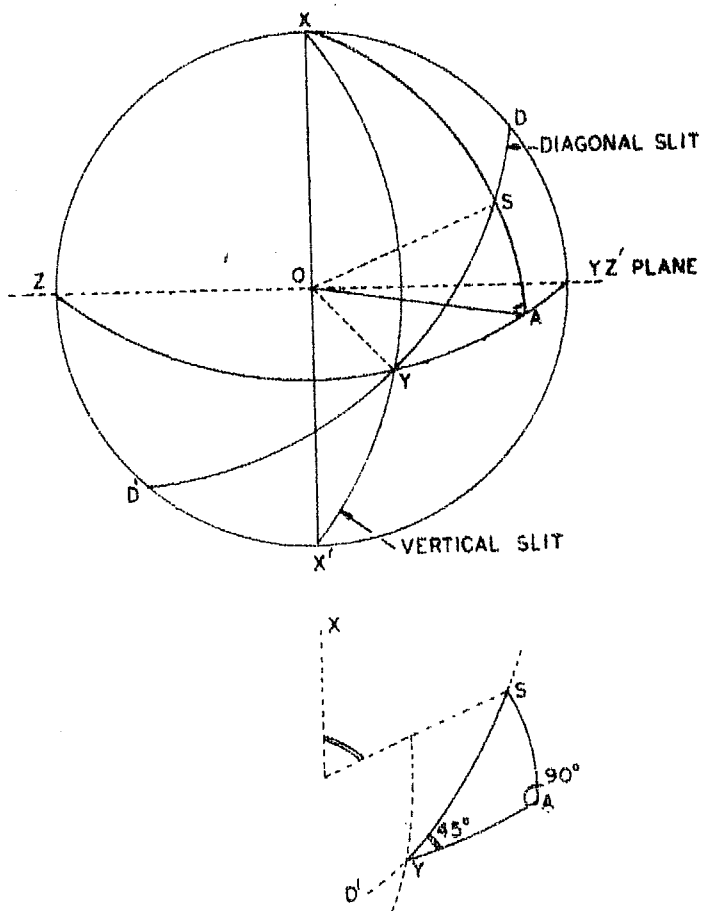


FIG. 12.6 - THE SCHEMATIC OF SOLAR SENSOR SLITS.

A 2.3. SOLAR SENSOR DATA REDUCTION:

The solar sensor used in the present flight was of analog type. The body of sensor was a hemisphere with three free slits, one vertical and the other two inclined at 45° to the vertical. The vertical slit had a thickness of .010" whereas diagonal slits had a thickness of .007." (figure A 2.5). A photodiode (Mullard BPY 10) placed at the center of the hemisphere was used as the basic sun sensor. Figure A 2.7 shows the plot of the output of the sensor during a typical precession cycle.

The information from this sensor was used to evaluate the precession half cone angle and the angle made by the rocket axis with respect to the sun. Referring to figure A 2.6 where XYX' and DYD' represent the vertical and diagonal slits respectively, it is seen that as the rocket spins about XOX' axis with a slow precession, the sun traces a helical path on the sphere about this axis. Assuming that diagonal slit sees the sun at S, from spherical trigonometry it is seen that angle $SYA = 45^{\circ}$, angle $YAS = 90^{\circ}$, and,

$$\cos (YOA) \cdot \cos 90 = \sin (YOA) \cdot \cot (SOA) - \sin 90 \cdot \cot 45$$

$$\text{or} \quad \tan (SOA) = \sin (YOA)$$

$$\text{or} \quad \cos (SOX) = \sin (YOA)$$

$$SOX = \arccos (\sin YOA) \quad (A 2.18)$$

The angle SOX defines the position of the sun with respect to the axis XOX' . The angle YOA was evaluated from the time displacement between the sighting of the sun by the diagonal and the vertical slits ($= \Delta T$). Since the sun follows a helical path as stated earlier the angle SNR can be obtained by,

:A 2.13:

$$\frac{\angle \text{SNR}}{360} \equiv \frac{\Delta T}{T}$$

$$\text{but } \angle \text{SNR} = \angle \text{YOA}$$

$$\therefore \angle \text{SOX} = \arctan \sin \left(\frac{360 \cdot \Delta T}{T} \right) \quad (\text{A 2.19})$$

Following the method described above the two values of ΔT found were, $\Delta T_1 = .021$, $\Delta T_2 = .019$ which yielded a mean precession half cone angle $\sim 1.5^\circ$. The position of the precession cone angle on the celestial sphere was determined as follows:

Taking latitude of launch site, $\phi = 8^\circ 32'34''$, Azimuth of launch, $Z = 256^\circ.16$, Elevation of rocket $h = 64^\circ$.

since, =

$$\sin \delta = \cos Z \cdot \cos \phi \cdot \cos h + \sin \phi \cdot \sin h \quad (\text{A 2.20})$$

$$\sin \delta = .0301$$

$$\text{or } \delta = 1^\circ 43' 10''.$$

Using this above values δ ; t , the hour angle was calculated from

$$\sin t = \frac{\cos h \cdot \sin \delta}{\cos \phi}$$

$$\text{thus, } t = 25^\circ 51' \text{ or } 115^\circ 51' \text{ and R.A.} = \text{L S T} - t \\ = 34^\circ 38' \text{ or } 134^\circ 38'$$

Only the second value was chosen since this was close to the zenith at the time of launch. The final precession point on the celestial sphere was described by,

$$\alpha_p = 134^\circ, \quad \delta_p = 3^\circ \quad (\text{A 2.21})$$

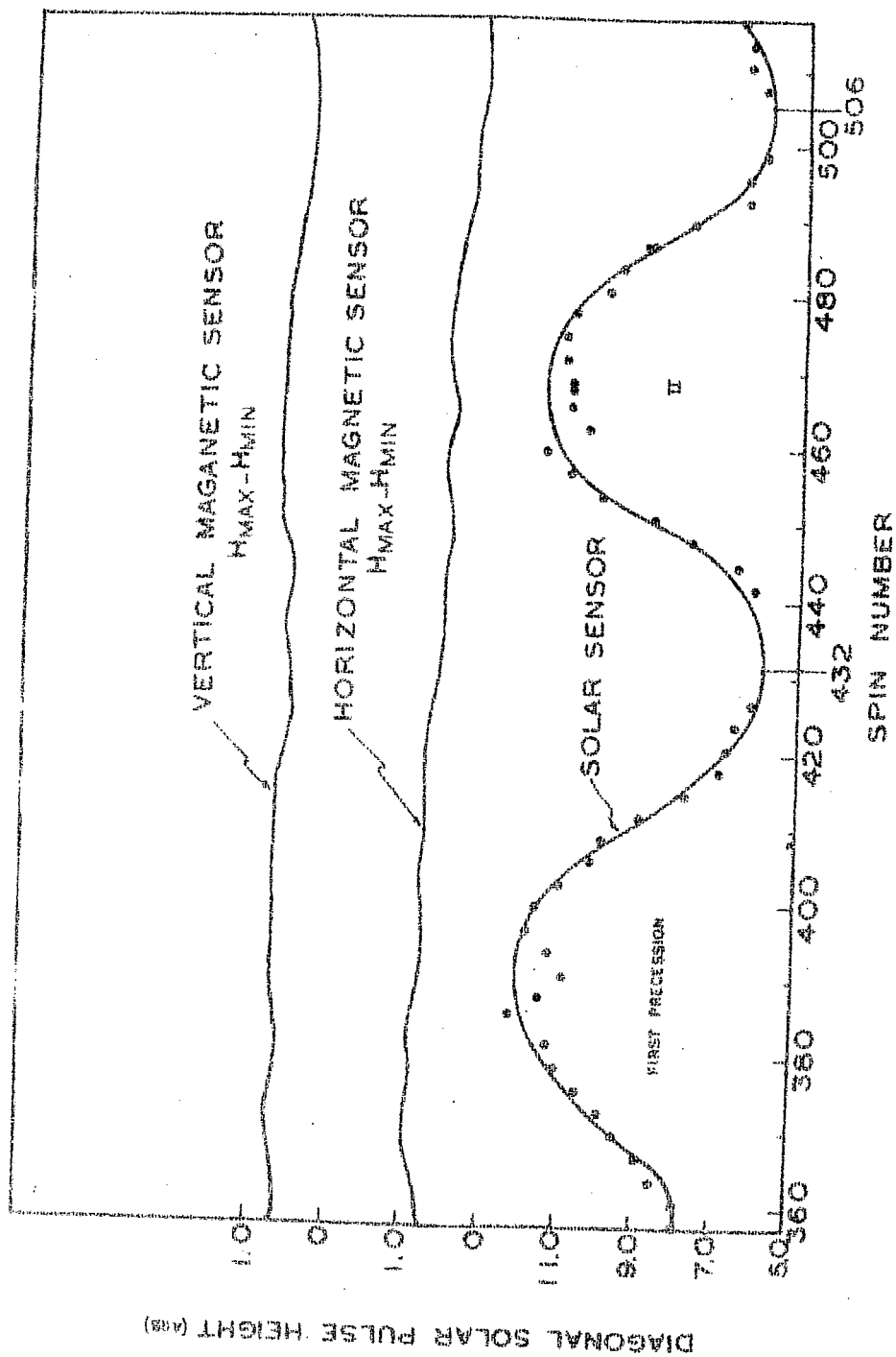


FIG. A27 SHOWS THE INFORMATION ON PRECESSION PERIOD DERIVED FROM SOLAR SENSOR.

:A.2.15:

Based on these data the calculated parameters for the sources which were in the field of view of the detector are given below:

<u>Source</u>	<u>Distance from detector normal</u>
Lup XR-1	3° 17'
Nor XR-2	7° 57'
Cen XR-1	27'
Cen XR-2	9° 10'
Cen XR-4	1° 34'

Aspect Parameters:

Date of launch	December 7, 1969
Time of launch	0035 UT
R.A. of sun	253° 24'
Decl. of sun	-22° 34'
R.A. of precession axis	134°
Decl. of precession axis	3°
Precession axis	78 x .1893 = 14.7654 sec.
Spin period	.1893 sec.
Precession cone angle	3°
R.A. of magnetic field	00 ^h 42 ^m
Decl. of magnetic field	31° 54'

A 3.1a. EFFICIENCY RESOLUTION AND ESCAPE X-RAYS OF THE DETECTOR:

The efficiencies of the detectors for the detection of X-ray in the present experiments are shown in figure A 3.1 and A 3.2. The detector efficiency at any given energy (E) is given by the product of the window transmission and the absorption of the incident radiation in the detection media. In case of proportional counter the window was 100 micron thick beryllium and detection media was 25 mm thick xenon gas at 1 atmospheric pressure. For the balloon experiments these were 0.8 mm Aluminium and 4 mm thick NaI (Tl) crystal respectively.

The efficiency of the detector thus will be given by the equation,

$$\epsilon(E) = \exp\left[-\mu_w(E) \cdot \rho_w \cdot X_w\right] \cdot \left[1 - \exp(-\mu_g(E) \cdot \rho_o \cdot X_o)\right]$$

where ρ_w and ρ_o are the densities of the window material and detector material respectively, $\mu_w(E)$ and $\mu_g(E)$, represent the mass absorption coefficient of the window material and of the detection media at energy E(keV). The efficiency curves shown in figures A 3.1 and A 3.2 have been derived using the mass absorption coefficients given by Allen (1963), Victoreen (1947) and Henke et al (1957).

The resolution of the proportional counter detector as a function of its geometry was also experimentally determined by placing radioactive sources at different portions on the window. The result of this test showed that the counter had an overall resolution of 20%. The resolution of the detector was approximated by $\sigma(E) = \sqrt{E}$.

A 3.1b. ESCAPE X-RAYS CORRECTION:

In addition, it is necessary to correct the calculated efficiency using the above equation for decrease in efficiency due to the escape radiation. No such calculations were necessary for Xenon counter since K-escape peak (34 keV) did not fall in the region of interest and at L-escape peak (~ 4 keV) the yield was very small. But for balloon experiment, since the detector used was NaI (Tl) crystal in which case the escape K-radiation (~ 32 keV) for iodine fell in the region of interest, photons whose energy exceeded the above limit may appear as photons of energy ~ 32 keV^{due} due to the above effect. The necessity for correcting for this effect has been shown by Staein and Lewin (1967), and detailed calculations of the escape probability K_α and K_β have been done by Liden and Starfelt (1954). Assuming P_α and P_β to be the probabilities that an incident photon will give rise to a K_α or K_β photons which escape from the detector with energies of E_{K_α} and E_{K_β} , we have calculated the escape probability using the equation (Overback 1969)

$$P_\alpha(E) = \int_0^{X_0} dx \mu e^{-\mu x} \cdot \frac{1}{2} \delta.w.f_\alpha \left(e^{-\mu_\alpha x} + e^{-\mu_\alpha (X_0 - x)} - \mu_\alpha x / (\mu_\alpha x) - \mu_\alpha (X_0 - x) E_1(\mu_\alpha (x - X_0)) \right)$$

and similarly,

$$P_\beta(E) = \int_0^{X_0} dx \mu e^{-\mu x} \cdot \frac{1}{2} \delta.w.f_\beta \left(e^{-\mu_\beta x} + e^{-\mu_\beta (X_0 - x)} - \mu_\beta x E_1(\mu_\beta x) - \mu_\beta (X_0 - x) E_1(\mu_\beta (X_0 - x)) \right)$$

where X_0 = thickness of the crystal = 1.468 gm.cm^{-2}

$E_{K_\alpha} = 32.5 \text{ keV}$, $E_{K_\beta} = 28.6 \text{ keV}$

A33

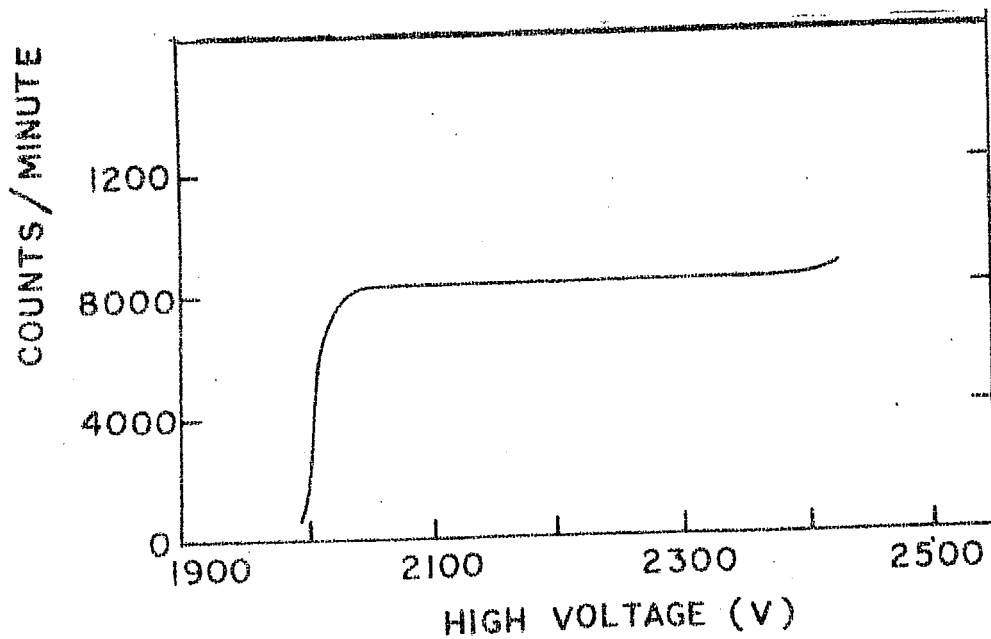
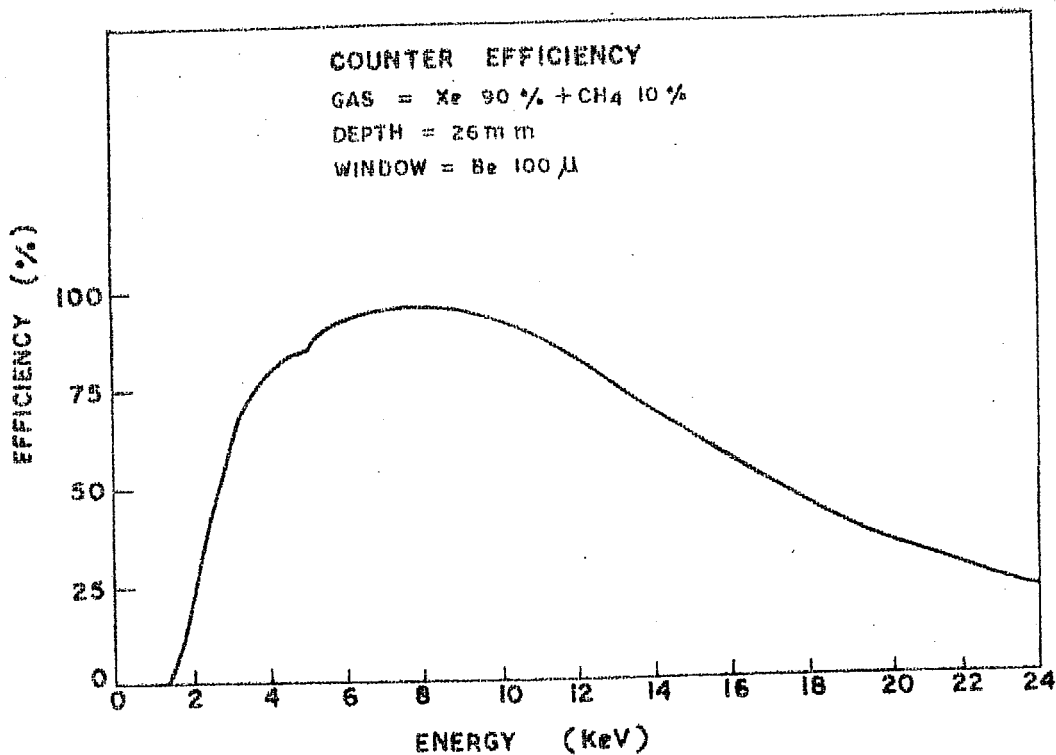


FIG. A31 - THE CALCULATED EFFICIENCY OF THE PROPORTIONAL COUNTER (UPPER). LOWER CURVE SHOWS VARIATION OF COUNT RATE WITH HIGH VOLTAGE.

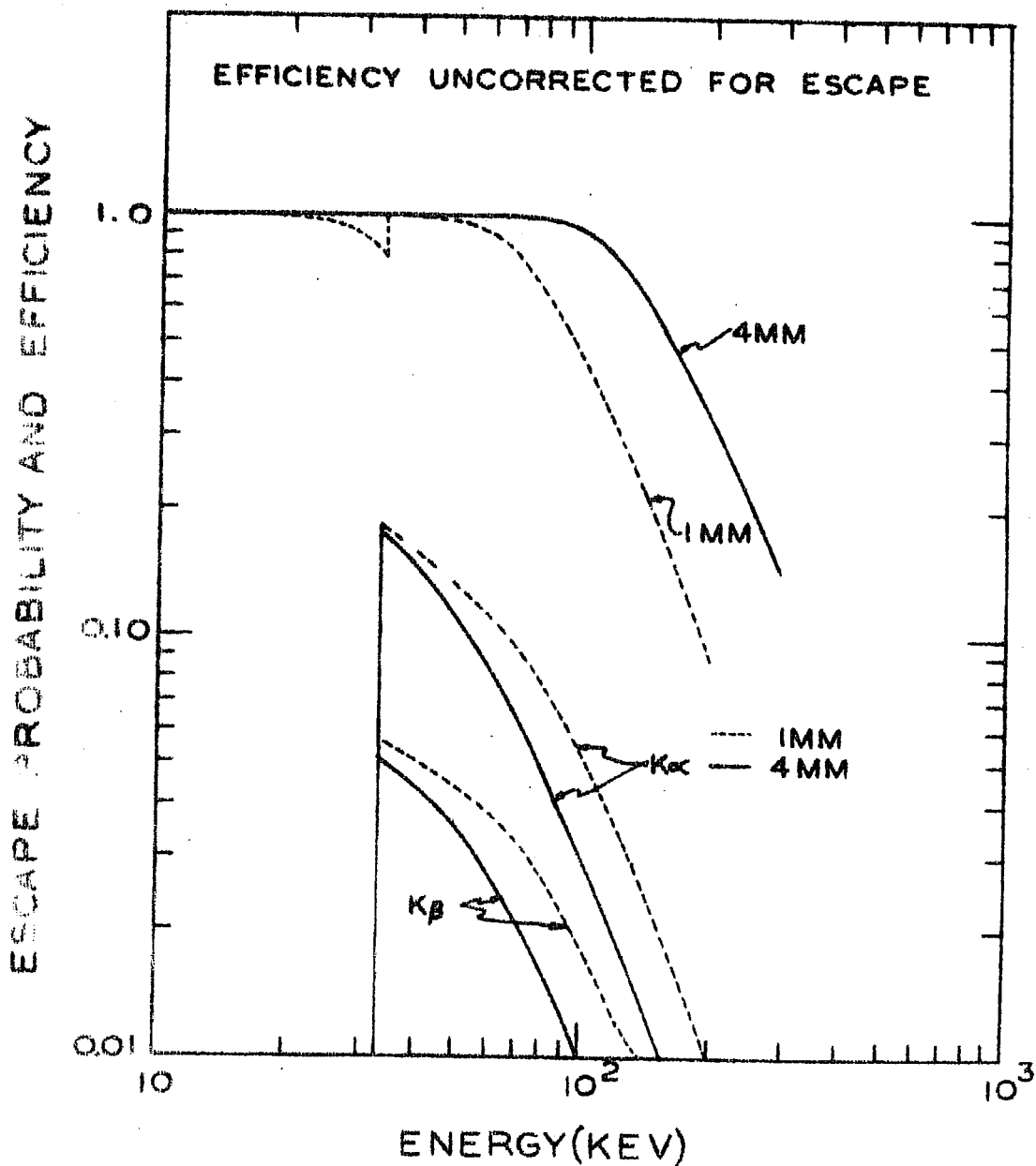


FIG: 132 THE FIGURE SHOWS THE DETECTION EFFICIENCY OF THE NaI(Tl) CRYSTAL FOR 4 MM AND 1 MM THICKNESS. THE ESCAPE PROBABILITY IS ALSO SHOWN.

μ_o = mass absorption coefficient of NaI (Tl)

$$\mu_{\alpha} = (EK_{\alpha}) = 6.62 \text{ cm}^2/\text{gms}$$

$$\mu_{\beta} = (EK_{\beta}) = 4.66 \text{ cm}^2/\text{gms}$$

δ is the fraction of photoelectric photons that originate in the K-shell = 0.875, ω is the K-fluorescence yield of iodine = 0.84. f_{α} and f_{β} are the fraction of K X-rays which are K_{α} and K_{β} X-rays respectively and are given by,

$$f_{\alpha} = 0.7937, f_{\beta} = 0.2063$$

The calculated values of P_{α} and P_{β} are plotted in A 3.2 which shows that at ≈ 33 keV, the escape probability of incident photons was $\approx 18\%$, which was a significant fraction and hence was considered in deriving the true spectrum of the incident radiation.

The resolution of the detector $\sigma(E)$ is usually, in terms of its standard deviation, given by,

$$\sigma(E) = a.E + b.E^{\frac{1}{2}}$$

the values of the constants a and b were determined experimentally by using the full width at half maximum resolution when the detector was irradiated by Cd^{109} (22 and 88 keV) and Am^{241} (59.5 keV).

A 3.2. EXPOSURE EFFICIENCY OF THE DETECTOR:

Collimator used in the present balloon flights was of cylindrical shape whose theoretical response is shown in figure A 3.3. To calculate the exposure efficiency for a source displaced at an angle θ with respect to the telescope

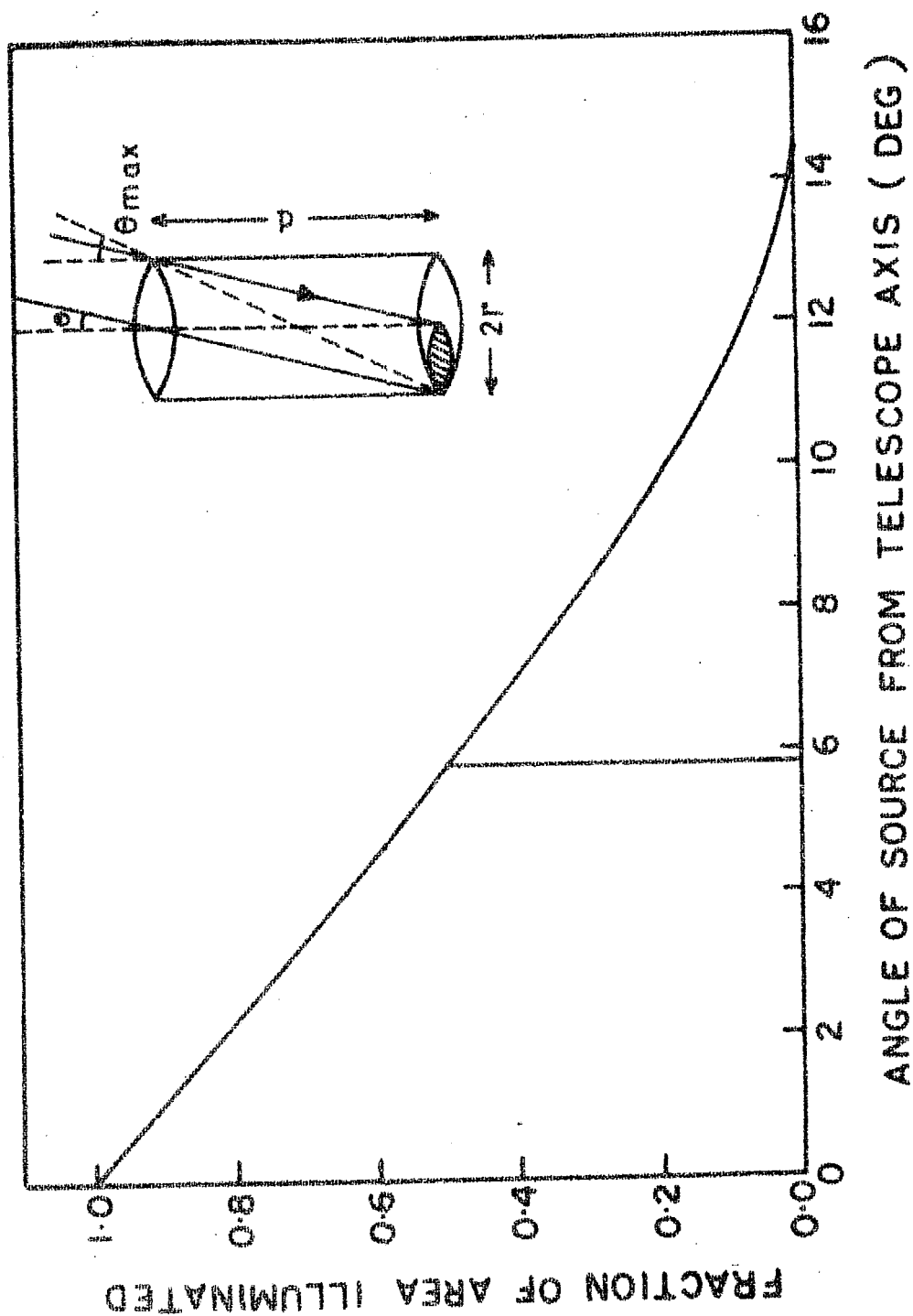


FIG. A33 - ANGULAR RESPONSE OF THE TELESCOPE AS A FUNCTION OF THE ANGLE BETWEEN THE SOURCE AND THE TELESCOPE.

:A 3.7:

axis, the following formulae were used,

$$\cos Z = \frac{\sin \delta - \sin \phi \sin h}{\cos \phi \cdot \cos h}$$

$$\sin h = \sin \phi \cdot \sin \delta + \cos \phi \cdot \cos \delta \cdot \cos t$$

where, h = elevation of the star,

δ = declination of the star,

ϕ = latitude of the place of observation

Z = azimuth of the star and t is the hour angle of the star given by,

t = local sidereal time (L.S.T.) - R.A. of the star.

After performing these calculations the angle between the telescope axis and source (θ) was calculated by

$$\cos \theta = \cos h_1 \cdot \cos h_2 \cdot \cos Z_1 \cdot \cos Z_2 + \cos h_1 \cdot \cos h_2 \cdot \sin Z_1 \cdot \sin Z_2$$

The effective transmission factor was then given by,

$$T_r (\text{coll}) = \left(1 - \frac{\theta}{\text{FWHM}}\right) \times 100 \text{ percent}$$

The elevation angle for the present flight was fixed at 72° for observations on Her X-1 and Cyg X-1.

A 3.3. SEPARATION OF SOURCE FROM BACKGROUND:

Observations of discrete X-ray sources at balloon altitudes are always carried out in the presence of secondary cosmic ray background as well as the cosmic diffuse X-ray background. It is, therefore, necessary to separate the background from the observed count rate to obtain the source flux.

To separate the effects of the background for evaluation of the true intensity of the source, the detector was made to alternately view in the direction of the source and 180° away for nearly equal time. Let B and N be the counts due to the background and the source respectively. Then the detector while looking towards the source registered (N + B) counts and when looking away from it registered B counts. The corresponding fluctuations are given by their standard deviations viz.,

$$\begin{aligned}\sigma(N + B) &= \sqrt{(N + B)} \\ \sigma(B) &= \sqrt{B}\end{aligned}$$

and by the law of propagation of errors,

$$\begin{aligned}\sigma(N) &= \sqrt{(N + B)^2 + (B)^2} \\ \text{i.e. } \sigma(N) &= (N + 2B)^{\frac{1}{2}}\end{aligned}$$

For the more general case of fluctuating background the average value \bar{B} of the background was used and then the signal level was defined as,

$$n = \frac{(N + B) - \bar{B}}{\sqrt{(N + B) + \bar{B}}}$$

This value of n was used for testing the χ^2 distribution to establish the genuineness of the signal.

A 3.4. SPECTRUM FOLDING:

From the data obtained describing the pulse height distribution of the incoming photons in different energy ranges the spectral information could be derived taking into account the following factors:

1. Detector area and field of view i.e. collimator transmission.

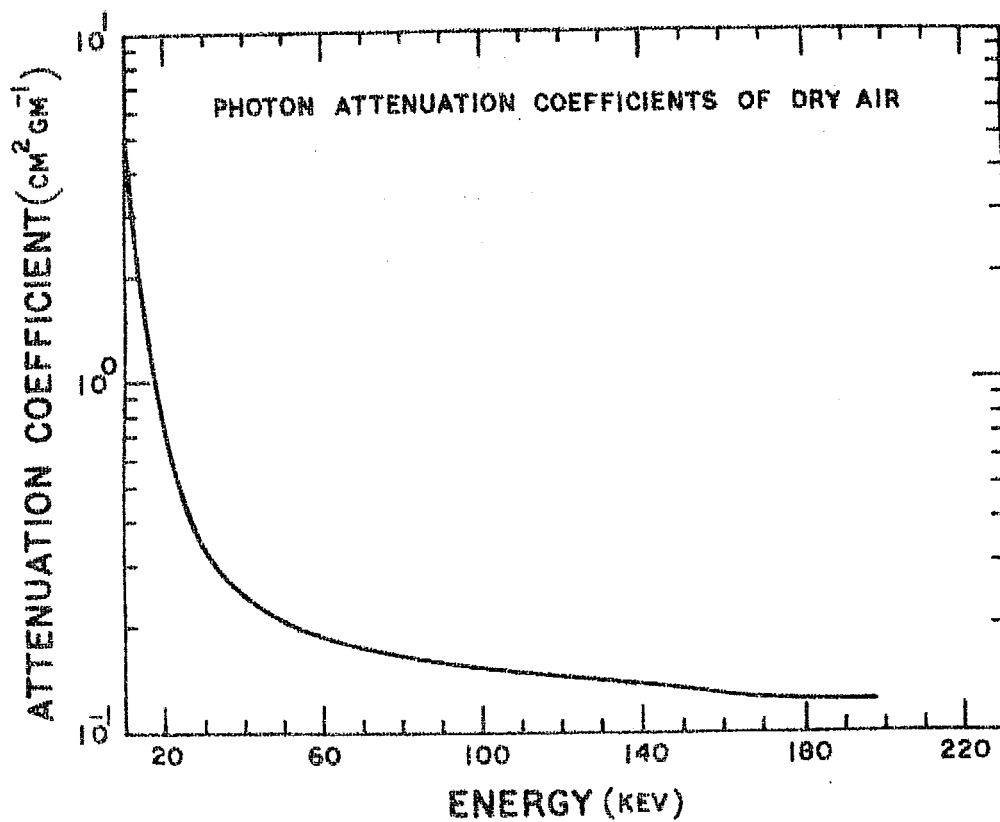


FIG. A3.4. THE FIGURE SHOWS THE MASS ATTENUATION COEFFICIENT USED IN ANALYSIS OF SPECTRA ABOVE 10 keV.

:A 3.10:

2. Finite resolution of the detector
3. Effect of escape radiation
4. The counter-detector efficiency.

To derive the spectrum of the source following procedure was adopted.

In case of balloon the payload floated at an altitude of $\sim 5 \text{ gm/cm}^2$.

At this altitude the incoming X-rays from the source are subjected to attenuation by the residual atmosphere above the detector. The attenuation coefficients of air were calculated taking the attenuation coefficient of nitrogen, oxygen and argon.

Figure A 3.4 shows the absorption coefficient of air above 10 keV. Absorption by detector window and collimator transmission were also taken into account while deriving the final spectrum as already described. In addition, the transmission through air was also taken into account. Let the actual photon spectrum of the source be,

$$\left[\frac{dN}{dE} \right]_D = A E^{-\alpha} \quad \text{or} \quad A \cdot \exp(E/kT)$$

then the attenuated spectra by atmosphere will be represented by,

$$\left[\frac{dN}{dE} \right]_1 = \left[\frac{dN}{dE} \right]_D \cdot e^{-\mu(E) \cdot g}$$

where $\mu(E)$ = attenuation coefficient of air and $g = g/\text{cm}^2$ of air along the line of sight. After correction for the efficiency $\epsilon(E)$ and escape probabilities P_α and P_β the primary spectrum

attenuated by air will be recorded as

$$\left[\frac{dN}{dE} (E) \right]_2 = \left[\frac{dN}{dE} (E) \right]_1 \left[C(E) - P_\alpha(E) - P_\beta(E) \right] + \left[\frac{dN}{dE} (E + EK_\alpha) \right]_1 \\ + P_\alpha(E + EK_\alpha) + \left[\frac{dN}{dE} (E + EK_\beta) \right]_1 + P_\beta(E + EK_\beta)$$

The above spectrum will be further modified by the resolution of the detector ($= \sigma(E)$) and the final spectrum recorded in the detector will be given by,

$$\left[\frac{dN}{dE} (E) \right]_{\text{final}} = \left[\frac{dN}{dE} (E') \right]_2 \frac{\exp.(-(E'-E)^2/(2\sigma(E')^2) dE'}{2\pi \sigma(E')^2}$$

The above equation formed the basis of the analysis of the whole data. Using this equation various possible values of the variable parameters of the spectrum (e.g. A, α , KT) were fed into a computer programme with known given values of these parameters. The resulting output was compared with the observed data. The best fit values of the parameter were then chosen by imposing the minimum χ^2 criteria as,

$$\chi^2 = \sum_E \left[\frac{C_{\text{theo}}(\Delta E) - C_{\text{obs}}(\Delta E)}{C_{\text{theo}}(\Delta E)} \right]^2$$

where $C_{\text{theo}}(\Delta E)$ and $C_{\text{obs}}(\Delta E)$ are the theoretical and observed counts in the energy interval ΔE .

x x x

REFERENCES

- Agrawal P., 1972, Ph.D. thesis, TIFR, Bombay.
- Agrawal P., Gokhale G., Iyengar V., Kunte P., Manchanda R. and Sreekantan B., 1972, TIFR preprint CR-X-A-18(72).
- Aikin A., 1971, COSPAR Symposium, Illinois, U.S.A.
- Ananthakrishnan S. and Ramanathan K., 1969, Nature 223 & 88.
- Ananthakrishnan S., 1969, Ph.D. thesis, PRL.
- Arp H., 1956, Astrn.J. 61,15.
- Avni Y., Bahcall J., Jon P., Bahcall N., Lamb F., 1973 Nature Phys. Sc. 246, 36.
- Bahcall J. and Bahcall N., 1972, Ap. J. letters, 178, L1.
- Baity W., Ulmer M., Wheaton W., Peterson L., 1973, Nature Phy. Sc. 245, 90.
- Baity W., Ulmer M., Peterson L., 1974, preprint.
- Barron D. and Budden K., 1959 Proc. Roy. Soc. A249, 387.
- Barth C., 1966, Ann. Geophys., 22, 98.
- Belian R., Conner J., Evans W., 1972, Ap. J., letters, 171,L87.
- Belrose J., 1968, Radiowave propagation, AGARD.
- Belrose J., 1957, Ph.D. thesis, Cambridge University.
- Bergamini R., Londrillo P. and Setti G., 1967, Nuovo Cimento, 52B, 495.
- Bingham R. and Clark C., 1969, Ap. J. 158, 207.
- Blaauw A., Galactic structure, 1964, page 435, Chicago University press.
- Bleeker J., Burger J., Deeranberg A., Scheepmaker A., Swanenburg B. and Tanaka Y., 1967, Ap. J. 147, 391.
- Boldt F., McDonald F., Riegler G. and Serlemitsos P., 1966, Phys. Rev. lett., 17, 447.
- Boldt E., Desai U. and Holt S., 1969, Ap. J. 156, 427.
- Boldt E., Desai U., Holt S. and Serlemitsos P., 1971, Ap.J. letters, 167, L1.
- Bolton C., 1972a, Nature 235, 21.

- Bolton C., 1972b, Nature Phys. Sc. 240, 124.
- Booker H., 1938, Phil. Trans. Roy. Soc. A237, 411.
- Bopp B., Grupsmith G. and Vanden Bout P., 1972, Ap. J. letters, 178, L5.
- Bowyer S., Byram E., Chubb T., Friedman H., 1965, Science 147, 394, 146, 1307.
- Bowyer S., Lampton M., Mack J., DeMendonca F., 1970, Ap. J. letters, 161, L1.
- Bracewell R., Budden K., Ratcliffe J., Straker T., Weeks K., 1951, Proc. Inst. Elect. Engrs. 98, III, 221.
- Braes L., Miley G., 1972, Nature 235, 147.
- Brannon P. and Hoffman T., 1971, J.G.R. 76, 4630,
- Brecher K. and Morrison P., 1967, Ap. J. letters, 150, L61.
- Brecher K. and Morrison P., 1969, Phys. Rev. letters, 23, 802.
- Brecher K., 1972, Nature 239, 325.
- Brecher K. and Morris P., 1973, Ap.J. letters, 180, L121.
- Brini D., Cattani D., Ciriegi U., Fulgini F., Galli M., Gandolfic A., Moretti E. and Sacchi C., 1965, Ann. Astrophys. 28, 1034.
- Brinkman A., Parsignault D., Schreier E, Gursky H., Kellogg E., Tananbaum H. and Giacconi R., Ap. J. 188, 603.
- Brucato R. and Kristion J., 1972, IAU Circ. 2421.
- Bunner A., Coleman P., Kraushaar W., McCammon D., 1971, Ap. J. letters, 167, L3.
- Burgers B. and Jones T., 1969, Nature, 224, 680.
- Burginyon G., Hill R., Seward F., Tarter C., Toor A., 1972, UCRL 74382.
- Byram E., Chubb T. and Friedman H., 1966, Science, 152, 66.
- Canizares C., McClintock J., Clark G., Lewin W., Schnopper H., Sprott G., 1973, Nature Phy. Sc. 241, 28.
- Carruthers G., 1968, Ap. J. 151, 269.
- Carver J., Mitchell P., Murray E., 1964, J.G.R., 69, 3755.
- Chakravarty S., 1971, Proc. Ind. Acad. Sci. A74, 99.

- Chamberlin J., 1961, Physics of the Aurora & Air glow Academic P., London.
- Chau W., 1973, Nature, Phys. Sc., 243, 133.
- Chevalier C. and Ilavarsky S., 1973, IAUC 2561.
- Chodil G., Mark H., Rodriques R., Seward F., Swift C., Hiltener W., Wallerstein G. and Manner F., 1967, Phys.Rev. letters 19, 681.
- Chodil G., Mark H., Rodriques R., Seward F., Swift C., Tusiel I., Hiltner W., Wallerstein G. and Mannery E., 1968, Ap. J. 154, 645.
- Chodil G., Mark H., Rodrigmes R. and Swift C., 1968, Ap.J. lett., 151, L1.
- Chodil G., Mark H., Rodriques R., Swift C., 1968, Ap. J. letters, 152, L45.
- CIRA., 1965, Cospar Intl. Ref. Atmosphere, North Holland, Amsterdam.
- Clark G., Lewin W. and Smith W., 1968, Ap. J., 151, 21.
- Clark G., Bradt H., Lewin W., Markert T., Schnopper H., Sprott G., 1972, Ap. J. letters, 177, L109.
- Cline T., Desai U., Klebesadal R., Strong I., 1973, Ap. J. letters, 185, L1.
- Cline T., Desai U., 1973, 13th Intl.Cosmic ray conf., Denval page 80 volt I.
- Clyne M. and Thrush B., 1959, Proc. Roy. Soc. A261, 159.
- Cocke W., Hintzen P., Scott J. and Worden S., 1973, IAUC 2543.
- Conner J., Evans W., Belian R., 1969, Ap. J. letters, 157, L157.
- Conner J., Evans W., Mook D., 1972, Nature Phy.Sc., 239, 125.
- Cooke B., Pounds K., Stewardson E. and Adams D., 1967, Ap.J. 150, 189.
- Cooke B., Pounds K., 1971, Nature Phy. Sc., 229, 144.
- Cowsik R., Kobetich E., 1971, Nature Phy. Sc., 739, 41.
- Crompton D. Hutchings J., 1972, Ap. J. letters, 178, L65.
- Cruddace R., Bowyer S., Lampton M., Mack J., Margon B., 1972, Ap. J. 174, 529.
- Davidson A., Henry J., Middleditch J., Harding E., 1972a, Ap. J. lett. 177, L97.

- Davidson A., Shulmon S., Fritz G., Meekins J., Henry R.,
Friedman H., 1972b, Ap. J. 177, 629.
- Davidson K., Ostriker J., 1973, Ap. J. 179, 585.
- Deeks D., 1966, Proc. Roy. Soc. 291, 413.
- Dennis B., Suri A., Frost K., 1973, Ap. J. 186, 97.
- Dolan J., 1970, Space Sc. Rev. 10, 830.
- Doxsey R., Murthy G., Rappaport S., Spencer J., Zaumen W.,
1972, Ap. J. letters, 176, L15.
- Doxsey R., Bradt H., Levine A., Murthy G., Rappaport S.,
Spada G., 1973, Ap. J. letters, 182, L25.
- Dyer C. and Morfil G., 1971, Ap. Sp. Sc., 14, 243.
- Edwards P., 1968, Nature 217, 43.
- Edwards P., Burtt, G., and Knox F., 1969, Nature 222, 1052.
- Elliot J., Murphy R. and Cruikshank D., 1973, IAUC 2454.
- Evans W., Belian R., Conner J., 1970, Ap. J. letters, 159, L57.
- Fabian A., Pringle J., Rees M., 1973a, IAUC 2555.
- Fabian A., Pringle J., Rees M., 1973b, Nature 244, 212.
- Felton J. and Morrison P., 1966, Ap. J. 146, 686.
- Finch and Leaton , 1957, preprint.
- Fisher P., Johnson H., Jordon W., Acton L., 1965, Ap.J., 143, 203.
- Forman W., Jones C., Liller W., 1972a, Ap. J. letters, 177, L103.
- Forman W., Kellogg E., Gursky H., Tananbaum H., Giacconi R.,
1972b, Ap. J. 178, 309.
- Francey R., Fenton A., Harries J., McCracken K., 1967, Nature
216, 773.
- Francey R., 1970, J.G.R., 75, 4849.
- Friedman H., 1960, In Physics of the upper atmosphere,
ed.- J.A. Ratcliffe, Academic press.
- Friedman H., Byram E., Chubb T., 1967, Science 156, 374.
- Friedman H., Byram E., 1967, Science 158, 257.
- Fritz G., Davidson A., Meekins J., Friedman H., 1971,
Ap. J. letters. 164, L81.

Frohlich A., 1972, IAUC 2436.

Fulgini F., Frontera F., 1973, Astrn. Ap., 28, 373.

Giacconi R., Paolini F., Gursky H., Rossi B., 1972, Phy. Rev. letters, 9, 439.

Giacconi R., Gursky H., Waters J., Rossi B., Clark G., Garmire G., Oda M. and Wada M., 1965, ASE preprint, 1003B.

Giacconi R., Gorenstein P., Gursky H. and Water J., 1967, Ap. J. letters, 148, L119.

Giacconi R., Kellogg E., Gorenstein P., Gursky H., Tananbaum H., 1971, Ap. J. letters, 165, L27.

Giacconi R., Murray S., Gursky H., Kellogg E., Schreier E., Matilsky T., Koch D. and Tananbaum H., 1973a, ASE 3249, preprint.

Giacconi R., Gursky H., Kellogg E., Levinson R., Schreier E., Tananbaum H., 1973b, Ap. J. 184, 227.

Gill S., 1951, Proc. Camp. Phil. Soc., 47, 96.

Glass I., 1969, Ap. J., 157, 215.

Gold T., 1968, Nature 218, 371.

Gorenstein P., Giacconi R. and Gursky H., 1967, Ap.J. lett. 150, L85.

Gorenstein P., Kellogg E., Gursky H., 1969, Ap. J., 156, 315.

Gorenstein P., Kellogg E., Gursky H., 1969, Ap.J., 156, 515.

Gorenstein P., Tucker W., 1972, Ap. J., 176, 333.

Gould R., Burbidge G., 1963, Ap. J., 138, 969.

Grader R., Hill R. and Stoering T., 1970, Ap. J., lett. 161, L45.

Gratton L., 1969, preprint.

Gribben J., 1971, Nature Phy. Sc., 233, 18.

Groth E., Nelson M., 1972, Ap. J., letters, 178, L111.

Guo D., Webber W., Damle S., 1973, 13th Int.cosmic ray Conf., Denver, vol. V.

Gursky H., Kellogg E., Leong C., Tananbaum H., Giacconi R., 1971, Ap. J. letters, 165, L43.

Gursky H., 1972, Ap. J. letters, 175, L141.

Gursky H., 1973, ASE, preprint, 3306.

- Harries J., McCracken K., Francey R., Fenton A., 1967, Nature 215, 38.
- Harries J., Tuchy I., Broderick A., Fenton K., Luyendy K., 1971, Nature Phy. Sc., 234, 149.
- Hayakawa S., Kato T., Makino F., Ogawa H., Tanaka Y., Yamoshila K., Matsnoka J., Myamoto S., Oda M. and Ogawara Y., 1971, Ap. Sp. Sc., 12, 104.
- Hayakawa S., 1973, X and gamma ray astronomy IAU, page 235.
- Haymes R., Ellis D., Fishman G., Glenn S. and Kurfess J., 1968, Ap. J. 151, L125.
- Haymes R. and Harnden Jr.F., 1970, Ap. J., 159, 1111.
- Henrickesen R., Chia T., 1972, Nature Phys. Sc., 240, 133.
- Henry R., Fritz G., Meekins J., Chubb T., Friedman H., 1971, Ap. J. letters, 163, L73.
- Hill R., Burginyon G., Griader R., Palmieri T., Seward F., Stoering J., 1972, Ap. J., 171, 519.
- Hinteregger H., 1965, Space Sc. Rev. 4, 461.
- Hjellming R. and Wade C., 1971a, Ap. J. letters, 166, L21.
- Hjellming R. and Wade C., 1971b, Nature, 234, 138.
- Hjellming R., 1973, preprint (Ap. J. 1973).
- Holt S., Boldt E., Schwartz D., Serlemitsos P., Bleach R., 1971, Ap. J. letters, 166, L65.
- Hoover R., Thomas R. and Underwood J., 1972, Space Sc. and Techn. 11, 2.
- Hunt R., Sciama D., 1972, Mon. Not. R.Astr. Soc., 157, 335.
- Hutchings J., Crampton D., Glaspey J., Walker G., 1973, Ap. J., 182, 549.
- Iyengar V., Manchanda R., Durgaprasad N., Gokhale G., Kunte P., Sreekantan B., 1974, TIFR, preprint, CR-XA-23(74).
- Jacchia L., 1970, Smith Ap. Obs. Space Rep. 313.
- Jackson J., 1972, Nature Phy. Sc., 236, 39.
- Jones C., Forman W., Tananbaum H., Schreier E., Gursky H., Kellogg E., Giacconi R., 1973a, Ap. J. letters, 181, L33.
- Jones C., Forman W., Liller W., 1973b, Ap.J. letters, 182, L109.

- Kane R. and Rao U., 1958, Proc. Ind. Ac. Sc. 67, 30.
- Kasturirangan K. and Rao U., 1972, Ap. Sp. Sc., 15, 161.
- Kato T., 1972, Ap. Sp. Sc., 12, 58.
- Kaufman P., Paes de Barros M., Viana E., 1970, Nature 228, 1080.
- Kawabata K., Fujimoto M., Sofue Y. and Fukai M., 1969, Publ. Astron. Soc., Japan, 21, 293.
- Kellogg E., Gursky H., Murray S., Tananbaum H., Giacconi R., 1971, Ap. J. letters, 169, L99.
- Kellogg E., Murray S., Giacconi R., Tananbaum H., Gursky H., As. & E., preprint 3245.
- Kitamura T., Matsuoka M., Miyomoto S., Nakagawa M., Oda M., Ogawara Y., Takagishi K., 1969, Nature, 224, 784.
- Klebesadel R., Strong I., Olson R., 1973, Ap. J. letters, 182, L85.
- Kopal Z., 1959, Close Binary systems (New York, John Wiley & Sons), 135.
- Kreplin R., Chupp T., Friedman H., 1962, J.G.R., 67, 2231.
- Kreplin R., 1961, Ann. Geophys., 17, 151.
- Kristiakowsky G. and Volpi G., 1957, J.Chem. Phys., 27, 114.
- Kristion J., Brucato R., Visvanathan N., Lanning H., Sandage A., 1971, Ap. J. letters, 168, L91.
- Krzeminski W., 1973, IAU 2612.
- Lamb F., Pethick C., Pines D., 1973, Ap. J. 184, 271.
- Lampton M., Bowyer S., Mack J., Margon B., 1971, Ap.J., 168, L1.
- Lampton M., Margon B., Bowyer S., 1972, Ap.J. letters, 171, L45.
- Lewin W., Clark G., Smith W., 1968, Ap.J. letters, 152, L49.
- Lewin W., Clark G. and Smith W., 1968, Can.Jl.Phy., 46, S409.
- L'Henneux J., 1974, Ap. J. letters, 187, L53.
- Li F. and Clark G., 1974, Ap. J. letters, 191, L33.
- Liden K. and Starfelt N., 1954, Ark. f. Fys., 7, 427.
- Liller W., 1972, IAU cir., 2415, 2427.
- Lindsay J., 1963, Trans. Amer. Geophys. Union, 44, 722.

- MacGregor A., Seward F., Turiel I., 1969, Ap.J. 161, 979.
- Manchanda R., Iyengar V., Agrawal P., Gokhele P., Kunte P., Sreekantan B., 1971, Nature Phy.Sc., 232, 190.
- Manchandra R., Iyengar V., Durgaprasad N., Gokhele G., Kunte P., Sreekantan B., 1973, Nature Phy. Sc., 244, 59.
- Margon B., Lampton M., Bowyer S., Cruddace R., 1971, Ap. J. letters 169, L23.
- Margon B., Bowyer S., Ston R., 1973, SSL preprint 14161.
- Matilsky T., Giacconi R., Gursky R., Kellogg E., Tananbaum H., 1972, Ap. J. letters, 174, L53.
- Matilsky T., Gursky H., Kellogg E., Tananbaum H., Murray S., Giacconi R., 1973, Ap. J. letters, 181, L753.
- Matteson I., 1971, Ph.D. thesis, Uni. of California, San Diego.
- Mavroyannis C. and Winckler C., 1961, Chemical Reactions in the lower and upper atmosphere Interscience publishers, 287.
- McCammon D., Bunner A., Coleman P., Kranshaar W., 1971, Ap. J. letters, 168, L33.
- McClintock J., Lewain W., Sullivan R., Clark G., 1969, Nature, 223, 1969.
- McClintock J., Clark G., Lewin W., Schnopper H., Canizares C., Sprött G., 1974, Ap. J. 188, 159.
- McCracken K., 1966, Science 154, 1000.
- McCray R., 1973, Nature Phy. Sc., 243, 94.
- Mechtley E. and Smith L., 1968, J.A.T.P. 30, 363.
- Merier R., 1970, Space Res. 10, 572.
- Meira L. Jr., 1971, J.G.R. 76, 202.
- Metzger A. and Dolan J., 1968, Astron. J., 73, S107.
- Mitra A., 1966, JATP, 28, 945,
1968, JATP, 30, 1065
1969, Space Res. 9, 418.
- Mohanty D., Balsubramaniam V., Swarup G., 1971, Nature 232, 191.
- Morton D., 1967, Ap. J., 147, 1017.
1969, Astn. Sp. Sc. 3, 117.
- Muller E., 1935, Z. Astrophys. 10, 52.
- Murdin P., 1972, IAUC Circ. 2433.

- Nakagawa M., Sakurai H. and Kitamura T., 1973, 13th Int. cosmic ray conf., Denver, U.S.A., paper 671.
- Nicolet M. and Aikin A., 1960, J.G.R. 65, 1469.
- Nicolet M., 1965, J.G.R., 70, 679, 691.
- Novick R., Weisskoff M., Berthelsdraf R., Linke R., Wolfe R., 1972, Ap. J. letters, 174, L8.
- Oda M., 1965, Int. conf. cosmic rays, Vol. 1, 68.
- Oda M., Gorenstein P., Gursky H., Kellogg E., Schrier E., Tananbaum H., Giacconi R., 1971, Ap. J. letters, 166, L1.
- Oda M., Wada M., Matsuoka M., Miyamoto S., Muranaka N., Ogawara Y., 1972, Ap. J. letters, 172, L13.
- Overbeck J., Womack E. and Tananbaum H., 1967, Ap.J., 150, 47.
- Overbeck J., Tananbaum H., 1968, Ap. J., 153, 899.
- Overbeck J., 1969, NASA-CR-1045.
- Palmieri T., Burginyon G., Grader R., Hill R., Seward F., Stoering J., 1971, Ap. J. 169, 33.
- Parsignault D., Gursky H., Kellogg E., Matilsky T., Murray S., Schreier E., Tananbaum H., Giacconi R., 1972, Nature Phy.Sc. 239, 123.
- Parthasarathy R. and Larfald G., 1965, University of Alaska report.
- Pearce J., 1969, J.G.R., 74, 853.
- Peterson L., Jacobson A., Pelling R. and Swartz D., 1968, Cand. Jl. Phys. 46, S437.
- Peterson L., 1973, X and gamma ray astronomy, ed-.Bradt and Giacconi, page 51.
- Petro L. and Hiltner W., 1972, Ap. J. letters, 181, L39.
- Poppoff I. and Whitten R., 1962, J.G.R. 67, 2986.
- Poppoff I. and Whitten R., 1969, Nature 224, 1187.
- Potemra T. and Zmuda A., 1970, J.G.R., 75, 7161.
- Pounds K., 1969, IAU Symp. No.37, Non-solar gamma and X-ray astronomy (Rome).
- Poveda A. and Woltjer L., 1968, Astn. J. 73, 65.
- Prakasarao A., Sharma D., Jayanthi U., Rao U., 1971, Ap. Sp. Sc. 10, 150.

Prakasarao A., Sharma D., Jayanthi U. and Rao U., 1971,
Ap. Space Sc., 10, 150.

Pringle J. and Rees M., 1972, Astr. & Ap. 21, 1.

Pringle J. and Rees M., 1972, Nature.

Pringle J., 1973, Nature Phy. Sc., 243, 90.

Rao U., Chitnis E., Sharma D., Prakasarao A., Jayanthi U.,
1971, Nature 224.

Rao U., Chitnis E., Prakasarao A., Jayanthi U., 1969, Ap. J.
letters, 157, L127.

Rappaport S., Zauman W., Doxsey R., 1971a, Ap. J. letters 168, L17.

Rappaport S., Doxsey R., Zauman W., 1971b, Ap. J. letters, 168, L43.

Rappaport S., Cash W., Doxsey R., Moore G., Borken R.,
1973, MIT - preprint, CSR-P-73-108.

Rawer K., 1962, The Ionosphere, FUP, New York, 1952.

Reigler G., Boldt E., Serlemitsos, P., 1968, Ap. J. 153, 195.

Reinert C.P., 1969, Ph.D. thesis (Unpublished), University
of Minnesota.

Richer H., Isherwood B., Fletcher M., Morbey C., 1972, IAUC 2431.

Roberts J., 1974, Ap. J. 187, 575.

Rocchia R., Rothenflug R., Boclet D. and Durouchoux P., 1969,
Saclay, preprint.

Rose M., 1968, Ap. J. 152, 245.

Rothschild R., Boldt E., Holt S., Serlemitsos P., 1974,
Ap. J. letters, 189, L13.

Rowan Robinson M., 1968, Mon. Not. R. Ast. Soc. 138, 445.

Ryle M., 1968, Ann. Rev. Astron. Ap. 6, 249.

Sanford P., Mason K. and Hawkins F., 1974, Ap. J. letters, 190, L55.

Schmidt M., 1968, Ap. J. 151, 393.

Schreier E., Gursky H., Kellogg E., Tananbaum H., Giacconi R.,
1971, Ap. J. letters, 170, L21.

Schreier E., Levinson R., Gursky H., Kellogg E., Tananbaum H.,
Giacconi R., 1972a, Ap. J. letters, 172, L31.

Schreier E., Giacconi R., Gursky H., Kellogg E., Tananbaum H.,
1972b, Ap. J., 178, L71.

- Schwartz D., 1969, Ph.D. thesis, Uni. of California, San diego, USA.
- Schwartz D., Gursky H., 1973, NASA SP.339.
- Sen H., Wyler A., 1960, J.G.R., 65, 3931.
- Seshadri K., Prakasarao A., Rao U., 1971, preprint.
- Setti G. and Rees M., 1970, Non-solar X and gamma ray astronomy (ed.- L.Gratton) page 352.
- Seward F., 1970, UCID - 15622, preprint.
- Seward F., 1974, preprint, UCRL-51 456.
- Shapiro S., 1973, Ap. J., 180, 531.
- Sheddy C., 1968, Radio Science 3, 792.
- Shukla P., Wilson B., 1970, preprint, Ap.J. 1971, 164, 265.
- Shulman S., Fritz G., Meekins J., Friedman H., 1971, Ap.J. letters, 168, L49.
- Silk J., 1969, Nature 221, 347.
- Silk J. and McCray R., 1969, Ap. letters 3, 59.
- Silk J., 1970, Sp. Sc. Rev. II, 671.
- Silk J., 1973, Ann. Rev. Astr. Astrophy.
- Smith H., Margon B. and Conti P., 1973, Ap.J. lett, 179, L125.
- Spada G., Bradt H., Doxsey R., Levine A., Rappaport S., 1974, preprint, Ap. J. press.
- Spencer N., Bogges R. and Taeush D., 1964, J.G.R., 69, 1367.
- Stein J. and Lewin W., 1967, J.G.R., 72, 383.
- Stothers R., 1972, Ap. J. 175, 431.
- Strong I., Klagesadel R., Olson R., 1974, Ap.J. lett, 188, L1.
- Stroud W. and Nordberg W., 1963, IGY Rocket report 7, 33.
- Subbaraya B., Satya Prakash and Pareek P., 1972, J.A.T.F.34, 155.
- Subbaraya B., Satya Prakash and Gupta S.P., 1971, Ind.J. Pure., Appl. 9, 626.
- Swider W., 1969, Rev. Geophys. 7, 573.
- Tananbaum H., Gursky H., Kellogg E., Levinson R., Schreier E., Giacconi R., 1972a, Ap. J. letters, 174, L143.

- Tananbaum H., Gursky H., Kellogg E., Giacconi R., Jones C., 1972b, Ap. J. letters, 177, L5.
- Thomas L., 1971, J.A.T.P., 33, 157.
- Thomas R., Busseli G., Clancy M., Davidson P., 1969, Ap. J. letters, 158, L151.
- Tinsley B., 1969, J.G.R. 74, 2327.
- Toor A., Groves D., Price R., Seward F., 1971, UCRL 27, 3605.
- Tucker W., Kellogg E., Gursky H., Giacconi R., Tananbaum H., 1972, ASE - preprint, 3075.
- Tulinov V., Shibaeva L. and Jackovler S., 1969, Space Res.9, 231.
- Tushy R., Davidson P., 1973, Nature Phy.Sc. 244, 121.
- Ulmer M., Baity W., Wheaton W., Peterson L., 1972, Ap.J.lett. 178, L61.
- Ulmer M., Baity W., Wheaton W., Peterson L., 1972a, Ap. J. lett., 178, L121.
- Ulmer M., Baity W., Wheaton W. and Peterson L., 1973a, Ap. J. letters, 181, L33.
- Ulmer M., Baity W., Wheaton W. and Peterson L., 1973b, Ap. J. letters 184, 117.
- U.S. Standard Atmosphere suppl., 1966, ESSA, NASA.
- Vanden Heuvel E. and Heisse E., 1972, Nature Phy.Sc., 239, 67.
- Vanden Heuvel E., 1973a, Nature 242, 71.
- Vanden Heuvel E., De Loore C., 1973b, Astron & Astrophy., 25, 387.
- Velinov P., 1968, J.A.T.P., 30, 1891.
- Vidal N., Wickramshinghe D., Peterson B., 1973, Ap.J.lett.182,L77.
- Waade C., Hjellming R., 1972, Nature 235, 271.
- Wagner Ch.V., 1966, J.A.T.P., 28, 607.
- Walborn N., 1973, Ap. J. letters, 179, L123.
- Watanabe K., 1958, Adv. Geophys. 5, 153.
- Webber W., 1962, J.G.R., 67, 5091.

Webber W. and Reinert C., 1970, Ap. J. 162, 883.

Webster B., Mordin P., 1972, Nature, Phy.Sc., 235, 37.

Weeks L. and Smith L., 1968, J.G.R., 73, 4835.

Wheaton W., Ulmer M., Baity W., Datlowe D., Elcon M., Peterson L.,
Klebesadel R., Strong I., Cline T., Desai U., 1973, Ap. J.
letters, 185, L57.

Whitten R., Poppoff I., Edmonds R. and Berming N., 1965,
J.G.R. 70, 1737.

Wildman P., Kerley M. and Schaw M., 1969, J.A.T.P., 31, 951.

Yentis D., Novick R., Vanden Bait P., 1972a, Ap. J., 177, 365.

Yentis D., Novick R., Vanden Bait P., 1972b, Ap. J., 177, 375.

Young J., Carruthers G., Helmes H., Johnson C., and Patterson N.,
1968, Science 160, 990.